



Project acronym and title:

SECURE – Subsurface Evaluation of Carbon capture
and storage and Unconventional Risks

**D2.2 Report on effects of long-term sequestration process in the
Borzecin structure – observation evidence of the injected gas
migration and possible leakage**

Authors and affiliation:

**Jan LUBAŚ, Wiesław SZOTT, Piotr ŁĘTKOWSKI, Andrzej GOŁĄBEK,
Krzysztof MIŁEK, Andrzej RYCHLICKI, Marcin WARNECKI, Mirosław
WOJNICKI, Jerzy KUŚNIERCZYK, Sławomir SZUFLITA, Stanisław
BIAŁY**

Oil and Gas Institute – National Research Institute, Lubicz 25A, 31-504
Krakow, Poland

Email of lead author:
szott@inig.pl

D2.2
Revision:1 (draft for definitive)

Disclaimer

This report is part of a project that has received funding by the *European Union's Horizon 2020 research and innovation programme* under grant agreement number 764531.

The content of this report reflects only the authors' view. The *Innovation and Networks Executive Agency (INEA)* is not responsible for any use that may be made of the information it contains.



Project funded by the European Commission within the Horizon 2020 Programme

Dissemination Level

PU	Public	X
CO	Confidential, only for members of the consortium (incl. the Commission Services)	
CL	Classified, as referred to in Commission decision 2001/844/EC	

Deliverable number:	D2.2
Deliverable name:	Report on effects of long-term sequestration
Work package:	WP2 – Risk assessment for leakage and induced seismicity: methodology and case studies
Lead WP/deliverable beneficiary:	TNO/INIG

Status of deliverable		
	By	Date
Submitted (Author(s))	Wiesław Szott (INIG)	05.05.2020
Verified (WP leader)	Jens Wollenweber (TNO)	18.05.2020
Approved (EB member)	Wolfram Kloppmann (BRGM)	
Approved (Coordinator)	Edward Hough (UKRI-BGS)	

Author(s)		
Name	Organisation	E-mail
Jan Lubaś	INIG	lubas@inig.pl
Wiesław Szott	INIG	szott@inig.pl
Piotr Łętkowski	INIG	letkowski@inig.pl
Andrzej Gołabek	INIG	golabek@inig.pl
Krzysztof Milek	INIG	milek@inig.pl
Andrzej Rychlicki	INIG	rychlicki@inig.pl
Marcin Warnecki	INIG	warnecki@inig.pl
Mirosław Wojnicki	INIG	wojnicki@inig.pl
Jerzy Kuśnierczyk	INIG	kusnierczyk@inig.pl
Sławomir Szuflita	INIG	szuflita@inig.pl
Stanisław Biały	INIG	bialy@inig.pl



Public introduction

Subsurface Evaluation of CCS and Unconventional Risks (SECURE) project is gathering unbiased, impartial scientific evidence for risk mitigation and monitoring for environmental protection to underpin subsurface geoenergy development. The main outputs of SECURE comprise recommendations for best practice for unconventional hydrocarbon production and geological CO₂ storage. The project is funded from June 2018–May 2021.

The project is developing monitoring and mitigation strategies for the full geoenergy project lifecycle; by assessing plausible hazards and monitoring associated environmental risks. This is achieved through a program of experimental research and advanced technology development that includes demonstration at commercial and research facilities to formulate best practice. It will meet stakeholder needs; from the design of monitoring and mitigation strategies relevant to operators and regulators, to developing communication strategies to provide a greater level of understanding of the potential impacts.

The SECURE partnership comprises major research and commercial organisations from countries that host shale gas plays and CCS sites at different stages of operation (from permitted to closed). SECURE is forming a durable international partnership with non-European groups; providing international access to study sites, creating links between projects and increasing our collective capability through exchange of scientific staff.

Executive report summary

As part of activities in Work Package 2 of the SECURE project, the aim of deliverable D2.2 is to evaluate the effects of the long-term CO₂-H₂S sequestration process in the Borzęcin (Poland) reservoir structure. The report includes all historical operational data determining assumed and implemented parameters of the process. In addition, various tests and analyses were performed on downhole, as well as surface samples of reservoir fluids, taken from selected wells of the Borzęcin reservoir. They were aimed at identifying the propagation and intensity of acid gas migration within the reservoir and potential leakage pathways towards the ground surface. Some of the tests such as soil gas or gas from downhole brine degassing analyses have never been conducted before, providing additional information on the safety of geological storage of acid gases within the Borzęcin structure. Corrosion potential of well tubings and cement were also examined and analysed as they are crucial elements of well completion and leakage prevention. The report is supplemented with a simulation model of the Borzęcin structure. The model was calibrated against available operational and measured data and used to determine basic characteristics of the sequestration process such as fluid saturations and compositions, their variation in time due to fluid migrations and the transition between various phases. The observation evidence of absent acid gas leakage from the Borzęcin structure was confirmed and explained by the simulation results of the sequestration process. The constructed and calibrated model of the structure was also used to predict the future performance of the current sequestration project. In addition, the capacity of the Borzęcin structure for increased sequestration is assessed by finding the optimum scenario of the risk-free sequestration performance.



Contents

Public introduction	ii
Executive report summary.....	ii
Contents	iii
1 Introduction	1
2 History of operation	2
2.1 Production phase.....	2
2.2 Injection phase	8
2.3 Summary and Conclusions.....	19
3 Measurements	20
3.1 Bottomhole sampling of reservoir water saturated with gas.....	20
3.2 Gas Analyses.....	35
3.3 Reservoir water analysis	50
3.4 PVT analysis.....	54
3.5 Soil gas analysis	60
3.6 Tubing Corrosion measurements and analysis	72
3.7 Influence of CO ₂ upon the strength of cement	75
3.8 <i>Summary and Conclusions</i>	76
4 Geological setting and modelling	78
4.1 Geological setting	78
4.2 Geological modelling	78
4.3 Summary and Conclusions.....	85
5 Dynamic simulation model	86
5.1 Model construction	86
5.2 Model calibration	94
5.3 Summary and Conclusions.....	106
6 Geomechanical model.....	107
6.1 Geomechanical description	107
6.2 Geomechanical simulations.....	107
6.3 Summary and Conclusions.....	114
7 Analysis of simulation results – detailed description of the ongoing sequestration process.....	115
7.1 Process basic parameters	115
7.2 Leakage risk factor analysis	118
7.3 Summary and Conclusions.....	125
8 Simulation forecasts and result analysis for the continuation scenario of the acid gas sequestration	127
8.1 Simulaton forecast assumptions.....	127
8.2 Simulation forecast results and analysis	127
8.3 Summary and Conclusions.....	139
9 Storage capacity analysis for a hypothetic full-scale CO₂ sequestration scenario at Borzęcin.....	140
9.1 Simulaton forecast assumptions.....	140
9.2 Simulation forecast results and analysis	140



9.3	Summary and Conclusions.....	152
10	Summary and Conclusions of the deliverable.....	153
11	References.....	156



FIGURES

Figure 2.1. Reservoir monthly gas production.....	3
Figure 2.2. Well monthly gas production. Wells: W1, W10, W11, W12, W21, W22.....	3
Figure 2.3. Well monthly gas production. Wells: W23, W24, W25, W26, W27.....	4
Figure 2.4. Well monthly gas production. Wells: W4, W6, W7, W29, W30, W31.....	4
Figure 2.5. Reservoir monthly water production.....	5
Figure 2.6. Well monthly water production. Wells: W1, W10, W11, W12, W21, W22.....	5
Figure 2.7. Well monthly water production. Wells: W23, W24, W25, W26, W27.....	6
Figure 2.8. Well monthly water production. Wells: W4, W6, W7, W29, W30.....	6
Figure 2.9. Bottom hole pressure. Wells: W1, W4, W6, W7, W10, W11, W12, W21, W22, W23, W24, W25, W26, W27, W29, W30, W31.....	7
Figure 2.10. Total gas production vs original gas in place. Total water production vs original water in place.....	7
Figure 2.11. Reservoir monthly gas injection. Fraction of total gas injection by 31.08.2019.....	9
Figure 2.12. Composition of injected gas.....	10
Figure 2.13. Reservoir monthly gas production.....	10
Figure 2.14. Well monthly gas production. Wells: W12, W21, W22.....	11
Figure 2.15. Well monthly gas production. Wells: W21, W24, W25, W26, W27.....	11
Figure 2.16. Well monthly gas production. Wells: W4, W6, W29, W31.....	12
Figure 2.17. Composition of produced gas. Well W4.....	12
Figure 2.18. Composition of produced gas. Well W21.....	13
Figure 2.19. Composition of produced gas. Well W22.....	13
Figure 2.20. Composition of produced gas. Well W24.....	14
Figure 2.21. Composition of produced gas. Well W27.....	14
Figure 2.22. Composition of produced gas. Well W31.....	15
Figure 2.23. CO ₂ concentration, c_{CO_2} , in gas produced by wells: W4, W21, W22, W24, W27, W31.....	15
Figure 2.24. Reservoir monthly water production.....	16
Figure 2.25. Well monthly water production. Wells: W24, W27 W21, W4 W22.....	16
Figure 2.26. Well monthly water production. Wells: W29, W12, W6, W25, W26.....	17
Figure 2.27. Reservoir monthly water injection.....	17
Figure 2.28. Well monthly water injection. Wells: W10, W11, W23, W29.....	18
Figure 2.29. Total gas production / injection vs original gas in place. Total water production / injection vs original water in place.....	18
Figure 2.30. Bottom hole pressure. Wells: W1, W4, W6, W7, W10, W11, W12, W21, W22, W23, W24, W25, W26, W27, W29, W30, W31.....	19
Figure 3.1. Bottomhole samplers driving to the B-4 well.....	22
Figure 3.2. Pulling out the samplers set from the lubricator - B-4 well.....	22
Figure 3.3. The work at the B-6 well.....	23
Figure 3.4. Samples taking from the bottomhole sampler.....	24
Figure 3.5. Overflow bailer after pulling out from the B-30 well.....	24
Figure 3.6. Sampling of bottomhole samples from the B-24 well.....	25
Figure 3.7. Sampling of bottomhole samples from the B-22 well – the view from slickline unit.....	27
Figure 3.8. Slickline unit.....	27
Figure 3.9. Bottomhole samplers pulled out from the B-22 well lubricator.....	27
Figure 3.10. Set of two bottomhole samplers after pulling out from the B-22 well.....	28
Figure 3.11. The bottom part of bottomhole sampler (No 514) after pulling out from the B-22 well.....	28
Figure 3.12. Sampling of bottomhole samples from the B-24 well.....	29
Figure 3.13. Bottomhole samplers pulled out from the B-24 well lubricator.....	30
Figure 3.14. Protection of bottomhole samples pulled out from the B-24 well.....	30
Figure 3.15. The B-24 well after completion of the work related to sampling.....	30
Figure 3.16. Bottomhole samplers driving to the B-4 well.....	31
Figure 3.17. The work at sampling from the B-6 well.....	32
Figure 3.18. Samplers driving to the B-6 well.....	33
Figure 3.19. Map of the Borzęcin reservoir – bottomhole samples taking.....	35
Figure 3.20. Composition of the gas dissolved in the Borzęcin reservoir water.....	36
Figure 3.21. CO ₂ concentration in the gas released from the bottomhole water versus the distance from the injecting well.....	38



Figure 3.22. H ₂ S concentration in the gas released from the bottomhole water versus the distance from the injecting well.	38
Figure 3.23. Composition comparison of samples of gas dissolved in water and of the extracted gas - well B-4.	39
Figure 3.24. Composition comparison of samples of gas dissolved in water and of the produced gas - well B-22.	40
Figure 3.25. Composition comparison of gas samples originating from the B-6 well.	41
Figure 3.26. Composition comparison of gas samples originating from the B-24 well.	42
Figure 3.27. Part of the surface installation – separate reduction-measurement systems of productive wells.	42
Figure 3.28. Composition of natural gas extracted from the Borzęcin reservoir.	43
Figure 3.29. Installation for acid gases injection to the Borzęcin reservoir.	44
Figure 3.30. Composition of acid gas injected directly to waters underlying the Borzęcin gas reservoir. .	44
Figure 3.31. Methane carbon and hydrogen isotope diagram presenting the origin of analysed gas. TO, thermogenic with oil; TC, thermogenic with condensate; TD, dry thermogenic; TH: thermogenic with high-temperature [7].	46
Figure 3.32. Carbon isotopic composition of methane versus carbon dioxide [8].	47
Figure 3.33. Variability of the isotope composition of hydrogen in methane.	48
Figure 3.34. Temporal variability of the hydrogen isotope composition in methane – gas samples from brine degassing.	48
Figure 3.35. Variability of the carbon isotope composition in methane in relation to the distance from the acid gas injection well (B-28) – gas samples from brine degassing drawn in 2019.	48
Figure 3.36. Variability of isotope composition of carbon in carbon dioxide.	49
Figure 3.37. Variability of isotope composition of carbon in carbon dioxide.	49
Figure 3.38. Variability of the carbon isotope composition in CO ₂ in the brine degassing gas in relation to the distance from the acid gas injection well (B-28) – in 2019.	50
Figure 3.39. Percentage of anions in samples from individual wells.	51
Figure 3.40. Percentage of cations in samples from individual wells.	51
Figure 3.41. The difference in the percentage of individual cations in the samples drawn at annual intervals on the example of the B-24 productive well.	52
Figure 3.42. Gas deviation factor Z – CME test of the produced gas.	58
Figure 3.43. Gas volume factor B _g – CME test of the produced gas.	58
Figure 3.44. Gas deviation factor Z of the injected gas generated by the PVTsim software.	59
Figure 3.45. Phase diagram of the injected gas generated by the PVTsim software.	59
Figure 3.46. Solubility of gases in Borzęcin reservoir water.	60
Figure 3.47. Location of wells in the area of the Borzęcin natural gas reservoir with soil gas sampling sites indicated.	61
Figure 3.48. Location of measuring points at the B-6 well.	62
Figure 3.49. Location of measuring points at the B-22 well.	62
Figure 3.50. Location of measuring points at the B-28 well.	62
Figure 3.51. Soil gas sampling from a monitoring well located within the B-28 well pad.	63
Figure 3.52. Soil gas sampling from a monitoring well located within 35 metres of the B-22 wellhead.	63
Figure 3.53. Installation of a drive-in probe at the B-23 well.	67
Figure 3.54. Location of measuring points (drive-in probes) around the B-23 well.	68
Figure 3.55. Installation of a drive-in probe at the B-24 well.	68
Figure 3.56. Location of measuring points (drive-in probes) around the B-24 well.	68
Figure 3.57. Hydrocarbons content in samples taken at the B-6, B-22 and B-28 wells.	71
Figure 3.58. Hydrocarbons content in samples taken at the B-22 and B-24 wells.	72
Figure 3.59. Schematic of corrosion measurements at constant well tubing depth.	73
Figure 3.60. Penetration (maximum pit depth) vs Depth.	73
Figure 3.61. Histograms of measured pit depths vs depth of well tubing. Depth range: 1350-1400 m.	74
Figure 3.62. Corrosion rates at various depth range of injecting well (W28) tubing.	74
Figure 4.1. Structural map of the Basal limestone top.	78
Figure 4.2. Structural map of the Basal limestone bottom.	79
Figure 4.3. Structural map of the Rotliegend bottom.	79
Figure 4.4. Variographic analysis of NTG: measured vs. theoretical semivariance in three main directions (vertical direction, minor and major horizontal directions).	80
Figure 4.5. Geological parameter (porosity, permeability, NTG) distributions along the vertical cross section (A-A').	83



Figure 4.6. NTG distribution at various geological layers (Basal limestone top and bottom, Rotliegend bottom).	83
Figure 4.7. Porosity distribution at various geological layers (Basal limestone top and bottom, Rotliegend bottom).	84
Figure 4.8. Permeability distribution at various geological layers (Basal limestone top and bottom, Rotliegend bottom).	84
Figure 5.1. 3D view of the reservoir simulation model.	86
Figure 5.2. Top view of the reservoir simulation model. Vertical cross section line A-A'	87
Figure 5.3. Vertical cross section of the reservoir simulation model along line A-A'	87
Figure 5.4. Top view of the reservoir simulation model including surrounding aquifer. Definitions of partially isolated reservoir regions.	88
Figure 5.5. Well W28 design.	89
Figure 5.6. Initial gas saturation along vertical cross section (A-A').....	90
Figure 5.7. Initial gas saturation at the Basal limestone top.....	90
Figure 5.8. Initial gas saturation at the Rotliegend top.....	90
Figure 5.9. Initial gas saturation at the Rotliegend bottom.....	90
Figure 5.10. Formation volume factor of original gas and injected gas at reservoir temperature.....	92
Figure 5.11. Viscosity of original gas and injected gas at reservoir temperature.....	93
Figure 5.12. Phase diagram of: original reservoir gas, injected gas, pure CO ₂	93
Figure 5.13. Solution of CO ₂ in reservoir brine under reservoir conditions vs pressure.	95
Figure 5.14. Solution of H ₂ S in reservoir brine under reservoir conditions vs pressure.....	95
Figure 5.15. Model calibration. Comparison of measured bottom hole pressure and simulation results. Well W1.	96
Figure 5.16. Model calibration. Comparison of measured bottom hole pressure and simulation results. Well W4.	96
Figure 5.17. Model calibration. Comparison of measured bottom hole pressure and simulation results. Well W6.	96
Figure 5.18. Model calibration. Comparison of measured bottom hole pressure and simulation results. Well W7.	96
Figure 5.19. Model calibration. Comparison of measured bottom hole pressure and simulation results. Well W10.	97
Figure 5.20. Model calibration. Comparison of measured bottom hole pressure and simulation results. Well W11.	97
Figure 5.21. Model calibration. Comparison of measured bottom hole pressure and simulation results. Well W12.....	97
Figure 5.22. Model calibration. Comparison of measured bottom hole pressure and simulation results. Well W21.....	97
Figure 5.23. Model calibration. Comparison of measured bottom hole pressure and simulation results. Well W22.....	98
Figure 5.24. Model calibration. Comparison of measured bottom hole pressure and simulation results. Well W23.....	98
Figure 5.25. Model calibration. Comparison of measured bottom hole pressure and simulation results. Well W24.....	98
Figure 5.26. Model calibration. Comparison of measured bottom hole pressure and simulation results. Well W25.....	98
Figure 5.27. Model calibration. Comparison of measured bottom hole pressure and simulation results. Well W26.....	99
Figure 5.28. Model calibration. Comparison of measured bottom hole pressure and simulation results. Well W27.....	99
Figure 5.29. Model calibration. Comparison of measured bottom hole pressure and simulation results. Well W28.....	99
Figure 5.30. Model calibration. Comparison of measured bottom hole pressure and simulation results. Well W30.....	99
Figure 5.31. Model calibration. Comparison of measured bottom hole pressure and simulation results. Well W31.....	100
Figure 5.32. Model calibration. Comparison of measured water-gas ratio and simulation results. Well W1.101	
Figure 5.33. Model calibration. Comparison of measured water-gas ratio and simulation results. Well W4.101	
Figure 5.34. Model calibration. Comparison of measured water-gas ratio and simulation results. Well W6.101	
Figure 5.35. Model calibration. Comparison of measured water-gas ratio and simulation results. Well W7.101	



Figure 5.36. Model calibration. Comparison of measured water-gas ratio and simulation results. Well W10.	102
Figure 5.37. Model calibration. Comparison of measured water-gas ratio and simulation results. Well W11.	102
Figure 5.38. Model calibration. Comparison of measured water-gas ratio and simulation results. Well W12.	102
Figure 5.39. Model calibration. Comparison of measured water-gas ratio and simulation results. Well W21.	102
Figure 5.40. Model calibration. Comparison of measured water-gas ratio and simulation results. Well W22.	103
Figure 5.41. Model calibration. Comparison of measured water-gas ratio and simulation results. Well W23.	103
Figure 5.42. Model calibration. Comparison of measured water-gas ratio and simulation results. Well W24.	103
Figure 5.43. Model calibration. Comparison of measured water-gas ratio and simulation results. Well W25.	103
Figure 5.44. Model calibration. Comparison of measured water-gas ratio and simulation results. Well W26.	104
Figure 5.45. Model calibration. Comparison of measured water-gas ratio and simulation results. Well W27.	104
Figure 5.46. Model calibration. Comparison of measured water-gas ratio and simulation results. Well W29.	104
Figure 5.47. Model calibration. Comparison of measured water-gas ratio and simulation results. Well W30.	104
Figure 5.48. Model calibration. Comparison of measured CO ₂ concentration and simulation results in gas produced by well W4.	105
Figure 5.49. Model calibration. Comparison of measured CO ₂ concentration and simulation results in gas produced by well W21.	105
Figure 5.50. Model calibration. Comparison of measured CO ₂ concentration and simulation results in gas produced by well W22.	105
Figure 5.51. Model calibration. Comparison of measured CO ₂ concentration and simulation results in gas produced by well W27.	105
Figure 5.52. Model calibration. Comparison of measured CO ₂ concentration and simulation results in gas produced by well W31.	105
Figure 6.1. 3D view of the geomechanical model.	107
Figure 6.2. Geomechanical model input data. Young modulus.	108
Figure 6.3. Geomechanical model input data. Poisson ratio.	108
Figure 6.4. Geomechanical model input data. Unconfined compressive strength.	108
Figure 6.5. Geomechanical model input data. Friction angle.	108
Figure 6.6. Geomechanical model input data. Biot coefficient.	109
Figure 6.7. Geomechanical model input data. Tensile strength.	109
Figure 6.8. Distribution of vertical stress.	110
Figure 6.9. Distribution of maximum horizontal stress.	111
Figure 6.10. Distribution of minimum horizontal stress.	112
Figure 6.11. Distribution of volumetric strain.	113
Figure 7.1. Evolution of relative average regional pressures.	115
Figure 7.2. Relative water encroachment from underlying aquifer to reservoir regions.	116
Figure 7.3. Relative water encroachment from surrounding aquifer to reservoir regions.	116
Figure 7.4. Relative pressure distribution along the vertical cross section connecting wells: W29, W22, W11.	117
Figure 7.5. Relative pressure distribution at the structure top.	117
Figure 7.6. Relative pressure distribution at the structure bottom.	117
Figure 7.7. Relative pressure at the completion interval of well W28.	118
Figure 7.8. Distribution of the formation breakdown pressure within the Borzęcin structure.	119
Figure 7.9. Diagram for the estimation of the threshold displacement pressure at the caprock – reservoir rock boundary under initial conditions.	119
Figure 7.10. Distribution of gas saturation along the vertical cross section (A-A') connecting wells: W29, W22, W11.	121
Figure 7.11. Distribution of gas saturation at the structure top.	121



Figure 7.12. Distribution of gas saturation at the structure mid depth.....	121
Figure 7.13. Distribution of CO ₂ concentration in the gas phase along the vertical cross section (A-A') connecting wells: W29, W22, W11.....	122
Figure 7.14. Distribution of CO ₂ concentration in the gas phase at the structure top.	122
Figure 7.15. Distribution of CO ₂ concentration in the gas phase at the structure mid depth.	122
Figure 7.16. Distribution of brine saturation along the vertical cross section (A-A') connecting wells: W29, W22, W11.....	123
Figure 7.17. Distribution of brine saturation at the structure top.	123
Figure 7.18. Distribution of brine saturation at the structure mid depth.	123
Figure 7.19. Distribution of CO ₂ solution in brine (immobile at $S_w < 0.1$, mobile otherwise) along the vertical cross section (A-A') connecting wells: W29, W22, W11.	124
Figure 7.20. Distribution of CO ₂ solution in brine (immobile at $S_w < 0.1$, mobile otherwise) at the structure top.	124
Figure 7.21. Distribution of CO ₂ solution in brine (immobile at $S_w < 0.1$, mobile otherwise) at the structure mid depth.	124
Figure 7.22. Distribution of maximum horizontal stress in the well W28 zone.	125
Figure 8.1. Reservoir monthly gas production. Extrapolation of the historical production decline trend.	127
Figure 8.2. Well monthly gas production. Historical well contribution to the reservoir production rate.	128
Figure 8.3. Reservoir monthly gas injection by well W28. Balanced CO ₂ and H ₂ S production.....	129
Figure 8.4. Composition of gas injected by W28.....	129
Figure 8.5. Evolution of average regional pressures.....	130
Figure 8.6. Relative water encroachment from surrounding aquifer to reservoir regions.	130
Figure 8.7. Relative water encroachment from underlying aquifer to reservoir regions.....	131
Figure 8.8. CO ₂ concentration in gas produced by wells W4, W21, W22, W27 and of total reservoir production.....	131
Figure 8.9. Average composition of reservoir gas - CO ₂ and H ₂ S components.....	132
Figure 8.10. Average composition of reservoir gas - main components (C ₁ , C ₂ , C ₃₊ , N ₂).	132
Figure 8.11. Contribution of various phases to total CO ₂ in reservoir.	133
Figure 8.12. Distribution of gas saturation along the vertical cross section (A-A') connecting wells: W29, W22, W11.	134
Figure 8.13. Distribution of gas saturation at the structure top in year.....	134
Figure 8.14. Distribution of gas saturation at the structure mid depth in year.....	134
Figure 8.15. Distribution of CO ₂ concentration in the gas phase along the vertical cross section (A-A') connecting wells: W29, W22, W11.....	135
Figure 8.16. Distribution of CO ₂ concentration in the gas phase at the structure top.	135
Figure 8.17. Distribution of CO ₂ concentration in the gas phase at the structure mid depth.....	135
Figure 8.18. Distribution of brine saturation along the vertical cross section (A-A') connecting wells: W29, W22, W11.....	136
Figure 8.19. Distribution of brine saturation at the structure top.	136
Figure 8.20. Distribution of brine saturation at the structure mid depth.	136
Figure 8.21. Distribution of CO ₂ solution in brine along the vertical cross section (A-A') connecting wells: W29, W22, W11.	137
Figure 8.22. Distribution of CO ₂ solution in brine at the structure top.	137
Figure 8.23. Distribution of CO ₂ solution in brine at the structure mid depth.....	137
Figure 8.24. Figure 9. Relative pressure distribution along the vertical cross section (A-A') connecting wells: W29, W22, W11.	138
Figure 8.25. Relative pressure distribution at the structure top.....	138
Figure 8.26. Relative pressure distribution at the structure bottom.....	138
Figure 9.1. Localization of the injecting wells including W40.	141
Figure 9.2. Reservoir monthly CO ₂ injection.	141
Figure 9.3. Regional monthly CO ₂ injection.....	142
Figure 9.4. Evolution of total CO ₂ injection.....	142
Figure 9.5. Contribution of trapping mechanisms to the total sequestration.	143
Figure 9.6. Average reservoir pressure.	143
Figure 9.7. Relative water encroachment from surrounding aquifer to reservoir regions.	144
Figure 9.8. Relative water encroachment from underlying aquifer to reservoir regions.....	144
Figure 9.9. Reservoir pressure distribution at the end of the injection phase (2029).....	145
Figure 9.10. Maximum pressures along well trajectories. Maximum pressures among all well trajectories.....	145
Figure 9.11. Distribution of pressure step across the caprock-reservoir rock boundary in 2029.	146



Figure 9.12. Pressure step across the caprock-reservoir rock boundary at the high structure point.....	146
Figure 9.13. Distribution of gas saturation along the vertical cross section (A-A') connecting wells: W29, W22, W11.....	148
Figure 9.14. Distribution of gas saturation at the structure top.....	148
Figure 9.15. Distribution of gas saturation at the structure mid depth.....	148
Figure 9.16. Distribution of CO ₂ concentration in the gas phase along the vertical cross section (A-A') connecting wells: W29, W22, W11.....	149
Figure 9.17. Distribution of CO ₂ concentration in the gas phase at the structure top.....	149
Figure 9.18. Distribution of CO ₂ concentration in the gas phase at the structure mid depth.....	149
Figure 9.19. Distribution of brine saturation along the vertical cross section connecting wells: W29, W22, W11.....	150
Figure 9.20. Distribution of brine saturation at the structure top.....	150
Figure 9.21. Distribution of brine saturation at the structure mid depth.....	150
Figure 9.22. Distribution of CO ₂ solution in brine along the vertical cross section connecting wells: W29, W22, W11.....	151
Figure 9.23. Distribution of CO ₂ solution in brine at the structure top.....	151
Figure 9.24. Distribution of CO ₂ solution in brine at the structure mid depth.....	151

TABLES

Table 3.1 Bottomhole sampling summary.....	34
Table 3.2. The isotope composition of analysed samples.....	45
Table 3.3. Average ionic composition of the Borzęcin reservoir brine.....	51
Table 3.4. Hydrogeochemical indicators for the analysed samples.....	54
Table 3.5. Main PVT Results.....	55
Table 3.6. Results of Constant Mass Expansion test (CME) of produced gas (B-22) at 20°C.....	56
Table 3.7. Results of Constant Mass Expansion test (CME) of produced gas (B-22) at 46.8°C.....	57
Table 3.8. Results of flash separation to the ambient conditions.....	59
Table 3.9. Results of gas solubility tests in the reservoir water.....	60
Table 3.10. Composition of soil gas samples drawn at the B-6 well.....	64
Table 3.11. Composition of soil gas in samples drawn at the B-28 well.....	65
Table 3.12. Composition of soil gas in samples drawn at the B-22 well.....	66
Table 3.13. Composition of soil air around the B-23 well.....	69
Table 3.14. Composition of soil air around the B-24 well.....	70
Table 3.15. Slurry composition [12].....	75
Table 3.16. Slurry properties [12].....	75
Table 3.17. Ionic water composition [12].....	75
Table 3.18. Test results [12].....	75
Table 4.1. Litho-stratigraphy of Borzęcin Structure – well W22.....	81
Table 4.2. Coefficients of geometric anisotropic semi-variogram.....	82
Table 5.1. Component parameters of Peng-Robinson equation of state for varying composition fluid in the Borzęcin structure model.....	91
Table 5.2. Component parameters of Peng-Robinson equation of state for varying composition fluid in the Borzęcin structure model, cont'd. Binary coefficients.....	91
Table 5.3. Lorentz-Bray-Clark viscosity modelling coefficients.....	91
Table 5.4. Composition of original fluid (gas) in the Borzęcin reservoir.....	92
Table 5.5. Analysis of gas-in-brine solution measurements.....	94
Table 5.6. Coefficients of RS models.....	94



1 Introduction

This report describes in detail the past, present and future status of the long-term acid gas sequestration process carried out in the Borzęcin structure in western Poland. It should be emphasized that the Borzęcin injection project was the first full scale, acid gas reinjection process of practical value into the original gas reservoir, put into operation in 1996 [1,2]. In 2004, a similar process at a larger scale has been realized in the Krechba field in Algeria by BP and Statoil [3] and the reinjection of produced CO₂ started at the K12-B in the Netherlands operated by GDF-SUEZ [4]. In the Borzęcin project, acid gas has been reinjected into the water-bearing zone underlying the gas cap, from which natural gas has been constantly produced.

Slightly different projects were then implemented in Sleipner gas field and Weyburn oil field. In the case of gas extracted from Sleipner, the recovered CO₂ is reinjected into the separate Utsira aquifer, Weyburn is a typical EOR-CO₂ project.

At that time, the sequestration of acid gases into the same reservoir was in the early stages of development. Together with K12-B, the Borzęcin project was then innovative on a global scale, also in the domain of reservoir engineering. It required the performance of detailed simulations with the assumption that it was possible to rationally reconcile the simultaneous recovery of gas and back injection of acid gases into the water-bearing zone, and that it would be in accordance with applicable laws and the principles of rational exploitation. The challenge was also to inject not sour natural gas, which was already done in Canada and the Netherlands, but an reactive mixture of H₂S and CO₂. It is necessary to emphasize the positive contributions of the District Mining Office that approved the implementation of such an innovative solution.

Borzęcin is considered to be a unique experimental plant which allows us to investigate the acid gas sequestration process for 24 years of its operation and possibly for a few more years to come. Contrarily to other large reservoirs, the small capacity of the onshore Borzęcin structure enables us to effectively control and analyse the detailed mechanisms taking part in the sequestration process at a relatively short term scale.



2 History of operation

The history of the Borzęcin project operation [5] includes two phases:

1. Production phase: production of the original natural gas,
2. Injection phase: continuation of the gas production concomitant with acid gas reinjection.

2.1 PRODUCTION PHASE

This phase started in 1972 and lasted until May 1996. In the time interval of: 1972 – 1976 only one well (W31) was operating. As the produced gas contained relatively high amounts of acid gas components (0.1% of H_2S , 0.3% of CO_2) a gas sweetening installation was constructed and put into operation in 1977. Then 6 more wells (W1, 4, 6, 7, 10, 11) started to produce gas. In 1982 – 1984, well W7 was flooded out and production was stopped. At that time a new well (W12) started to operate. In 1985 – 1987 10 new producers (W21- 30) were put in operation. Well W28 was found unsuccessful. Wells W10 and W1 were stopped in 1985 and 1987, respectively, both due to high water-gas ratio.

Increasing number of producers resulted in an approximately steady production rate in the years 1977 – 1987 (Figure 2.1). Later on, underlying and/or surrounding aquifers caused relatively fast watering out of the producing wells (Figure 2.5) and, consequently, more than 3-fold reduction of the gas production in the years 1988 - 1996.

Although waterflooding occurred in many producing wells, the aquifers were not effective enough to maintain the average reservoir pressure in the dominant south-eastern part of the reservoir (Figure 2.9). This pressure declined by more than 60% of its initial value by the end of 1995 when the recovery coefficient of the original-gas-in-place (OGIP) exceeded 70% (Figure 2.10).

Detailed data on the reservoir operation during this phase are shown in the figures on the following pages:

- Figure 2.1 – reservoir monthly gas production,
- Figure 2.2, Figure 2.3, Figure 2.4 – monthly gas production of individual wells: W1, W10, W11, W12, W21, W22, W23, W24, W25, W26, W27, W4, W6, W7, W29, W30, W31.
- Figure 2.5. Reservoir monthly water production,
- Figure 2.6, Figure 2.7, Figure 2.8 – monthly water production of individual wells: W1, W10, W11, W12, W21, W22, W23, W24, W25, W26, W27, W4, W6, W7, W29, W30.
- Figure 2.9 – bottom hole pressure of individual wells: W1, W4, W6, W7, W10, W11, W12, W21, W22, W23, W24, W25, W26, W27, W29, W30, W31.
- Figure 2.10 – total gas and water production as a percentage of original gas and water in place, respectively.

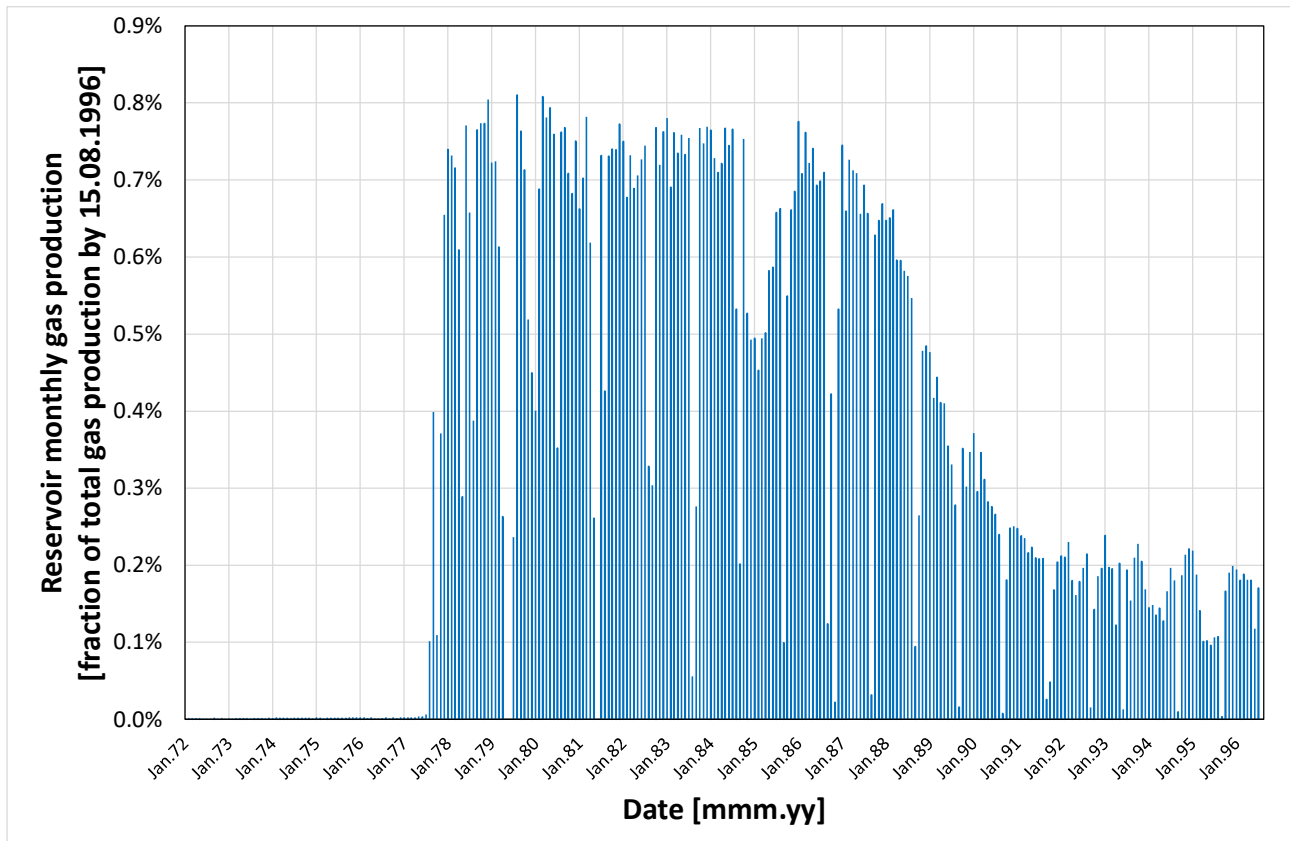


Figure 2.1. Reservoir monthly gas production.

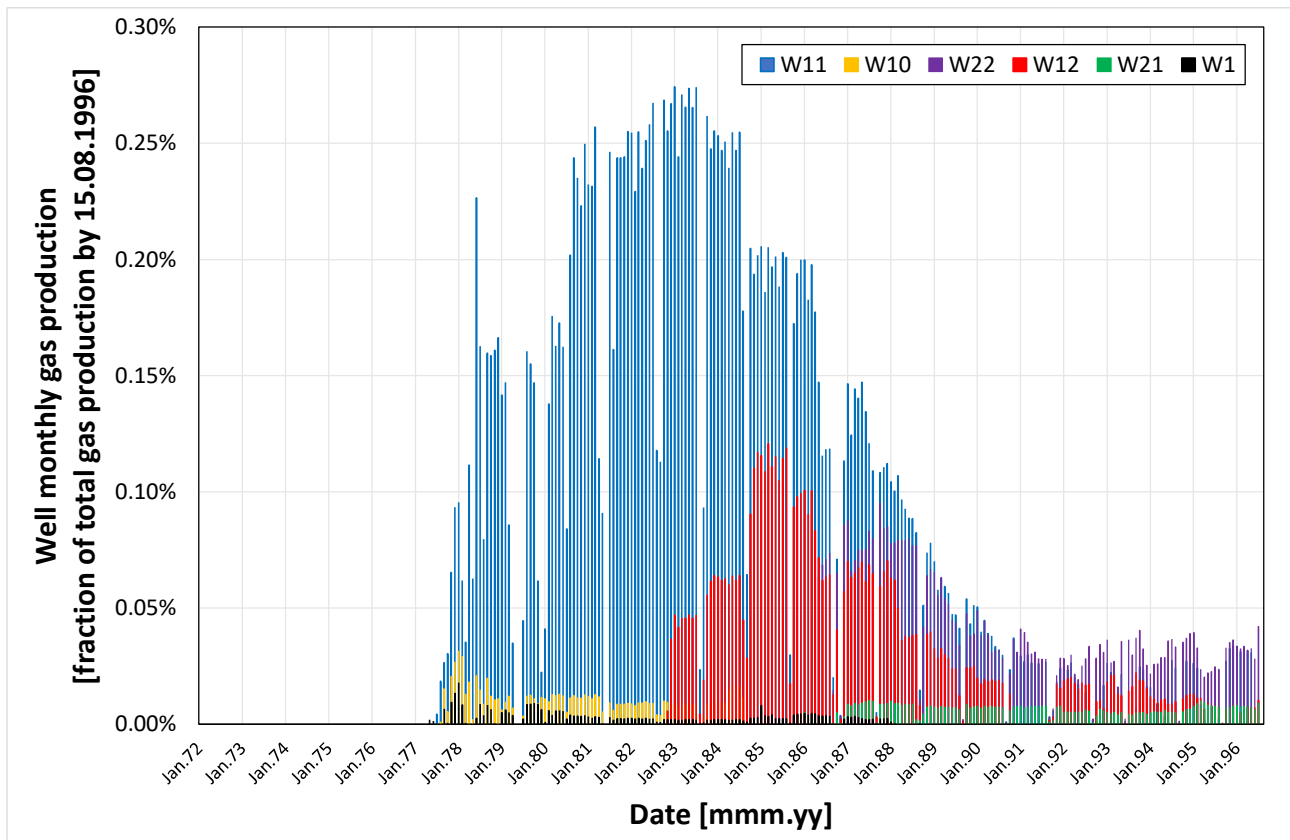


Figure 2.2. Well monthly gas production. Wells: W1, W10, W11, W12, W21, W22.

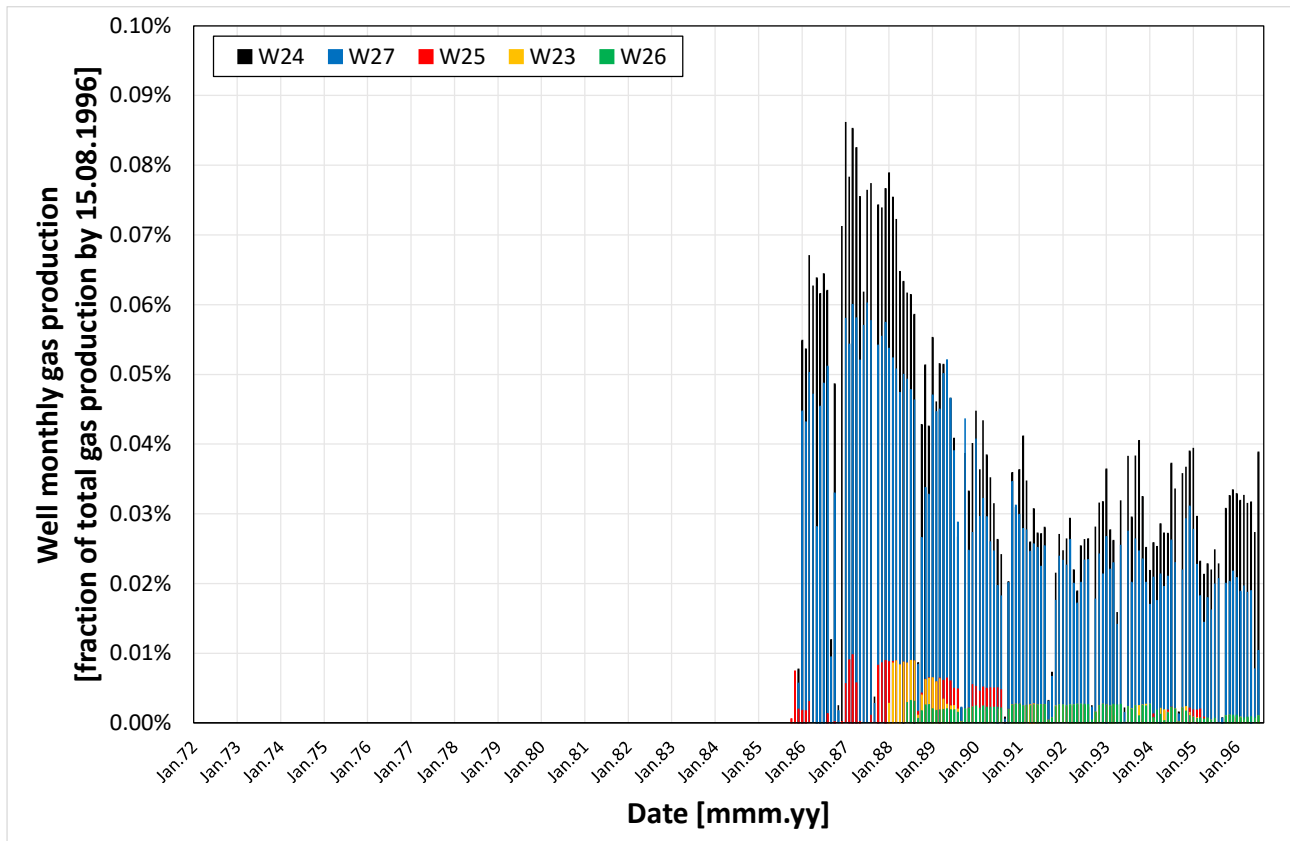


Figure 2.3. Well monthly gas production. Wells: W23, W24, W25, W26, W27.

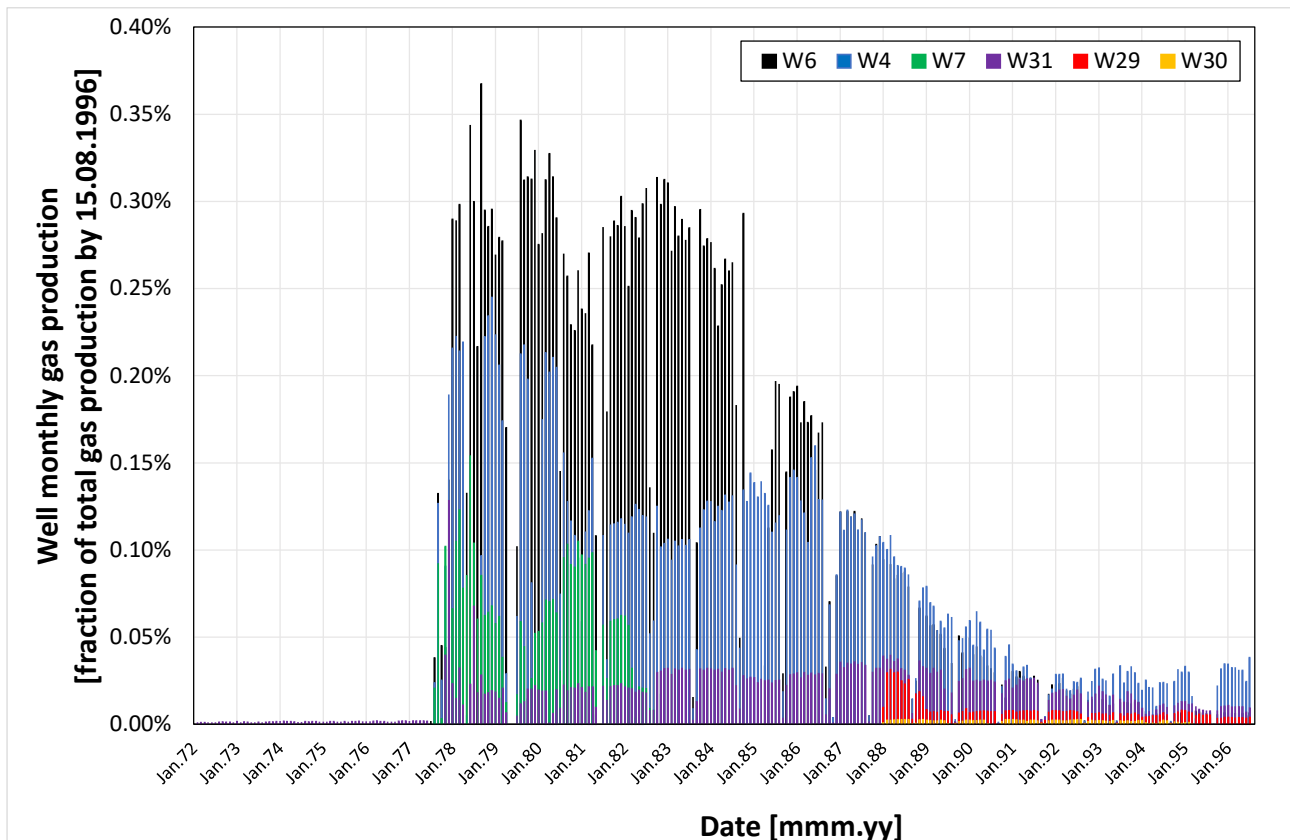


Figure 2.4. Well monthly gas production. Wells: W4, W6, W7, W29, W30, W31.

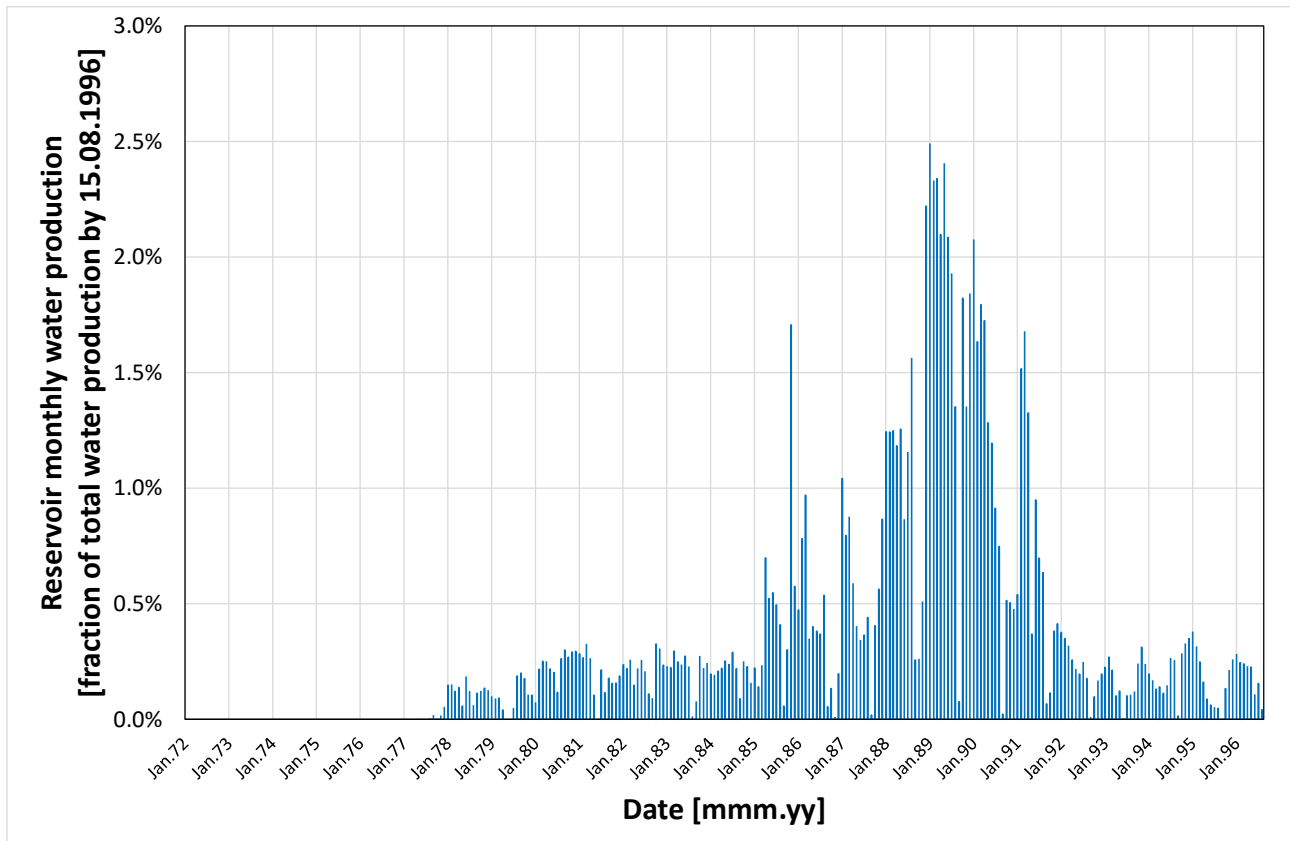


Figure 2.5. Reservoir monthly water production.

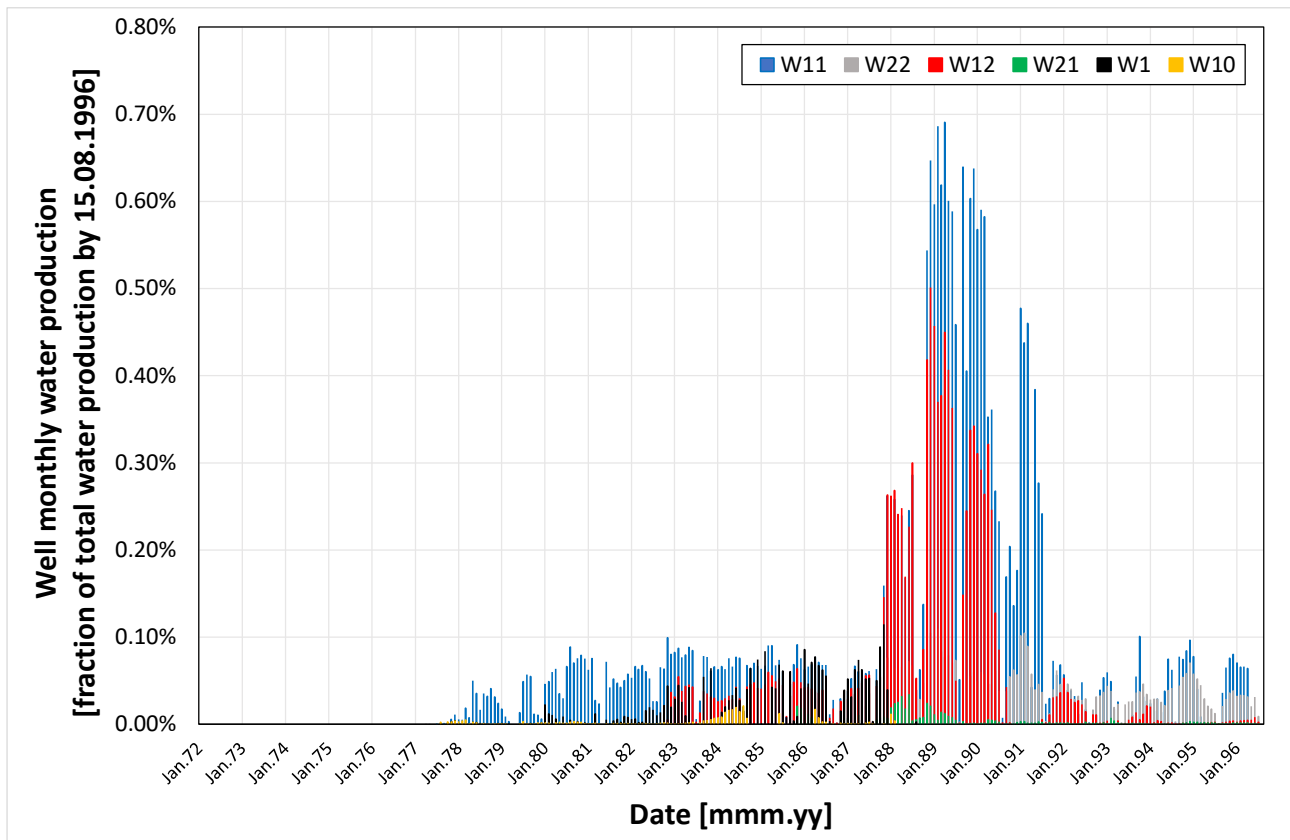


Figure 2.6. Well monthly water production. Wells: W1, W10, W11, W12, W21, W22.

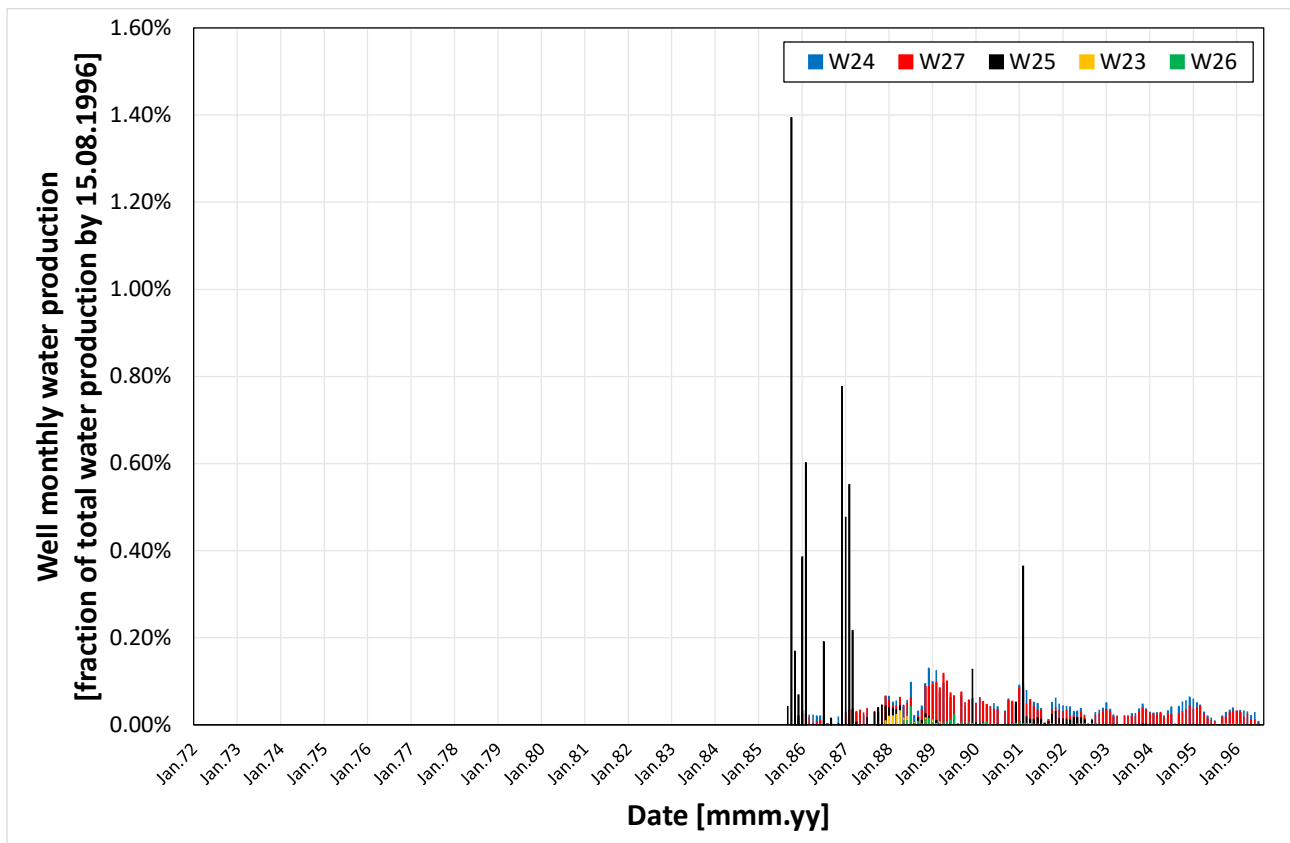


Figure 2.7. Well monthly water production. Wells: W23, W24, W25, W26, W27.

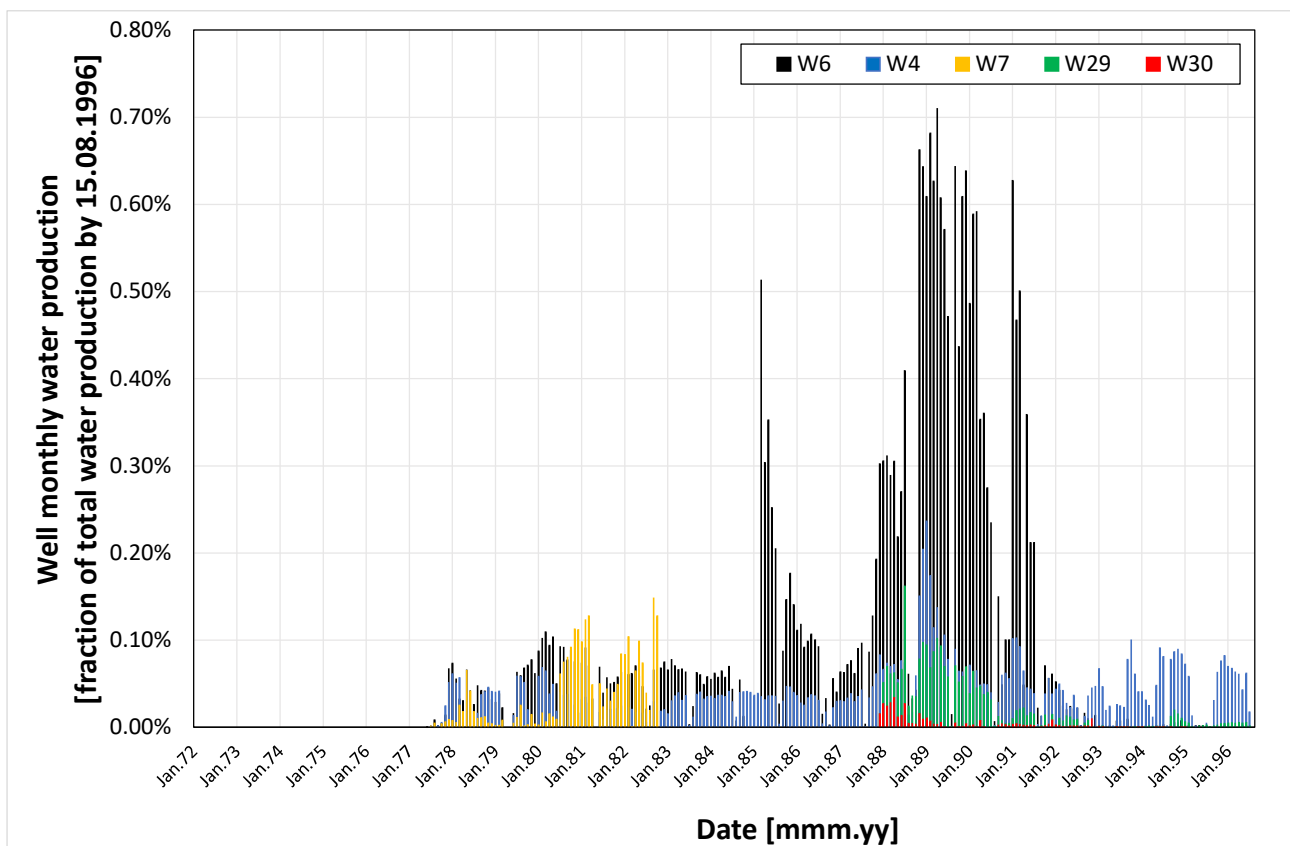


Figure 2.8. Well monthly water production. Wells: W4, W6, W7, W29, W30.

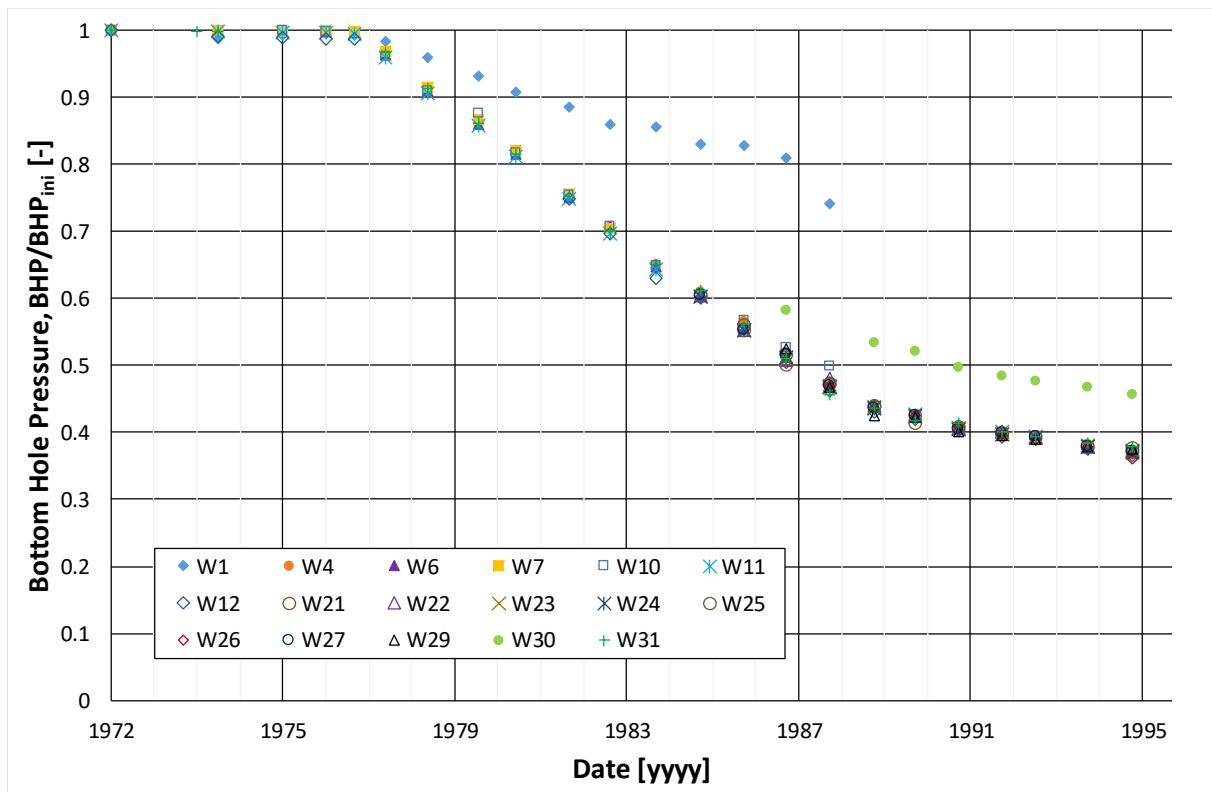


Figure 2.9. Bottom hole pressure. Wells: W1, W4, W6, W7, W10, W11, W12, W21, W22, W23, W24, W25, W26, W27, W29, W30, W31.

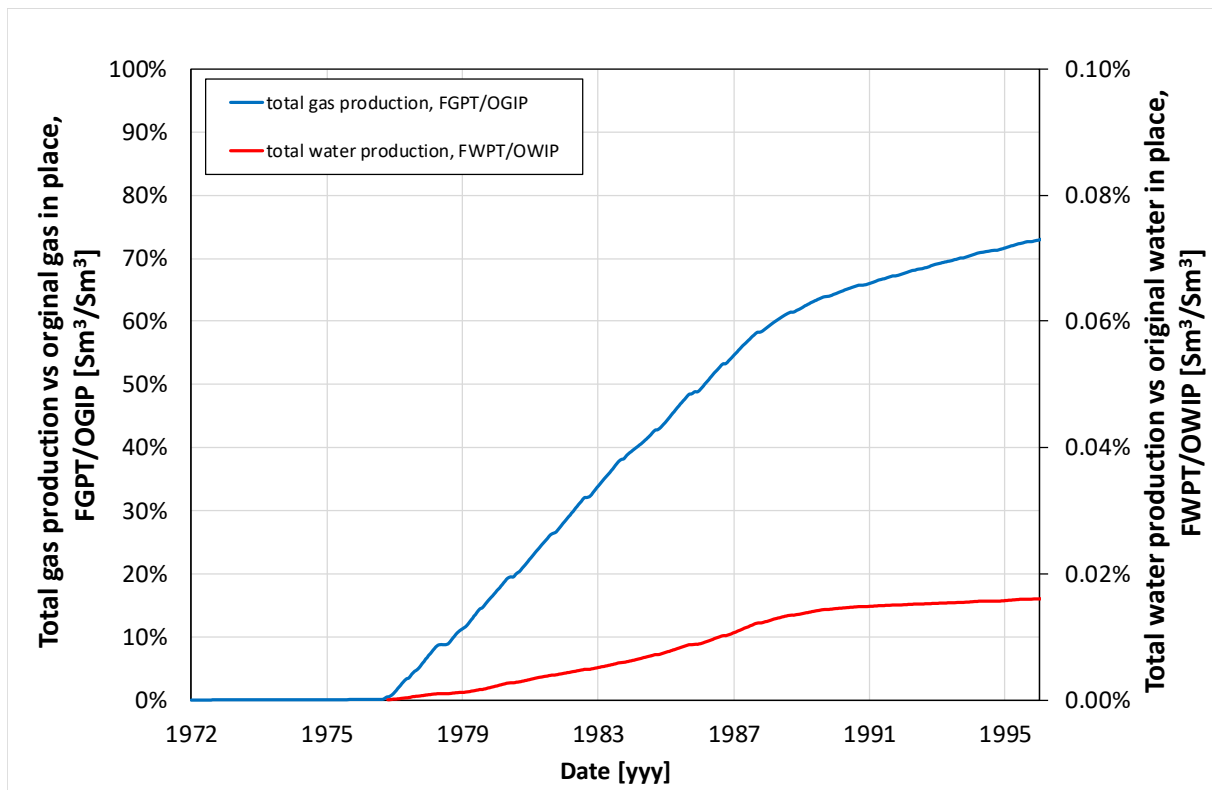


Figure 2.10. Total gas production vs original gas in place. Total water production vs original water in place.



2.2 INJECTION PHASE

In 1976, the MEA (monoethanolamine) gas sweetening installation was launched in order to remove the acid gas components from the produced gas stream. Until 1995, the acid gas components that constitute the waste product from the sweetening installation were burned in special furnaces in a stream of natural gas and emitted through a forty-meter long chimney into the atmosphere. The operation of the hydrogen sulphide afterburning installation existing at Borzęcin at that time caused air pollution and became troublesome due to the need to periodically replace the corroded fragments. It also posed a real threat because the corrosion of the chimney almost lead to a collapse several times as a result of heavy storms.

The produced gas sweetening installation generated large amounts of acid gases. In order to cope with this problem, the injection process was devised and implemented on the Borzęcin structure. The development and implementation of reinjection technology encountered many difficult obstacles and took many years. As a part of the resulting targeted project co-financed by the Scientific Research Committee and the Polish Oil and Gas Company (POGC), the "Technical Design Project for the Acid Gas Injection Installation to the Borzęcin Reservoir Zone" was submitted by INiG in 1995 to the Operator, which put into operation the installation in January 1996. The necessary installations were prepared by POGC and significant parts of the apparatus (acid gas compressor and separators) were provided by INiG.

The reinjection technology consisted in the injection of the gas sweetening products back to the underlying, water-bearing zone of the structure, beneath the original gas reservoir cap. This reinjection has become the key element of the Borzęcin project.

This phase started in the beginning of 1996, when 67% of the original gas in place (OGIP) had already been recovered, and has been continued until the present date. In 1996, well W28 was converted from the producing type into an injector and completed within the water-bearing zone underlying the gas reservoir. This well has been continuously injecting an acid gas mixture as obtained from the gas sweetening process. The amount and composition of the injected gas are directly dependent upon the amount and composition of the gas produced by all the other wells. It should be noted that the composition of the injected gas significantly changed in 2012 (Figure 2.12) due to the modernization of the sweetening installation by creating a compact DGA (diglycolamine) assembly with the injection unit. This composition remained roughly constant afterwards.

The producing wells were gradually watered out and removed from the list of gas producers. They include the following wells and their final years of their operation: W23 – 1997, W26 – 1999, W25 – 2000, W31 – 2001, W12 – 2003, W29 – 2003, W6 – 2007, W24 – 2013. At that time wells W10, 11, 23, 29 were converted from gas production to water injection.

This phase was characterized by the further reduction of gas production (Figure 2.13). At the end of the analysed interval of operation (August 2019), the gas production rate amounts to $\frac{1}{3}$ of its initial value (1996 – 1997). In the analysed phase, the recovery factor of OGIP increased only by 10% (Figure 2.29). This fact together with the reinjection of acid gases, water injection, and aquifer activities resulted in a much slower decrease of the reservoir pressure (Figure 2.30) during this phase.

Detailed data on the reservoir operation during this phase are shown in the following figures:

- Figure 2.11 – monthly, acid gas injection by W28,
- Figure 2.12 – composition of the injected gas,
- Figure 2.13 – Reservoir monthly gas production,
- Figure 2.14, Figure 2.15, Figure 2.16 – monthly gas production of individual wells: W12, W21, W22, W23, W24, W25, W26, W27, W4, W6, W29, W31,
- Figure 2.17, Figure 2.18, Figure 2.19, Figure 2.20, Figure 2.21, Figure 2.22 – composition of gas produced by the following wells: W4, 21, 22, 24, 27, 31. The figures show varying composition of the produced gas that is a direct evidence of the injected gas migration. Note: composition of gas produced by the others wells were not included due to their constant composition of original reservoir gas,
- Figure 2.23 – detailed CO₂ concentrations applied to the model calibration procedure described below,
- Figure 2.24 – reservoir monthly water production,
- Figure 2.25, Figure 2.26, – monthly water production of individual wells: W4, W6, W12, W21, W22, W24, W25, W26, W27 W29,
- Figure 2.27 – reservoir monthly water injection,
- Figure 2.28 – monthly water injection by wells: W10, W11, W23, W29.



- Figure 2.29 – total gas production / injection vs original gas in place. Total water production / injection vs original water in place,
- Figure 2.30 – bottom hole pressure measured in individual wells: W1, W4, W6, W7, W10, W11, W12, W21, W22, W23, W24, W25, W26, W27, W29, W30, W31.

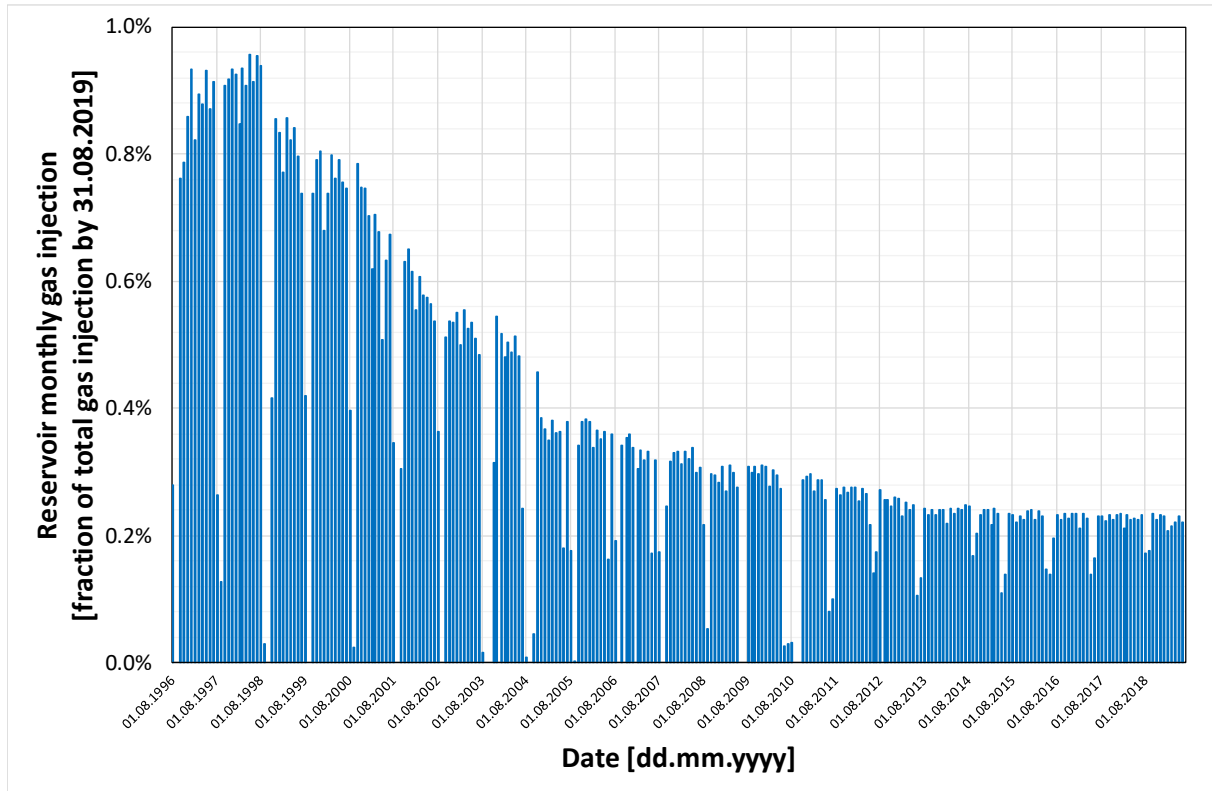


Figure 2.11. Reservoir monthly gas injection. Fraction of total gas injection by 31.08.2019.

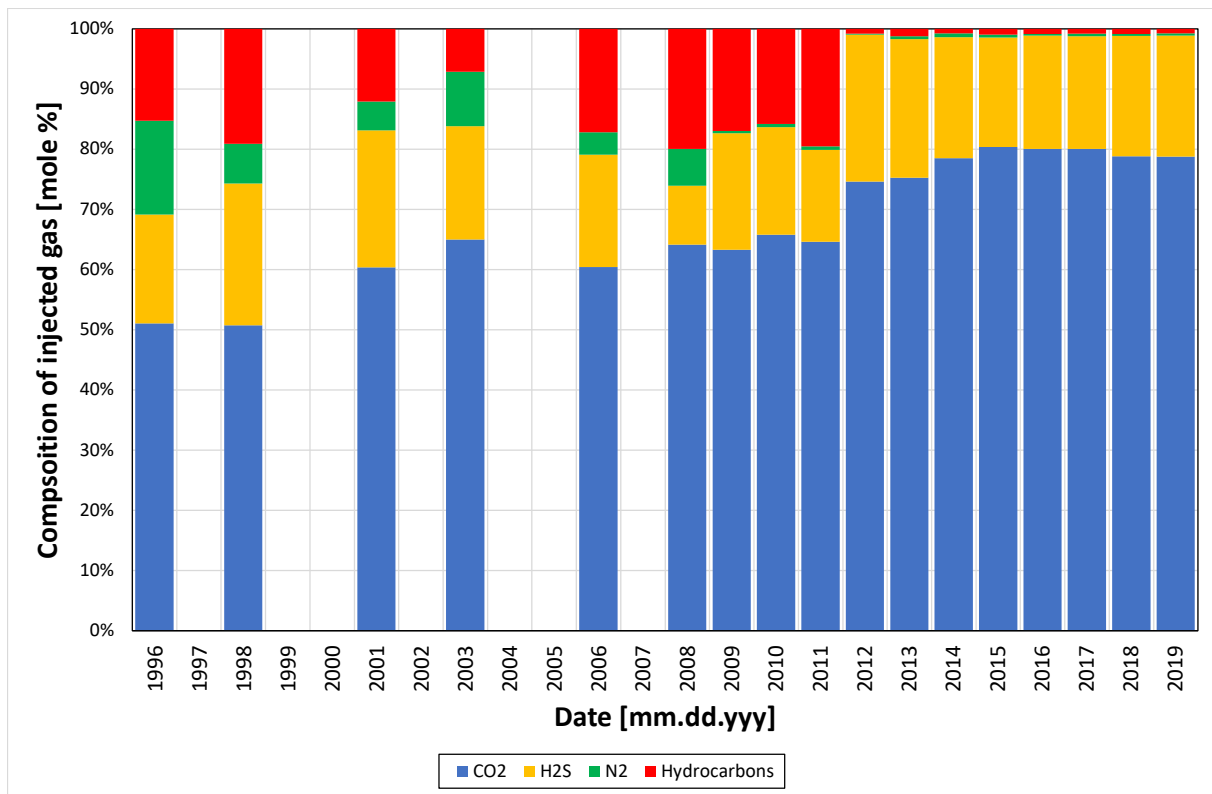


Figure 2.12. Composition of injected gas.

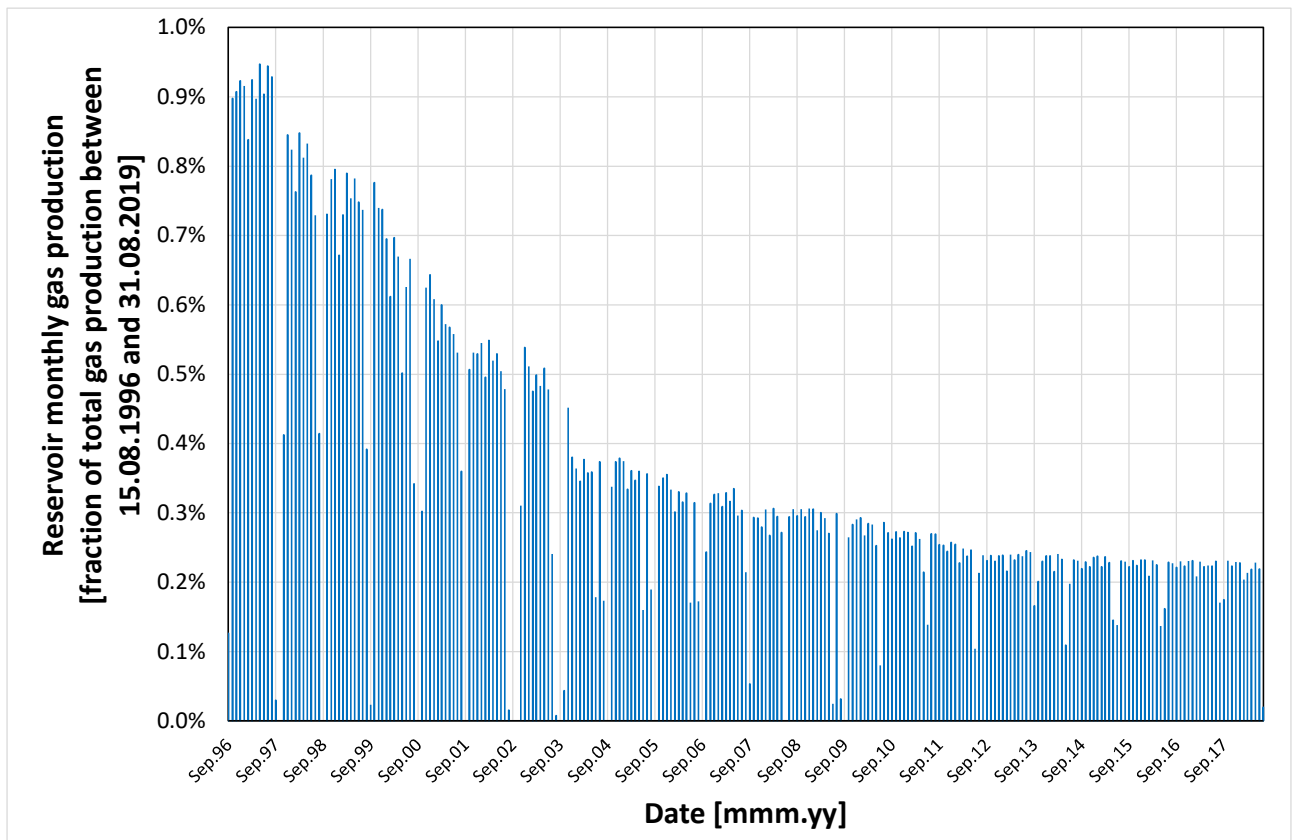


Figure 2.13. Reservoir monthly gas production.

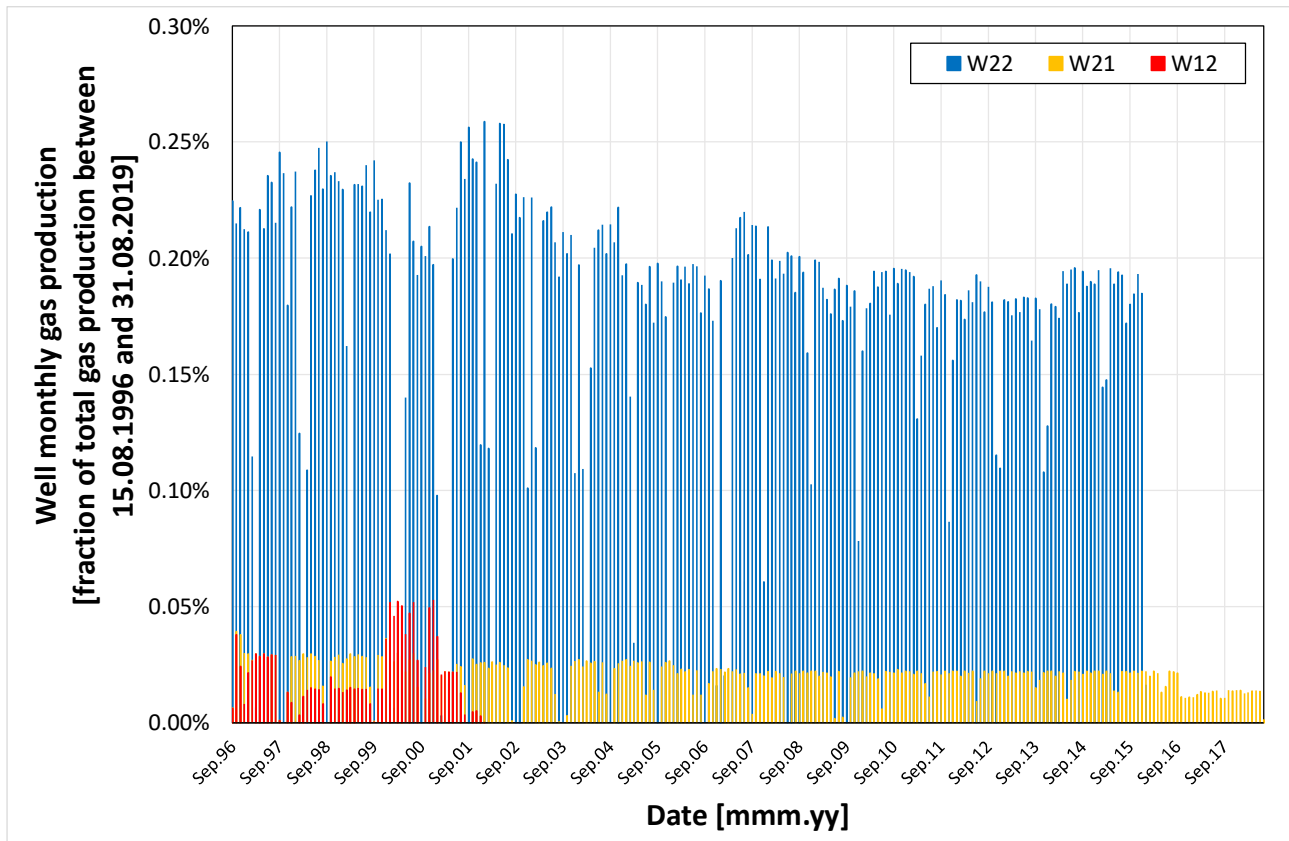


Figure 2.14. Well monthly gas production. Wells: W12, W21, W22.

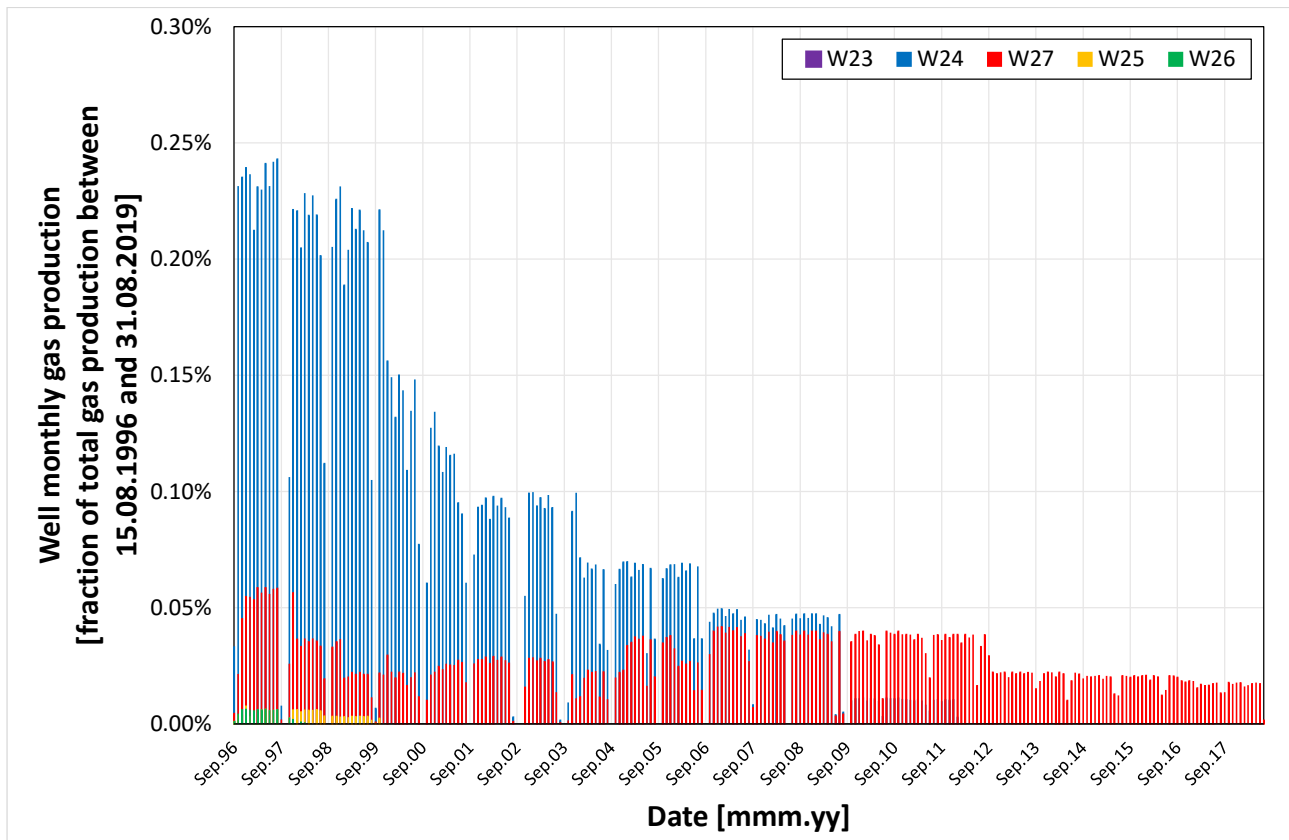


Figure 2.15. Well monthly gas production. Wells: W21, W24, W25, W26, W27.

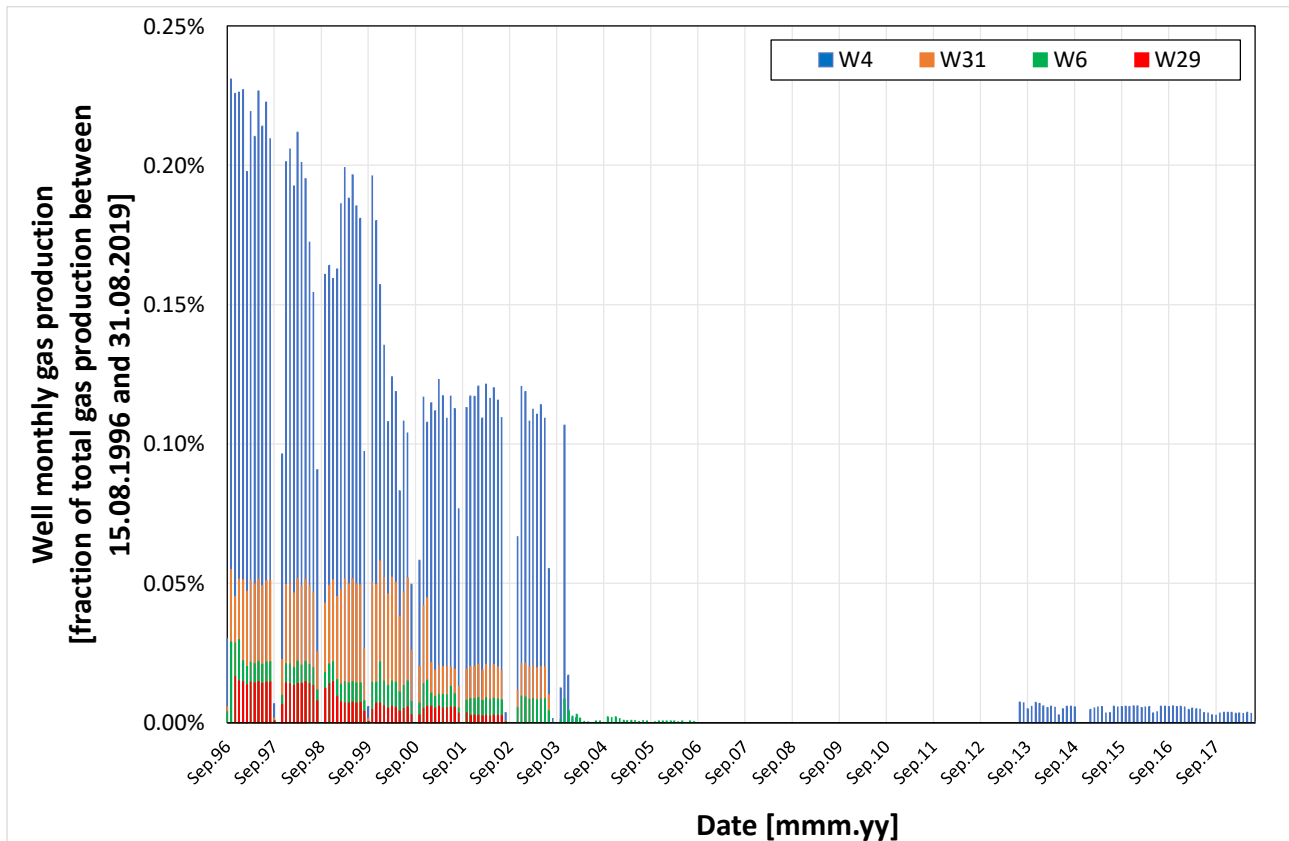


Figure 2.16. Well monthly gas production. Wells: W4, W6, W29, W31.

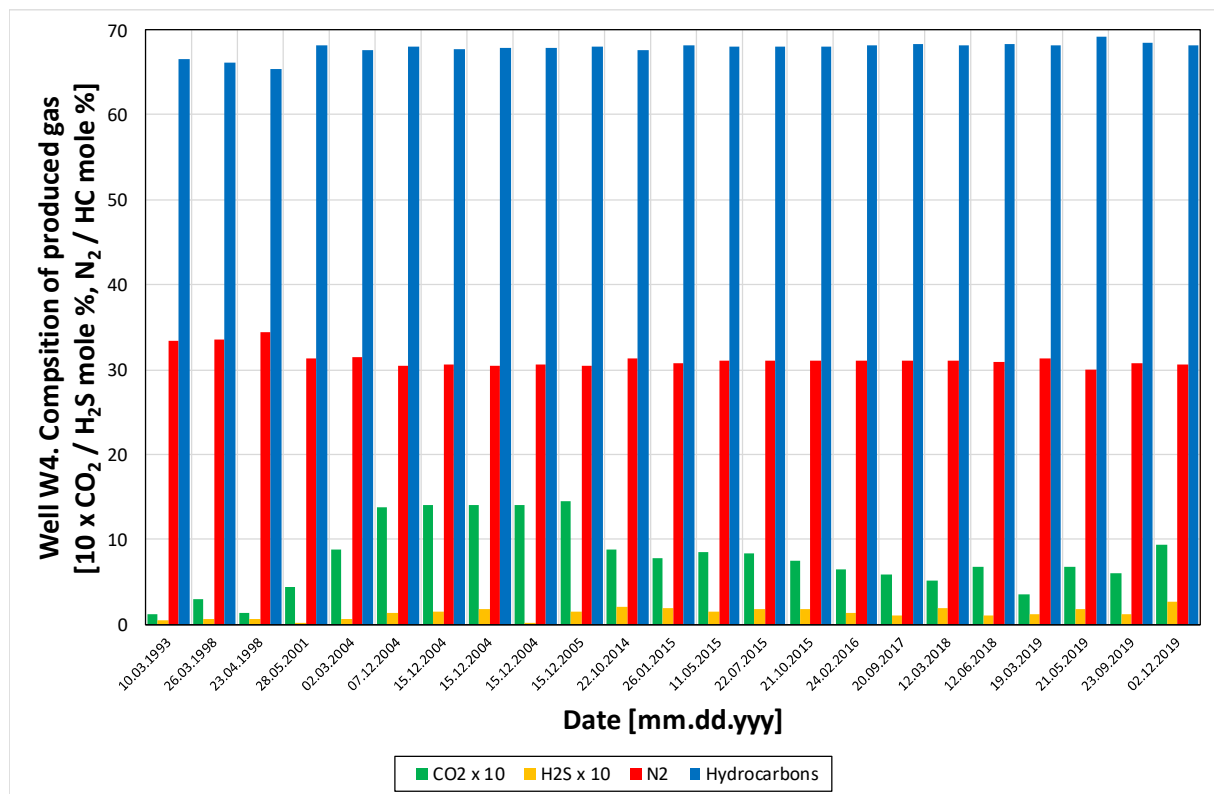


Figure 2.17. Composition of produced gas. Well W4.

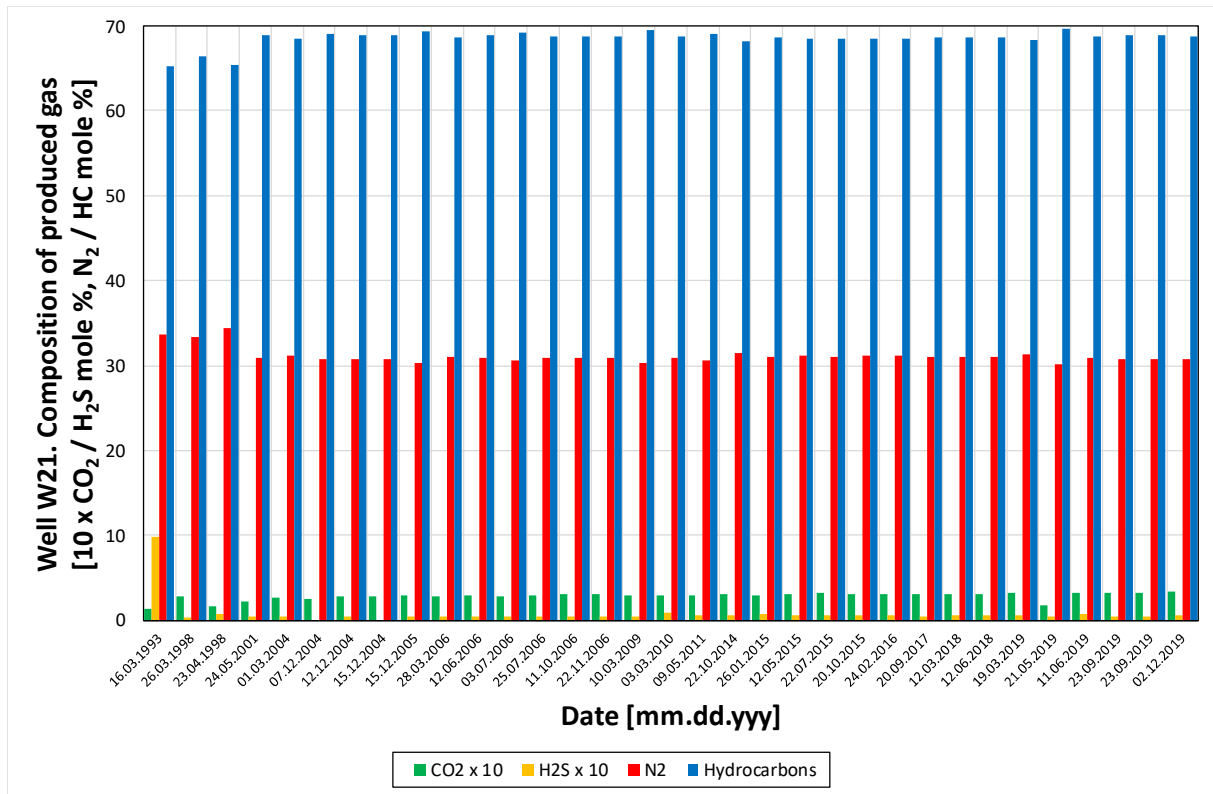


Figure 2.18. Composition of produced gas. Well W21.

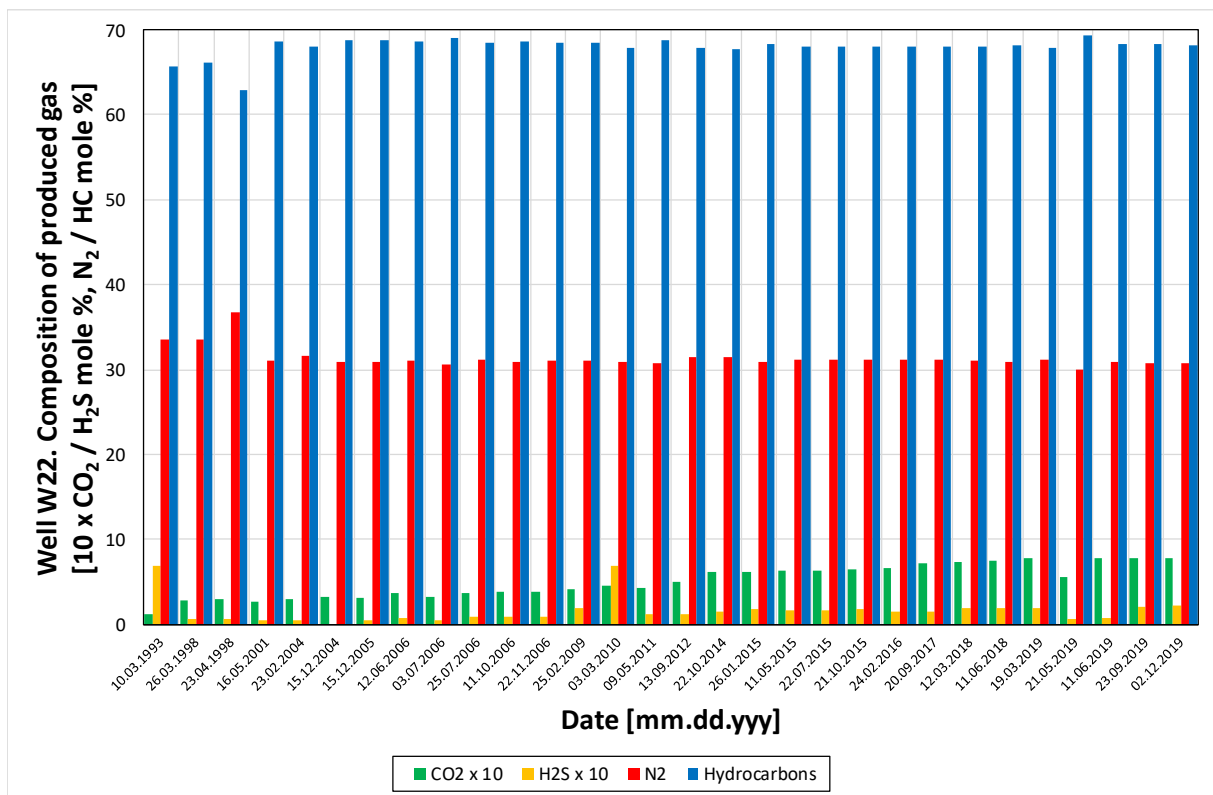


Figure 2.19. Composition of produced gas. Well W22.

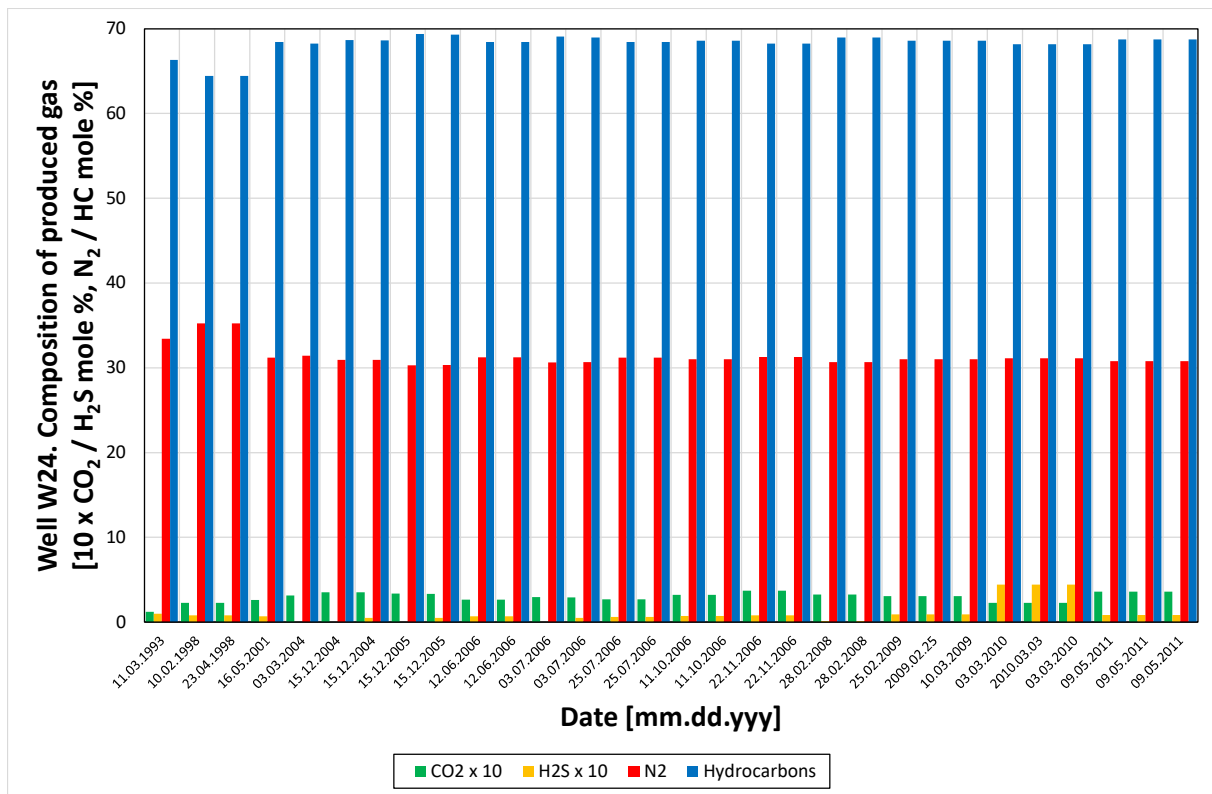


Figure 2.20. Composition of produced gas. Well W24.

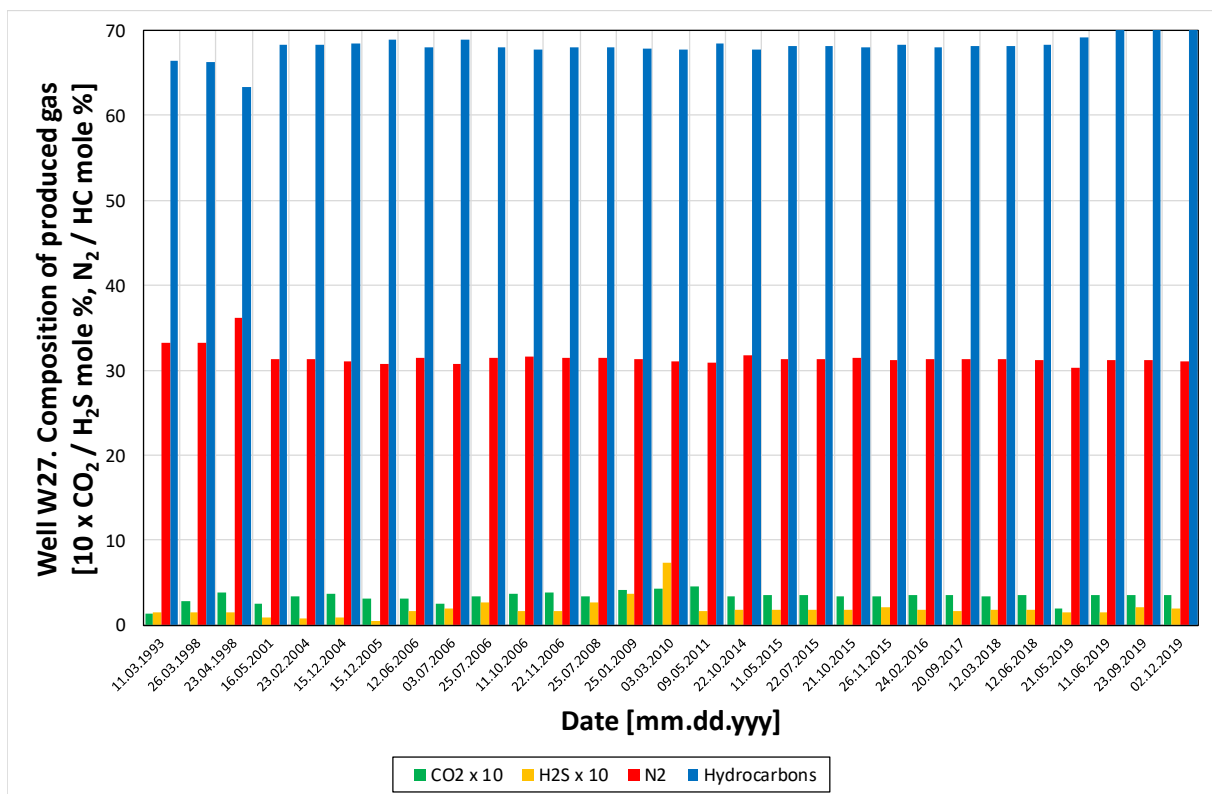


Figure 2.21. Composition of produced gas. Well W27.

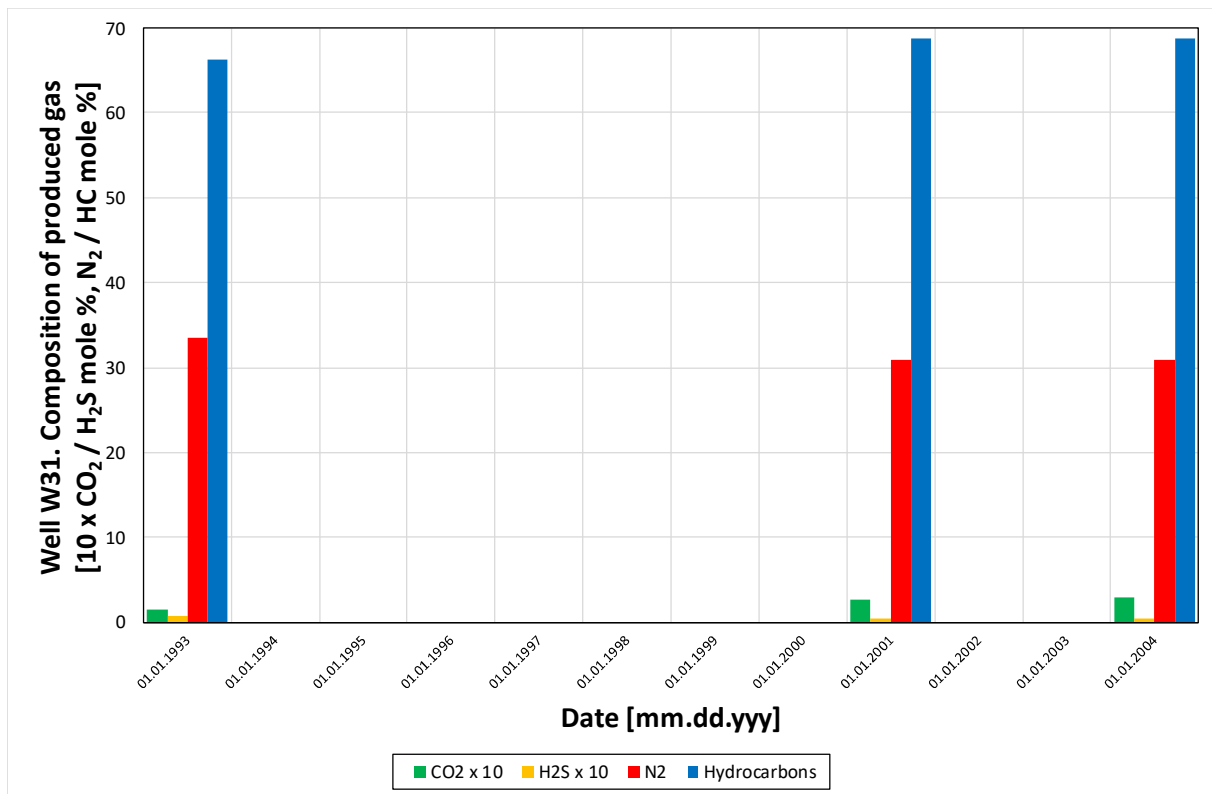


Figure 2.22. Composition of produced gas. Well W31.

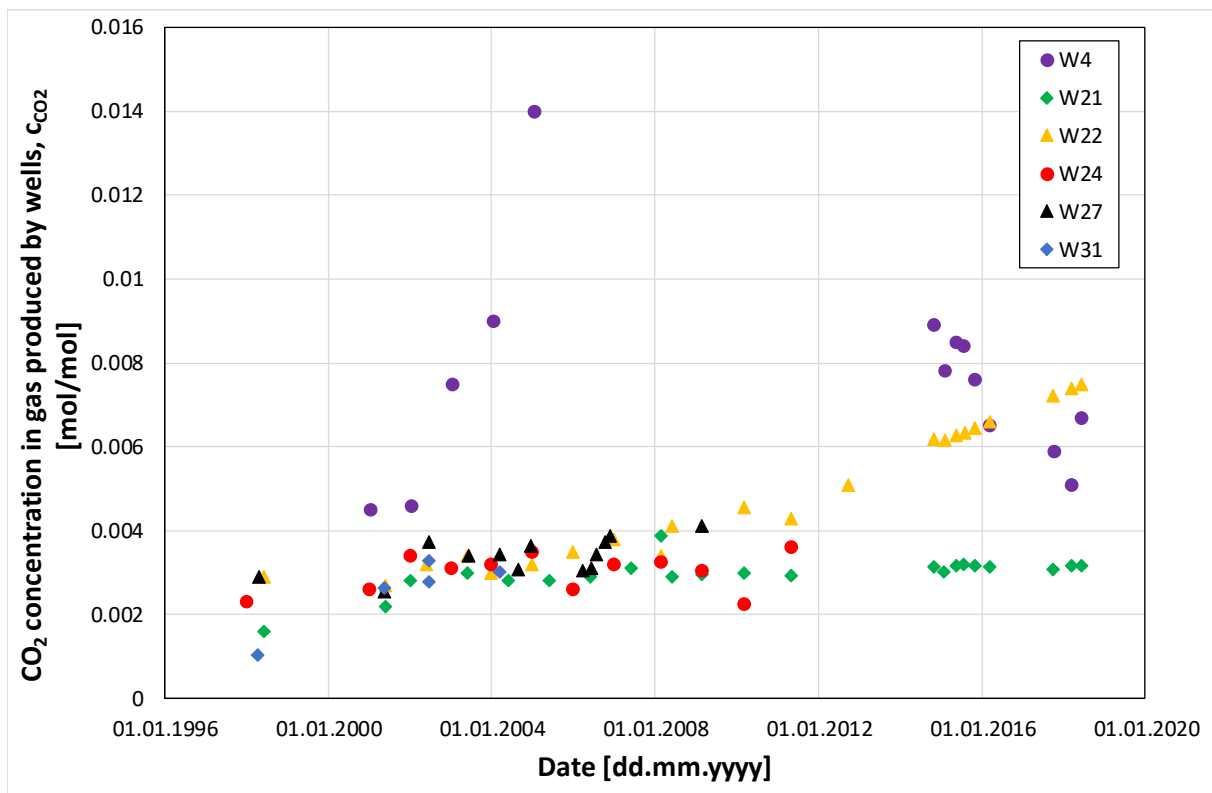


Figure 2.23. CO₂ concentration, c_{CO_2} , in gas produced by wells: W4, W21, W22, W24, W27, W31.

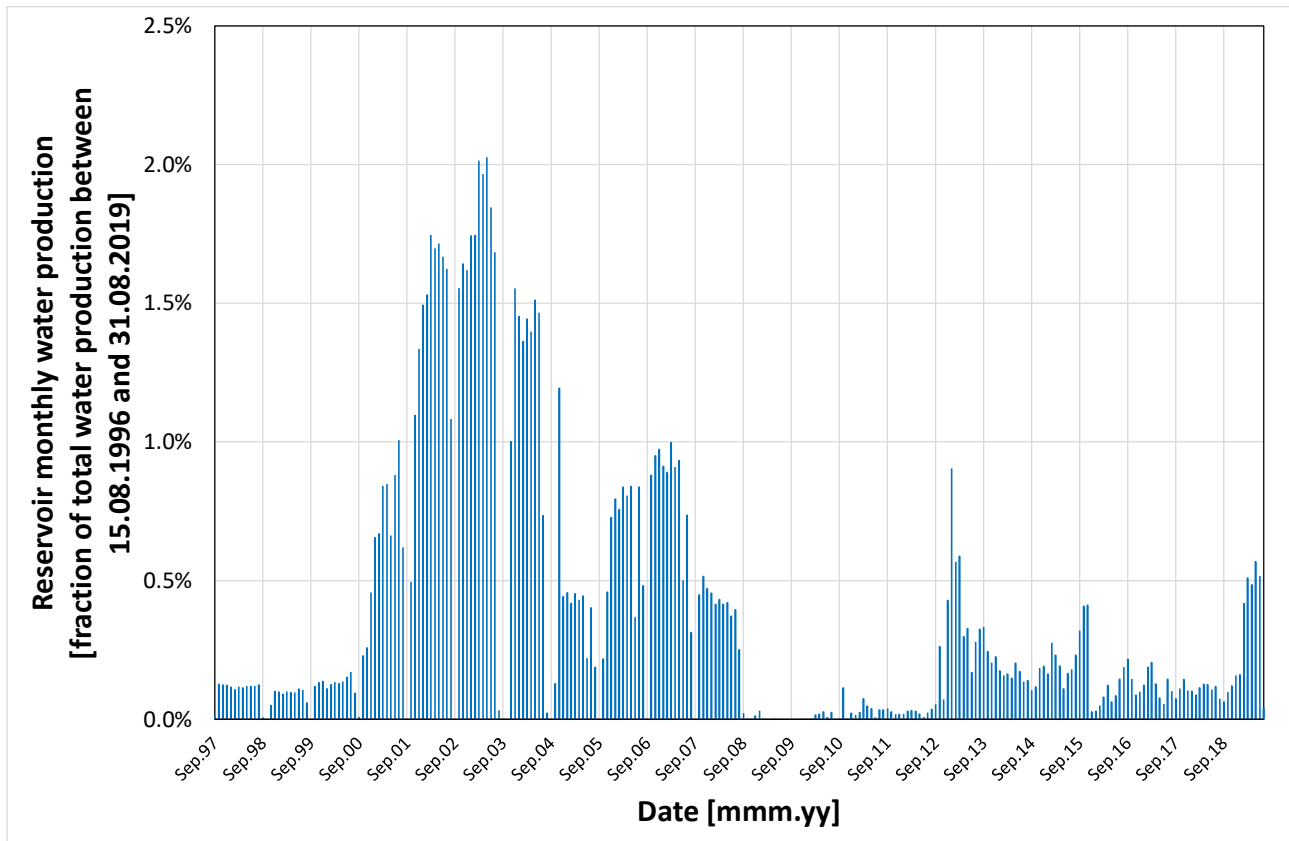


Figure 2.24. Reservoir monthly water production.

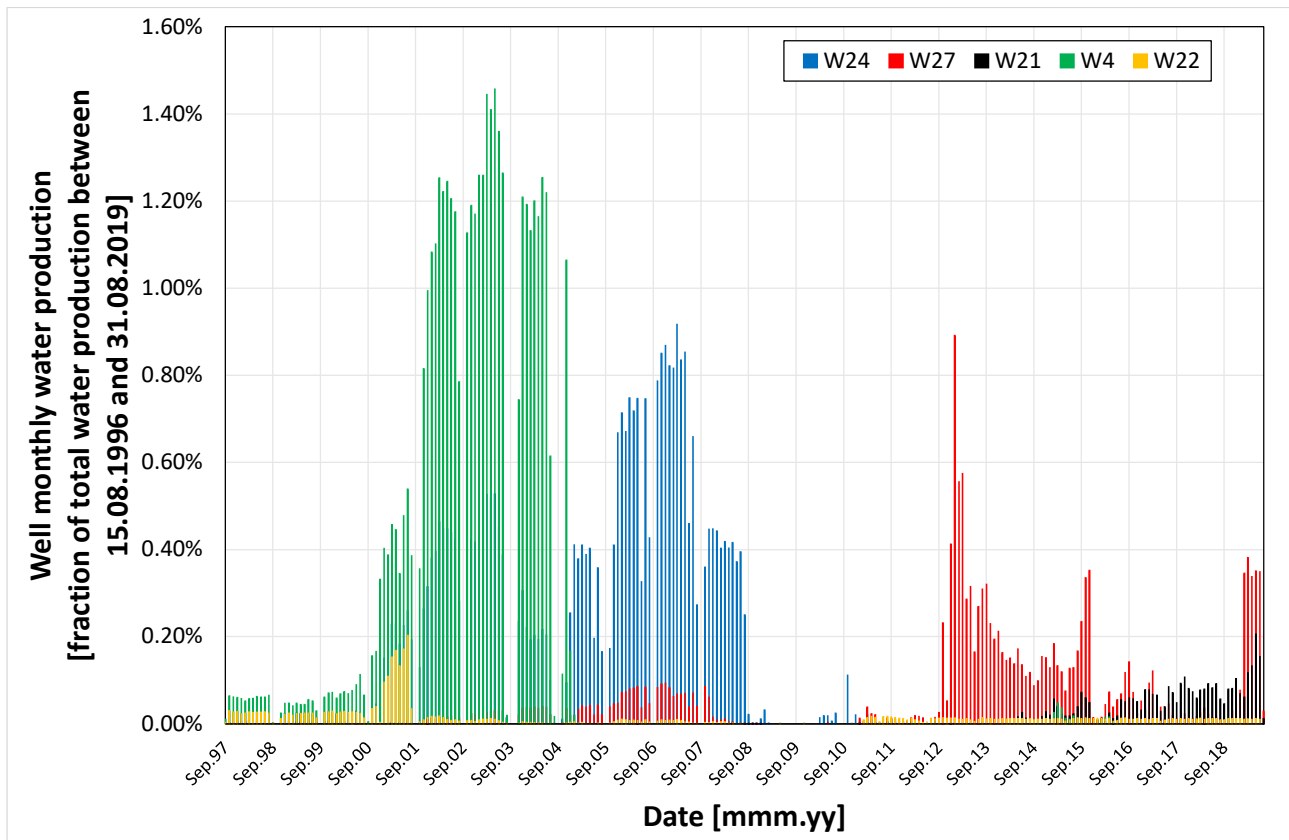


Figure 2.25. Well monthly water production. Wells: W24, W27 W21, W4 W22.

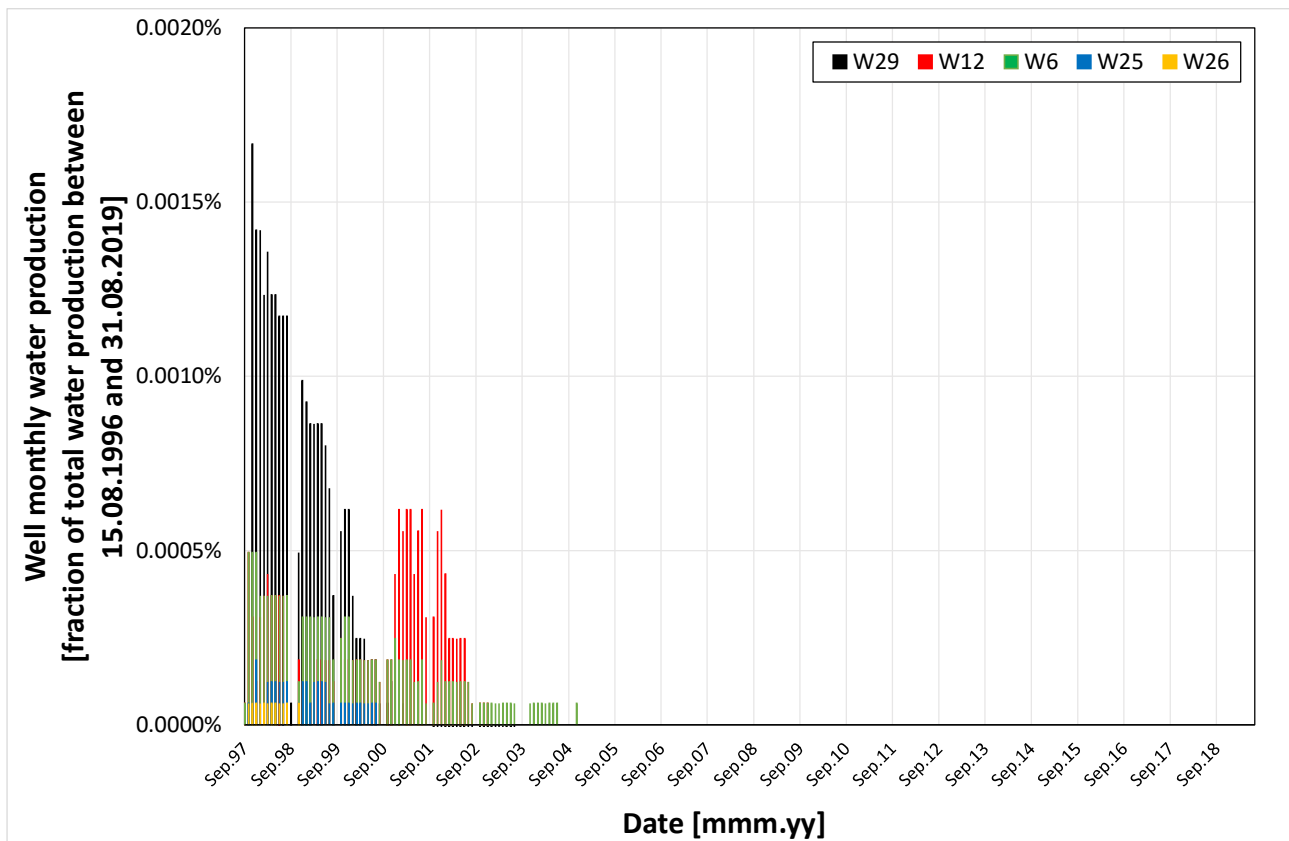


Figure 2.26. Well monthly water production. Wells: W29, W12, W6, W25, W26.

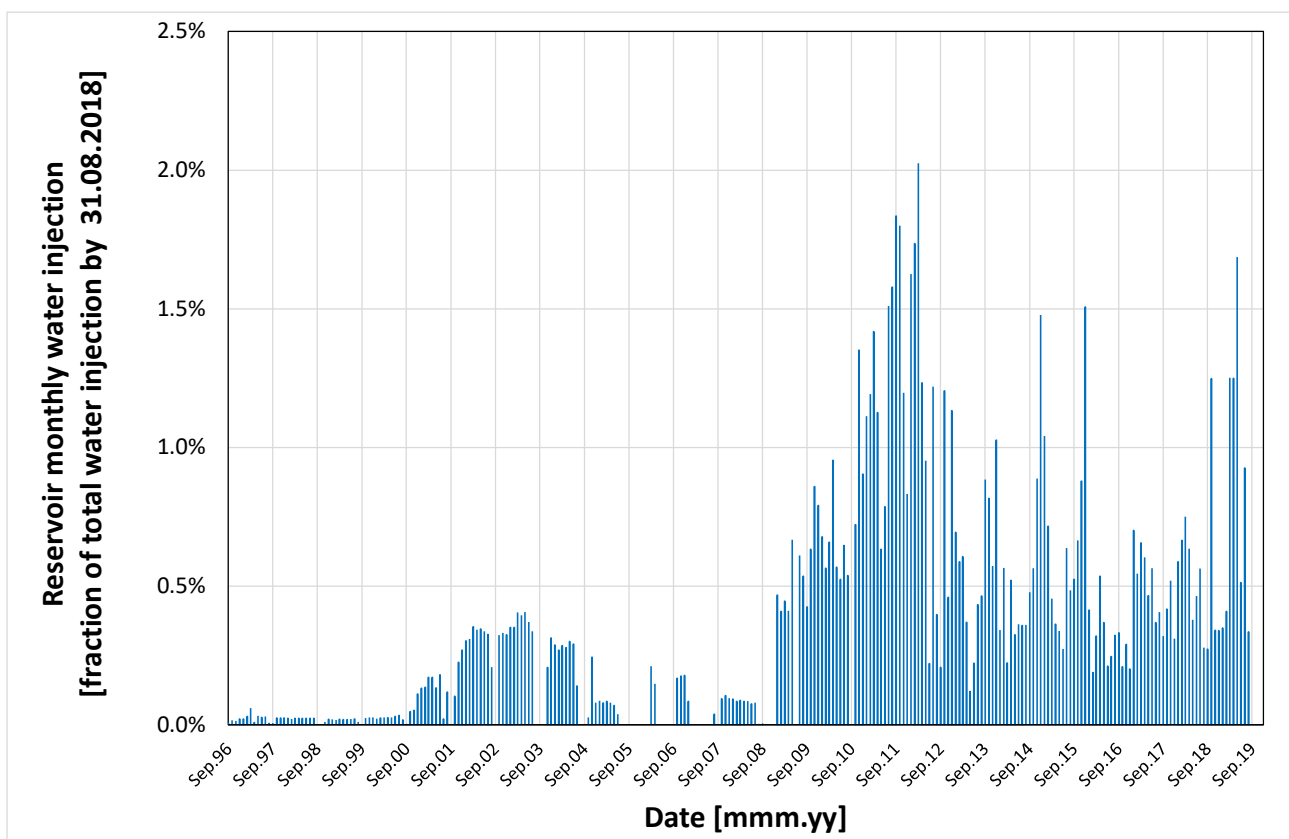


Figure 2.27. Reservoir monthly water injection.

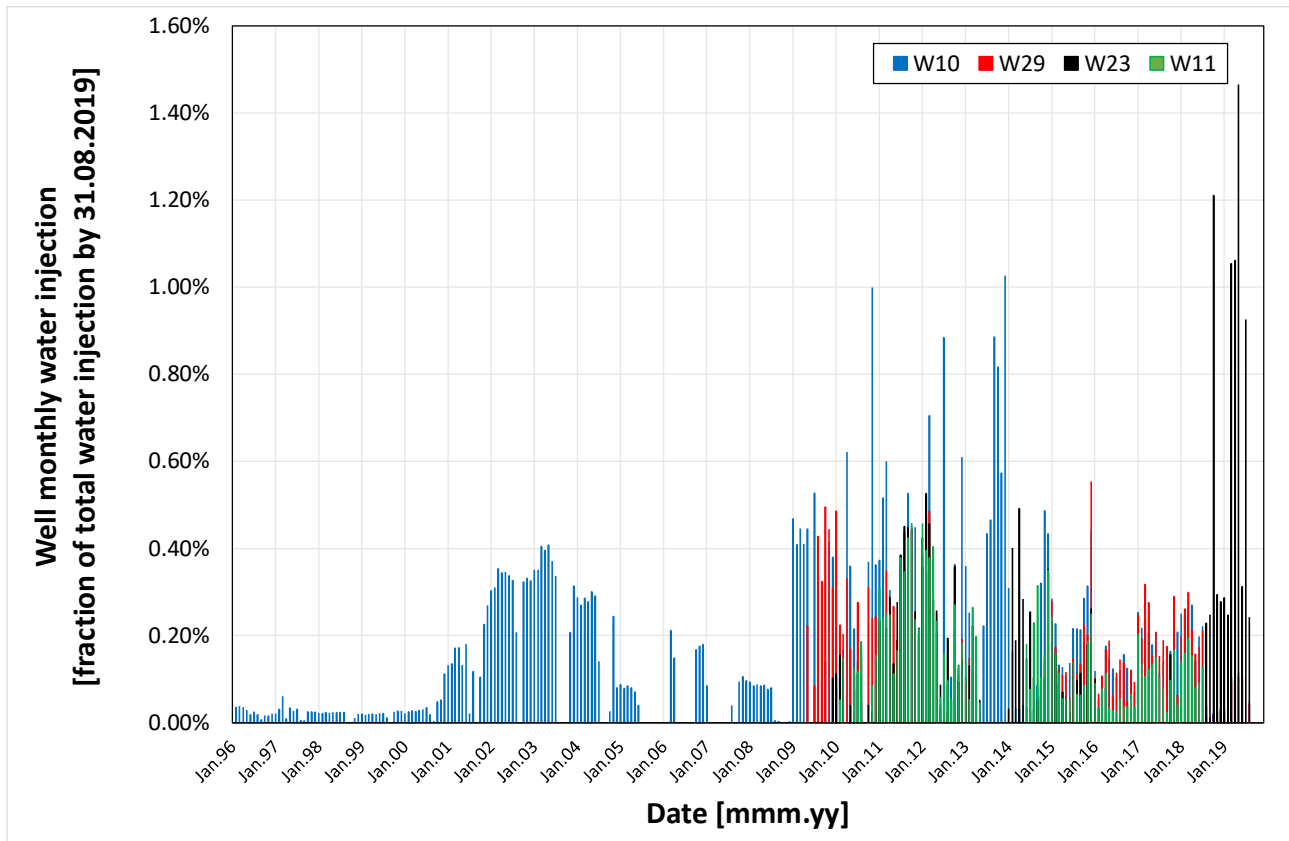


Figure 2.28. Well monthly water injection. Wells: W10, W11, W23, W29.

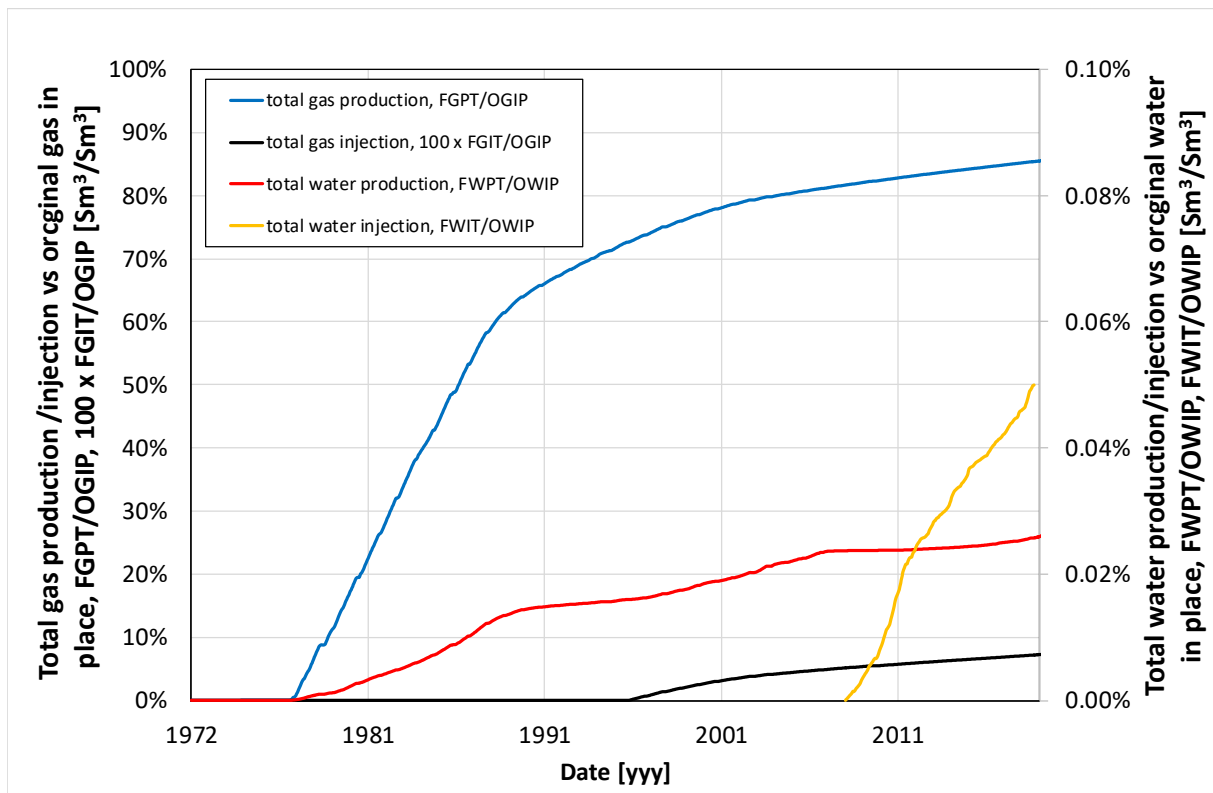


Figure 2.29. Total gas production / injection vs original gas in place. Total water production / injection vs original water in place.

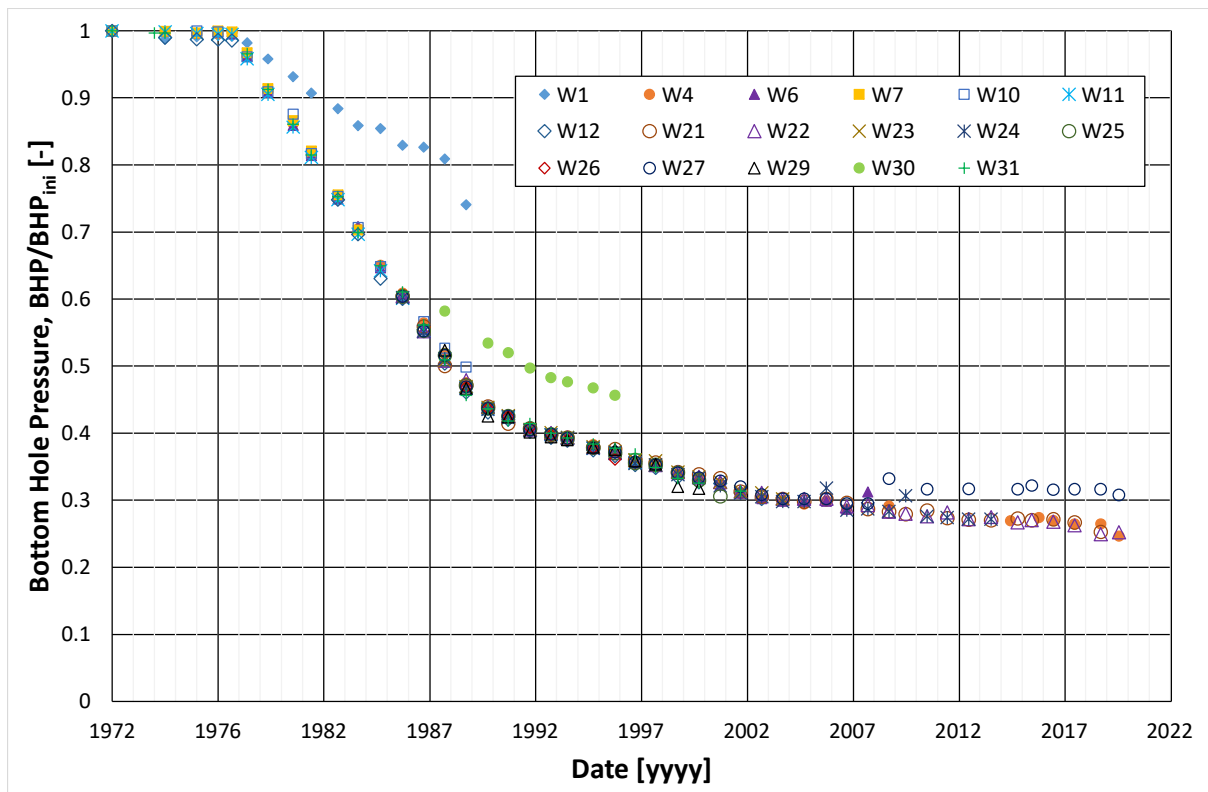


Figure 2.30. Bottom hole pressure. Wells: W1, W4, W6, W7, W10, W11, W12, W21, W22, W23, W24, W25, W26, W27, W29, W30, W31.

2.3 SUMMARY AND CONCLUSIONS

In this chapter, we describe the operational history of the Borzęcin Project. Its key elements consist of gas production data of the Borzęcin gas field (since 1972) and concomitant (since 1996) acid gas injection data of the injection activities targeted at the water-bearing zone underlying the gas cap of the Borzęcin field. These data are characterized by a steady decline of the production rate and proportional decline of the injection rate as the injection gas originates from the sweetening process of the produced gas. Another consequence of this is the roughly constant composition of the injection gas (in particular, in the recent 8 years) containing about 78% of CO₂ and 20% of H₂S.

Although the acid gas is injected into the water-bearing zone, the injected gas migrates to the producing wells completed only in the gas-bearing zone of the Borzęcin structure which is evidenced by the varying composition of the produced gas containing increasing acid gas components above their original various. This indicates migration paths of the injected gas in free gas state induced by buoyance mechanisms in the water-bearing zone and by pressure gradients in the gas cap of the structure. This migration takes place due to the limited effects of acid gas solution in the reservoir brine (more gas in the free phase) and the migration of acid gasses in the free phase significantly dominates over their migration in the brine saturated with dissolved gas. The detailed description of all the involved mechanisms leading to the effective migration of the gas injected in the structure is given in Chapter 7 as a result of the matched simulation model that reproduces the project operational data.

The above migration effects of the injected gas also result in making a few leakage risks possible. They include leakage pathways across the caprock and as a spill-out beyond the structural trap in addition to the pathway via induced fractures and along well trajectories. These possibilities analysed in Chapter 7.



3 Measurements

3.1 BOTTOMHOLE SAMPLING OF RESERVOIR WATER SATURATED WITH GAS

Within the SECURE project a decision was made to take bottomhole samples of reservoir water, i.e. brine situated immediately below the gas reservoir to obtain a more consistent picture of acid gas plume migration in the Borzęcin structure. In the following text, the letter "B" is used instead of "W". Because of full hydrodynamic communication, the water- and gas-bearing zones remain in equilibrium. Water underlying the gas reservoir remains naturally saturated with natural gas. The re-injected acid gases, injected by the B-28 production well to the flooded layer, partly dissolve in formation water adjacent to the well. The gas volumes, which did not dissolve in water, can remain in aquifer waters in the form of immobile dispersed bubbles. Having exceeded the critical gas saturation of the brine, the mixture of acid gases will gravitationally migrate upwards in the reservoir, and will penetrate the gas zone leading to a gradual mixing with the reservoir gas. Composition changes of gas produced by individual production wells, and actually the occurrence of increased CO₂ and/or H₂S concentrations provides information on the propagation of acid gases plume migration in the gas zone of the Borzęcin sequestration structure. For a proper migration analysis within the aquifer (where the acid gases are injected) it is required to acquire additional difficultly obtainable data. Bottomhole samples of reservoir water saturated with gas should be taken – so-called PVT samples. In the history of the Borzęcin sequestration operation such samples were not obtained before. Small volumes of liquid are sampled by means of bottomhole samplers driven into the well bottom. After lowering to a pre-set depth, the sampler is hermetically closed and the fluid (gas/oil/water) remains isolated in its chamber preserving the pressure and temperature at the moment of sampling, hence in-situ reservoir conditions. Taking such bottomhole samples allows the determination of the composition of gas dissolved/dispersed in the reservoir water before these gases will penetrate to the gas zone of the structure. After pulling out the sampler from the well, the obtained sample of water saturated with gas was subject to separation, which resulted in obtaining the gas, entirely dissolved and/or dispersed in the water phase at in-situ reservoir conditions, and degassed reservoir water.

Bottomhole reservoir sampling is technically challenging. Cooperation was necessary between the reservoir operator (POGC), a measuring group having *inter alia* a slickline service (Exalo), and a team of INiG – PIB staff preparing the bottomhole samplers, managing the sampling operation, and securing the obtained fluids for further studies and analyses.

The sampling of bottomhole samples from the Borzęcin sequestration structure was carried out in two series. The first of them was performed in September 2018. Then the work on productive wells was consecutively started: B-4, B-27, B-6, B-30, and B-24. The second series of bottomhole sampling was carried out in July 2019 and comprised wells: B-21, B-22, B-24, B-4, and B-6. A short description of those actions, including photographic documentation, is presented below.



Year 2018

The sampling of bottomhole samples of reservoir water was performed on 4-7 September 2018. The work was aimed at obtaining water saturated with gas, underlying the Borzęcin natural gas reservoir.

Borzęcin-4

Before the operations described below the well was blown out on 24 August 2018. This operation consisted in reducing the pressure in the well and burning out the gas in a flare. The blowing out was aimed at eliminating a certain volume of water in the production tubing, which would affect the planned measurements of pressure distribution in the well. Reservoir water was sampled on 4 September 2018. During the described operations the well was in a static state (production was stopped). Before sampling, a drift mandrel (44 mm in diameter) with an overflow bailer was introduced to the well. The drift mandrel was lowered to a depth of 1435 m b.g.l., according to the sampling plan. After pulling out the set, approx. 1000 cm³ of fluid were obtained from the bailer. Then pressures in the well were measured at selected depths.

Operations in the well were carried out at:

- static bottomhole pressure at a depth of 1420 m b.g.l. BHPs = 40.7 bar,
- bottomhole temperature at a depth of 1420 m b.g.l. BHT = 48.5°C
- static wellhead pressure WHPs = 34.0 bar,
- wellhead temperature WHT= 19°C.

After completion of operations described above the bottomhole sampling of reservoir water started. 2 PVT bottomhole samplers were prepared, joined together (in tandem) and driven in one go into the Borzęcin-4 production well to a depth of 1428 m b.g.l., which was approx. 32 m below the shoe of production tubing. Specifications of both samplers used were previously verified in the PVT laboratory. Sampler Leutert No 950 - the top one, has a capacity of 610 cm³, while sampler Leutert No 514 - the bottom one, has a capacity of 620 cm³.

Once the pressure chambers closed, at a pre-set sampling depth and at a set time, the bottomhole samplers were pulled out to the surface. Immediately, both samplers were properly opened and the collected fluid separated, i.e. the reservoir brine saturated with hydrocarbon gas. This treatment resulted in obtaining the gas from degassing of reservoir water and degassed brine.

The fluid taken by sampler No 950 consisted of 418 cm³ of gas (382 Ncm³ – reference conditions DIN 1343), which under thermobaric reservoir conditions was dissolved and dispersed in the reservoir water, and 610 cm³ of degassed brine. Hence the estimated water saturation with gas was 0.63 Nm³/m³ of brine.

In a similar way, the collection of fluid by sampler No 514 resulted in 447 cm³ of gas (408 Ncm³) and 620 cm³ of degassed brine. The water saturation with gas was an estimated 0.66 Nm³/m³ of brine.

It should be mentioned that, because of technical aspects of the collection of fluids from the sampler and their separation, the measured water and gas volumes can differ from the in-situ reservoir values. During the transfer of saturated reservoir (water from the sampler) and separation, most samples remained representative for quantitative analyses (gas and water for chemical analyses). Precise fluid volume measurements, albeit carried out carefully, may carry an error resulting from technical limitations of downhole sampling.

The acquired gas and water samples were properly protected in tight, closed containers, to prevent release to or contact with atmospheric air. Afterwards they were transported to the INiG – PIB laboratory to carry out further tests and analyses. The sampling operation is depicted in Figure 3.1 and Figure 3.2, below.



Figure 3.1. Bottomhole samplers driving to the B-4 well.

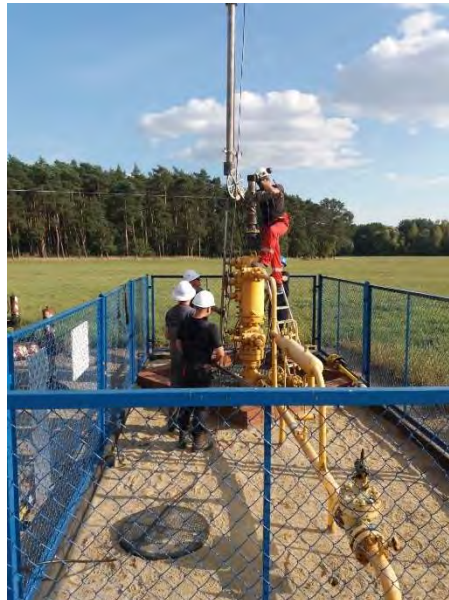


Figure 3.2. Pulling out the samplers set from the lubricator - B-4 well.

Borzęcin-27

Before operations described below the well was blown out on 24 August 2018. The work related to sampling bottomhole samples of reservoir water started on 5 September 2018. During the operations the well was in a static state. A drift mandrel (44 mm in diameter) with an overflow bailer was introduced to the well. This set stopped at a depth of 1399 m b.g.l., i.e. approx. 4 m below the shoe of production tubing. After pulling out the set it was found to be entirely dry and in the overflow bailer no fluid was found. Traces of a solid fraction were visible on the drift mandrel, in the form of sand saturated with dark hydrocarbon fraction. The distribution of pressure and temperature was measured, which also confirmed the lack of water in the well. Because of this the operation of driving bottomhole samplers was given up.

Operations in the well were carried out at:

- static bottomhole pressure at a depth of 1392 m b.g.l. BHPs = 48.9 bar,
- bottomhole temperature at a depth of 1392 m b.g.l. BHT = 47.1°C
- static wellhead pressure WHPs = 43.5 bar,
- wellhead temperature WHT = 20°C.

Borzęcin-6



The Borzęcin-6 well, drilled in 1970, was used to extract gas from the reservoir in the years 1977-2007. Currently it is a flooded observational well, through which, after appropriate preparation, the injection of liquid waste to the reservoir can be carried out (if necessary). The sampling of reservoir water from the well started on 6 September 2018. During the described operations the well was in a static state. Before samplers driving, a drift mandrel (44 mm in diameter) with an overflow bailer was introduced to the well. The drift mandrel was lowered to a depth of 1443 m b.g.l., according to the sampling plan, 45 m below the shoe of production tubing. After pulling out the set, a sample of watery fluid was obtained from the bailer, at an amount of approx. 1000 ml.

Operations in the well were carried out at:

- static wellhead pressure WHPs = 1 bar,
- wellhead temperature WHT = 21°C,
- actual bottomhole parameters were not measured.

After completion of the operations described above, the sampling of reservoir water bottomhole samples started. 2 PVT bottomhole samplers were prepared, joined together (in tandem) and driven in one go to the Borzęcin-6 productive well to a depth of 1441 m b.g.l., i.e. approx. 43 m below the shoe of production tubing. Once the pressure chambers closed, samplers were pulled out to the surface. Immediately, both samplers were properly opened and the collected fluid separated, i.e. the reservoir brine saturated with hydrocarbon gas. This treatment resulted in obtaining the gas from degassing of reservoir water and degassed brine.

Sampler No 950 yielded 220 cm³ of gas (201 Ncm³), which under thermobaric reservoir conditions was dissolved and dispersed in the reservoir water, and 610 cm³ of degassed brine. Hence the estimate water saturation with gas was 0.33 Nm³/m³ of brine.

In a similar way, the collection of fluid sampled by sampler No 514 resulted in 216 cm³ of gas (197 Ncm³) and 620 cm³ of degassed brine. The estimated water saturation with gas was 0.32 Nm³/m³ of brine.

The acquired samples of gas and water were properly protected in tightly closed containers preventing release to or contact with atmospheric air. Afterwards they were transported to the INiG – PIB laboratory to carry out further tests and analyses. The sampling operation is depicted in Figure 3.3 and Figure 3.4, below.



Figure 3.3. The work at the B-6 well.



Figure 3.4. Samples taking from the bottomhole sampler.

Borzecin-30

The gas production by the Borzecin-30 well was finished in 1995 due to its gradual flooding. Currently, it is an observation well. The sampling of reservoir water from this well started on 6 September 2018. During the described operations the well was in a static state. A drift mandrel (44 mm in diameter) with an overflow bailer was driven in the well. The shoe of production tubing is situated at a depth of 1424 m b.g.l. The drift mandrel stopped at a depth of 1415 m b.g.l. (it was periodically sticking from a depth of 1100 m), so it did not go beyond the production tubing. After pulling the set out it was found that the bailer did not contain any fluid, and the workshop is covered with a gluey paste, dark grey in colour –Figure 3.5. Because of the above the operation of bottomhole samplers driving was given up.

Operations in the well were carried out at:

- static wellhead pressure WHPs = 44 bar,
- wellhead temperature WHT = 19°C,
- actual bottomhole parameters were not measured.



Figure 3.5. Overflow bailer after pulling out from the B-30 well.



Borzęcin-24

The Borzęcin-24 well was one of the wells, used for the gas production from the reservoir. No production is carried out since February 2013. During the workover carried out in November 2014 the set of production tubing in the well was replaced. Unfortunately, a loss of part of tubing was registered, i.e. 81 lin. m. of production set 2 2/3 API, below a depth of 1343 m b.g.l. The last tubing that was pulled out was entirely damaged by corrosion. Despite the reconstruction work, aimed at resuming the production from the well, it remains out of operation. The sampling of reservoir water from the well started on 7 September 2018. During the described operations the well was in a static state. Before samplers driving, a drift mandrel (44 mm in diameter) with an overflow bailer was introduced to the well. The drift mandrel was lowered to a depth of 1330 m b.g.l., which at the same time was 11 m above the shoe of production tubing. After pulling out the set, a sample of watery fluid was obtained from the bailer, at an amount of approx. 1000 cm³.

Operations in the well were carried out at:

- static wellhead pressure WHPs = 1 bar,
- wellhead temperature WHT = 20°C,
- actual bottomhole parameters were not measured.

After completion of operations described above the sampling of reservoir water bottomhole samples started. 2 PVT bottomhole samplers were prepared, joined together (in tandem) and driven in one go to the Borzęcin-24 productive well to a depth of 1330 m b.g.l., i.e. approx. 11 m above the shoe of production tubing. Once the pressure chambers closed, samplers were pulled out to the surface. Immediately both samplers were properly opened and the collected fluid separated, i.e. the reservoir brine saturated with hydrocarbon gas. This treatment resulted in obtaining the gas from degassing of reservoir water and degassed brine.

The outcome of fluid collection by sampler No 950 consisted in obtaining 167 cm³ of gas (153 Ncm³), which under thermobaric reservoir conditions was dissolved and dispersed in the reservoir water, and 610 cm³ of degassed brine. Hence the estimate water saturation with gas was 0.25 Nm³/m³ of brine.

In a similar way, the collection of fluid sampled by sampler No 514 resulted in obtaining 125 cm³ of gas (114 Ncm³) and 620 cm³ of degassed brine. The estimated water saturation with gas was 0.18 Nm³/m³ of brine.

The acquired samples of gas and water were properly protected in tightly closed containers, preventing any release to or contact with atmospheric air. Afterwards they were transported to the INiG – PIB laboratory to carry out further tests and analyses. The sampling operation is depicted in Figure 3.6.



Figure 3.6. Sampling of bottomhole samples from the B-24 well.



Year 2019

The second sampling series of bottomhole samples of reservoir water was performed on 15-18 July 2019. The work was aimed at obtaining water saturated with gas underlying the natural gas reservoir.

Borzęcin-21

Before operations described below, the well was blown out on 27 June 2019. The work related to sampling bottomhole samples of reservoir water was started on 15 July 2019. During the operations, the well was in a static state. A drift mandrel (44 mm in diameter) with an overflow bailer was introduced to the well. This set was driven to a planned depth of 1431 m b.g.l., i.e. approx. 4 m above the shoe of production tubing. After pulling out the set no fluid was found in the bailer. The distribution of pressure and temperature was measured in the well, which also confirmed the lack of water. Because of the above, the operation of driving bottomhole samplers was given up.

Operations in the well were carried out at:

- static bottomhole pressure at a depth of 1430 m b.g.l. BHPs = 39.6 bar,
- bottomhole temperature at a depth of 1430 m b.g.l. BHT = 48.0°C
- static wellhead pressure WHPs = 35.2 bar,
- wellhead temperature WHT = 29°C.

Borzęcin-22

The well is situated on the top of the reservoir structure. The sampling of reservoir water from the well started on 16 July 2019. During the operations the well was in a static state. Before samplers driving, a drift mandrel (44 mm in diameter) with an overflow bailer was introduced to the well. The drift mandrel was lowered to a depth of 1420 m b.g.l., which at the same time was 1 m below the shoe of production tubing. After pulling out the set, a sample of watery fluid was obtained from the bailer, at an amount of approx. 1000 cm³.

After completion of the operations described above the sampling of reservoir water bottomhole samples started. 2 bottomhole PVT samplers were prepared, joined together in tandem (sampler No 950 - top, sampler No 514 - bottom) and driven in one go to the well to a depth of 1420 m b.g.l., which was 1 m below the shoe of production tubing. Once the pressure chambers closed, samplers were pulled out to the surface. The sampling operation is depicted in Figure 3.7, Figure 3.8, Figure 3.9 and Figure 3.10 below.

Operations in the well were carried out at:

- static bottomhole pressure at a depth of 1410 m b.g.l. BHPs = 39.0 bar,
- bottomhole temperature at a depth of 1410 m b.g.l. BHT = 47.3°C
- static wellhead pressure WHPs = 34.7 bar,
- wellhead temperature WHT = 21°C.

The entire bottom sampler (No 514) was covered with thick mud of dark colour –Figure 3.11. After careful visual inspection it was found that a metal screen in the sampler's nose, protecting against possible inflow of undesired solid pollutants to the sampler's working chamber, was damaged.



Figure 3.7. Sampling of bottomhole samples from the B-22 well – the view from slickline unit.



Figure 3.8. Slickline unit.



Figure 3.9. Bottomhole samplers pulled out from the B-22 well lubricator.



Figure 3.10. Set of two bottomhole samplers after pulling out from the B-22 well.



Figure 3.11. The bottom part of bottomhole sampler (No 514) after pulling out from the B-22 well.

Immediately, both samplers were properly opened and the collected fluid separated. This treatment resulted in obtaining the gas from degassing of reservoir water and degassed brine.

Sampler No 950 yielded 415.5 cm³ of gas (380.6 Ncm³), which under thermobaric reservoir conditions was dissolved and dispersed in the reservoir water, and 610 cm³ of degassed brine. Hence the estimated water saturation with gas was 0.62 Nm³ of hydrocarbon gas in 1 m³ of brine.

In a similar way, sampler No 514 resulted in obtaining 412 cm³ of gas (375 Ncm³) and 620 cm³ of degassed brine. The estimated water saturation with gas was 0.60 Nm³/m³ of brine.

The acquired samples of gas and water were properly protected in leak-tight containers, preventing any release to or contact with atmospheric air impossible. Afterwards they were transported to the INiG – PIB laboratory to carry out further tests and analyses.

Borzęcin-24

The Borzęcin-24 well is turned out of gas production. Despite reconstruction works, it was not possible to resume its operation. The sampling of reservoir water from the well started on 17 July 2019. The work was carried out in a similar way as in 2018. During the described operations the well was in a static state. Before samplers driving, a drift mandrel (44 mm in diameter) with an overflow bailer was introduced to the well. The



drift mandrel was lowered to a depth of 1330 m b.g.l. After pulling out the set, a sample of watery fluid was obtained from the bailer, at an amount of approx. 1000 cm³.

Operations in the well were carried out at:

- static wellhead pressure WHPs = 1 bar,
- wellhead temperature WHT = 21°C,
- actual bottomhole parameters were not measured.

After completion of the operations described above, the sampling of reservoir water bottomhole samples started. 2 PVT bottomhole samplers were prepared, joined together (in tandem) and driven in one go to the well to a depth of 1330 m b.g.l., which was approx. 11 m above the shoe of production tubing. Once the pressure chambers closed, samplers were pulled out to the surface. Immediately, both samplers were properly opened and the collected fluid separated, i.e. the reservoir brine saturated with hydrocarbon gas. This treatment resulted in obtaining the gas from degassing of reservoir water and degassed brine.

Sampler No 950 yielded 115 cm³ of gas (105 Ncm³), which under thermobaric reservoir conditions was dissolved and dispersed in the reservoir water, and 610 cm³ of degassed brine. Hence the estimated water saturation with gas was 0.17 Nm³/m³ of brine.

Sampler No 514 yielded 180 cm³ of gas (163 Ncm³) and 620 cm³ of degassed brine. The estimated water saturation with gas was 0.27 Nm³/m³ of brine.

The samples of gas and water acquired in the above way were properly protected in leak-tight containers, to prevent any release to or contact with atmospheric air. Afterwards they were transported to the INiG – PIB laboratory to carry out further tests and analyses. The sampling operation is depicted in Figure 3.12, Figure 3.13, Figure 3.14 and Figure 3.15, below.



Figure 3.12. Sampling of bottomhole samples from the B-24 well.



Figure 3.13. Bottomhole samplers pulled out from the B-24 well lubricator.



Figure 3.14. Protection of bottomhole samples pulled out from the B-24 well.



Figure 3.15. The B-24 well after completion of the work related to sampling.



Borzecin-4

The bottomhole sampling of reservoir water was made on 17 July 2019. The work was carried out in a similar way as in 2018. During the described operations the well was in a static state. Before samplers driving, a drift mandrel (44 mm in diameter) with an overflow bailer was introduced to the well. It was possible to drive the sampler to a depth of 1430 m b.g.l. as against the planned 1435 m b.g.l. After pulling out the set, a sample of watery fluid was obtained from the bailer, at an amount of approx. 1000 cm³.

Operations in the well were carried out at:

- static wellhead pressure WHPs = 34.5 bar,
- wellhead temperature WHT = 20°C,
- actual bottomhole parameters were not measured.

After completion of the operations described above the sampling of reservoir water bottomhole samples started. 2 PVT bottomhole samplers were prepared, joined together (in tandem) and driven in one go to the Borzecin-4 productive well to a depth of 1428 m b.g.l., which was approx. 32 m below the shoe of production tubing. Once the pressure chambers closed, samplers were pulled out to the surface. Immediately both samplers were properly opened and the collected fluid separated, i.e. the reservoir brine saturated with hydrocarbon gas. This treatment resulted in obtaining the gas from degassing of reservoir water and degassed brine.

Sampler No 514 (bottom one) yielded 192 cm³ of gas (175 Ncm³), which under thermobaric reservoir conditions was dissolved and dispersed in the reservoir water, and 610 cm³ of degassed brine. Hence the estimate water saturation with gas was 0.29 Nm³/m³ of brine. Because sampler No 950 became unsealed, it was not possible to acquire the second bottomhole sample of reservoir water.

After the samples were appropriately marked and sealed the collected material was transported to the INiG – PIB laboratory to carry out further tests and analyses. The sampling operation is depicted in Figure 3.16, below.



Figure 3.16. Bottomhole samplers driving to the B-4 well.

Borzecin-6

The bottomhole sampling of reservoir water from the well started on 18 July 2019. During the described operations the well was in a static state. Before samplers driving, a drift mandrel (44 mm in diameter) with an overflow bailer was introduced to the well. The drift mandrel was lowered to a depth of 1443 m b.g.l., planned in the design. After pulling out the set, a sample of watery fluid was obtained from the bailer, at an amount of approx. 1000 cm³.

Operations in the well were carried out at:



- static wellhead pressure WHPs = 1 bar,
- wellhead temperature WHT = 20°C,
- actual bottomhole parameters were not measured.

After completion of the operations described above the sampling of reservoir water bottomhole samples started. 2 PVT bottomhole samplers were prepared, joined together (in tandem) and driven in one go to the Borzęcin-6 well to a depth of 1441 m b.g.l., which was approx. 43 m below the shoe of production tubing. Once the pressure chambers closed, samplers were pulled out to the surface. Immediately, both samplers were properly opened and the collected fluid separated, i.e. the reservoir brine saturated with hydrocarbon gas. This treatment resulted in obtaining the gas from degassing of reservoir water and degassed brine.

Sampler No 950 yielded 136 cm³ of gas (124 Ncm³), which under thermobaric reservoir conditions remained dissolved in the reservoir water, and 610 cm³ of degassed brine. Hence the estimated water saturation with gas was 0.20 Nm³/m³ of brine.

In a similar way, the outcome of fluid collection by sampler No 514 consisted in obtaining 140 cm³ of gas (128 Ncm³), which under thermobaric reservoir conditions remained dissolved in the reservoir water, and 620 cm³ of degassed brine. The estimated water saturation with gas was 0.21 Nm³/m³ of brine.

The samples of gas and water acquired in the above way were properly marked, sealed, and then transported to the INiG – PIB laboratory to carry out further tests and analyses. The sampling operation is depicted in Figure 3.17 and Figure 3.18, below.



Figure 3.17. The work at sampling from the B-6 well.



Figure 3.18. Samplers driving to the B-6 well.

Within the SECURE project 10 operations of bottomhole sampling of reservoir water underlying the Borzęcin gas reservoir were carried out in the years 2018–2019. Such samples were never acquired before.

The majority of bottomhole sampling operations were successful. Samples of reservoir water saturated with gas were obtained from wells B-4, B-6, B-22, and B-24. In wells B-4, B-6, and B-24 it was possible to obtain the research material twice - year after year - which is an additional advantage for comparative analyses. Despite attempts, no bottomhole samples from wells B-21, B-27, and B-30 were obtained. The main reason was the lack of water at the pre-set depth of samplers driving – albeit there were attempts to drive them to the maximum safe depth determined by the drift mandrel with an overflow bailer driven down to the well.

Table 3.1 presents a summary of the different stage of reservoir water bottomhole sampling. Figure 3.19 presents the location of wells on the map of Borzęcin reservoir. The B-28 well, through which the acid gases are re-injected, was marked with a black square. The wells, from which it was possible to take samples of reservoir water are marked with green circles, while those, from which despite efforts made it was not possible, with red ones.



Table 3.1 Bottomhole sampling summary.

Well number	Well status	Sampling date	Blowing out	Drift depth (m b.g.l.)	Tubing shoe depth (m b.g.l.)	Sampling depth (m b.g.l.)	Sampling result	Gas in water saturation [Nm ³ /m ³]
B-4	producing	4.09.2018	yes	1435	1396	1425	Positive	0.63
						1428	Positive	0.66
B-27	producing	5.09.2018	yes	1399	1395	cancelled	Negative	-
							Negative	-
B-6	closed in	6.09.2018	no	1443	1398	1438	Positive	0.33
						1441	Positive	0.32
B-30	closed in	6.09.2018	no	1415	1424	cancelled	Negative	-
							Negative	-
B-24	closed in	7.09.2018	no	1330	1341	1327	Positive	0.25
						1330	Positive	0.18
B-21	producing	15.07.2019	yes	1431	1435	cancelled	Negative	-
							Negative	-
B-22	producing	16.07.2019	no	1420	1419	1417	Positive	0.62
						1420	Positive	0.60
B-24	closed in	17.07.2019	no	1330	1341	1327	Positive	0.17
						1330	Positive	0.27
B-4	producing	17.07.2019	no	1430	1396	1425	Negative	-
						1428	Positive	0.29
B-6	closed in	18.07.2019	no	1443	1398	1438	Positive	0.20
						1441	Positive	0.21

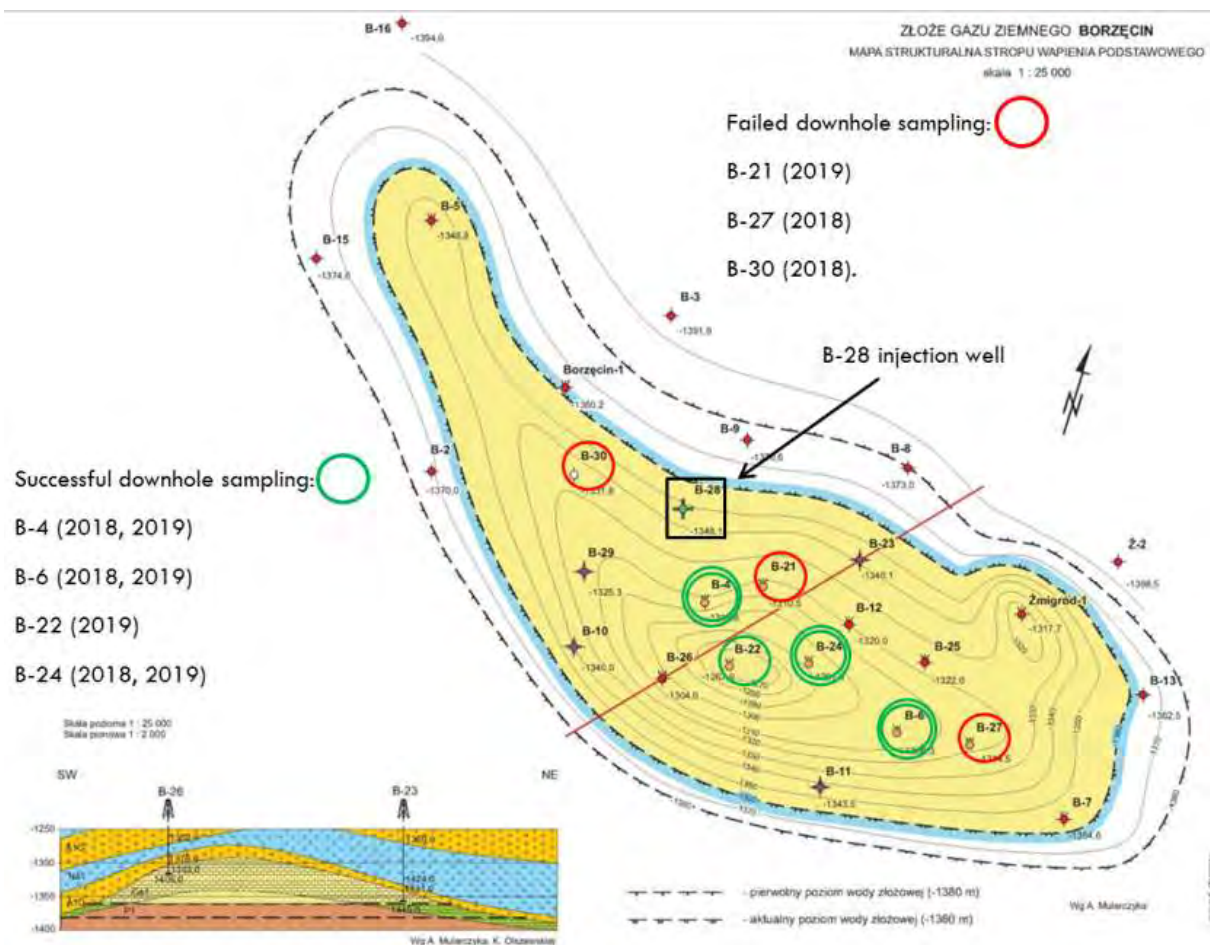


Figure 3.19. Map of the Borzęcin reservoir – bottomhole samples taking.

3.2 GAS ANALYSES

As previously described, after the separation of water and gas phases (originated due to degassing resulting from pressure reduction in the sampler), gas and water samples for further tests were obtained. Their volume was measured, they were then sealed for transport to the laboratory. Water samples were subject to detailed physical and chemical analyses. The samples of gas released from the reservoir water were subject to chromatographic analyses and isotope composition determinations. Relevant tests of phase properties of reservoir fluids were carried out in the PVT (Pressure-Volume-Temperature) laboratory. The acquired data were successively transferred to the team developing a numerical simulation model of the Borzęcin sequestration structure. The assessment of risk accompanying a long-term process of acid gases sequestration, using the example of Borzęcin natural gas reservoir, was the overriding objective.

3.2.1. Chemical composition

Methodology of gas chemical composition determination

To perform chromatographic analyses of the following components: O₂, N₂, CO, CO₂, C₁, C₂, C₃, i-C₄, n-C₄, i-C₅, n-C₅, neo-C₅, and of a sum of hydrocarbons C₆, C₇, C₈, C₉, and C₁₀ a two-channel valve gas chromatograph was used: AGILENT 7890 A and a system of columns and detectors:

- thermal conductivity detector (TCD), flame ionisation detector (FID), and capillary columns: HP-PLOT/Q and HP-MOLESIEVE 5A,
- flame ionisation detector (FID) and an HP-PONA capillary column.



During gas analysis, argon was used as a carrier gas, with a flow gradient from 3 ml/min to 6 ml/min. A temperature programme was used from 35°C to 260°C. The temperature of 30°C was maintained for fifteen minutes, the temperature increase ranged then from 15°C to 25°C per minute. The maximum temperature was held for 6.5 minutes. Working temperatures were: nickel catalyst - 375°C, FID detectors - 300°C, and the inlet and the TCD detector - 200°C.

To determine trace amounts of CO and CO₂ additional equipment was used - a Nickel Catalyst Tube G2747A connected with a flame ionisation detector. The gas sample is split in the column and passed with a hydrogen additive through the catalyst, which converts CO and CO₂ into methane, due to which it is possible to determine very small amounts of those gases.

Sampling loops were used (although the system is equipped also with a typical split/splitless inlet).

To perform chromatographic analyses of sulphur compounds as well as of helium and hydrogen, a two-channel valve gas chromatograph AGILENT 7890 A with ChemStation software was used together with a system of columns and detectors:

- thermal conductivity detector (TCD) and a Molecular Sieve 5A Ultimetall packed column,
- flame photometric detector (FPD) and a capillary column DB-1 of Agilent Technologies.

Nitrogen was used as the carrier gas. Certified gas standards were used to carry out calibration. The uncertainty of individual components measurement is 3%. After the calibration the chromatographic systems are every day checked by means of standards.

Discussion of results

The gas acquired from the degassing of bottomhole samples of reservoir water was subject to *inter alia* chromatographic analysis. The recording in the tested gas composition of increased (in respect to the natural) concentrations of components of the gas injected to the reservoir (such as CO₂ and H₂S) is an important piece of information on directions and intensity of acid gases migration in the Borzęcin sequestration structure aquifer. The results of gas, dissolved in the brine underlying the Borzęcin reservoir, analyses performed under the SECURE project implementation are presented below, simplified to the main components. Figure 3.20 presents the composition of the gas dissolved in the Borzęcin reservoir water.

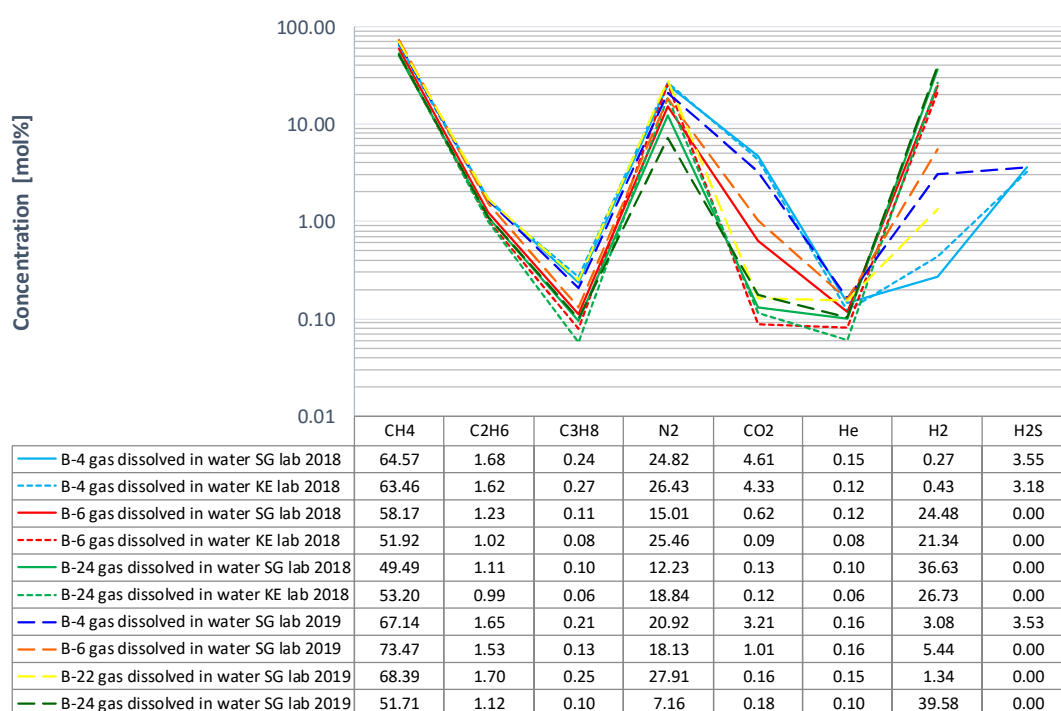


Figure 3.20. Composition of the gas dissolved in the Borzęcin reservoir water



It should be noted that from certain wells (B-4, B-6, B-24) samples were taken twice (in 2018 and 2019), and in addition a part of those samples were additionally analysed in separate laboratories - hence the SG lab and KE lab indication.

Methane is the main hydrocarbon component of the gas released from the reservoir water, with an average content of approx. 60% mol% based on 10 analyses. The next are ethane (1.4 mol%) and propane (0.16 mol%) - the other hydrocarbon components are on a negligibly low level (below the significance level to the studied phenomena) and they were not included in the presented specification. The non-hydrocarbon components are dominated by nitrogen (approx. 20 mol%), carbon dioxide is next (on average 1.5 mol%, but in samples originating from the B-4 well its amount is highest reaching 4.6 mol%). Small amounts of helium (on average slightly more than 0.1 mol%) were also identified in each sample. Also, strongly varying hydrogen concentrations were determined in the studied gases. For two productive wells (B-4 and B-22), the values are relatively low, i.e. on average approx. 1.3 mol%, while for the other wells, turned out from gas production, the hydrogen concentrations were much higher - on average 30 mol%. The highest hydrogen concentrations (reaching almost 40 mol%) were recorded in the B-24 well, which will be discussed hereafter. Hydrogen sulphide, on an average level of 3.4 mol%, was identified only in the gas samples from the B-4 well.

Figure 3.21 presents the CO₂ concentration, determined in the gas originating from degassing of water obtained by bottomhole samplers in selected wells of the Borzęcin sequestration facility, versus the distance from the injecting well (B-28). The tests show that water originating from the Borzęcin-4 well is saturated to the largest extent with carbon dioxide and hydrogen sulphide, hence the acid gases re-injected to water-bearing layers. In each of three analyses of gas released from the B-4 reservoir water the determined concentrations exceeded many times the levels observed in the other wells from which bottomhole samples were taken (B-6, B-22, B-24). The analysis of arrangement and mutual distances of the aforementioned wells to the injecting well, i.e. the B-28, helps to understand the concentration distribution. As shown in Figure 3.19, the B-4 well is situated closest to the well injecting acid gases. Moreover, it is situated south of B-28, that is in the direction of the expected migration of acid gases upwards the structure, directed by gravity forces, but also by a depression of pressure caused by continuous gas extraction from the reservoir - now by four wells, i.e.: B-4, B-21, B-22 (most productive), and B-27.

Like for carbon dioxide, Figure 3.22 presents H₂S concentrations in the gas released from water versus the distance from the injecting well. It should be noted that the gas containing hydrogen sulphide at an average level of 3.4 mol% was detected only in samples originating from the B-4 well (along a straight line 630 m away from the injection well B-28). This is a very high concentration, considering that in samples from the other wells hydrogen sulphide was not identified at all. The above measurements and studies undoubtedly enhance the information on dynamics and migration directions of acid gases in the water phase - that is in the water-saturated layers underlying the gas reservoir, to which CO₂ and H₂S are directly injected.

Figure 3.23 presents the chemical composition of gases originating from the Borzęcin-4 well. The result of analyses of the sample of gas released from the reservoir water sampled in September 2018 by the bottomhole sampler No 950 (top in the set) is marked in blue - the analysis was performed by the laboratory of the SG Department at the INiG – PIB Krakow. The result of analysis of the sample of gas released from the reservoir water sampled in September 2018 by the bottomhole sampler No 514 (bottom in the set) is marked in green - the analysis was performed by the laboratory of the KE Department at the INiG – PIB Krosno. Both samples were taken at the same time by two separate samplers, joined and driven together to the well to a depth allowing to immerse them in the reservoir water saturated with gas. The results of both laboratories are very close. Methane is the main gas component, with an average concentration of approx. 64 mol%. Also, ethane (1.65 mol%) and propane (0.25 mol%) can be distinguished among hydrocarbon components - the other hydrocarbon components are on a negligibly low level. The non-hydrocarbon components are dominated by nitrogen (25 mol%), carbon dioxide (4.5 mole%), and hydrogen sulphide (3.4 mol%). Also, small amounts of hydrogen (0.3 mol%) and helium (approx. 0.13 mol%) were determined.

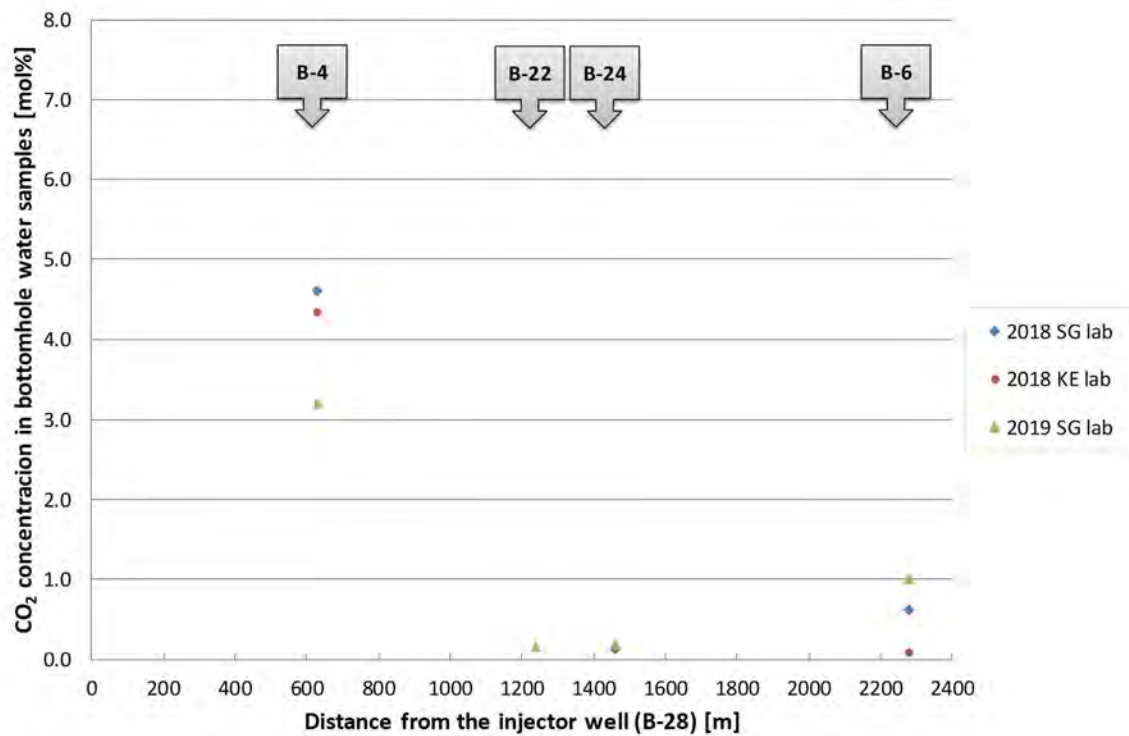


Figure 3.21. CO₂ concentration in the gas released from the bottomhole water versus the distance from the injecting well.

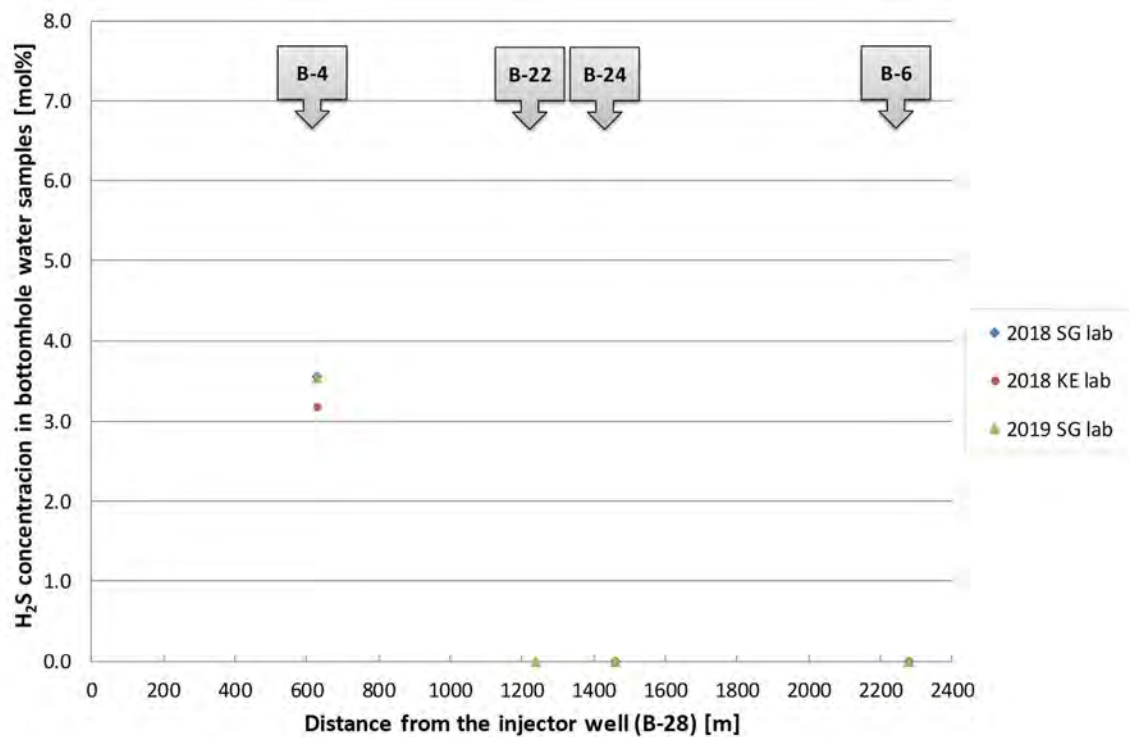


Figure 3.22. H₂S concentration in the gas released from the bottomhole water versus the distance from the injecting well.



The composition of dissolved gas released from the B-4 reservoir water is marked in grey, but this sample was taken in July 2019, so nearly after a year. Approx. a 10 times higher concentration of hydrogen (up to 3 mol%) was noticed - mainly accompanied by lower nitrogen concentrations. This situation can be possibly explained by the fact that in 2018 the B-4 well was blown out 10 days before the bottomhole sampling, but not a year later. Such decisions are made by the reservoir operator (POGC in this case) and are related to periodical reconstruction works or planned measurements in selected wells of a specific reservoir. The pressure depression in the B-4 well, caused by blowing out, allowed most likely the release and separation of hydrogen from the water phase to the gas phase, which significantly reduced its concentration in water samples taken a few days later. A higher hydrogen concentration is most likely related to electrochemical corrosion processes, which widely occur in an aqueous environment in the presence of hydrogen sulphide and steel from the well completion. In a year-to-year comparison, concentrations of the other components of gas released from the reservoir water are on a relatively the same level.

Because B-4 is a still producing, the composition of gas extracted in 2019 is marked in red in Figure 3.23. Substantial differences are visible in CO₂ and H₂S concentrations between the gases released from water and the extracted gas. Increased amounts of carbon dioxide and hydrogen sulphide in water as against natural concentrations present in the extracted reservoir gas can be related to large differences in individual gases solubility in water (that was the subject of laboratory tests presented in subsection 3.4), but they are primarily the effect of acid gases re-injection through the B-28 well situated nearby.

During separation of bottomhole water samples, its saturation with gas was estimated at approx. 0.5 Nm³ of gas in 1 m³ of brine.

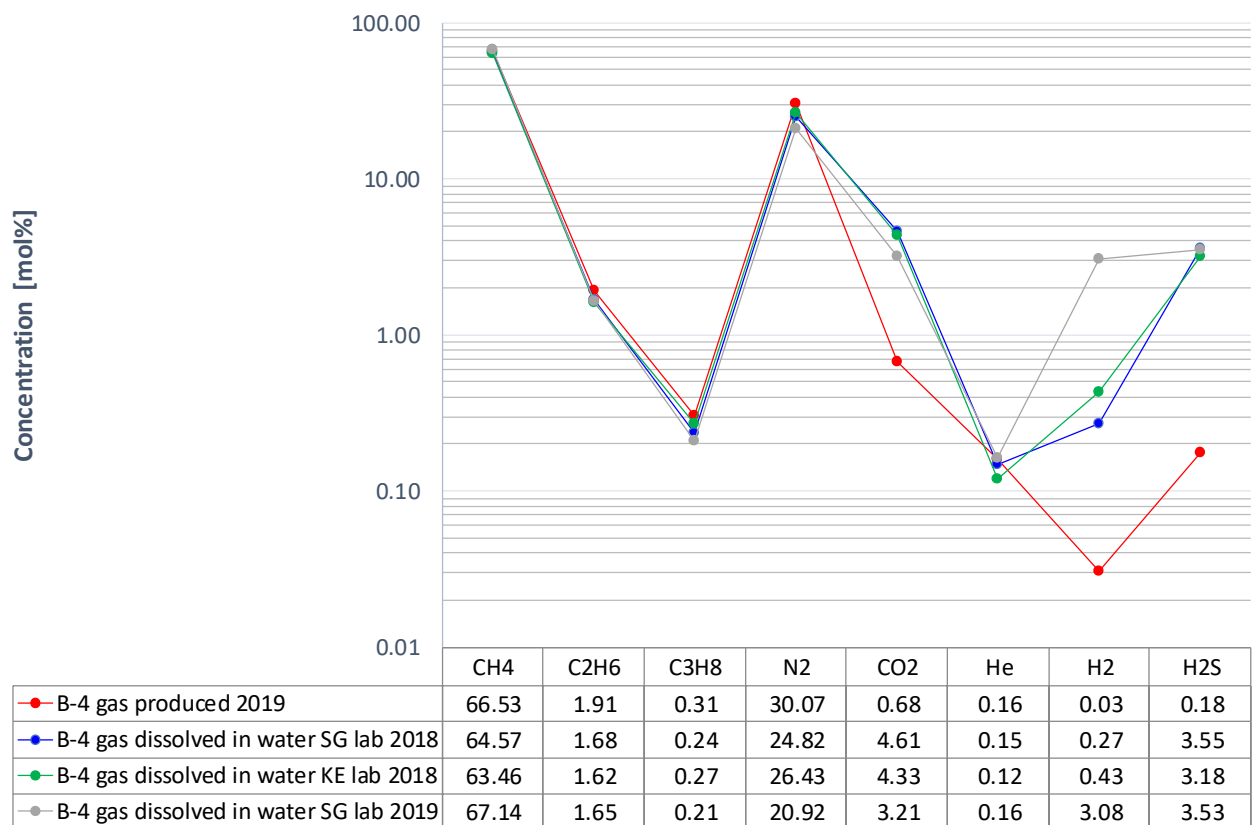


Figure 3.23. Composition comparison of samples of gas dissolved in water and of the extracted gas - well B-4.

Figure 3.24 shows the chemical composition of gases originating from the second productive well, from which it was possible to take bottomhole samples of water, i.e. B-22. This is currently the most productive well of the reservoir (provides approx. 80% of the entire production). The composition of gas released from the bottomhole water sample is presented in grey, while the composition of produced gas is indicated in red. The content of hydrocarbon components in both samples is on a similar level. In the gas released from water 1.3 mol% of hydrogen was determined, which is related to corrosion. As compared with the gas dissolved in water originating from the B-4 well, the CO₂ concentration is very low, and H₂S was not found at all. This allows to



draw the conclusion, that the migration of injected acid gases, contrarily to the B-4 well, did not reach the B-22 well yet, despite a high pressure gradient in the well resulting from intensive gas extraction.

During separation of the bottomhole water sample its saturation with gas was estimated at approx. 0.6 Nm³/1m³ of brine.

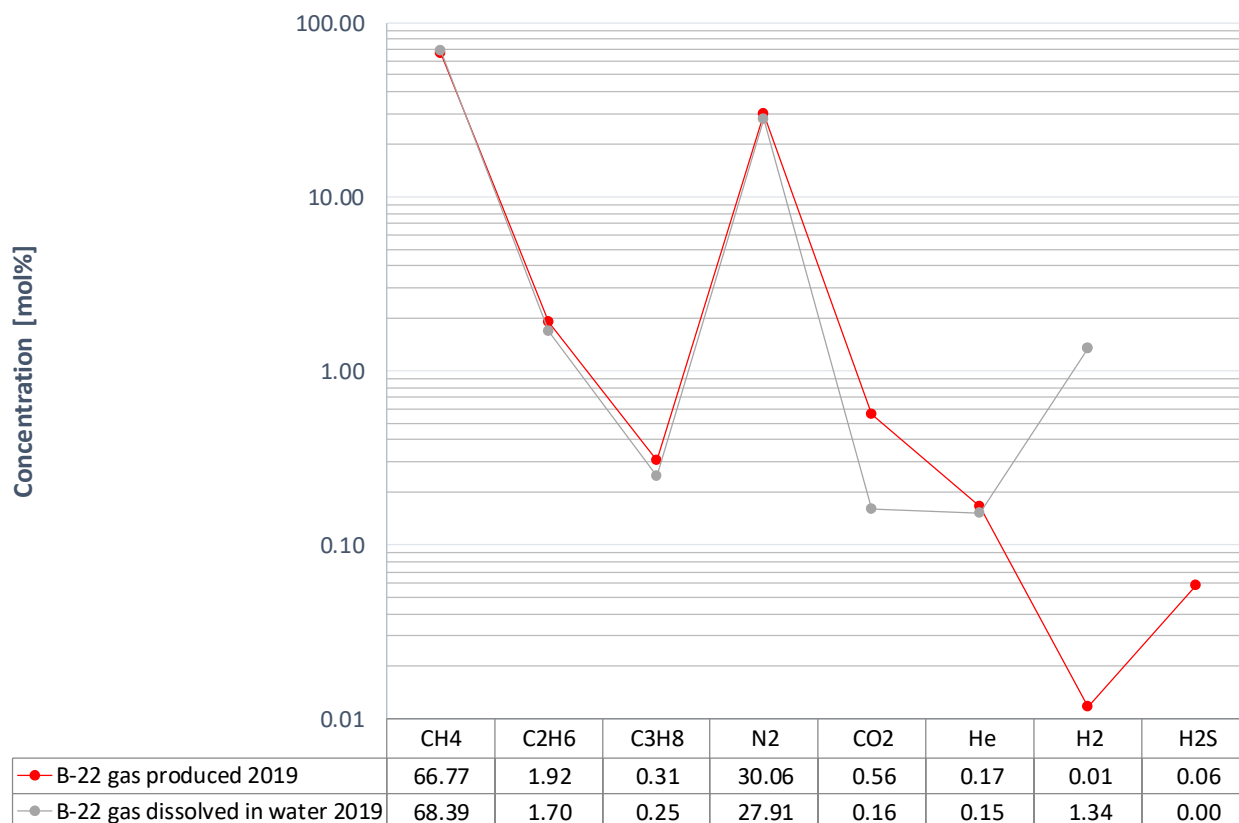


Figure 3.24. Composition comparison of samples of gas dissolved in water and of the produced gas - well B-22.

Figure 3.25 shows the chemical composition of gases originating from the B-6 well, out-of-operation at present day and having the status of an observation well. Significant differences in the methane, nitrogen, and hydrogen concentrations were recorded in the gas composition. Especially a reduced hydrogen concentration in the 2019 sample is striking, compared to the two similar analyses from 2018, which seems difficult to explain. Perhaps this is an error related to a failed sampling process. The well remained out-of-operation since 2007 and during the last year, i.e. between bottomhole water sampling operations under the SECURE project, no work was carried out on it. It is also not possible that hydrogen accumulated in the well could escape to the atmosphere at any stage of bottomhole samplers driving operations.

No hydrogen sulphide was found in any of the analysed samples, while the carbon dioxide concentration on average is 0.6 mol%, so it maintains on a very low level - comparable with the Borzęcin reservoir gas. On this basis it is necessary to conclude that the acid gases migration did not reach the B-6 well zone, which anyhow, due to the lack of pressure gradient resulting from the well closing, was rather improbable.

During separation of the bottomhole water sample, its saturation with gas was estimated at approx. 0.3 Nm³/1m³ of brine.

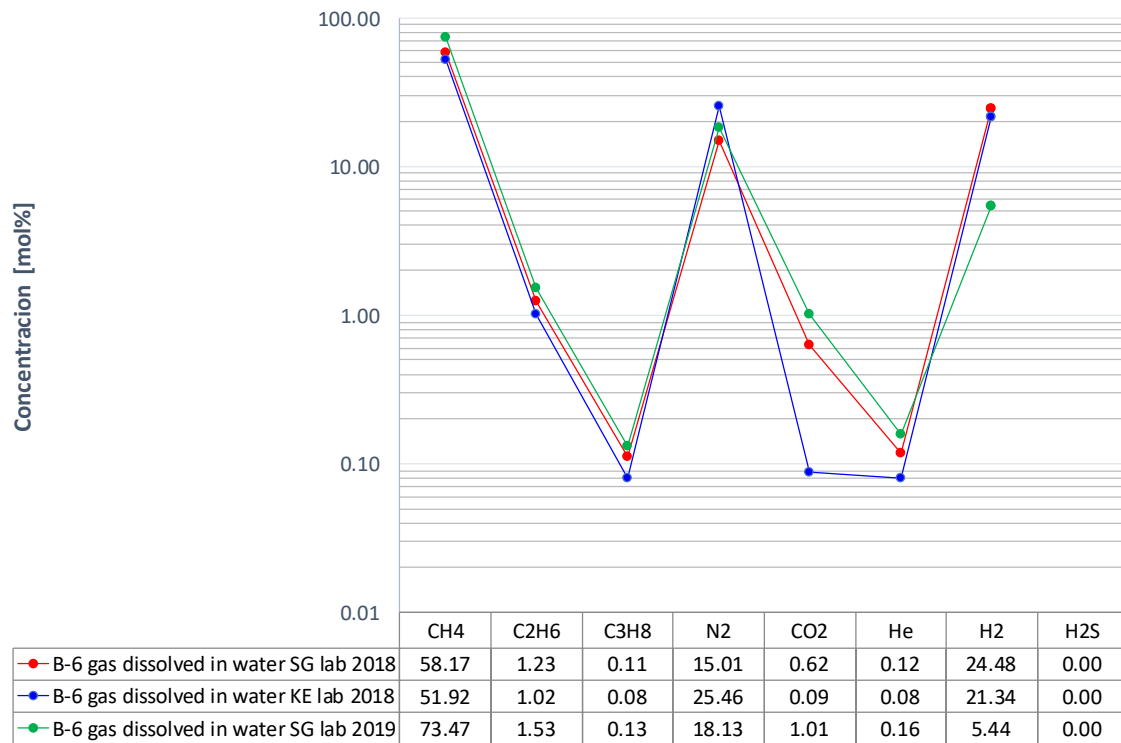


Figure 3.25. Composition comparison of gas samples originating from the B-6 well.

Figure 3.26 shows chemical compositions of gases originating from the B-24 well, out-of-operation since 2013. During the treatment-service work carried out in 2014, the set of lifting casing in the well was replaced. Unfortunately, part the of casing pipes was lost, which was left in the well. The last pulled out production tubing pipe was entirely damaged by corrosion. Despite reconstruction works, no satisfactory gas extraction was achieved and the well remains out of operation.

Some information on the well history was provided here to explain the fact that in the gas originating from the B-24 well, record hydrogen concentrations of 26÷40 mol% were registered. Unexpectedly high hydrogen concentrations were the reason for transferring the backup gas samples to an additional laboratory (KE marking), to verify the analysis.

The confirmed very high hydrogen concentration is related to progressing corrosion of the lost part of the tubing. The bottomhole brine was sampled approx. 13 m above the place of tubing failure. It features a very low degree of saturation with gas, estimated on average at 0.2 Nm³/1m³, therefore already small amounts of hydrogen can substantially increase its percentage concentration. The well remained out of operation for years, and this results in a limited exchange of water between the well annulus and the aquifer. This provides favourable conditions for progressive corrosion, which leads to continuous water saturation with hydrogen. At very high hydrogen concentrations, the methane, nitrogen, and also other gas components contents are necessarily proportionally lower.

No hydrogen sulphide was found in any of the analysed samples, which could be partially related to the H₂S consumption during the corrosion reaction. The carbon dioxide concentration on average is 0.14 mol%, so it maintains on a very low level. It should be concluded, that the acid gases migration did not reach also the out-of-operation B-24 well.

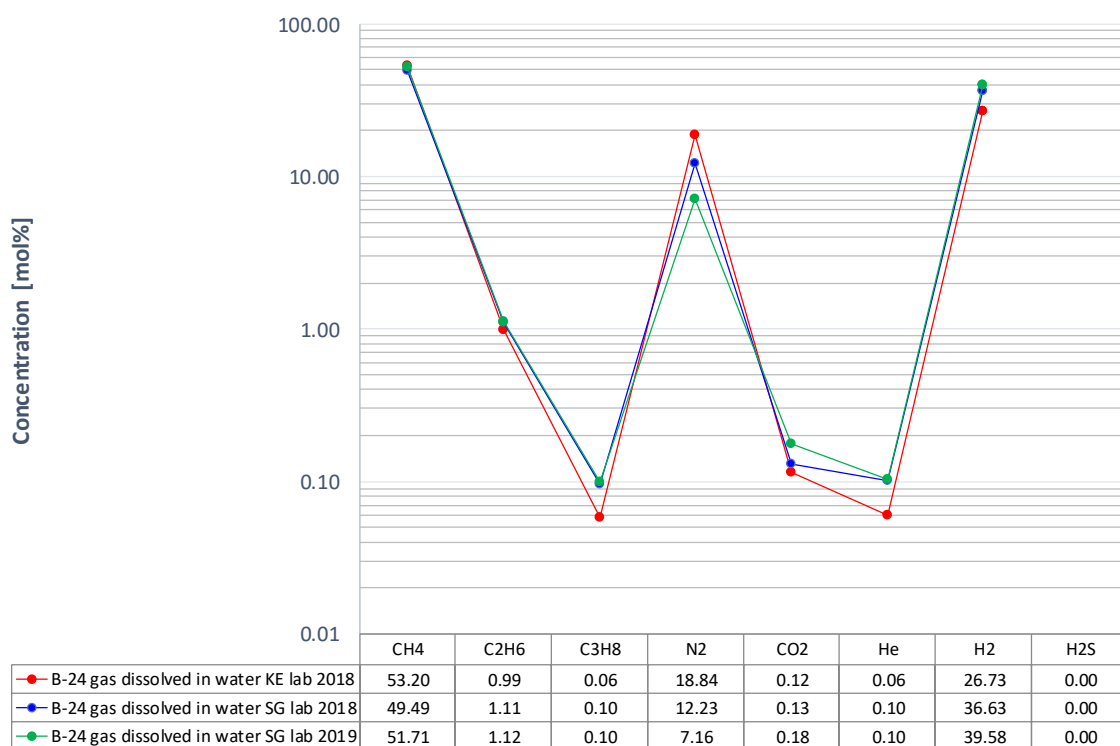


Figure 3.26. Composition comparison of gas samples originating from the B-24 well.

Analyses of produced gas

The gas from the Borzęcin reservoir is now extracted by four productive wells, i.e.: B-4, B-21, B-22, and B-27. Samples of the gas, extracted by individual wells, and of water lifted together with gas, were taken from the surface installation in May 2019. The acquired fluids were subjected to the planned analyses and tests.

Figure 3.27 presents part of surface development situated in the area of the Borzęcin Gas Plant. The samples for testing were taken from the visible reduction-measurement lines, separate for each productive well.



Figure 3.27. Part of the surface installation – separate reduction-measurement systems of productive wells.

Figure 3.28 shows chemical compositions of gases extracted now from the Borzęcin reservoir. The performed analyses show that methane prevails among hydrocarbon gas components, with an average content of 66.77 mol%, the next ones are ethane (1.91 mol%), and propane (0.31 mol%) - the other hydrocarbon components due to their negligible, to the analysed phenomena, concentrations were omitted in the presented specification.



The non-hydrocarbon components are dominated by nitrogen (on average 30.16 mol%), carbon dioxide is next (on average 0.41 mol%, but in samples originating from the B-4 well its amount is highest - 0.68 mol%). During the previously presented discussion of analysis results of gases released from bottomhole water samples, the samples from only the B-4 well showed increased CO₂ and H₂S concentrations. As it is known, the B-4 well is located closest to the well injecting the acid gases. So, there is a phenomenon of increasingly great penetration of the injected gas to the extracted gas.

Also, small amounts of helium (on average 0.18 mol%, at relatively small concentration differences between the wells) were identified in each of the 4 extracted gases. In addition, small hydrogen concentrations (approx. 0.01 mol%, but in the B-4 again the highest, 0.03 mol%) were determined in the tested gases.

Hydrogen sulphide was identified in the gas from each well. Its amount is highest in the gas from the B-4 (0.18 mol%) and from the B-27 (0.15 mol%), albeit the analysis of archive data shows that H₂S concentrations exceeding 0.2 mol% were determined in the past.

The composition of extracted gas is monitored by the reservoir operator in quarterly intervals.

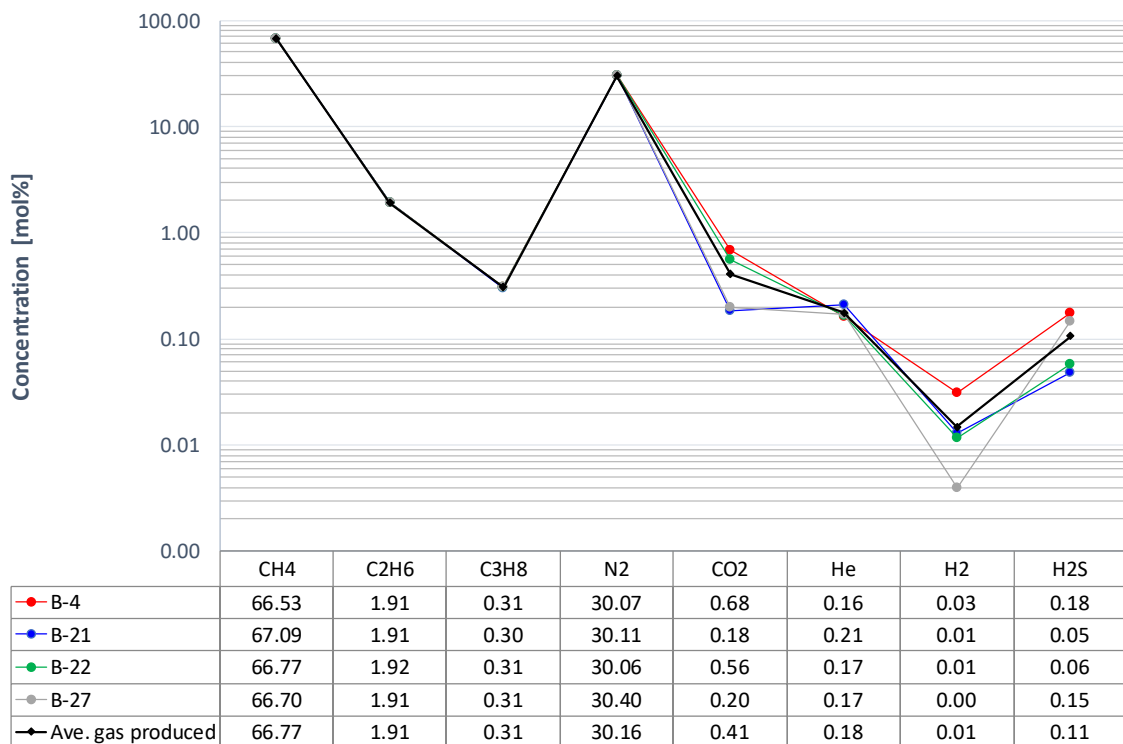


Figure 3.28. Composition of natural gas extracted from the Borzęcin reservoir.

Analyses of injected gas

In February 2020 a pressurised gas sample (5.5 MPa) was taken from the acid gases injection installation, to perform the tests and analyses planned in the project.

Figure 3.29 shows part of the acid gases injection installation situated in the area of the Borzęcin Gas Plant.



Figure 3.29. Installation for acid gases injection to the Borzęcin reservoir.

Figure 3.30 shows the current chemical composition of acid gases re-injected into the Borzęcin reservoir. The last 3 analyses of a POGC, Zielona Góra Branch, laboratory (marked ZG lab) and the last analysis of INiG – PIB, carried out under the SECURE project (marked KE lab), were used.

Carbon dioxide prevails among the main gas components (with an average concentration of 79.9 mole%), hydrocarbon sulphide is next (on average 19.0 mol%). In general, the acid components ($\text{CO}_2 + \text{H}_2\text{S}$) constitute now 99% of the injected gas composition. Minute amounts of hydrocarbon components are the remainder. Methane was identified, with an average content of 0.93 mol%, the next ones are ethane (0.04 mol%), and propane (0.01 mol%) - the other hydrocarbon components were omitted in the presented specification due to their negligible concentration. Trace amounts of helium and hydrogen appear occasionally; in most cases, both gases are below the threshold of method detectability (<0.01 mol% for He and <0.001 mol% for H_2).

The composition of the injected gas is monitored by the reservoir operator in quarterly intervals.

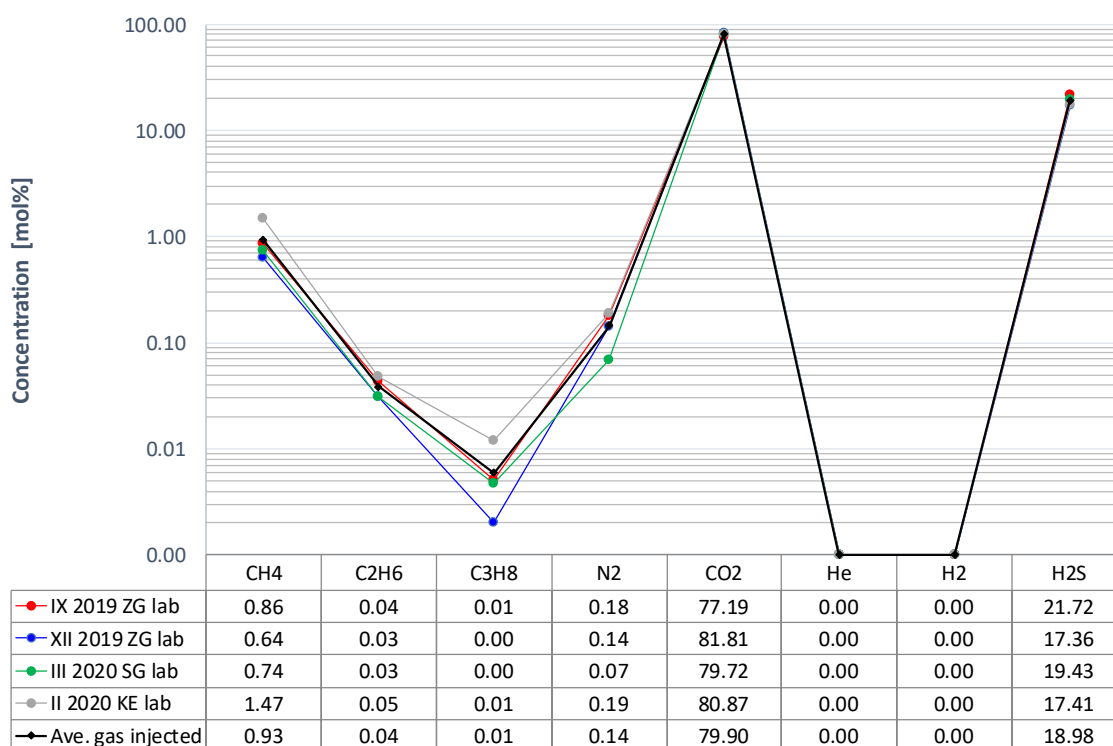


Figure 3.30. Composition of acid gas injected directly to waters underlying the Borzęcin gas reservoir.



3.2.2. Isotopic composition

The determination of isotope composition of stable carbon, hydrogen and nitrogen isotopes in gas dissolved in brine and in the produced (free) gas to investigate the possible temporal/spatial variability and to make an attempt to assess the migration of the injected gas components based on analyses from individual wells. In 2018, isotope determination was carried out for gas from degassing of downhole reservoir brine samples from the B-4, B-6 and B-24. A year later, in addition to repeated isotope determination in the above wells, an analysis for the B-22 well was also successfully completed. These are the first studies of this type at that site. In addition to that, the isotope composition of gas produced from B-4, B-21, B-22 and B-27 wells was analysed. The isotope composition of the produced gas was analysed in previous years and on a larger scale by a team led by Dr. Pleśniak from the University of Wrocław [6]. As part of the isotope analyses, the values of carbon ($\delta^{13}\text{C}$) in methane, ethane, propane and carbon dioxide, deuterium (δD) in methane, and nitrogen ($\delta^{15}\text{N}$) in molecular nitrogen were determined. In total, in the framework of the SECURE project, the above isotope composition was determined for 11 samples, including 3 brine degassing gas samples drawn in 2018, 4 brine gas degassing samples and 4 produced gas samples drawn in 2019.

Methodology of isotopic composition determination

The isotopic composition of stable carbon, hydrogen and nitrogen isotopes was performed in The Oil and Gas Geochemistry Laboratory of INiG-PIB using a Delta V Advantage Isotope Ratio Mass Spectrometer.

The gas samples are separated on a Trace GC Ultra chromatograph using a 30-meter HP-PLOT/Q capillary column with a diameter of 0,32 mm. The temperature program starts at 35° C (maintained for 4 minutes). Then temperature increases to 210°C (maintained for 5 minutes). The inlet temperature is 150° C. Subsequent separated gas components leaving the column are burnt in reactors of the GC IsoLink device and then they are transferred on the IRMS.

The analytical error is related to the analytical error of the device and the error of the certified standard. Prior to the analysis, a repeatability test (a tenfold reference gas test) is performed. The uncertainty for carbon test must be less than 0,05‰ and for hydrogen than 0,5‰ (otherwise no determinations are made). The uncertainty of the used standards is 0,2‰ for carbon and 3‰ for hydrogen.

Results

The isotope composition of carbon in methane ranged from -35.9‰ to -34.4‰ (average -35.1‰), in ethane from -30.57‰ to -30.1‰ (average -30.2‰), in propane from -26.4‰ to -26.0‰ (average -26.2‰), and in carbon dioxide from -17.58‰ to -3.71‰ (average -10.4). The isotope composition of hydrogen in methane was in the range of: -133.5±-106.9 ‰ (average -118.4 ‰), while the isotope composition of nitrogen ranged from -0.4 to 5.2 ‰ (average 3.4 ‰). The complete results of isotope analyses are presented in Table 3.2

Table 3.2. The isotope composition of analysed samples

	Well No	Sampling date	$\delta^{13}\text{C-C}_1$ [‰ vs. PDB]	$\delta^{13}\text{C-C}_2$ [‰ vs. PDB]	$\delta^{13}\text{C-C}_3$ [‰ vs. PDB]	$\delta^{13}\text{C-CO}_2$ [‰ vs. PDB]	$\delta\text{D-C}_1$ [‰ vs. VSMOW]	$\delta^{15}\text{N-N}_2$ [‰ vs. air]
Produced gas	B-4	21.05.2019	-34.8	-30.3	-26.3	-14.7	-116.3	5.2
	B-21	21.05.2019	-34.6	-30.2	-26.4	-12.4	-115.9	4.6
	B-22	21.05.2019	-34.4	-30.2	-26	-13.9	-117.8	5.2
	B-27	21.05.2019	-34.8	-30.3	-26.4	-12.5	-117.1	4.8
Gas released from the brine	B-22	16.07.2019	-35.9	-30.4	-26	-6	-133.5	4.9
	B-4	17.07.2019	-35	-30.5	-26.1	-16.2	-120.8	1.8
	B-6	18.07.2019	-35.2	-30.5	-26.3	-6.5	-120.5	3.6
	B-24	17.07.2019	-35.3	-30.1	*	-6.7	-128.5	-0.4



B-4	17.07.2018	-34.8	-30.2	-26.3	-17.6	-110.8	3.8
B-6	18.07.2018	-35.2	-30.4	-26.3	-4.5	-106.9	2.4
B-24	17.07.2018	-35.6	-30.6	-26.3	-3.7	-114.6	1.6
Average		-35.1	-30.3	-26.2	-10.4	-118.4	3.4
Min		-35.9	-30.6	-26.4	-17.6	-133.5	-0.4
I Quartile		-35.3	-30.5	-26.3	-14.7	-120.8	1.8
Median		-35.0	-30.3	-26.3	-12.4	-117.1	3.8
III Quartile		-34.8	-30.2	-26.1	-6.0	-114.6	4.9
Max		-34.4	-30.1	-26.0	-3.7	-106.9	5.2

Discussion

A comparison of the stable isotopes of carbon and hydrogen in methane, using the graph presented in Figure 3.31 makes it possible to determine the genetic type of the gas being analysed. All applied points corresponding to the samples analysed are within the area of dry thermogenic gas (Figure 3.31).

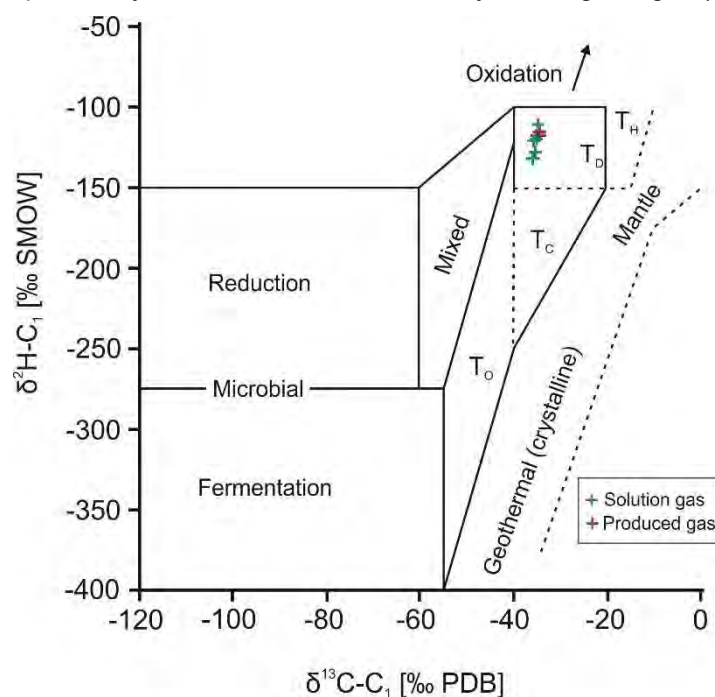


Figure 3.31. Methane carbon and hydrogen isotope diagram presenting the origin of analysed gas. TO, thermogenic with oil; TC, thermogenic with condensate; TD, dry thermogenic; TH: thermogenic with high-temperature [7].

Another method to determine genetic characteristics of the analysed gas based on the isotope composition is to compare the values of stable isotopes of carbon in carbon dioxide and in methane (Figure 3.32).

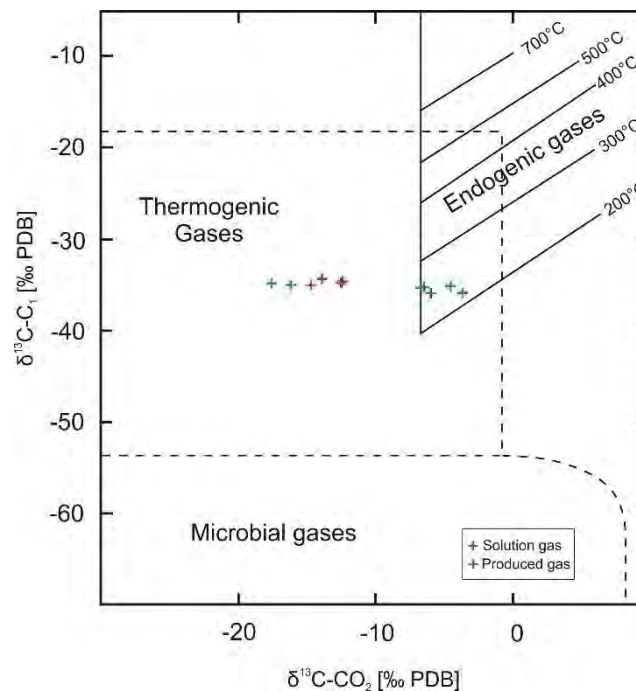


Figure 3.32. Carbon isotopic composition of methane versus carbon dioxide [8].

The location of points corresponding to the analysed samples on the graph of the $\delta^{13}\text{C-C}_1$ and $\delta^{13}\text{C-CO}_2$ relationships indicates mainly the thermogenic origin of the gas, although a shift of some points towards the area typical for endogenous gases is also noticeable (Figure 3.32). The shift of those results towards the area of endogenic gases can be attributed to the enrichment of carbon dioxide in the heavy ^{13}C isotope and it applies to some of the samples of gas dissolved in brine, drawn both, in 2018 and 2019. In the samples of gas dissolved in brine carbon isotopic composition of CO_2 could be shifted towards heavier values as a result of easier dissolving of isotopically lighter CO_2 in brine. Such dissolving results in enrichment of CO_2 with ^{13}C in natural gas. The enrichment of carbon dioxide in a heavier isotope may result from pressure changes in the reservoir caused by annual downtime and release of gas from the blind parts of the reservoir (ventilation/homogenisation). Said enrichment in the heavier ^{13}C isotope can also result from the reduction of carbon dioxide.

Changes in the isotope composition

The isotope composition of carbon in methane, ethane and propane appears to be unchanged and independent of the type of gas sample drawn and the time of sampling. The differences in the extreme values of carbon isotope composition in methane are about 1.5‰ (approximately 4%) and, in ethane and propane, ca. 0.4 ‰ (approximately 1.5%) (Table 3.2).

However, changes in the isotope composition of hydrogen in methane are noticeable. The isotope composition of hydrogen in the extracted gas samples is distinguished by enrichment in a heavier isotope, the deuterium, relative to gas samples from brine degassing drawn in 2019 (Figure 3.33). Produced gas samples were drawn two months before the brine downhole samples from which the gas was obtained. A difference in the isotope composition of the hydrogen between the samples from brine degassing drawn at annual intervals is also evident. Samples drawn in 2018 are characterised by being enriched in heavy hydrogen isotope, compared to samples drawn the following year (Figure 3.34). The isotope composition of hydrogen in methane reveals some changing in time trend since, as demonstrated by the analyses completed, the later the sampling time, the greater is the depletion of the heavier hydrogen isotope (Table 3.2; Figure 3.33). Figure 3.35 shows spatial variability of the carbon isotope composition in the gas from brine degassing, based on the series of measurements carried out in 2019. in relation to the distance from the well for injecting acid gases (B-28). Some results (except for the closest B-4 well) show a characteristic trend of depletion of the heavier carbon isotope as the distance from the B-28 well increases (Figure 3.35). However, such conclusions should be taken with caution as the differences are close to the analytical uncertainty.

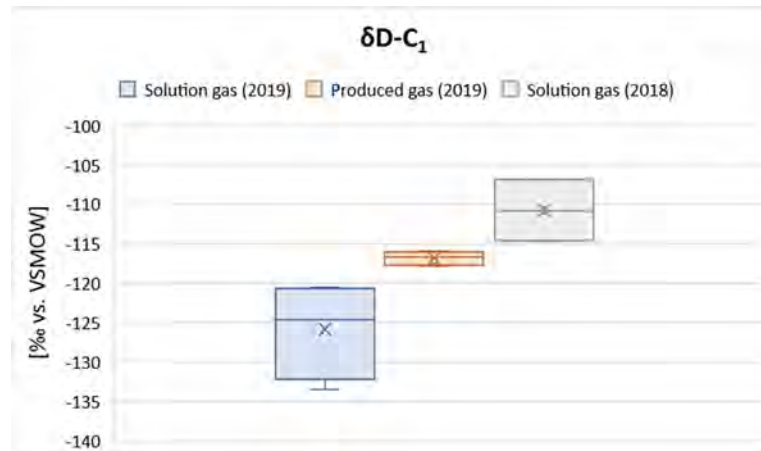


Figure 3.33. Variability of the isotope composition of hydrogen in methane.

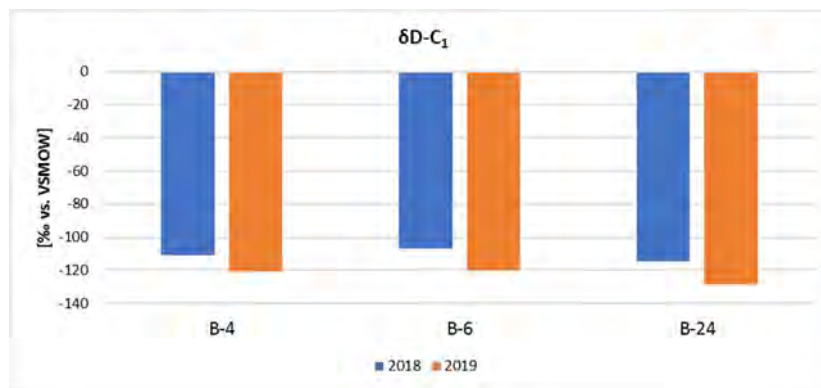


Figure 3.34. Temporal variability of the hydrogen isotope composition in methane – gas samples from brine degassing.

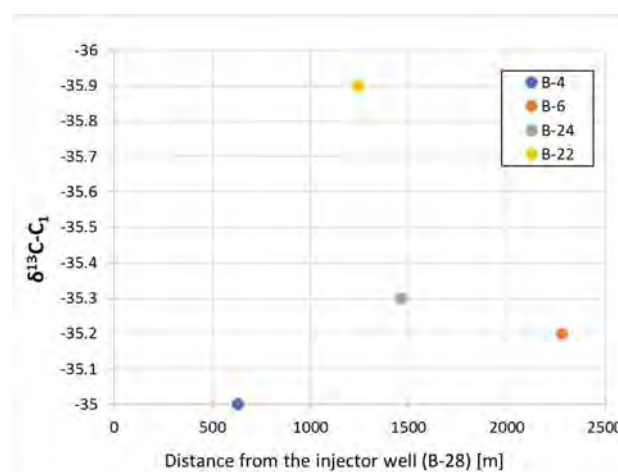


Figure 3.35. Variability of the carbon isotope composition in methane in relation to the distance from the acid gas injection well (B-28) – gas samples from brine degassing drawn in 2019.

The variability in the carbon isotope composition is noticeable in the case of carbon dioxide. Samples of the extracted gas are characterised the depletion of CO₂ of the heavier carbon isotope, compared to gas samples from brine degassing (Figure 3.36). For the brine degassing gas analyses, results should be distinguished for



samples from the B-4 well, characterised by a noticeably lower content of the heavier carbon isotope in CO₂ than in the others during both, the first (2018) and the second (2019) measuring series (Figure 3.37).

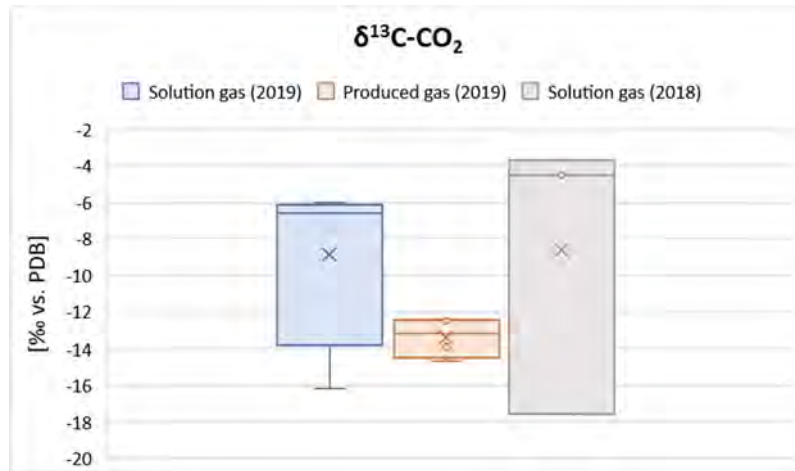


Figure 3.36. Variability of isotope composition of carbon in carbon dioxide.

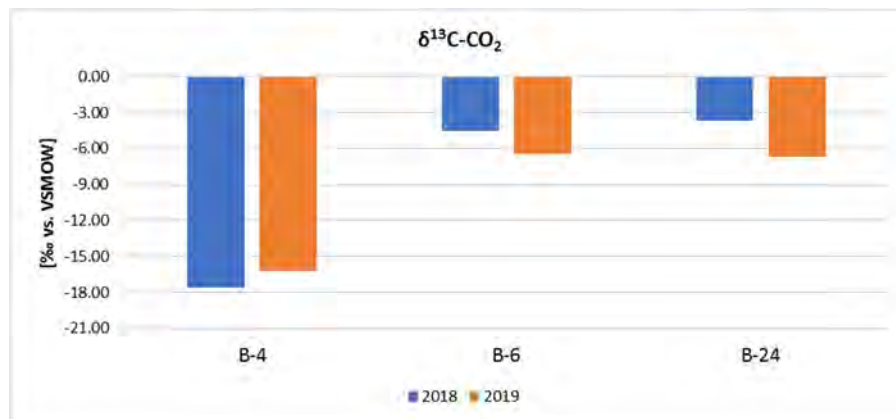


Figure 3.37. Variability of isotope composition of carbon in carbon dioxide.

The B-4 well, for which the lowest $\delta^{13}\text{C-CO}_2$ values were noticed, standing out from the other analysed gas samples from the brine degassing, is located closest to the B-28 productive well for injecting acid gases (Figure 3.38).

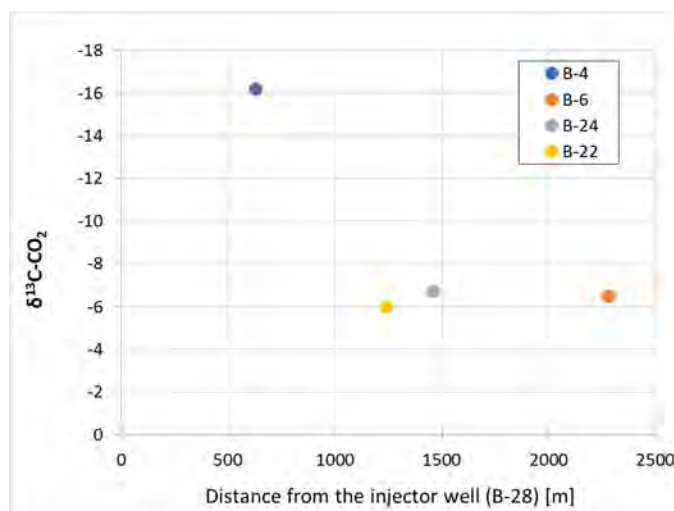


Figure 3.38. Variability of the carbon isotope composition in CO₂ in the brine degassing gas in relation to the distance from the acid gas injection well (B-28) – in 2019.

3.3 RESERVOIR WATER ANALYSIS

The analyses of physiochemical parameters of bottom water underlying the Borzęcin reservoir were carried out by testing downhole samples drawn from the productive wells B-4, B-6, B-24 and B-22 and surface samples of water drawn from the wells B-21, B-22 and B-27. The tests of the downhole samples in wells B-4, B-6 and B-24 were repeated at approximately one-year interval.

In most cases, the analysed water is reservoir brine. Only the samples drawn from the B-22 (downhole sample) and B-22 (surface sample) wells indicate condensation water and will not be a part of further considerations.

The extracted liquid was colourless to yellowish green colour. In most cases, the liquid had an opalescent suspension of sulphides visible to the naked eye. The odour of hydrogen sulphide was clearly perceptible.

The amount of substances dissolved in the analysed samples falls within the range 228-251 g/l and 243 g/l on average. The density ranges from 1.153 ÷ 1.166 g/cm³, 1.156 g/cm³ on average. The average conductivity is 205 mS/cm. The pH of the samples analysed ranges from 4.5 to 6.5, with an average of 5.4. The chemical composition of the brine analysed is dominated by chloride and sodium ions. The percentage of chloride ion among anions is greater than 99%, while that of sodium ions among cations is ~ 78% (Figure 3.39 and Figure 3.40). The averaged percentage of anions and cations (% mval) is shown in Table 3.3.

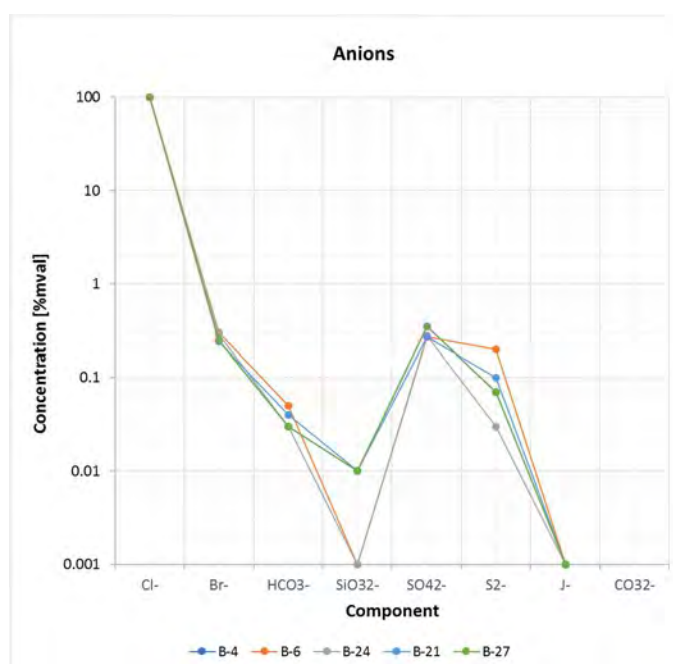


Figure 3.39. Percentage of anions in samples from individual wells.

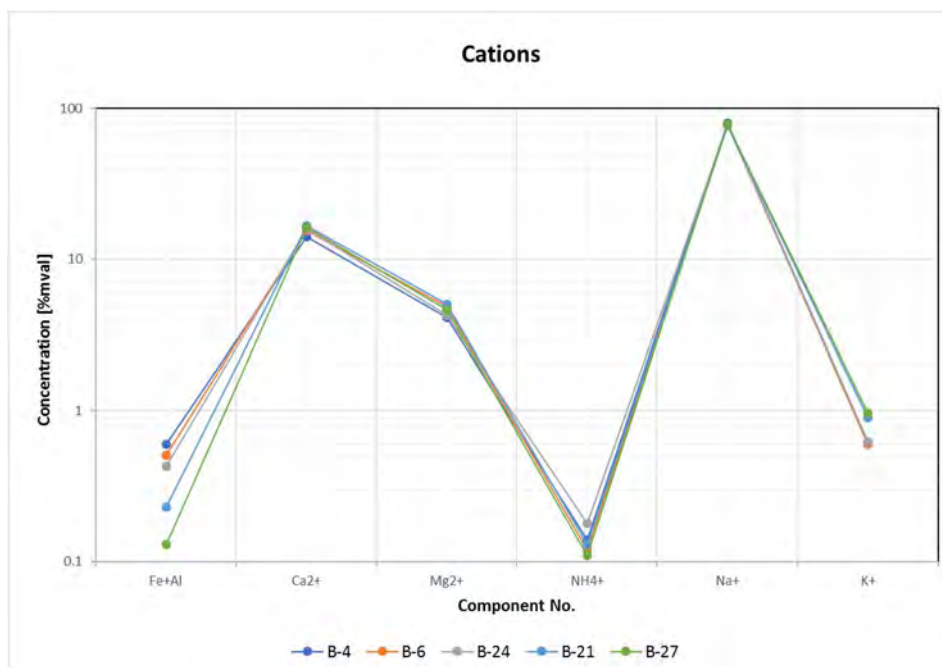


Figure 3.40. Percentage of cations in samples from individual wells.

Table 3.3. Average ionic composition of the Borzęcin reservoir brine.

Anions	Component	Concentration [%mval]
	Cl ⁻	99.37
	Br ⁻	0.26
	HCO ₃ ⁻	0.03
	SiO ₃ ²⁻	0.01



Cations	SO ₄ ²⁻	0.28
	S ²⁻	0.08
	J-	<0.001
	CO ₃ ²⁻	0.0
	Fe+Al	0.38
	Ca ²⁺	15.75
	Mg ²⁺	4.59
	NH ₄ ⁺	0.14
	Na ⁺	78.40
	K ⁺	0.74

The chemical analyses repeated for the same wells at an annual interval did not show significant changes in the concentration of individual components over time either. A slight increase in the percentage of Na⁺, NH₄⁺ and Mg²⁺ cations can be observed at the cost of the Ca²⁺ and K⁺ ones. However, those changes are slight, below 1 percentage point (Figure 3.41).

Differences in the concentration of individual components between samples drawn from individual wells are insignificant and, in the case of anions, even negligible (on average below 0.1 percentage point). For cations, the differences observed, mainly concerning Ca²⁺ and K⁺, are slightly higher and amount to a maximum of ~ 3 percentage points.

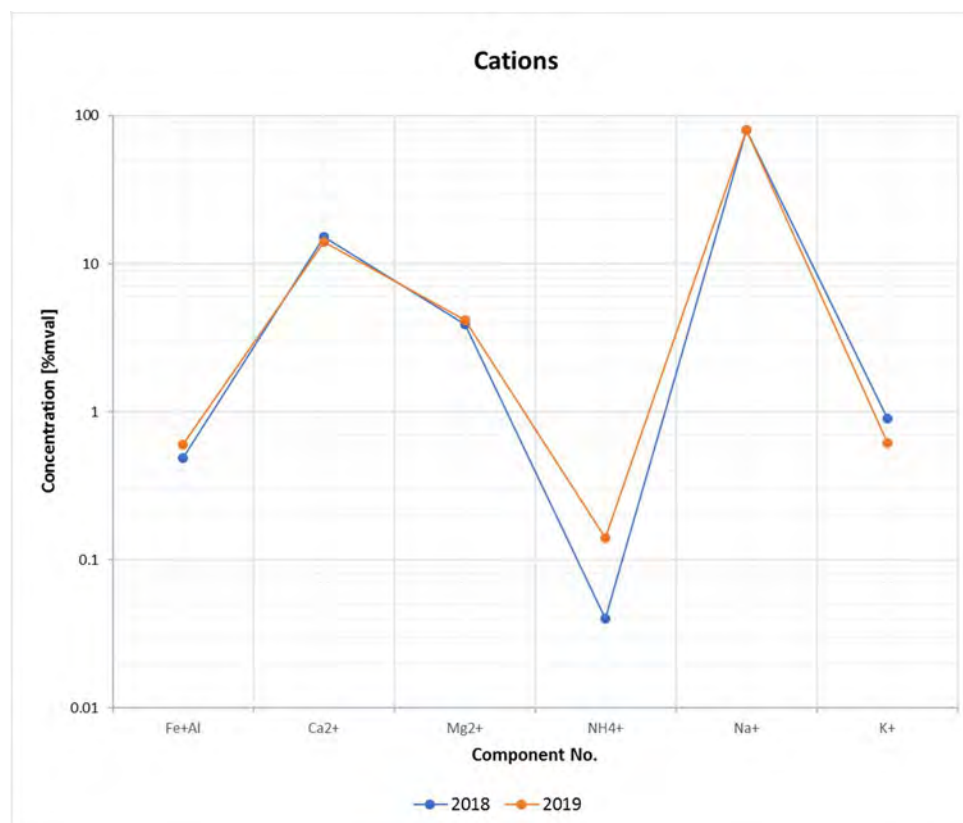


Figure 3.41. The difference in the percentage of individual cations in the samples drawn at annual intervals on the example of the B-24 productive well.



In the analysed water samples, the presence of dissolved hydrogen sulphide was found in the range of 0.015-0.065 g/l (0.039 g/l on average) and sulphides in the range of 0.0016-0.0056 (0.0033 g/l on average).

Salinity and alkalinity of the brine calculated by the Palmer method [9], take the following averaged values:

- First order salinity: 79.45
- Second order salinity: 20.49
- Second order alkalinity: 0.05.

Table 3.4 presents a set of hydrochemical indicators calculated on the basis of the ionic content of individual components. In the case of productive wells where tests were performed twice, an averaged value from two analyses was presented.



Table 3.4. Hydrogeochemical indicators for the analysed samples.

Ion ratio	B-24	B-6	B-4	B-21	B-27	Average	Min	Max	Change Max/min %
Cl ⁻ /HCO ₃ ⁻	3616.62	2855.54	2464.37	3138.45	2221.98	2859.39	2221.98	3616.62	62.8
Cl ⁻ /(HCO ₃ ⁻ +CO ₃ ²⁻)	3616.62	2855.54	2464.37	3138.42	2221.98	2859.38	2221.98	3616.62	62.8
Cl ⁻ /Br ⁻	348.30	374.48	351.99	361.64	407.90	368.86	348.30	407.90	17.1
Cl ⁻ /SO ₄ ²⁻	355.79	372.07	367.18	313.51	337.73	349.26	313.51	372.07	18.7
Na ⁺ /Cl ⁻	0.82	0.83	0.83	0.77	0.80	0.81	0.77	0.83	7.5
Na ⁺ /Ca ²⁺	4.86	4.88	4.95	4.60	4.78	4.81	4.60	4.95	7.7
Na ⁺ /(Ca ²⁺ +Mg ²⁺)	3.87	3.85	3.84	3.53	3.70	3.76	3.53	3.87	9.5
Na ⁺ /SO ₄ ²⁻	292.02	306.91	304.04	241.32	271.16	283.09	241.32	306.91	27.2
Ca ²⁺ /Mg ²⁺	3.92	3.72	3.47	3.32	3.51	3.59	3.32	3.92	18.1
(%Cl- %Na)/%Mg	5.09	4.65	4.82	4.44	4.64	4.73	4.44	5.09	14.6
%SO ₄ x100/%Cl	0.28	0.27	0.36	0.32	0.30	0.31	0.27	0.36	31.2

3.4 PVT ANALYSIS

Constant Mass Expansion (CME) tests were carried out to determine significant parameters of the extracted gas, i.e. the gas volume factor – B_g and the gas deviation factor Z . They consist in the sample volume expansion in a pressure cell at a pre-set testing temperature. The total mass of the sample does not change – its volume and possibly phase state change (depending on the tested reservoir fluid). The CME test was performed on gas from the B-22 well (considered identical with the Borzęcin reservoir gas) at two temperatures, i.e. ambient (20°C) and reservoir (46.8°C) temperature. Results of CME tests are presented in Tables (Table 3.5, Table 3.6 and Table 3.7) and graphs showing changes of parameters B_g (Figure 3.42) and Z (Figure 3.43) versus pressure. Considering safety issues and instrument limitations, dictated by a high hydrogen sulphide content, experimental CME tests of the injected acid gas were abandoned. The gas deviation factor Z (Figure 3.44) and the phase diagram (Figure 3.45) of the acid gas were generated, based on its composition, by means of the PVTsim simulation software. In the presented phase diagram (Figure 3.45) it is illustrated that the injected mixture of acid gases, under reservoir conditions, exists only in the gas phase. The condensation of a certain (small) amount of liquid from the injected gas can occur in the well at the existence of particular thermobaric conditions – determined by the saturation curves.

After contact tests, a flash separation experiment was performed on a part of the sample from the test chamber – one-stage separation from a pressure of 99 bar to 1 bar at ambient temperature (Table 3.8). The results obtained from the flash separation experiment were indispensable for appropriate balancing of the CME experiment.

The determination of solubility (R_s) both of the extracted gas and the acid gas re-injected to the reservoir brine was a significant test for considerations and simulation of migration of the injected gases in the aquifer underlying the Borzęcin reservoir. Solubility tests were carried out at the reservoir temperature and in five pressure steps (Table 3.9), based on which the solubility curve was drawn. The injected acid gas features definitely much higher solubility in the reservoir brine, even 23 times more – depending on the pressure, than the extracted gas. Table 3.9 presents results of solubility tests and Figure 3.46– a graph of solubility coefficient versus pressure.



Table 3.5. Main PVT Results.

Reservoir conditions		
Reservoir pressure (initial)	15.55	MPa
Reservoir pressure (current)	3.97	MPa
Reservoir temperature	46.8	°C
Constant mass expansion study at 46.8°C (320.0 K)		
Dew point pressure	Not found	MPa
Gas volume factor B_g at actual reservoir conditions	0.00974	m ³ /Nm ³
Gas deviation factor Z at actual reservoir conditions	0.887	-
Constant mass expansion study at 20.0°C (293.1 K)		
Dew point pressure	Not found	MPa
Solubility study in the reservoir water at 46.8°C (320.0 K)		
Produced gas		
at actual pressure 3.97 MPa	0.248	Nm ³ /m ³
at initial pressure 15.5 MPa	0.801	Nm ³ /m ³
Injected gas		
At actual pressure 3.97 MPa	5.80	Nm ³ /m ³
At initial pressure 15.5 MPa	7.31	Nm ³ /m ³
Flash separation to ambient conditions		
from: 99.05 bar; 20.0°C		
to: 0.985 bar; 20.0°C (ambient)		
Flash GLR	-	Nm ³ /m ³
Flashed Gas Gravity (air = 1)	0.6989	-
Flashed Gas Density	0.9036	kg/m ³
Flash Liquid Density	No liquid	g/cm ³



Table 3.6. Results of Constant Mass Expansion test (CME) of produced gas (B-22) at 20°C.

Pressure	Sample Volume	Gas Volume Factor	Gas Deviation Factor Z	Liquid Sample Volume
P	V	B _g	Z	V _L
MPa	cm ³	m ³ /Nm ³	-	%V _{dp}
1	2	3	4	5
49.131	24.97	0.00275	1.241	-
44.228	26.24	0.00289	1.174	-
39.325	27.90	0.00307	1.110	-
34.421	30.06	0.00331	1.046	-
29.518	32.80	0.00361	0.979	-
24.615	37.41	0.00411	0.931	-
19.711	44.86	0.00493	0.894	-
14.808	58.39	0.00642	0.874	-
12.356	70.15	0.00772	0.877	-
9.905	88.69	0.00975	0.888	-
5.658	162.12	0.01783	0.928	-
4.619	201.15	0.02212	0.940	-
3.893	240.76	0.02648	0.948	-
3.040	312.04	0.03432	0.959	-
2.442	391.27	0.04303	0.966	-



Table 3.7. Results of Constant Mass Expansion test (CME) of produced gas (B-22) at 46.8°C.

Pressure	Sample Volume	Gas Volume Factor	Gas Deviation Factor Z	Liquid Sample Volume
P	V	B _g	Z	V _L
MPa	cm ³	m ³ /Nm ³	-	%V _{dp}
1	2	3	4	5
49.131	27.45	0.0030	1.249	-
44.228	28.92	0.0032	1.185	-
39.325	30.88	0.0034	1.125	-
34.421	33.43	0.0037	1.066	-
29.518	37.05	0.0041	1.013	-
24.615	42.25	0.0046	0.964	-
19.711	50.98	0.0056	0.931	-
14.808	66.98	0.0074	0.919	-
12.356	80.23	0.0088	0.918	-
11.140	89.35	0.0098	0.922	-
6.325	161.08	0.0177	0.944	-
5.139	200.14	0.0220	0.953	-
4.310	239.98	0.0264	0.958	-
3.981	260.59	0.0287	0.961	-
3.344	311.71	0.0343	0.966	-
2.682	391.30	0.0430	0.972	-

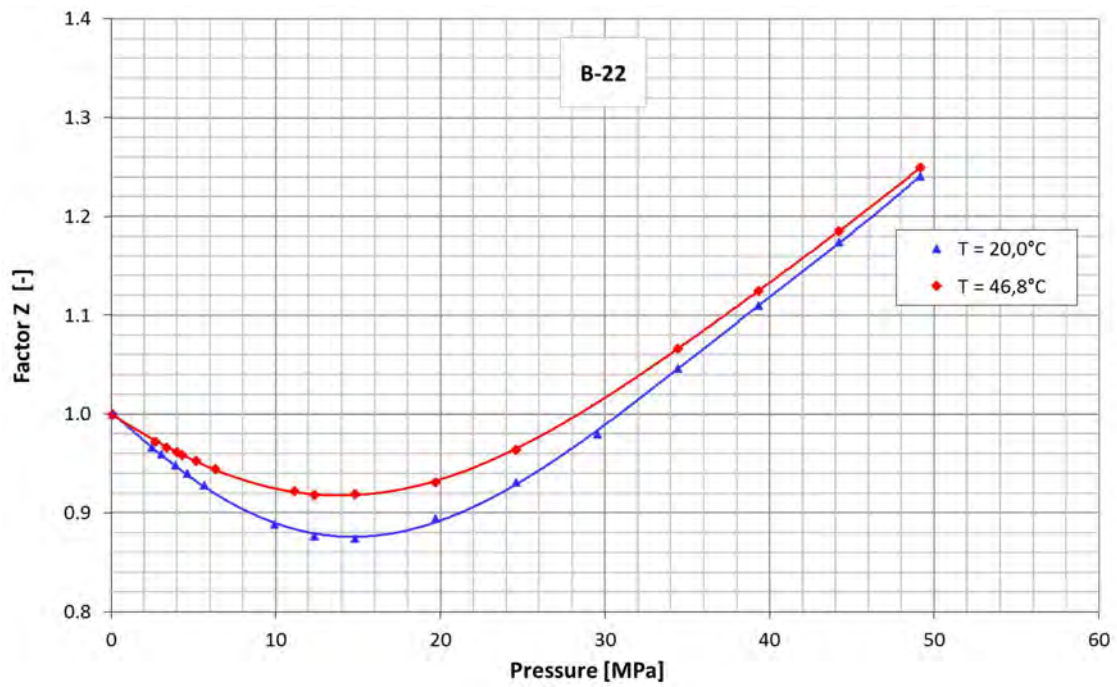


Figure 3.42. Gas deviation factor Z – CME test of the produced gas.

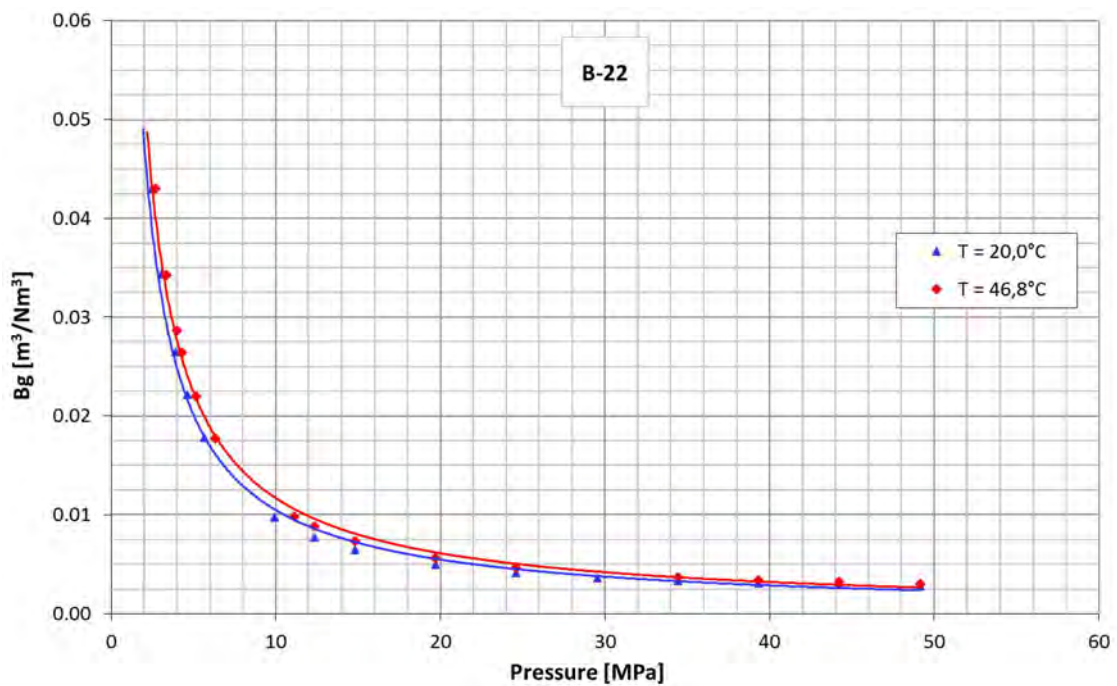


Figure 3.43. Gas volume factor B_g – CME test of the produced gas.



Table 3.8. Results of flash separation to the ambient conditions.

Pressure	Temperature	Flash GLR	Flashed Gas Gravity	Z Factor	Gas Volume Factor B_g
bar	°C	Nm ³ /m ³	air = 1	-	m ³ /Nm ³
99.05	20.0	-	-	0.887	0.00974
0.985	20.0	0.0	0.699	-	1.00

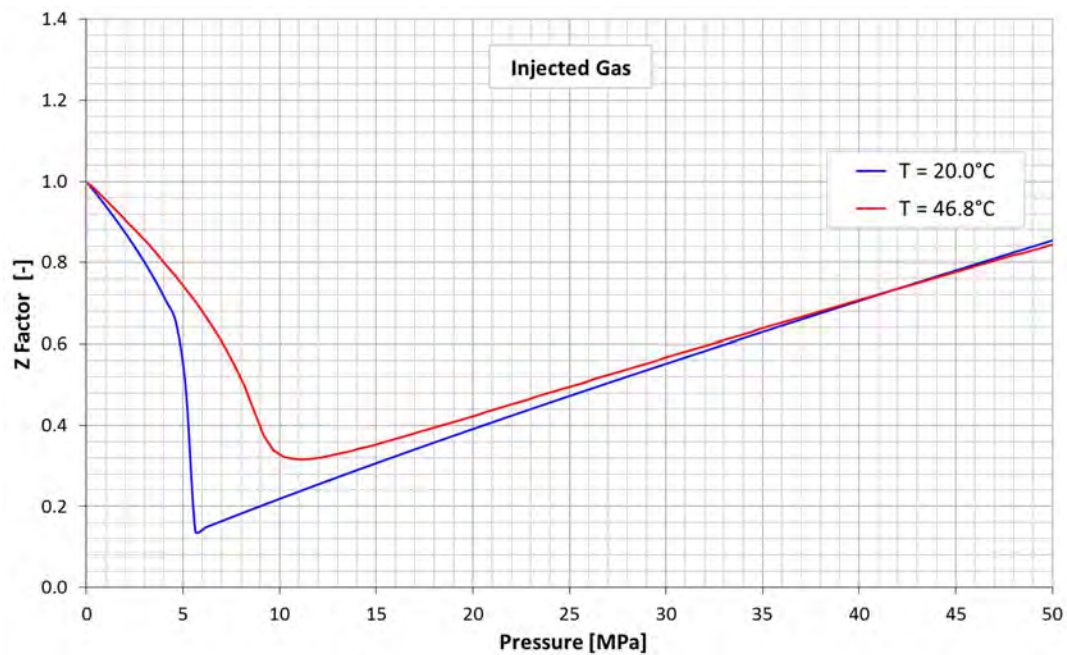


Figure 3.44. Gas deviation factor Z of the injected gas generated by the PVTsim software.

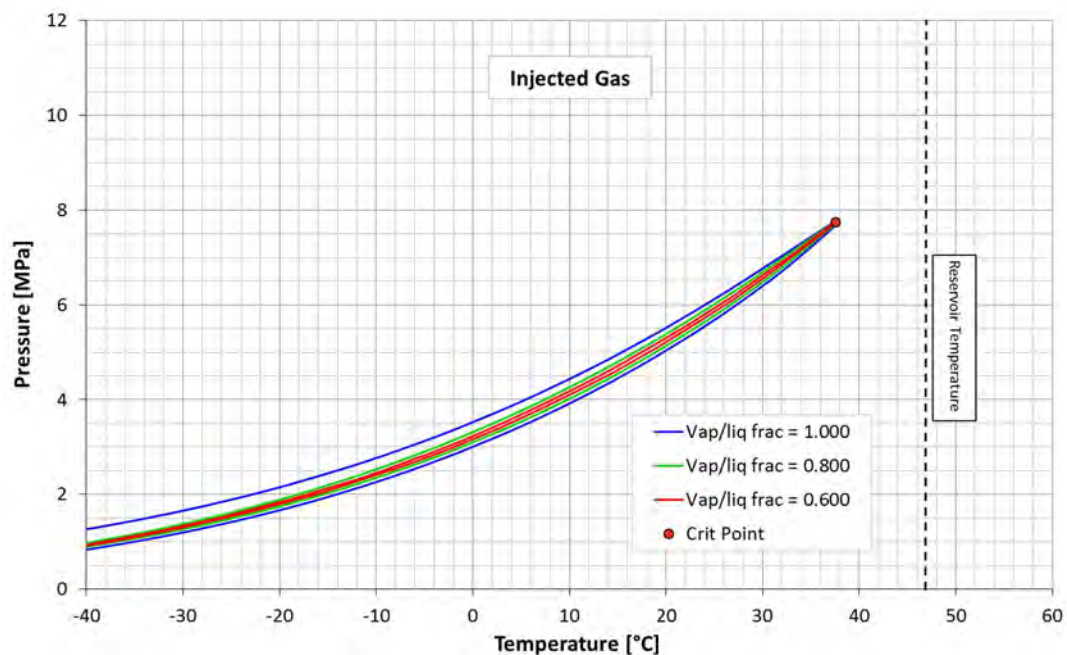


Figure 3.45. Phase diagram of the injected gas generated by the PVTsim software.



Table 3.9. Results of gas solubility tests in the reservoir water.

Pressure [MPa]	Solubility [Nm ³ /m ³]	
	Produced gas	Injected gas
0.10	0.000	0.00
2.00	0.13	3.20
3.97	0.25	5.80
9.72	0.56	7.09
15.5	0.80	7.31

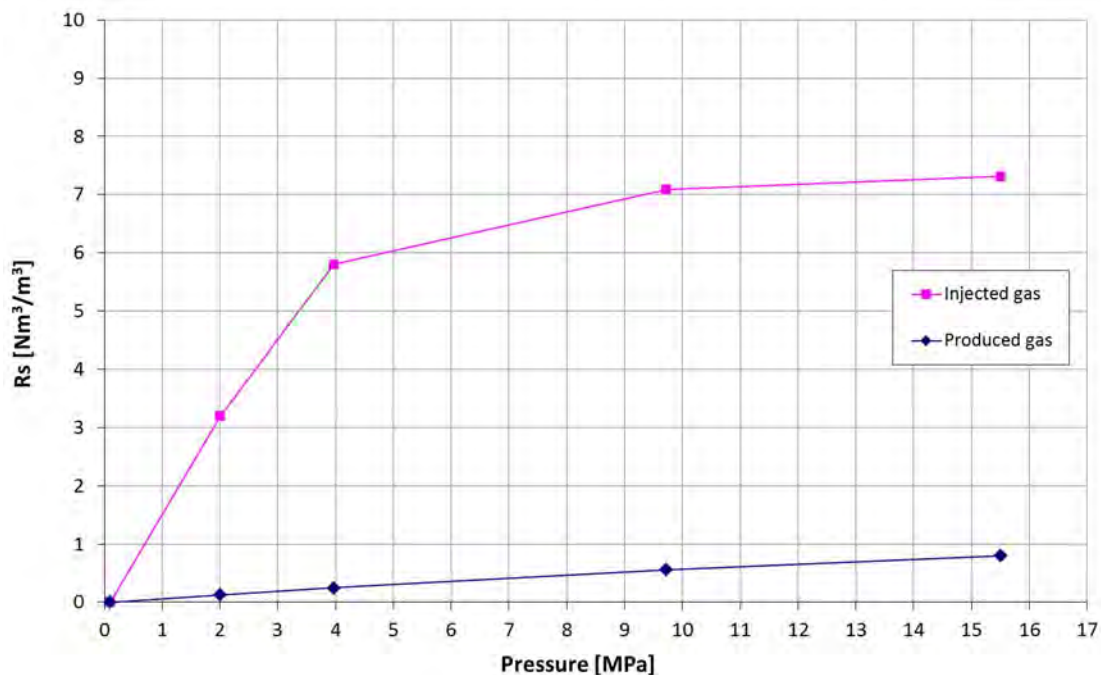


Figure 3.46. Solubility of gases in Borzęcin reservoir water.

3.5 SOIL GAS ANALYSIS

Selection of wells for examination – measurement series 1-3

In order to determine the potential impact of acid gas injection into the Borzęcin reservoir and investigate possible leakage, the measurements of soil gas composition were carried out. The gas samples were taken from monitoring wells located at three production wells, that is B-6 – a now abandoned observation well, although the most gas has been produced so far from that reservoir, B-22 – currently the most efficient production well (80% of current production), and B-28 – a well injecting acid gases into the aquifer underlying the natural gas reservoir – Figure 3.47.

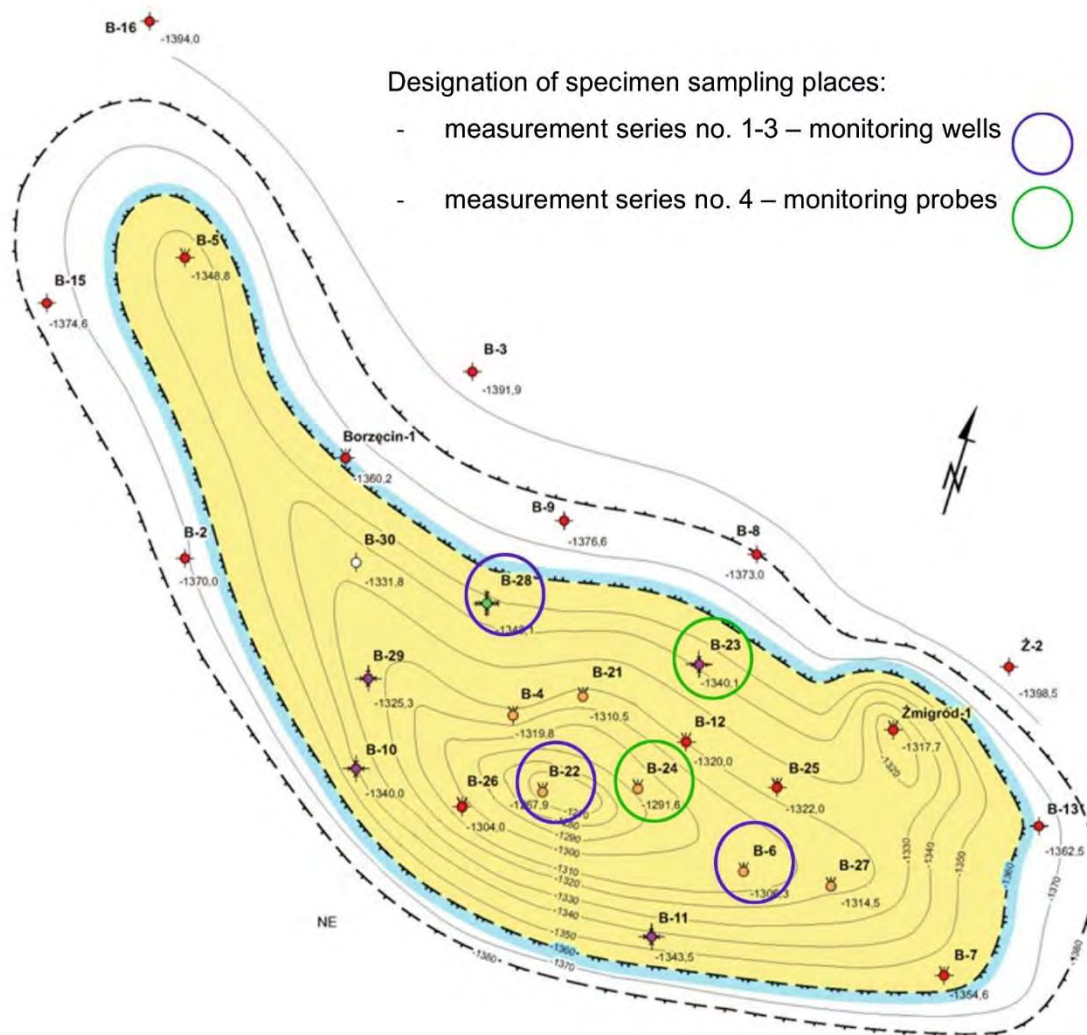


Figure 3.47. Location of wells in the area of the Borzęcin natural gas reservoir with soil gas sampling sites indicated.

The B-28 well was drilled in 1987. Despite the intensification of efforts, including two-stage acid treatment, it failed producing on a commercial scale and it was intended to be abandoned. In 1994, reconstruction works were carried out on the well to adapt it to injecting acid gases (CO₂, H₂S). In January 1996, with the B-28 well, the process of reinjection of acid gases into the reservoir and, more precisely, directly into the aquifer underlying the Borzęcin natural gas reservoir, was initiated. Acid gases are waste products from the amine sweetening plant for natural gas extracted from the Borzęcin reservoir. The present composition of the injected gas is as follows:

Component	Percentage
CO ₂	77.2
H ₂ S	21.7
CH ₄	0.9
N ₂	0.18

The B-28 well is a key component of the acid gas reinjection system at the Borzęcin sequestration facility, and its proper technical condition is crucial for the safety of the entire project.

Soil gas sampling from monitoring wells – measurement series 1-3



The monitoring wells were installed on October 23-25, 2019. They were located directly at the wells (at the wellhead within the near well zone) and at a distance of approx. 35 metres from the wellhead. The location of the measuring points is shown in Figure 3.48, Figure 3.49 and Figure 3.50, below.



Figure 3.48. Location of measuring points at the B-6 well.

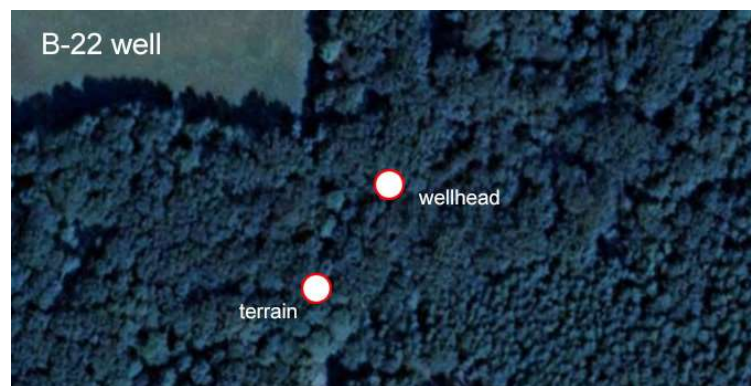


Figure 3.49. Location of measuring points at the B-22 well.



Figure 3.50. Location of measuring points at the B-28 well.

The gas was sampled from six 2-metre-deep monitoring wells. A monitoring well was made of PE pipe embedded in gravel backfill. In the lower part of the pipe, along an 80 cm section, there was a perforation made enabling the free inflow of soil gas. The sampling was carried out using glass pipettes and a vacuum pump (Figure 3.51 and Figure 3.52).



Figure 3.51. Soil gas sampling from a monitoring well located within the B-28 well pad.



Figure 3.52. Soil gas sampling from a monitoring well located within 35 metres of the B-22 wellhead.

Determination of the sampled gas composition – measurement series 1-3

The composition of gas sampled in the first three measurement series was examined by the INiG – PIB Department of Production Technology laboratory. Chromatographic analyses of the sampled gas were performed using a two-channel valve Clarus 680 GC Perkin Elmer-Arnel chromatograph with thermal conductivity (TCD) and flame ionisation (FID) detectors. The apparatus was coupled with TotalChrom Navigator software. The chromatographic system is periodically calibrated with the certified standard gas mixtures. Before each analysis, the device was tested and checked with the reference mixture. A total of three measurement series were completed, the results of which are given in Table 3.10, Table 3.11 and Table 3.12, below.



Table 3.10. Composition of soil gas samples drawn at the B–6 well.

Component	Content [% mol]					
	21/11/2019		17/01/2020		26/02/2020	
	wellhead	field	wellhead	field	wellhead	field
oxygen	20.9	19.9	21.1	20.7	20.5	20.5
nitrogen	79.0	79.6	78.8	78.9	76.9	76.5
carbon dioxide	0.08	0.56	0.09	0.39	0.06	0.24
hydrogen sulphide	n.i.	n.i.	n.i.	n.i.	n.i.	n.i.
helium	n.i.	n.i.	n.i.	n.i.	n.i.	n.i.
methane	0.0279	0.0073	n.i.	0.0193	2.4707	2.6402
ethane	0.0004	0.0005	n.i.	0.0015	0.1143	0.1147
propane	n.i.	n.i.	n.i.	n.i.	0.0116	0.0116
i-butane	n.i.	n.i.	n.i.	n.i.	0.0020	0.0020
n-butane	n.i.	n.i.	n.i.	n.i.	0.0019	0.0019
neo-pentane	n.i.	n.i.	n.i.	n.i.	n.i.	n.i.
i-pentane	n.i.	n.i.	n.i.	n.i.	0.0003	0.0004
n-pentane	n.i.	n.i.	n.i.	n.i.	0.0002	0.0003
2,3-dimethylbutane	n.i.	n.i.	n.i.	n.i.	n.i.	n.i.
2-methylpentane	n.i.	n.i.	n.i.	n.i.	n.i.	n.i.
3-methylpentane	n.i.	n.i.	n.i.	n.i.	n.i.	n.i.
n-hexanes	n.i.	n.i.	n.i.	n.i.	n.i.	n.i.
benzene	n.i.	n.i.	n.i.	n.i.	n.i.	n.i.
C ₆ – unidentified	n.i.	n.i.	n.i.	n.i.	n.i.	n.i.
Σ-C ₆	–	–	–	–	–	–
2,4-dimethylpentane	n.i.	n.i.	n.i.	n.i.	n.i.	n.i.
2-methyl-hexane	n.i.	n.i.	n.i.	n.i.	n.i.	n.i.
3-methyl-hexane	n.i.	n.i.	n.i.	n.i.	n.i.	n.i.
2,3-dimethylpentane	n.i.	n.i.	n.i.	n.i.	n.i.	n.i.
n-heptane	n.i.	n.i.	n.i.	n.i.	n.i.	n.i.
toluene	n.i.	n.i.	n.i.	n.i.	n.i.	n.i.
C ₇ – unidentified	n.i.	n.i.	n.i.	n.i.	n.i.	n.i.
Σ-C ₇	–	–	–	–	–	–
2,3,4-trimethylpentane	n.i.	n.i.	n.i.	n.i.	n.i.	n.i.
2,2-dimethylhexane	n.i.	n.i.	n.i.	n.i.	n.i.	n.i.
2,4-dimethylhexane	n.i.	n.i.	n.i.	n.i.	n.i.	n.i.
2-methylheptane	n.i.	n.i.	n.i.	n.i.	n.i.	n.i.
3-methylheptane	n.i.	n.i.	n.i.	n.i.	n.i.	n.i.
n-octane	n.i.	n.i.	n.i.	n.i.	n.i.	n.i.
xylenes	n.i.	n.i.	n.i.	n.i.	n.i.	n.i.
C ₈ – unidentified	n.i.	n.i.	n.i.	n.i.	n.i.	n.i.
Σ-C ₈	–	–	–	–	–	–
Σ-C ₉	n.i.	n.i.	n.i.	n.i.	n.i.	n.i.
Σ-C ₁₀	n.i.	n.i.	n.i.	n.i.	n.i.	n.i.
Σ-C ₁₁	n.i.	n.i.	n.i.	n.i.	n.i.	n.i.
Σ-C ₁₂	n.i.	n.i.	n.i.	n.i.	n.i.	n.i.
TOTAL	100.0000	100.0000	100.0000	100.0000	100.0000	100.0000



Table 3.11. Composition of soil gas in samples drawn at the B-28 well.

Component	Content [% mol]					
	21/11/2019		17/01/2020		26/02/2020	
	wellhead	field	wellhead	field	wellhead	field
oxygen	18.7	19.2	21.5	21.0	21.3	21.5
nitrogen	80.5	80.0	78.3	78.6	78.1	78.1
carbon dioxide	0.23	0.75	0.07	0.40	0.05	0.10
hydrogen sulphide	n.i.	n.i.	n.i.	n.i.	n.i.	n.i.
helium	n.i.	n.i.	n.i.	n.i.	n.i.	n.i.
methane	0.5633	0.0025	0.0755	0.0463	0.5096	0.2582
ethane	0.0039	n.i.	0.0025	0.0012	0.0185	0.0950
propane	0.0002	n.i.	0.0002	0.0001	0.0018	0.0010
i-butane	0.0001	n.i.	n.i.	n.i.	0.0004	0.0001
n-butane	0.0002	n.i.	n.i.	n.i.	0.0003	0.0001
neo-pentane	n.i.	n.i.	n.i.	n.i.	n.i.	n.i.
i-pentane	n.i.	n.i.	n.i.	n.i.	n.i.	n.i.
n-pentane	n.i.	n.i.	n.i.	n.i.	n.i.	n.i.
2.3-dimethylbutane	n.i.	n.i.	n.i.	n.i.	n.i.	n.i.
2-methylpentane	n.i.	n.i.	n.i.	n.i.	n.i.	n.i.
3-methylpentane	n.i.	n.i.	n.i.	n.i.	n.i.	n.i.
n-hexanes	n.i.	n.i.	n.i.	n.i.	n.i.	n.i.
benzene	n.i.	n.i.	n.i.	n.i.	n.i.	n.i.
C ₆ – unidentified	n.i.	n.i.	n.i.	n.i.	n.i.	n.i.
Σ-C ₆	–	–	–	–	–	–
2.4-dimethylpentane	n.i.	n.i.	n.i.	n.i.	n.i.	n.i.
2-methyl-hexane	n.i.	n.i.	n.i.	n.i.	n.i.	n.i.
3-methyl-hexane	n.i.	n.i.	n.i.	n.i.	n.i.	n.i.
2.3-dimethylpentane	n.i.	n.i.	n.i.	n.i.	n.i.	n.i.
n-heptane	n.i.	n.i.	n.i.	n.i.	n.i.	n.i.
toluene	n.i.	n.i.	n.i.	n.i.	n.i.	n.i.
C ₇ – unidentified	n.i.	n.i.	n.i.	n.i.	n.i.	n.i.
Σ-C ₇	–	–	–	–	–	–
2.3.4-trimethylpentane	n.i.	n.i.	n.i.	n.i.	n.i.	n.i.
2.2-dimethylhexane	n.i.	n.i.	n.i.	n.i.	n.i.	n.i.
2.4-dimethylhexane	n.i.	n.i.	n.i.	n.i.	n.i.	n.i.
2-methylheptane	n.i.	n.i.	n.i.	n.i.	n.i.	n.i.
3-methylheptane	n.i.	n.i.	n.i.	n.i.	n.i.	n.i.
n-octane	n.i.	n.i.	n.i.	n.i.	n.i.	n.i.
xylenes	n.i.	n.i.	n.i.	n.i.	n.i.	n.i.
C ₈ – unidentified	n.i.	n.i.	n.i.	n.i.	n.i.	n.i.
Σ-C ₈	–	–	–	–	–	–
Σ-C ₉	n.i.	n.i.	n.i.	n.i.	n.i.	n.i.
Σ-C ₁₀	n.i.	n.i.	n.i.	n.i.	n.i.	n.i.
Σ-C ₁₁	n.i.	n.i.	n.i.	n.i.	n.i.	n.i.
Σ-C ₁₂	n.i.	n.i.	n.i.	n.i.	n.i.	n.i.
TOTAL	100.0000	100.0000	100.0000	100.0000	100.0000	100.0000



Table 3.12. Composition of soil gas in samples drawn at the B-22 well.

Component	Content [% mol]					
	21/11/2019		17/01/2020		26/02/2020	
	wellhead	field	wellhead	field	wellhead	field
oxygen	19.7	19.8	21.2	21.2	20.9	20.6
nitrogen	78.5	78.8	78.7	78.6	76.2	77.0
carbon dioxide	0.28	0.42	0.08	0.16	0.15	0.14
hydrogen sulphide	n.i.	n.i.	n.i.	n.i.	n.i.	n.i.
helium	n.i.	n.i.	n.i.	n.i.	n.i.	n.i.
methane	1.4204	0.9745	0.0274	0.0066	2.5757	2.1501
ethane	0.0091	0.0045	0.0008	0.0001	0.1372	0.0992
propane	0.0015	0.0003	0.0001	n.i.	0.0134	0.0107
i-butane	0.0002	n.i.	n.i.	n.i.	0.0024	0.0019
n-butane	0.0001	n.i.	n.i.	n.i.	0.0022	0.0018
neo-pentane	n.i.	n.i.	n.i.	n.i.		n.i.
i-pentane	n.i.	n.i.	n.i.	n.i.	0.0006	0.0004
n-pentane	n.i.	n.i.	n.i.	n.i.	0.0004	0.0002
2.3-dimethylbutane	n.i.	n.i.	n.i.	n.i.	n.i.	n.i.
2-methylpentane	n.i.	n.i.	n.i.	n.i.	n.i.	n.i.
3-methylpentane	n.i.	n.i.	n.i.	n.i.	n.i.	n.i.
n-hexanes	n.i.	n.i.	n.i.	n.i.	n.i.	n.i.
benzene	n.i.	n.i.	n.i.	n.i.	n.i.	n.i.
C ₆ – unidentified	n.i.	n.i.	n.i.	n.i.	n.i.	n.i.
Σ-C ₆	–	–	–	–	–	–
2.4-dimethylpentane	n.i.	n.i.	n.i.	n.i.	n.i.	n.i.
2-methyl-hexane	n.i.	n.i.	n.i.	n.i.	n.i.	n.i.
3-methyl-hexane	n.i.	n.i.	n.i.	n.i.	n.i.	n.i.
2.3-dimethylpentane	n.i.	n.i.	n.i.	n.i.	n.i.	n.i.
n-heptane	n.i.	n.i.	n.i.	n.i.	n.i.	n.i.
toluene	n.i.	n.i.	n.i.	n.i.	n.i.	n.i.
C ₇ – unidentified	n.i.	n.i.	n.i.	n.i.	n.i.	n.i.
Σ-C ₇	–	–	–	–	–	–
2.3.4-trimethylpentane	n.i.	n.i.	n.i.	n.i.	n.i.	n.i.
2.2-dimethylhexane	n.i.	n.i.	n.i.	n.i.	n.i.	n.i.
2.4-dimethylhexane	n.i.	n.i.	n.i.	n.i.	n.i.	n.i.
2-methylheptane	n.i.	n.i.	n.i.	n.i.	n.i.	n.i.
3-methylheptane	n.i.	n.i.	n.i.	n.i.	n.i.	n.i.
n-octane	n.i.	n.i.	n.i.	n.i.	n.i.	n.i.
xylenes	n.i.	n.i.	n.i.	n.i.	n.i.	n.i.
C ₈ – unidentified	n.i.	n.i.	n.i.	n.i.	n.i.	n.i.
Σ-C ₈	–	–	–	–	–	–
Σ-C ₉	n.i.	n.i.	n.i.	n.i.	n.i.	n.i.
Σ-C ₁₀	n.i.	n.i.	n.i.	n.i.	n.i.	n.i.
Σ-C ₁₁	n.i.	n.i.	n.i.	n.i.	n.i.	n.i.
Σ-C ₁₂	n.i.	n.i.	n.i.	n.i.	n.i.	n.i.
TOTAL	100.0000	100.0000	100.0000	100.0000	100.0000	100.0000

Among the results from the first three measurement series, no values were observed which could suggest uncontrolled emission (leakage) of injected acid gases into the soil air. However, due to the presence of higher hydrocarbons in some samples, it was decided to perform another series of measurements, taking into account an increased number of measuring points around the indicated productive wells.



Selection of wells for examination – measurement series 4

Two wells were selected for further examination:

- B-23 – the well injecting liquid waste into the reservoir;
- B-24 – the well in which progressing corrosion has led to a partial loss of extraction tubing.

The B-23 well has been producing gas from the reservoir since 1988. The initial output of 7 Nm³/min decreased consistently to fall below 1 m³/min in 1995. The well has been inactive since December 1997 due to water encroachment. In 2004, the well was reconstructed to adapt it for liquid waste injection. In 2005 and 2007, absorbency tests were performed on the well. For two years it has been one of the four wells through which liquid waste to the Borzęcin reservoir is injected. That well was selected for soil air examination.

The B-24 well has been one of the wells used to extract gas from the reservoir since 1985. The initial gas output (up to 60 Nm³/min) consistently decreased to reach an average of slightly above 1 Nm³/min in 2012. At the same time, water extraction was increasing up to 63 m³/month. It has been abandoned since February 2013. During service and workover carried out in November 2014, the producing tubing was replaced in the well. Unfortunately, some of the tubing was lost, i.e. 81 running metres of the 2 3/8 API production tubing set, below the depth of 1343 m. The last excavated tube was completely destroyed by corrosion. Despite the workover aimed at resuming production from the well. Satisfactory gas production was not achieved and the well remains inactive.

Within the SECURE project, the downhole reservoir water sampling was performed twice in the B-24 well (in September 2018 and July 2019). The sampling depth was 1.330 m below ground level. Chemical analyses of the gas separated from the brine demonstrated an increased concentration of hydrogen – over 30 mol%, which, given the above producing tubing issue, can prove the occurrence of electrochemical corrosion and hydrogen release in the well. Therefore, the B-24 well was selected for the extended examination of the soil air composition.

Soil gas sampling from drive-in probes – measurement series 4

Around the two wells selected for measurements, 18 driven-in monitoring probes were deployed, each with a 1 m depth, 9 units per well. The measuring points were located within approx. 25 m and 50 m distances from the wells and at the wells themselves (Figure 3.53, Figure 3.54, Figure 3.55 and Figure 3.56).

A hammer drill was used to make the holes for the probes. Then, a perforated PE pipe with a socket with a built-in measuring connector was placed in the holes. Perforation made on a part of the pipe allowed free flow of soil gas into the probe. The probes were installed in such a manner that the measuring connections were located at the ground surface.



Figure 3.53. Installation of a drive-in probe at the B-23 well.



Figure 3.54. Location of measuring points (drive-in probes) around the B-23 well.



Figure 3.55. Installation of a drive-in probe at the B-24 well.



Figure 3.56. Location of measuring points (drive-in probes) around the B-24 well.

After 9 days, soil air samples from the installed probes were drawn into glass bulbs and handed over for further analysis. Samples were taken from 16 holes. Sampling soil air from two probes located beside the B-24 well was unsuccessful. That was presumably caused by the groundwater level being too high, preventing free flow of air into the probes.



Determination of the sampled gas composition – measurement series 4

Examination of gas composition from 16 samples contained in glass bulbs within the fourth measurement series was performed by the INiG-PIB Department of Geology and Geochemistry laboratory.

The molecular composition of soil air is given in Table 3.13 and Table 3.14. The components were normalised against 100% gas. Unfortunately, it was not possible to analyse methane for methane isotopic composition due to its low concentration in the samples available.

Table 3.13. Composition of soil air around the B-23 well.

	B23-1	B23-2	B23-3	B23-4	B23-5	B23-6	B23-7	B23-8	B23-9
	Content [% mol]								
O₂	20.0	18.9	18.9	18.1	18.0	19.4	18.6	21.0	18.8
N₂	79.7	79.9	79.3	80.2	80.2	79.4	79.6	78.9	79.2
CO₂	0.29	1.16	1.78	1.73	1.86	1.19	1.83	0.10	2.09
CO	0.0034	0.0002	0.0002	0.0008	0.0005	0.0004	0.0002	0.0001	0.0003
H₂S	<0.0001	<0.0001	<0.0001	<0.0001	<0.0001	<0.0001	<0.0001	<0.0001	<0.0001
H₂	0.010	<0.001	<0.001	<0.001	<0.001	0.003	<0.001	<0.001	<0.001
He	<0.001	<0.001	<0.001	<0.001	<0.001	<0.001	<0.001	<0.001	<0.001
C₁	0.0007	0.0001	0.0001	0.0001	0.0106	0.0008	0.0016	0.0038	0.0003
C₂	<0.0001	<0.0001	<0.0001	<0.0001	0.0003	0.0001	<0.0001	0.0001	0.0001
C₃	<0.0001	<0.0001	<0.0001	<0.0001	<0.0001	<0.0001	<0.0001	<0.0001	0.0001
I-C₄	<0.0001	<0.0001	<0.0001	<0.0001	<0.0001	<0.0001	<0.0001	<0.0001	<0.0001
N-C₄	<0.0001	<0.0001	<0.0001	<0.0001	<0.0001	<0.0001	<0.0001	<0.0001	0.0002
neo-C₅	<0.0001	<0.0001	<0.0001	<0.0001	<0.0001	<0.0001	<0.0001	<0.0001	<0.0001
I-C₅	<0.0001	<0.0001	<0.0001	<0.0001	<0.0001	<0.0001	<0.0001	<0.0001	0.0001
N-C₅	<0.0001	<0.0001	<0.0001	<0.0001	<0.0001	<0.0001	<0.0001	<0.0001	0.0002
C₆	<0.0001	<0.0001	<0.0001	<0.0001	<0.0001	<0.0001	<0.0001	<0.0001	0.0002
C₇	<0.0001	<0.0001	<0.0001	<0.0001	<0.0001	<0.0001	<0.0001	<0.0001	0.0001
C₈	0.0001	<0.0001	0.0026	0.0001	0.0001	<0.0001	0.0001	<0.0001	0.0001
C₉	<0.0001	<0.0001	<0.0001	0.0001	<0.0001	<0.0001	<0.0001	<0.0001	<0.0001
C₁₀	<0.0001	<0.0001	<0.0001	<0.0001	<0.0001	<0.0001	<0.0001	<0.0001	<0.0001



Table 3.14. Composition of soil air around the B-24 well.

	B24-1	B24-2	B24-3	B24-4	B24-5	B24-6	B24-7	B24-8	B24-9
	Content [% mol]								
O₂	20.3	20.3	-	21.0	20.6	20.6	20.6	-	20.5
N₂	78.9	79.1	-	78.9	79.2	79.0	78.9	-	79.3
CO₂	0.71	0.65	-	0.07	0.24	0.38	0.50	-	0.18
CO	0.0003	0.0003	-	0.0002	0.0003	0.0002	0.0005	-	0.0059
H₂S	<0.0001	<0.0001	-	<0.0001	<0.0001	<0.0001	<0.0001	-	<0.0001
H₂	<0.001	<0.001	-	<0.001	<0.001	<0.001	<0.001	-	0.019
He	<0.001	<0.001	-	<0.001	<0.001	<0.001	<0.001	-	<0.001
C₁	0.0001	0.0001	-	0.0002	0.0001	0.0001	0.0001	-	0.0008
C₂	<0.0001	<0.0001	-	<0.0001	<0.0001	<0.0001	<0.0001	-	0.0001
C₃	<0.0001	<0.0001	-	<0.0001	<0.0001	<0.0001	<0.0001	-	0.0002
I-C₄	<0.0001	<0.0001	-	<0.0001	<0.0001	<0.0001	<0.0001	-	<0.0001
N-C₄	<0.0001	<0.0001	-	<0.0001	<0.0001	<0.0001	<0.0001	-	<0.0001
neo-C₅	<0.0001	<0.0001	-	<0.0001	<0.0001	<0.0001	<0.0001	-	<0.0001
I-C₅	<0.0001	<0.0001	-	<0.0001	<0.0001	<0.0001	<0.0001	-	<0.0001
N-C₅	<0.0001	<0.0001	-	<0.0001	<0.0001	<0.0001	<0.0001	-	<0.0001
C₆	<0.0001	<0.0001	-	<0.0001	<0.0001	<0.0001	<0.0001	-	<0.0001
C₇	<0.0001	<0.0001	-	<0.0001	<0.0001	<0.0001	<0.0001	-	<0.0001
C₈	<0.0001	<0.0001	-	<0.0001	0.0001	<0.0001	<0.0001	-	<0.0001
C₉	<0.0001	<0.0001	-	<0.0001	<0.0001	<0.0001	<0.0001	-	<0.0001
C₁₀	<0.0001	<0.0001	-	<0.0001	<0.0001	<0.0001	<0.0001	-	<0.0001

Analysis of the results

The potential negative impact of acid gases injection into the Borzęcin reservoir should be considered primarily in terms of the possibility of direct uncontrolled leakage of acid gases into the soil air along the production well structure. That process could then be manifested by an increased content of, in particular, CO₂ as the dominant component, and the presence of H₂S in the soil air. In order to determine the potential of such hazards, a total of 24 monitoring wells/probes were deployed, and 34 soil air samples were drawn for examination.

Uncontrolled emission of acid gases into the soil

Among all the results of analyses carried out in series 1-4, including the B-28 well used for injecting acid gases into the reservoir, no values were observed that could suggest uncontrolled emission of injected gases into the soil air. Analysing the results, it should be kept in mind that carbon dioxide is a gas that is part of typical soil air, and the main factors affecting its level include the activity of microorganisms and the roots of higher plants, temperature, humidity, depth, soil aeration degree, and atmospheric pressure. Furthermore, the area where the research was conducted should be taken into account. In the case of the four wells, it was an agricultural area, and forest for the B-6 well. Organic substances occurring naturally in the soil or penetrating into it as a result of human activity (natural fertilizers, crops residues) are subject to digestion and fermentation processes during which biogenic gas is generated, which consists mainly of carbon dioxide (CO₂) and methane (CH₄). It can therefore be concluded that the low methane concentrations found in some samples are also a consequence of natural processes occurring in the soil. The CO₂ levels observed (0.05% - 2.09%) should therefore be assumed to be absolutely normal for the type of area, which is also supported by literature data [10]. Moreover, the lack of even trace amounts of hydrogen sulphide (H₂S) in the samples examined proves the absence of uncontrolled emissions into the soil.



Occurrence of natural gas exhalation from the reservoir

Out of the first three measurement series, completed at the B-6, B-22 and B-28 wells, the results of the third measurement series at the B-6 well and the first and third series at the B-22 well depart from the typical soil air composition that can be found in agricultural areas (Figure 3.57). The high level of methane (approx. 2.5%) and, in particular, the presence of higher hydrocarbons is likely to result from local gas exhalations from the reservoir. Those exhalations may take place along casing and cement, which may be indicated by higher levels of contaminants in the samples drawn directly at the wells.

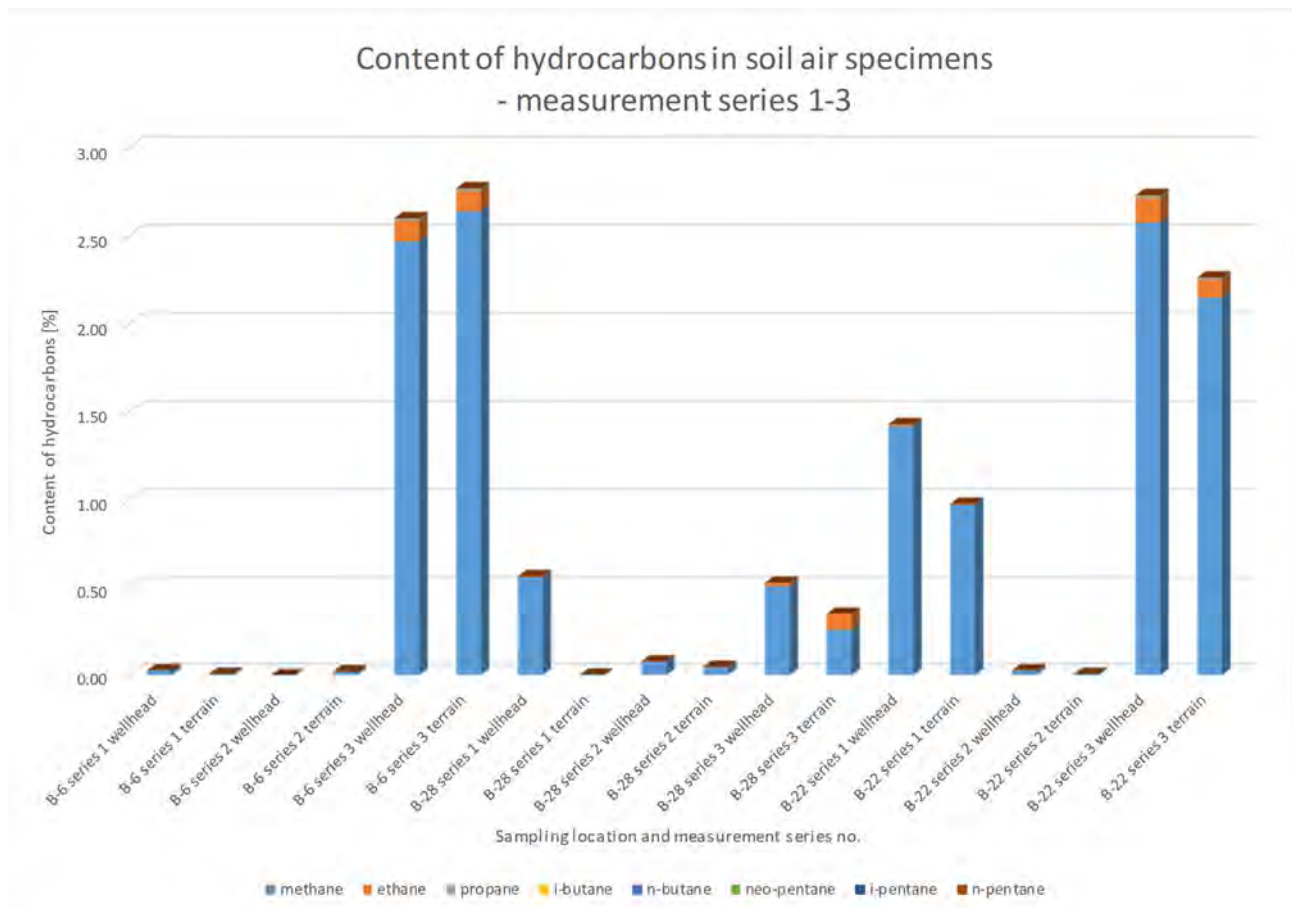


Figure 3.57. Hydrocarbons content in samples taken at the B-6, B-22 and B-28 wells.

Increased methane and ethane values in samples drawn from the B-28 well, in the first and third series, due to the trace content of C₃ and higher hydrocarbons, are most likely caused by natural processes occurring in the soil. Those compounds may also have an anthropogenic origin, e.g. soil pollution by ongoing farming and the use of heavy equipment. The remaining samples from series 1-3 contained insignificant amounts of methane, which can be considered as the regional geochemical background.

The fourth measurement series was completed at the B-23 and B-24 wells. The presence of small amounts of methane in soil air samples (up to 0.01%) is a consequence of digestion and fermentation processes (e.g. natural fertilisers), during which biogenic gas is produced. In none of the samples was the content of higher hydrocarbons found in quantities which could imply significant gas exhalations from the reservoir (Figure 3.58).

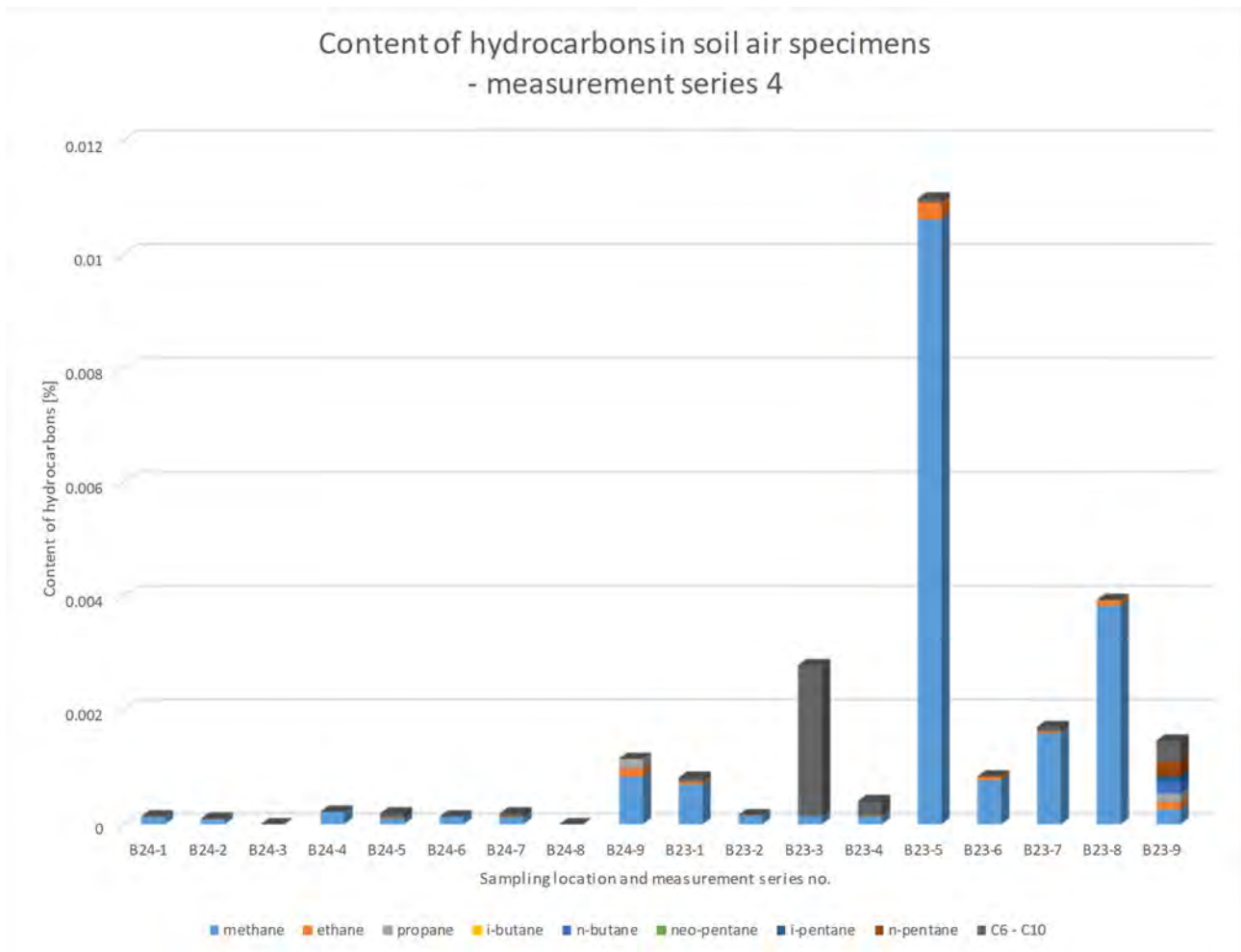


Figure 3.58. Hydrocarbons content in samples taken at the B-22 and B-24 wells.

3.6 TUBING CORROSION MEASUREMENTS AND ANALYSIS

The process of injecting acid gases is associated with very high potential corrosivity, resulting from the partial pressure of CO₂ and H₂S and the temperature which is favourable for corrosion processes. According to API 6A and NACE MR 01.75, the CO₂ and H₂S partial pressures were estimated to exceed 0.21 kPa and 0.34 kPa, respectively, that implies highly corrosive conditions.

Therefore, in order to monitor a possible risk of metal tubing corrosion, measurements of corrosion profile were performed in the injecting well W28 from 2002 till 2018. Nine measurements were done by the project operator (Polish Oil and Gas Company – POGC) with a multi-finger imaging tool (a device by Sondex) [11]. Those measurements were analysed as part of the SECURE study order to obtain detailed information on the corrosion rates.

The corrosion profile provides the corrosion pit depths measured at the whole range of tubing lengths (depths) with the resolution of approx. 9.5 m. The angular resolution of the measurements was 15°. An example of such measurements at selected depth is shown in Figure 3.59.



**Cross Section at depth
1370.82 m**
Nominal ID = 62.0 mm
Nominal OD = 73.0 mm
Remaining wall area = 98 %
Tool deviation = 1 °
Finger 10 Penetration = 1.63 mm

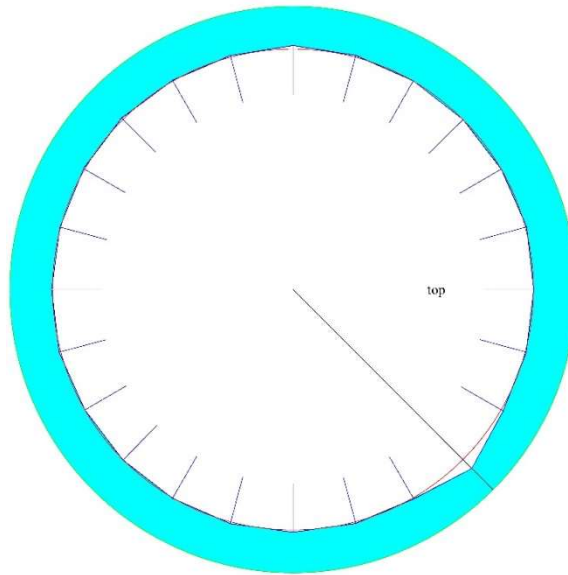


Figure 3.59. Schematic of corrosion measurements at constant well tubing depth.

The corrosion profiles of all measurements in terms of penetration (maximum pit depth) vs tubing depth is shown in Figure 3.60.

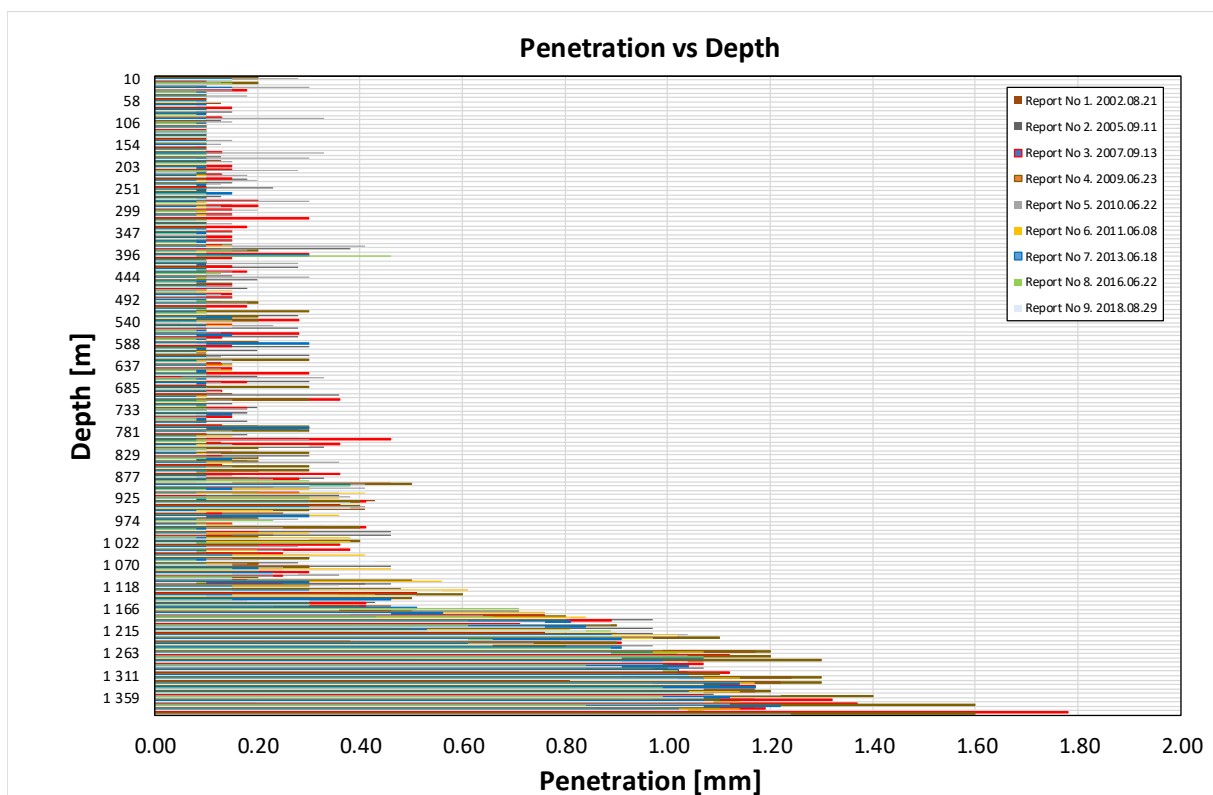


Figure 3.60. Penetration (maximum pit depth) vs Depth.

All the measurements were grouped into 4 tubing depth ranges (0-380 m, 1050-1100 m, 1250-1300 m, 1350-1400 m) selected by similar corrosion trends within each range. The measurements were analysed statistically; that exemplary case is shown in Figure 3.61 for the range of 1350-1400 m.

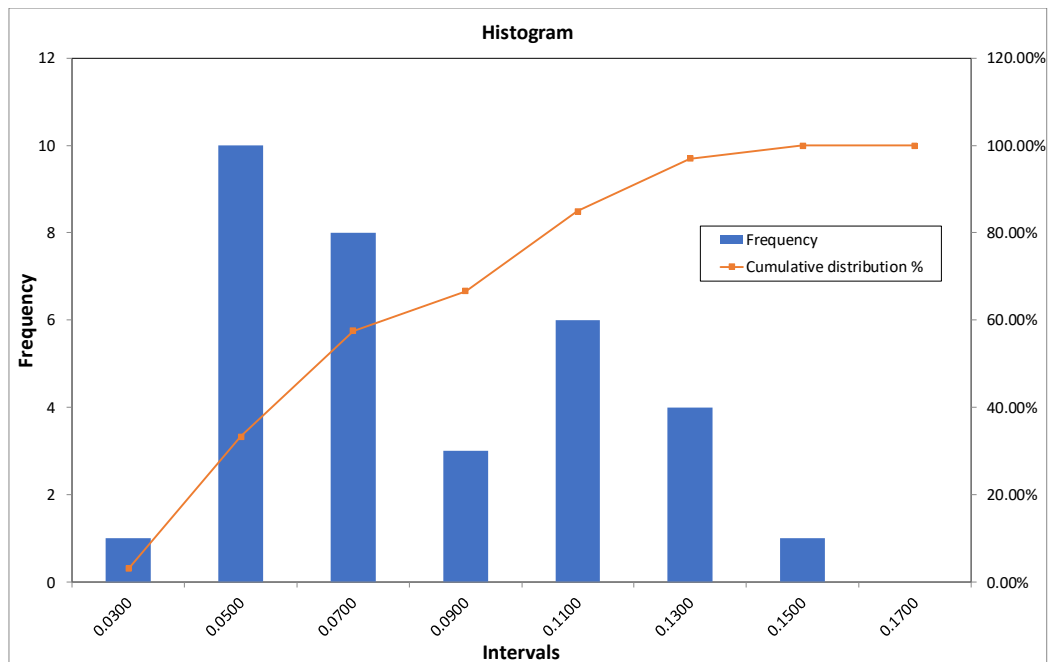


Figure 3.61. Histograms of measured pit depths vs depth of well tubing. Depth range: 1350-1400 m.

Based on this analysis, the corrosion rate was determined as a function of tubing depth. The corrosion rate dependence of the depths is shown in Figure 3.62 in terms of maximum, average (+/- standard deviation) and minimum values. Obviously, the corrosion rate increases with the tubing depth and reaches the maximum value of 0.18 (+/-0.02) mm/year. From this value and thickness of tubing wall (8.6 mm), the probability of the tubing full penetration can be determined as a function of time.

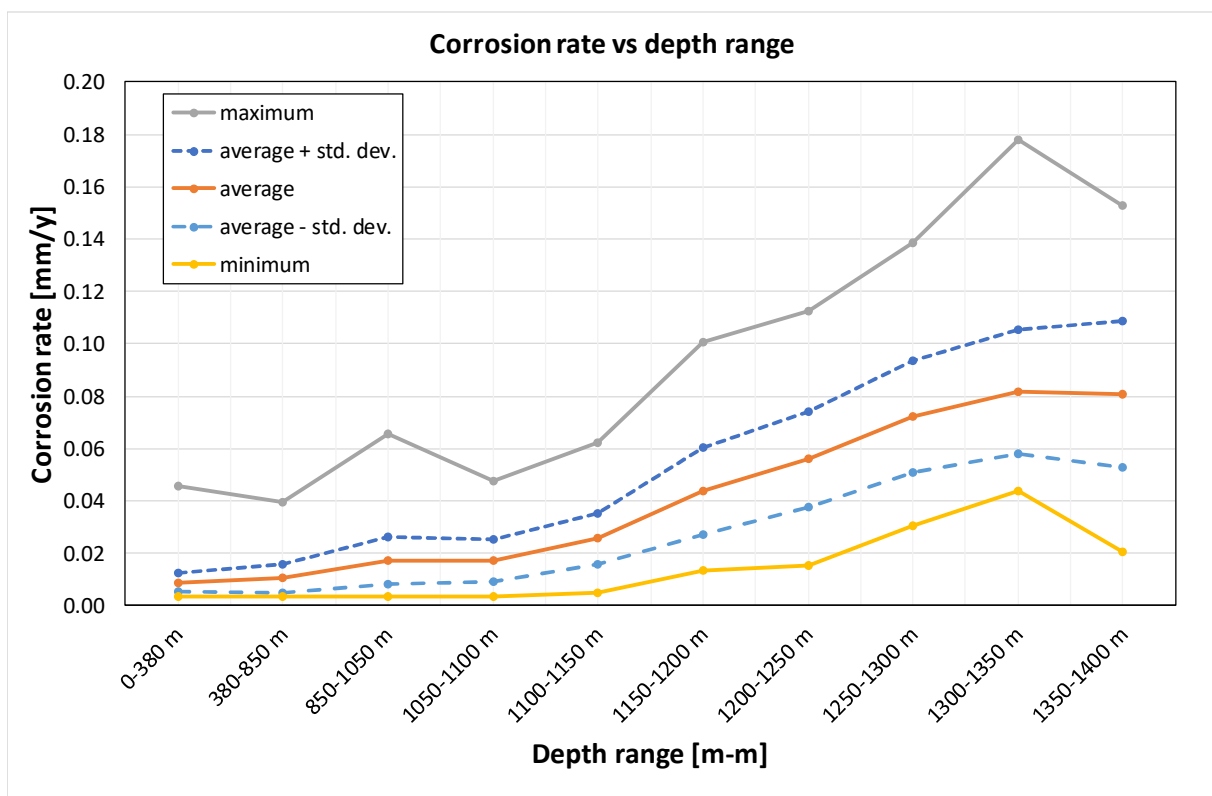


Figure 3.62. Corrosion rates at various depth range of injecting well (W28) tubing.



3.7 INFLUENCE OF CO₂ UPON THE STRENGTH OF CEMENT

In order to determine the influence of CO₂ gas upon the basic parameter (compressive strength) of the cement, long-term laboratory studies were performed on the samples of the typical cement slurry composition also used in well W28. The studies were carried out by INiG-PIB in the 90s of the last century. The slurry composition, its properties, and ionic water content are shown in Table 3.15, Table 3.16, and Table 3.17, respectively.

The cement samples were placed under the conditions of elevated temperature (80°C) and pressure (20 MPa) for up to 180 days and measured for the compressive strength. The tests were performed on 21 samples. The averaged results obtained for the samples kept in CO₂ and natural gas environment (for comparison) are shown in Table 3.18 [12].

Table 3.15. Slurry composition [12].

Component	Value
Tartaric acid (settin retarder) [kg]	0.5
Fly ash [kg]	500
Portland cement CEM I 32.5 kg]	500
Tap water [m ³]	0.5

Table 3.16. Slurry properties [12].

Property	Value
Density [kg/m ³]	1690
Fluidity [mm]	255
Yield point [Pa]	4.6
Plastic viscosity [mPa·s]	34.5

Table 3.17. Ionic water composition [12].

Ion	Content [g/l]
Mg ⁺²	2.92
Ca ⁺²	8.42
K ⁺	0.50
Na ⁺	55.80
Cl ⁻	109.90

Table 3.18. Test results [12].

Storage time [days]	Compressive strength [MPa]	
	with CO ₂	without CO ₂
28	22.5	22.5
90	29.0	27.5
180	29.7	28.2

The test results showed the increase of cement compressive strength over time for CO₂ environment as compared to the natural gas environment. In addition, no signs of carbonate corrosion were found.



3.8 SUMMARY AND CONCLUSIONS

Bottomhole sampling of reservoir water saturated with gas

The results of the test and analyses of downhole bottom-water samples are an essential source of knowledge concerning the phenomena occurring in the sequestration structure as a consequence of acid gas injection. Downhole sampling operation is much more complicated and more expensive than surface fluid sampling. Moreover, taking downhole samples from the initially selected wells could be impossible because of some technical issues that emerge directly during the operation. Such problems were encountered during downhole sampling undertaken within the realisation of the subtask. Despite the mentioned difficulties, downhole samples of water saturated with gas are very valuable material for research, and their proper utilisation gives a lot of useful information for better understanding of the processes occurring within the Borzęcin reservoir. So far, such samples have never been obtained before.

Chemical composition of gas

The results of solution gas analysis revealed that the acid gas injected into the aquifer through the B-28 injector well migrate southwards towards the B-4 well. The investigations proved that this is the main direction of the injected acid gas plume propagation. Water taken from the B-4 well is most intensely saturated with reinjected carbon dioxide and hydrogen sulphide. In each of the three analyses of gas separated from B-4 reservoir water, the concentration of CO₂ and H₂S exceeded many times the levels observed in the other downhole-sampled wells (B-6, B-22, B-24). The B-4 well is closest to the B-28 (injector well). Moreover, it's located in the direction consistent with the expected migration of acid gas upward the structure, driven by gravity forces as well as by pressure depression caused by continuous gas production from the reservoir (especially by the B-4 and B-22 wells).

Other actions within the task were related to the surface sampling of gas and associated water. As in the case of gas separated from the reservoir water, the chemical analysis of produced gas confirmed the inflow of the injected acid gas into the gas produced by the B-4 well. Furthermore, an increased concentration of CO₂ was also recorded in the gas produced by the B-22 well, which may indicate that the migration zone of the injected acid gas is going to affect the major production well (B-22).

Gas samples from the acid gas reinjection facility were also taken to the chemical analysis. The results confirmed stability in the composition of the gas over time. Currently, after the modernisation of the acid gas sweetening facility, the reinjected gas is composed mainly (in 99%) of carbon dioxide and hydrogen sulphide, while the hydrocarbon components represent less than 1% mole.

Isotopic composition of gas

The high dynamics of individual phases system occurring in the structure of the Borzęcin reservoir implies temporal and spatial variability in the isotope composition of the analysed gas from brine degassing and of the produced gas. The system is subject to periodic disturbances related to the process of reservoir exploitation, repeated injection of acid gases and liquid waste coming from outside the reservoir. Moreover, the solubility of CO₂ in brine and isotope fractionation (hydrogen between methane and brine) may also affect the isotope composition of carbon in CO₂ and hydrogen in methane for the brine degassing samples. Also, other processes, as microbial or abiotic oxidation of C₁ might play role in the $\delta^2\text{H}$ (C₁) variations.

Reservoir water analysis

Based on the physiochemical parameters and hydrochemical indicators presented above, it can be stated that the bottom water underlying the Borzęcin reservoir, to which acid gas is injected, is composed of approximately 24% Cl-Na binary brine. According to the Sulin classification [13], it is a calcium chloride type brine. The values of hydrochemical coefficients indicate a high degree of alteration (through water-rock interaction) of the brine analysed. It is a quality typical of highly metamorphosed fossil brines originating from formations with very high hydrogeological sealing. Local variability in the chemical composition of brine is highly related to the performance of the wells injecting liquid waste. Reservoir water with diverse chemistry account for the majority of liquid waste injected, originating from the nearby oil and gas production facilities.

PVT analysis

The PVT studies of produced natural gas as well as reinjected acid gas allowed for the phase behaviour analysis of tested fluids. Both experimental studies and computer simulations showed that under current thermobaric conditions, there is no risk of condensation of the liquid phase at any of the stages of the natural



gas production and acid gas reinjection processes. The determining factor here, apart from the gas composition, is low reservoir pressure (resulting from ongoing exploitation of the Borzęcin gas field), and above all, the reservoir temperature exceeding the critical temperature concerning both tested gases.

The ability to dissolve the produced and reinjected gases in the reservoir water was also examined. The studies showed that acid gas has excellent solubility in Borzęcin reservoir water. In the current thermobaric reservoir conditions, the solubility of acid gas is about 20 times higher than of the produced gas. This feature indicates that a significant volume of acid gas injected directly into the aquifer dissolves in water and migrate within the structure, remaining in the water zone. This is a positive phenomenon when concerning acid gas sequestration within an active gas reservoir. The dissolution of CO₂ and H₂S in the reservoir water delays the breakthrough of these components into the natural gas zone.

Soil gas analysis

To conclude, it should be stated that the soil air analyses carried out so far did not reveal surface leaks of acid gases injected into the Borzęcin structure. Periodically elevated hydrocarbon concentrations at the B-6 and B-22 wells are likely to occur due to natural gas exhalation. To ascertain what their origin is, it is recommended to perform long-term monitoring tests on the identified wells.

Tubing Corrosion measurements and analysis

The process of injecting CO₂ and/or other acid gases is typically associated with significant potential corrosivity of metal tubing and/or casing components of the injecting wells. In the analysed case of the Borzęcin project relevant corrosion tests were performed and showed relatively high corrosion rate reaching 0.18 mm/year. This effect confirms the necessity of corrosion monitoring and possible replacement of the corroded component during the sequestration project.

Influence of CO₂ upon the strength of cement

The injecting of CO₂ and/or other acid gases may affect properties of the cement used in injecting well constructions. This clearly requires the use of proper cement types. The cement used in the Borzęcin project wells was subject to long-time laboratory tests of the influence of CO₂ upon the cement properties. As a result, no signs of carbonate corrosion were found and the presence of CO₂ environment increased the cement compressive strength over time as compared to the natural gas environment.

4 Geological setting and modelling

4.1 GEOLOGICAL SETTING

The Borzęcin natural gas field was discovered in 1969 in the region of the Zielona Góra basin in the southern part of the Pre-Sudetic Monocline [14]. The Borzęcin structure includes an anticline with two local uprisings. The portions of the Borzęcin reservoir composed of the Basal limestone and Rotliegend sandstone formations. The first accumulation of gas was discovered at the depth of 1380 m in intervals which included Rotliegend and carbonate horizons of the Zechstein. Both pay horizons are hydrodynamically connected. The top of the reservoir is confined by overlying Zechstein strata and the bottom by underlying water. Borzęcin is the only reservoir discovered so far in the Zechstein limestone and Rotliegend sandstone formations of the Polish Lowland which contains gas with a high H_2S concentration.

4.2 GEOLOGICAL MODELLING

In order to better understand the effects of acid gas reinjection to the Borzęcin structure and to monitor quantities that are not available for direct measurements, a simulation model of the structure was constructed and calibrated. At first, a geological model was generated based on the data provided by the Borzęcin project operator. They include a set of structural maps of main structure horizons: the Basal limestone and the Rotliegend sandstone formations. Those maps are shown in Figure 4.1, Figure 4.2, Figure 4.3.

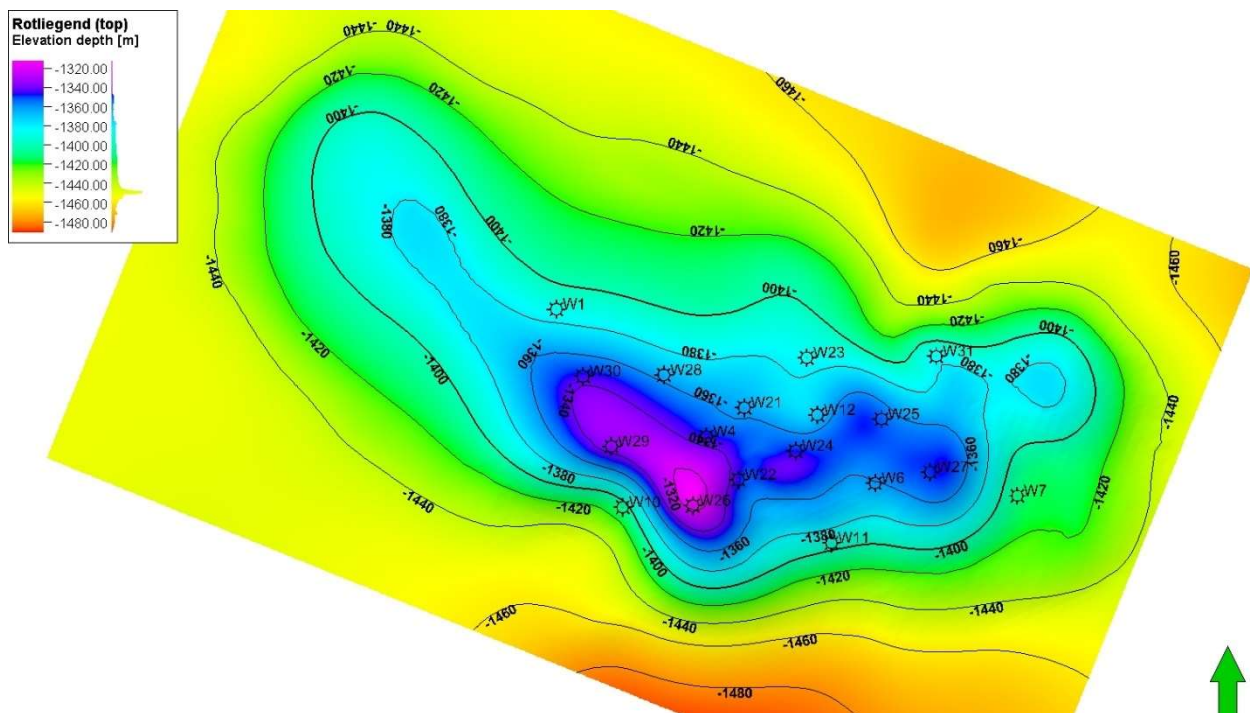


Figure 4.1. Structural map of the Basal limestone top.

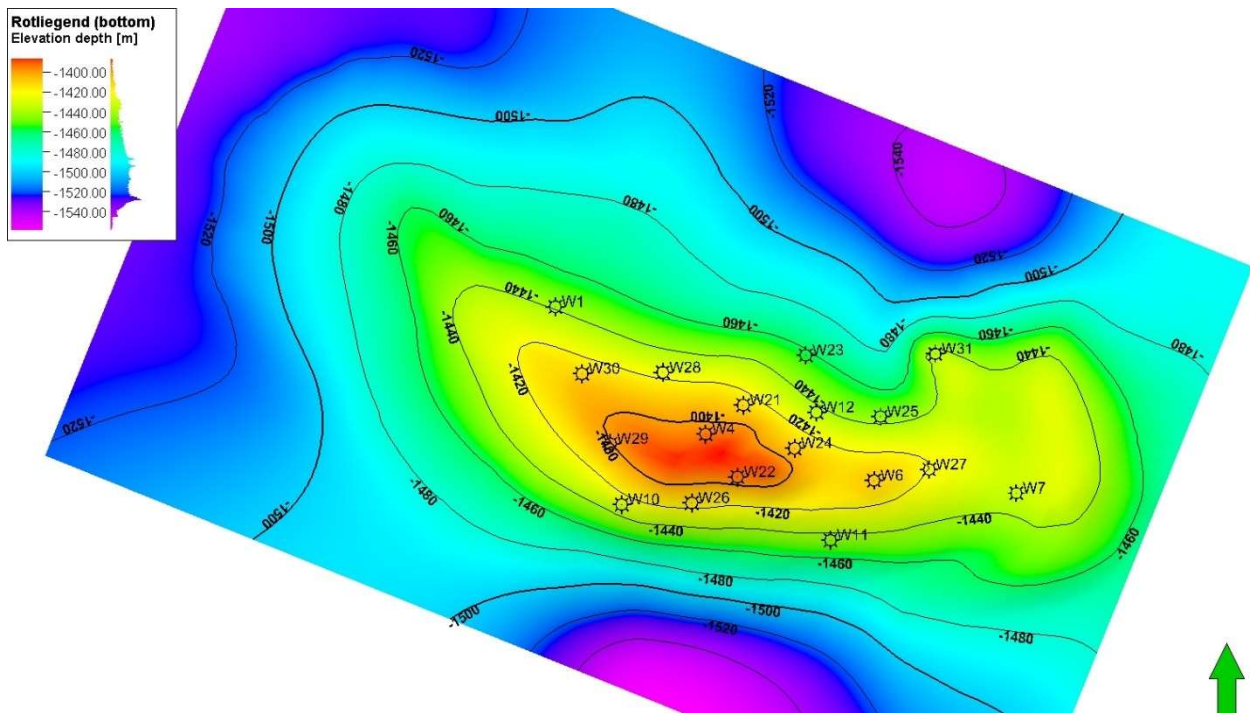


Figure 4.2. Structural map of the Basal limestone bottom.

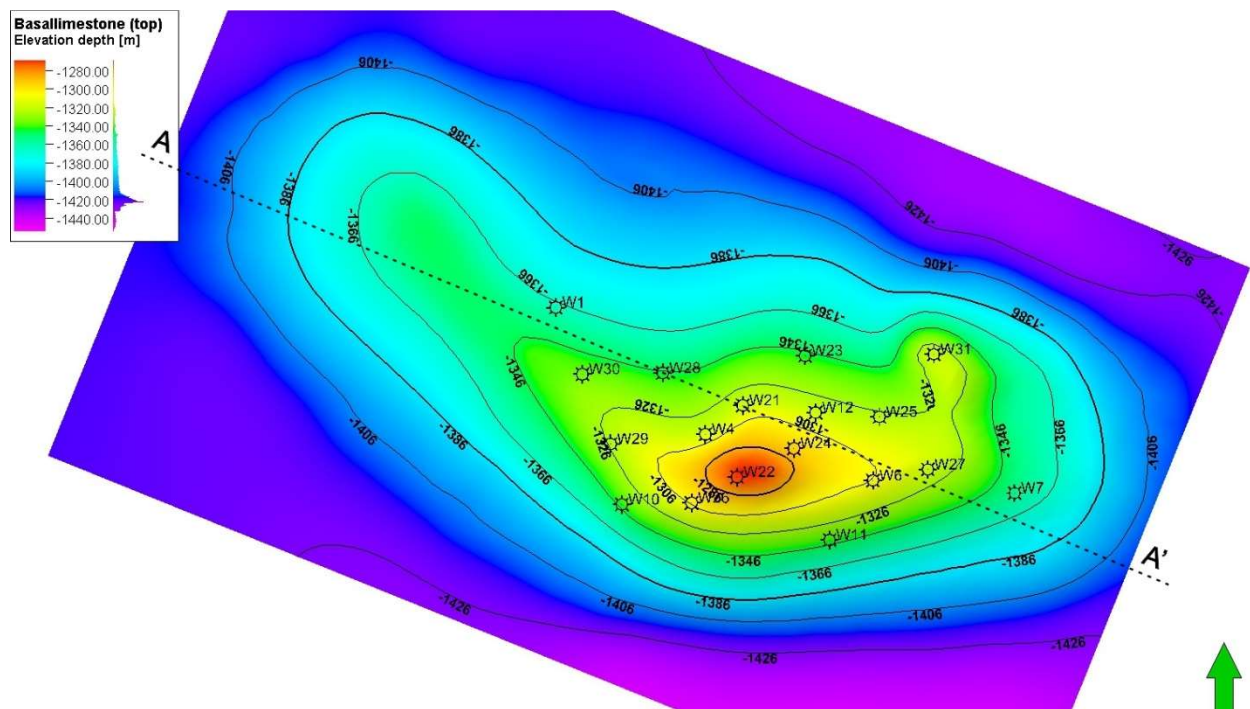


Figure 4.3. Structural map of the Rotliegend bottom.

In order to generate a basic parametric model of the structure, well survey data were used that include: geophysical log profiles, core sample measurements, well test results, etc. Those data resulted in lithological, stratigraphic and geophysical detailed structures for all tested wells. An example of such results is shown in Table 4.1 for well W22.

In order to generate spatial distributions of basic geological parameters (porosity, permeability, NTG), a variographic analysis was performed for each of those parameters. An example of such analysis is shown in Figure 4.4 for NTG.

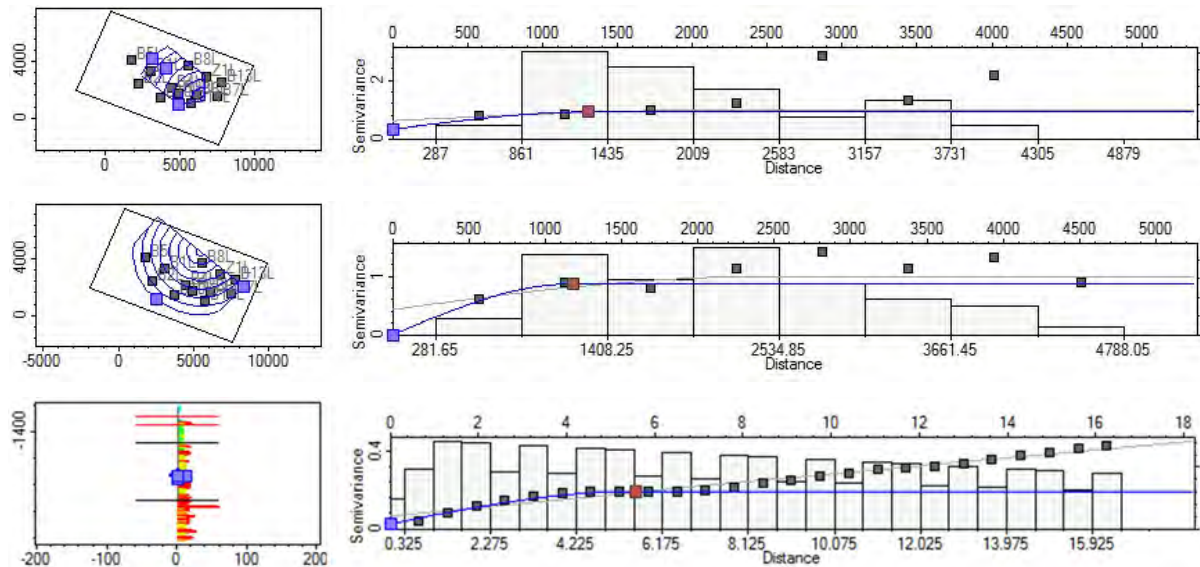


Figure 4.4. Variographic analysis of NTG: measured vs. theoretical semivariance in three main directions (vertical direction, minor and major horizontal directions).

Resulting variogram coefficients (sill, main range values – Table 4.2) together with parameter values determined at well positions were input parameters to generate stochastic realizations of corresponding distributions. Averaging of such realizations resulted in the final distributions constituting a parameter model of the structure. Figure 4.5, Figure 4.6, Figure 4.7, Figure 4.8 present spatial distributions of the main parameters: NTG, porosity, permeability along A-A' vertical cross section, at the Basal limestone top and bottom and at the Rotliegend bottom.



Table 4.1. Litho-stratigraphy of Borzęcin Structure – well W22.

Period	Thickness [m]	Top MD [m]	Bottom MD [m]	Top TVDSS [m bsl]	Bottom TVDSS [m bsl]	Lithology [-]	Porosity [%]	Permeability [mD]	Brine density [g/cm ³]
Quaternary and Tertiary	340.0	0.0	340.0	-90.0	250.0	clays, pleystocene and holocene sands, oligocene dark gray clays and olive gray clays	15.00	50.0	
Keuper-Rhaetian	0.0	340.0	340.0	250.0	250.0	claystones with sandstones and mudstones interbeds by gypsum with anhydrite series	n/a	n/a	
Upper Muschelkalk	0.0	340.0	340.0	250.0	250.0	limestones , anhydrite dolomite and lime-marl parts	n/a	n/a	
Middle Muschelkalk	45.0	340.0	385.0	250.0	295.0	limestones , anhydrite dolomite and lime-marl part	15.00	350.0	
Lower Muschelkalk	155.0	385.0	540.0	295.0	450.0	limestones , anhydrite dolomite and lime-marl part	15.00	350.0	
Upper Bunter - Ret	129.0	540.0	669.0	450.0	579.0	claystones, clayshells, dolomites and sandstones mudstones	15.00	100.0	
Middle Bunter	215.0	669.0	884.0	579.0	794.0	claystones, clayshells, dolomites and sandstones mudstones	15.00	100.0	
Lower Bunter	305.0	884.0	1189.0	794.0	1099.0	claystones, clayshells, dolomites and sandstones mudstones	15.00	100.0	
Upper Red Pelite (Transitional Pelite)	21.0	1189.0	1210.0	1099.0	1120.0	aller	1.50	0.0005	
Youngest Halite	0.0	1210.0	1210.0	1120.0	1120.0		n/a	n/a	
Saline Red Pelite	0.0	1210.0	1210.0	1120.0	1120.0		n/a	n/a	
Younger Halite	15.0	1210.0	1225.0	1120.0	1135.0	leine	1.50	0.0005	
Main Anhydrite	32.0	1225.0	1257.0	1135.0	1167.0		1.50	0.0005	
Grey Pelite	3.0	1257.0	1260.0	1167.0	1170.0		1.50	0.0005	
Basal Anhydrite	25.0	1260.0	1285.0	1170.0	1195.0	stassfurt	1.50	0.0005	1.1460
Main Dolomite	15.0	1285.0	1300.0	1195.0	1210.0		15.00	200.0	1.1460
Upper Anhydrite	39.0	1300.0	1339.0	1210.0	1249.0	werra	1.50	0.0005	
Oldest Halite	6.0	1339.0	1345.0	1249.0	1255.0		1.50	0.5000	
Lower Anhydrite	13.5	1345.0	1358.5	1255.0	1268.5		1.50	0.0005	
Zechstein Limestone	76.0	1358.5	1434.5	1268.5	1344.5		9.12	3.704	
Kupferschiefer	0.0	1434.5	1434.5	1344.5	1344.5		n/a	n/a	
Rotliegend	30.5	1434.5	1465.0	1344.5	1375.0	unbored	14.85	8.855	
Carboniferous/unbored	0.0	1465.0	1465.0	1375.0	1375.0		n/a	n/a	

well coordinates: x = 4797.03, y = 1747.67; well elevation = 90 m asl;



Table 4.2. Coefficients of geometric anisotropic semi-variogram.



Perameability	Basal limestone	Rotliegend
Sill, b [mD ²]	0.4933	0.2068
Range, a :		
Vertical direction [m]	7.346	6.166
Minor horizontal direction [m] / azimuth [°]	1233.397 / 220.7	1774.681 / 220.7
Major horizontal direction [m] / azimuth [°]	1438.719 / 310.7	1168.068 / 310.7
Porosity	Basal limestone	Rotliegend
Sill, b [-]	0.5494	0.2863
Range, a :		
Vertical direction [m]	8.409	6.006
Minor horizontal direction [m] / azimuth [°]	1083.792 / 220.7	1290.355 / 220.7
Major horizontal direction [m] / azimuth [°]	1562.359 / 310.7	842.550 / 310.7
Vshale	Basal limestone	Rotliegend
Sill, b [-]	0.2014	0.3758
Range, a :		
Vertical direction [m]	5.569	4.389
Minor horizontal direction [m] / azimuth [°]	1180.155 / 220.7	1377.846 / 220.7
Major horizontal direction [m] / azimuth [°]	1307.109 / 310.7	643.533 / 310.7

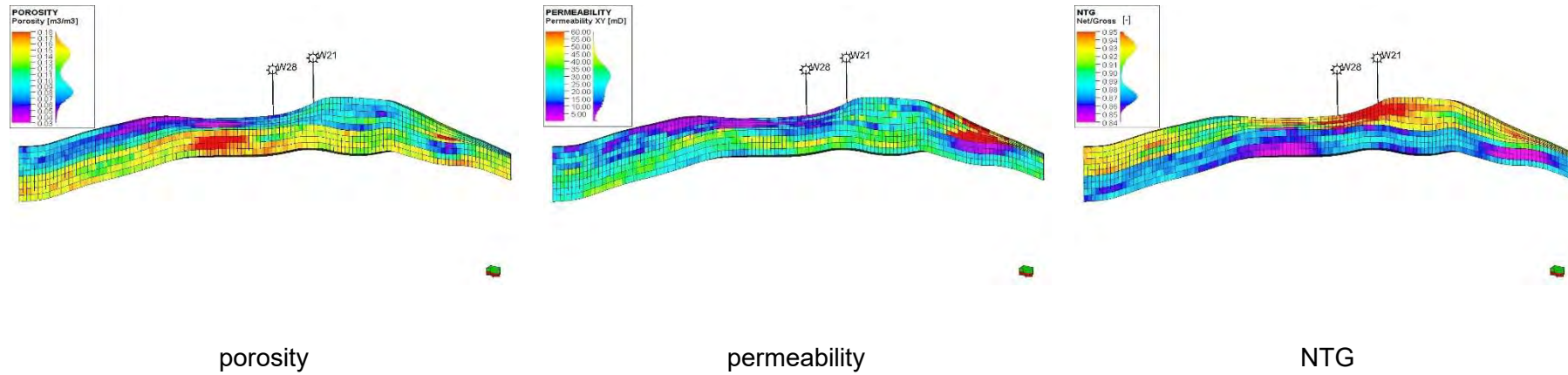


Figure 4.5. Geological parameter (porosity, permeability, NTG) distributions along the vertical cross section (A-A').

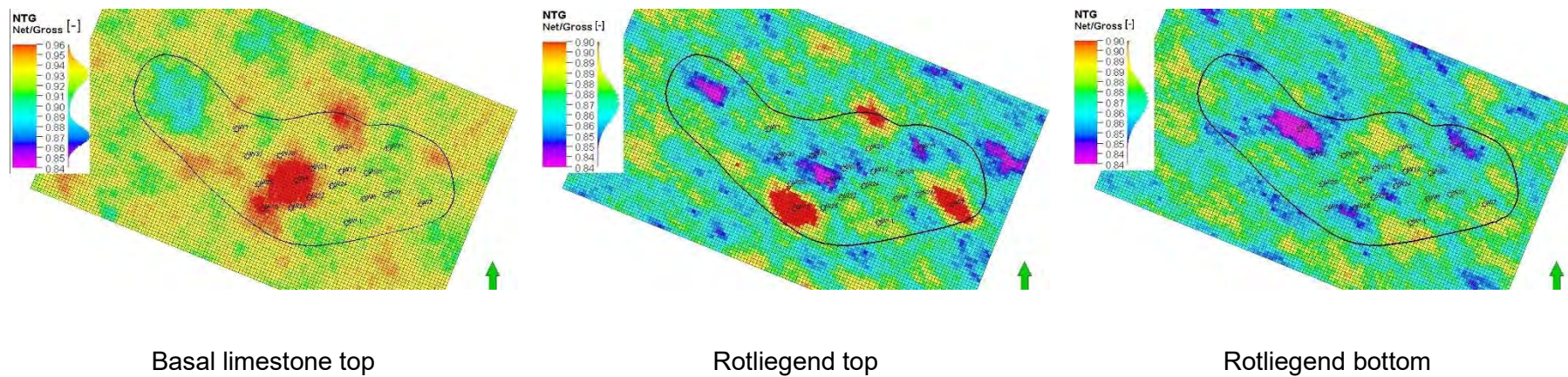


Figure 4.6. NTG distribution at various geological layers (Basal limestone top and bottom, Rotliegend bottom).

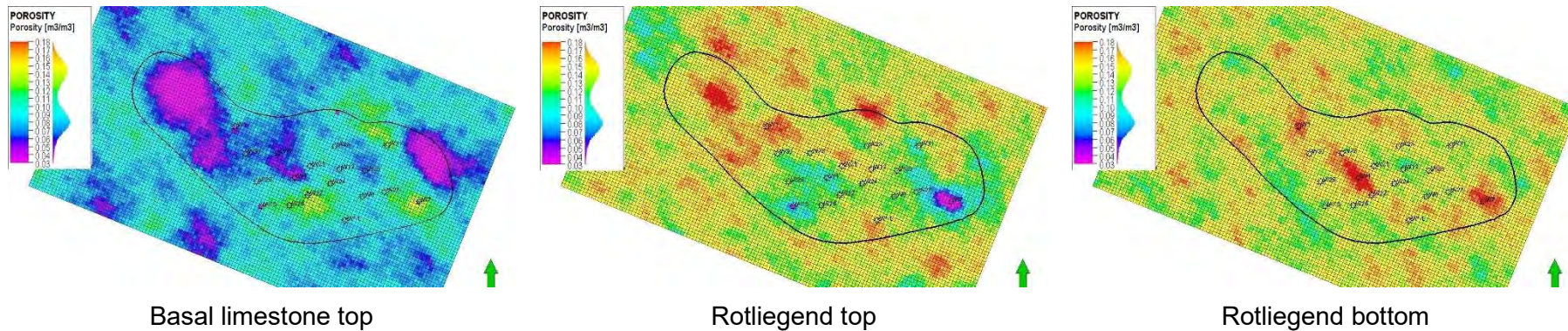


Figure 4.7. Porosity distribution at various geological layers (Basal limestone top and bottom, Rotliegend bottom).

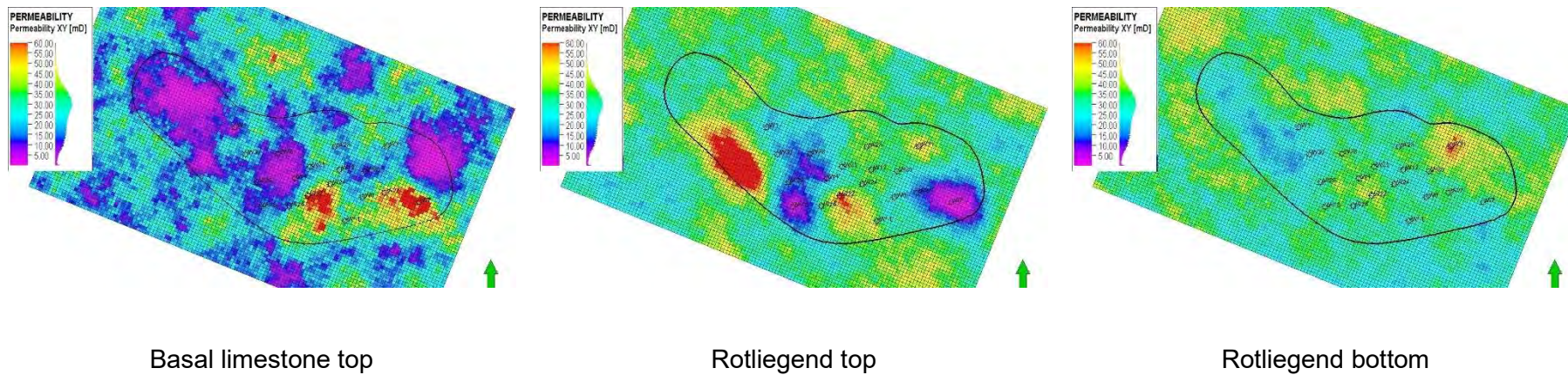


Figure 4.8. Permeability distribution at various geological layers (Basal limestone top and bottom, Rotliegend bottom).



4.3 SUMMARY AND CONCLUSIONS

As is commonly accepted, the geology of a structure planned for sequestration projects constitutes a basic criterion of the structure selection and the description of this geology has to be included prior to further analyses of the structure under consideration. Therefore, this chapter includes a detailed description of the geological setting of the Borzęcin structure. The geological data are subsequently quantified into the numerical model that includes both structural and parametric properties of the Borzęcin structure. The need of the geological model is indispensable for the quantitative modelling of the complex processes taking place in the Borzęcin structure during the acid gas injection project.



5 Dynamic simulation model

5.1 MODEL CONSTRUCTION

The geological model described in the previous chapter was used as an input to construct the updated dynamic simulation model of the Borzęcin structure [15]. The model grid in its basic part consists of 9 layers with their thickness varying between 5 and 13 m. Lateral sizes of the grid blocks equal to 80×80 m and enumerate up to 77×128 blocks. The 3D view of the model is shown in Figure 5.1. Its top view together with line A-A', defining a vertical cross section position, is shown in Figure 5.2. The cross section of the model structure is shown in Figure 5.3. The water-gas contact at the structure top defines reservoir contour and device the model into the inner reservoir part and the outer surrounding aquifer part as shown in Figure 5.4. In addition, the bottom layer of the model connects to underlying aquifer represented by an analytical model of the Carter-Tracy type.

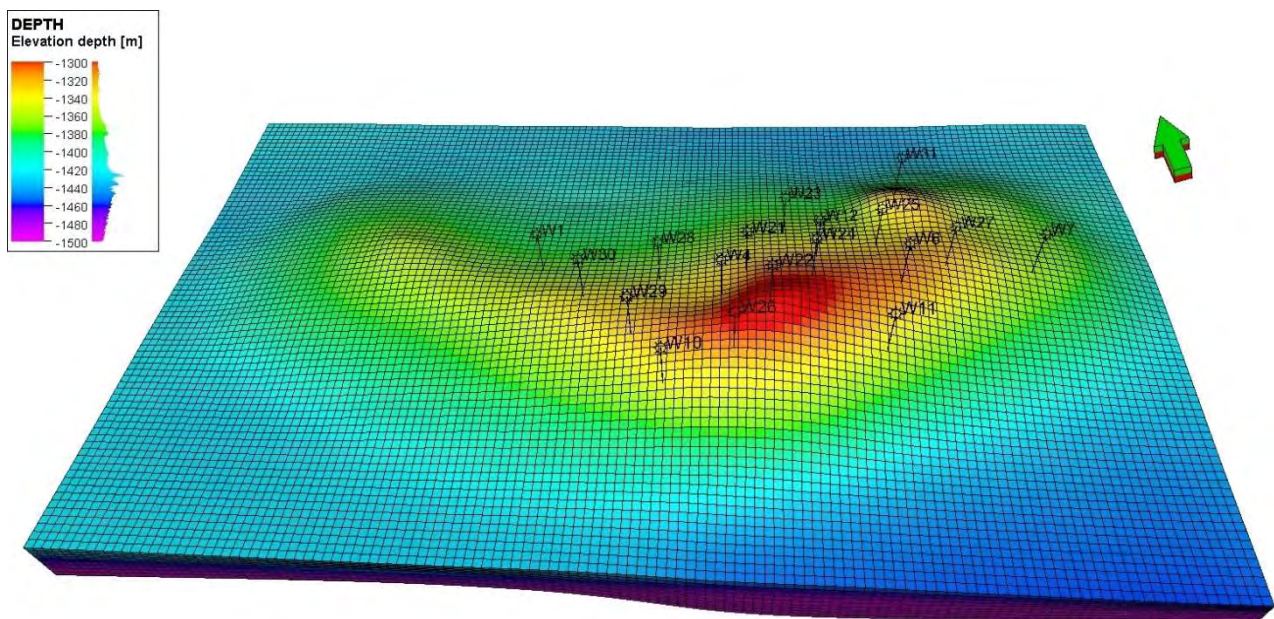


Figure 5.1. 3D view of the reservoir simulation model.

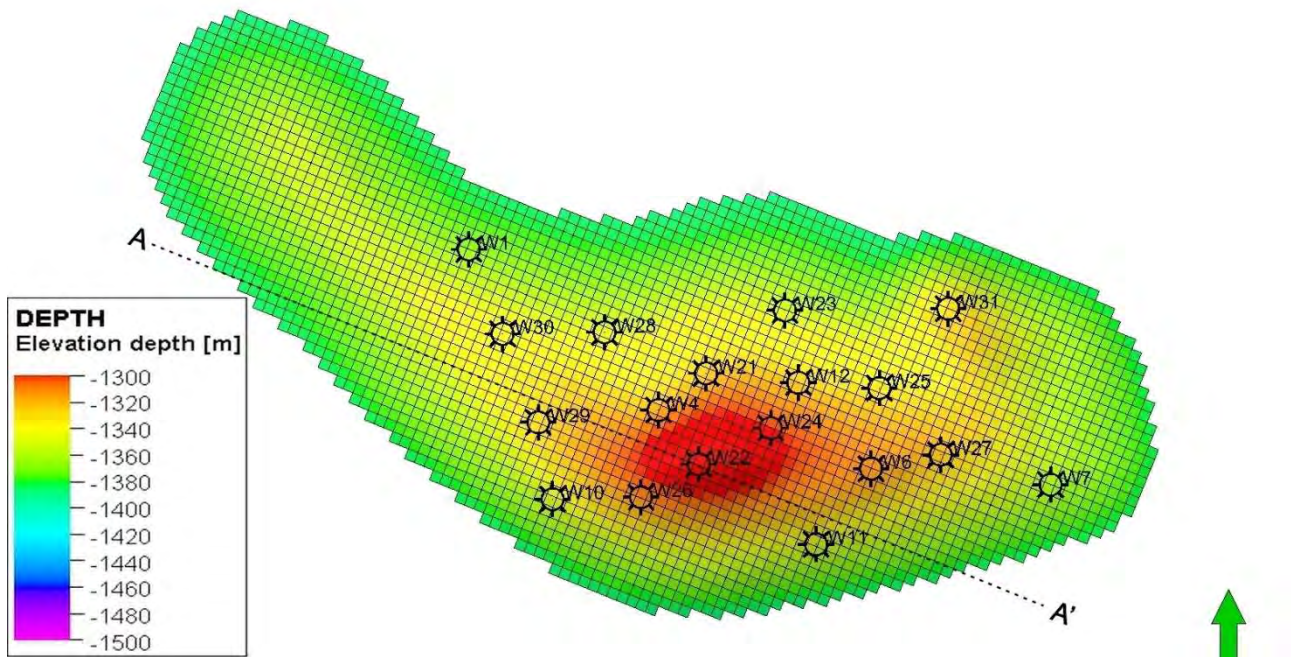


Figure 5.2. Top view of the reservoir simulation model. Vertical cross section line A-A'.

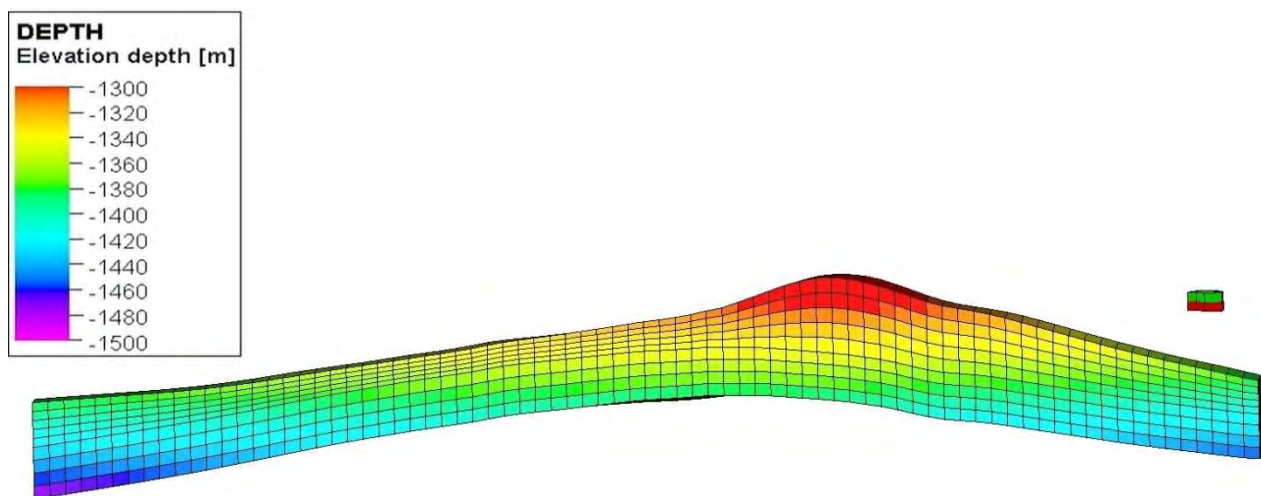


Figure 5.3. Vertical cross section of the reservoir simulation model along line A-A'.

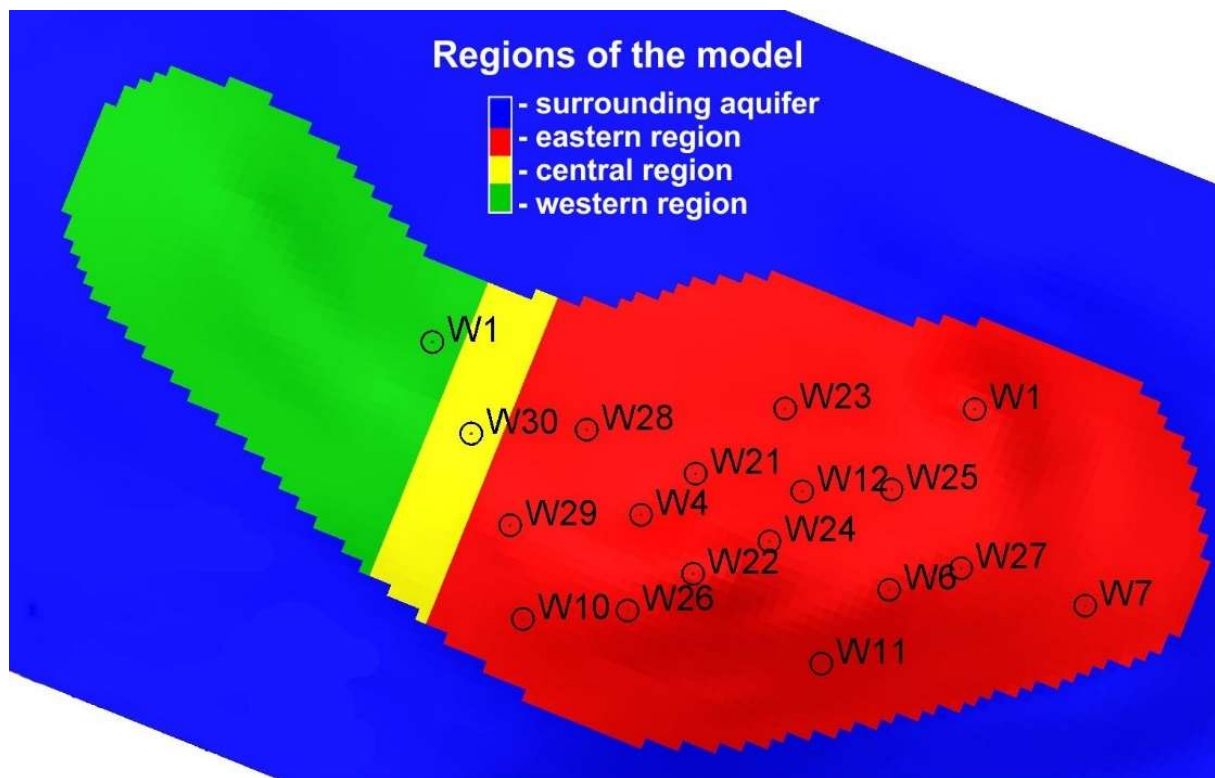


Figure 5.4. Top view of the reservoir simulation model including surrounding aquifer. Definitions of partially isolated reservoir regions.

Well data (well localizations, trajectories, diameters, completion intervals) were implemented into the model based on the information obtained from the reservoir operator. An example of well design is shown in Figure 5.5 for well W28.

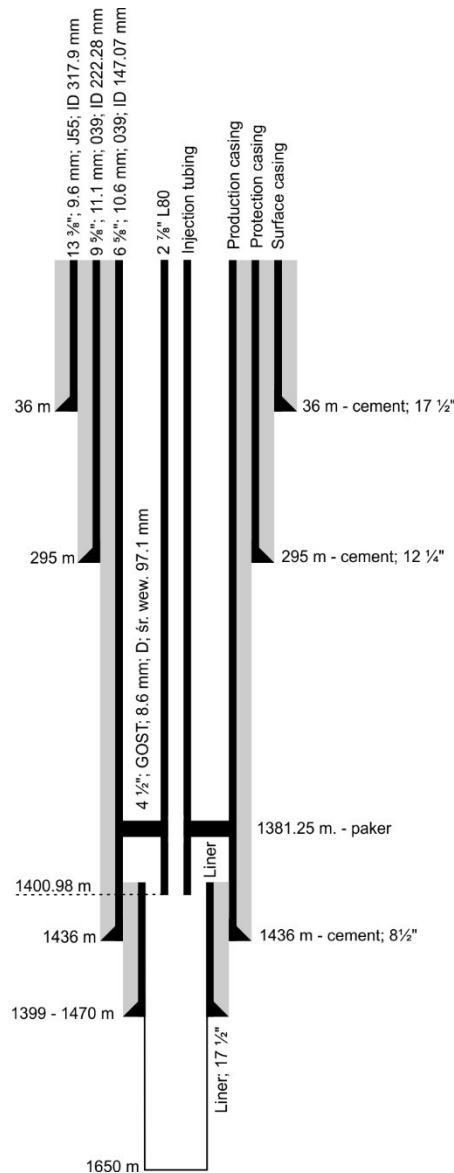


Figure 5.5. Well W28 design.

Model properties are supplemented with water saturation, S_w , and gas saturation, $S_g = 1 - S_w$, functions of capillary pressure, P_c , and relative permeabilities for water, k_{rw} , and gas, k_{rg} , in the water-gas system. The former was assumed of the following type:

$$P_c = P_a \frac{1}{(S_w^*)^\lambda} \text{ where:}$$

$$S_w^* = \frac{S_w - S_{wir}}{1 - S_{wir}}$$

Parameters: end-point capillary pressure, P_a , power law exponent, λ , irreducible water saturation, S_{wir} of these formula were determined to reconstruct (average) water saturation profiles measured in the wells of the reservoir as the functions of the height above the gas-water contact and their values were found to be:

$$P_a = 0.5 \text{ bar,}$$



$\lambda = 0.1$ in the Basal limestone,
 $\lambda = 0.5$ in the Rotliegend sandstone,
 $S_{wir} = 0.1$.

The resultant initial gas saturation distribution in the reservoir was presented in Figure 5.6, Figure 5.7, Figure 5.8, Figure 5.9 along A-A' vertical cross section and at various layers of the model.

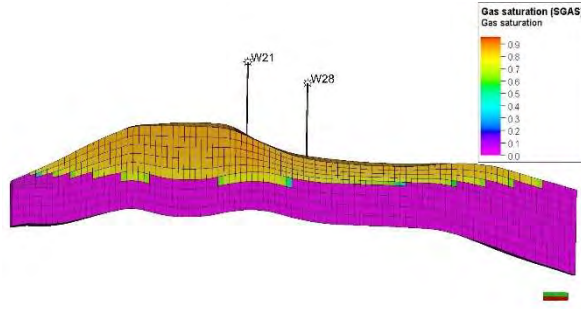


Figure 5.6. Initial gas saturation along vertical cross section (A-A').

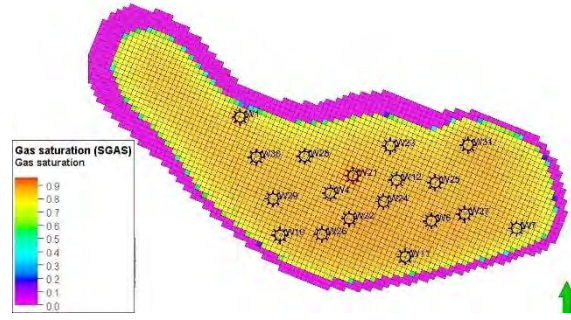


Figure 5.7. Initial gas saturation at the Basal limestone top.

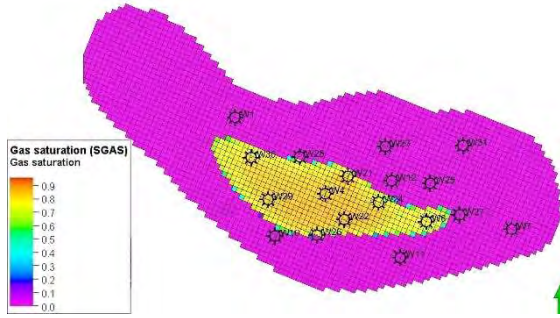


Figure 5.8. Initial gas saturation at the Rotliegend top.

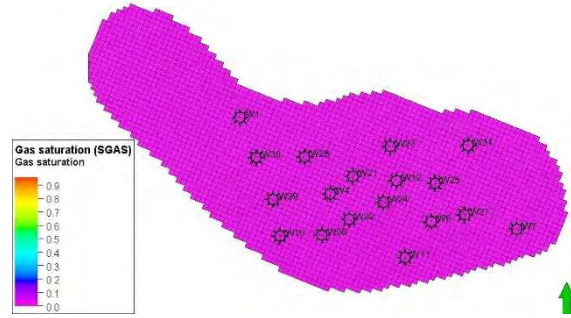


Figure 5.9. Initial gas saturation at the Rotliegend bottom.

As no measurements were performed for relative permeabilities of samples from the Borzęcin structure, then their dependence of fluid saturations were assumed to be those of the neighbouring reservoirs located in the same formations. They accept the following form:

$$k_{rw} = (S_w^*)^{3+2\alpha_1}$$

$$k_{rg} = (S_g^*)^2 \left[1 - (S_g^*)^{1+\alpha_2} \right]$$

$$\text{where: } S_g^* = \frac{S_g - S_{gr}}{1 - S_{wir} - S_{gr}}$$

with: $\alpha_1 = 0.5$ for the Basal limestone,
 $\alpha_1 = 1.0$ for the Rotliegend sandstone.
 $\alpha_2 = -1$
 $S_{gr} = 0.1$

In order to take into account varying composition of the gas within the structure and consequently, its varying properties, a composition model of the structure was constructed that adopted Peng-Robinson equation of state. Six components (N_2 , CO_2 , H_2S , C_1 , C_2 , C_{3+}) of that gas were assumed with EOS parameters given in Table 5.1 and Table 5.2. In Table 5.3 coefficient of the viscosity model by Lorentz-Bray-Clark are shown.



Table 5.1. Component parameters of Peng-Robinson equation of state for varying composition fluid in the Borzęcin structure model.

Component	Molecular weight [kg-mole]	Tcrit [K]	Pcrit [bar]	Vcrit [m ³ /kg-mole]	Zcrit [-]	Vol shift [-]	Acentric factor [-]	Parachor [dyne/cm]	Omega A [-]	Omega B [-]
N ₂	28.013	146.95	33.9439	0.09	0.29115	-0.13601	0.04	41	0.45724	0.0778
CO ₂	44.01	31.55	73.8659	0.094	0.27407	-0.04958	0.225	78	0.45724	0.0778
H ₂ S	34.076	100.45	89.3687	0.098	0.28195	-0.10798	0.1	80	0.45724	0.0778
C ₁	16.043	-82.55	46.0421	0.098	0.28472	-0.14863	0.013	77	0.45724	0.0778
C ₂	30.07	32.28	48.8387	0.148	0.28463	-0.10863	0.0986	108	0.45724	0.0778
C ₃₊	44.097	96.65	42.4552	0.200	0.27616	-0.0835	0.1524	150.3	0.45724	0.0778

Table 5.2. Component parameters of Peng-Robinson equation of state for varying composition fluid in the Borzęcin structure model, cont'd. Binary coefficients.

Name	N ₂	CO ₂	H ₂ S	C ₁	C ₂	C ₃₊
N ₂						
CO ₂	-0.017					
H ₂ S	0.1767	0.0974				
C ₁	0.0311	0.12	0.08			
C ₂	0.0515	0.12	0.0833	0		
C ₃₊	0.0848	0.12	0.081	0	0	

Table 5.3. Lorentz-Bray-Clark viscosity modelling coefficients.

a ₁	a ₂	a ₃	a ₄	a ₅
0.10230	0.02336	0.05853	-0.04076	0.00933



Original gas composition is presented in Table 5.4. Basic properties (formation volume factor, B_g , and viscosity, μ_g) of that gas and the gas injected to the structure are shown in Figure 5.10 and Figure 5.11, respectively. In addition, the phase diagram of the gases involved in the project (original gas, injected gas, pure CO_2) is shown in Figure 5.12.

Assumed reservoir brine properties from the obtained data are:

- density: $\rho_w = 1100 \text{ kg/m}^3$,
- formation volume factor: $B_w = 1.011 \text{ Rm}^3/\text{Sm}^3$ @ $P = 154.8 \text{ bar}$, $T = 46.8^\circ\text{C}$,
- compressibility: $c_w = 4.5 \times 10^{-5} \text{ 1/bar}$,
- viscosity: $\mu_w = 0.66 \text{ cP}$, @ $P = 154.8 \text{ bar}$, $T = 46.8^\circ\text{C}$,
- viscosibility: $1/\mu_w d\mu_w/dp = 6 \times 10^{-5} \text{ 1/bar}$.

Table 5.4. Composition of original fluid (gas) in the Borzęcin reservoir.

Component	Mole fraction
N_2	0.36300
CO_2	0.00284
H_2S	0.00129
C_1	0.61100
C_2	0.01970
C_{3+}	0.00461

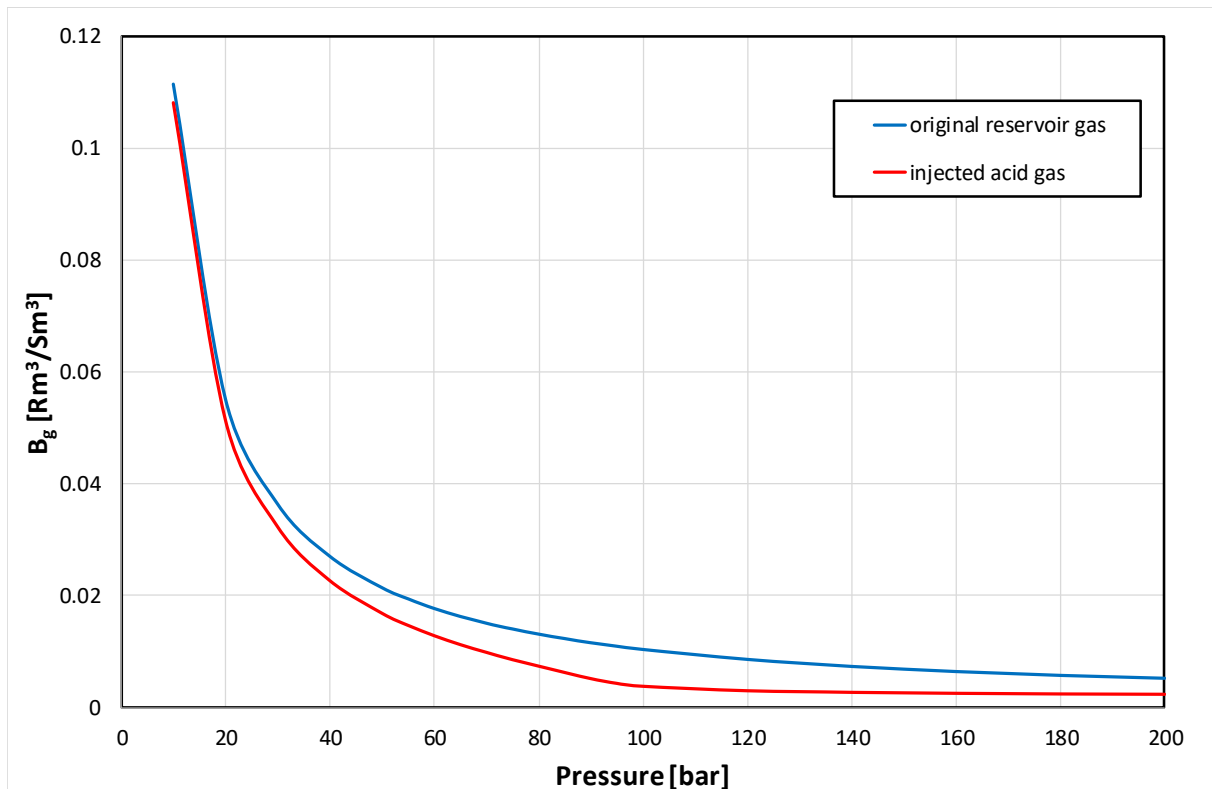


Figure 5.10. Formation volume factor of original gas and injected gas at reservoir temperature.

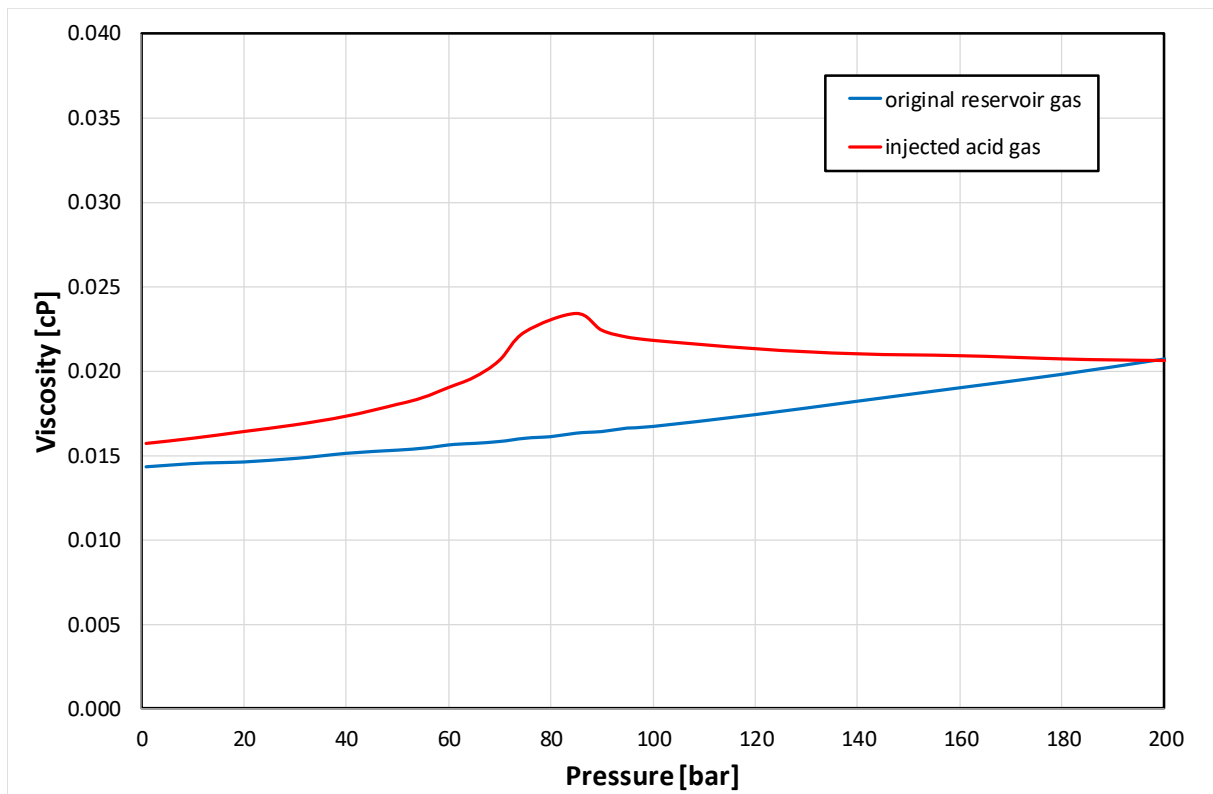


Figure 5.11. Viscosity of original gas and injected gas at reservoir temperature.

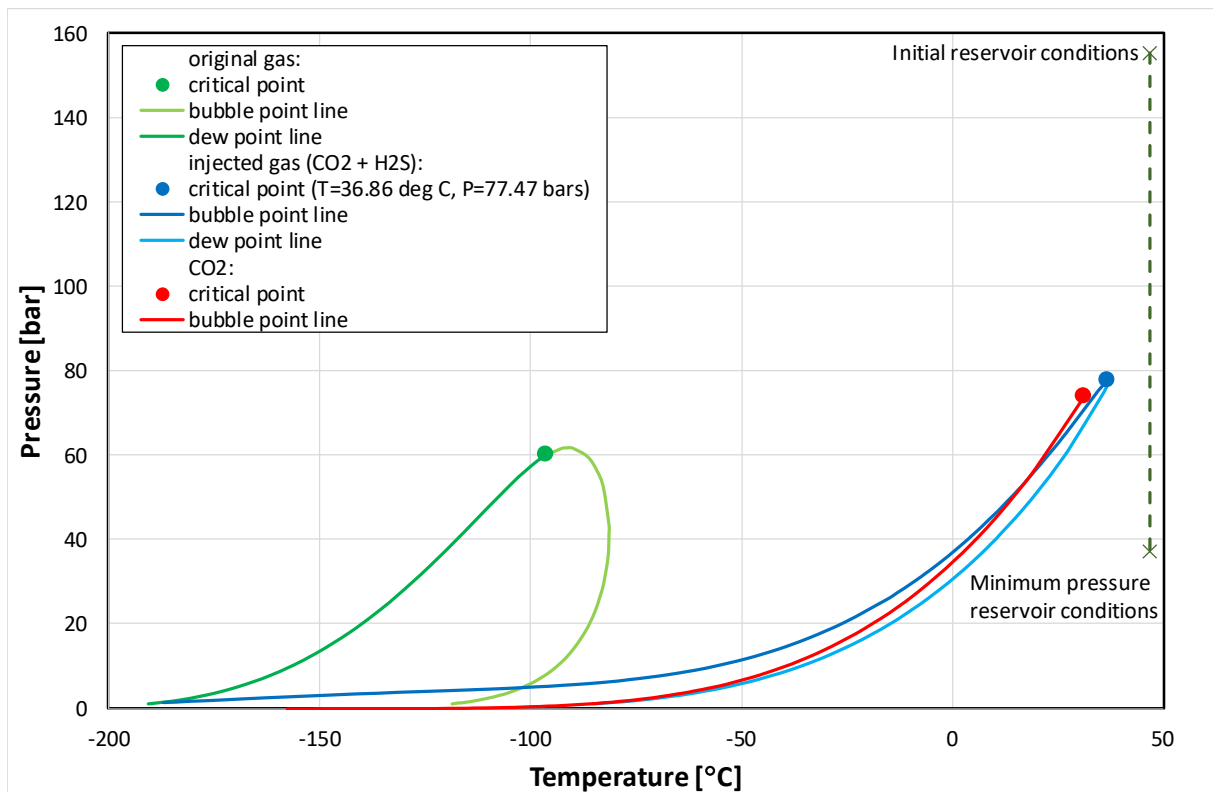


Figure 5.12. Phase diagram of: original reservoir gas, injected gas, pure CO₂.



In order to take into account effects of CO₂ and H₂S solubility in the reservoir brine, appropriate dependences of those solubilities upon varying reservoir pressures at the reservoir temperature were determined based on the measurements presented in Chapter 3. The measurement results were transformed to appropriate quantities (Table 5.5) and the following correlations of CO₂/H₂S solubility, $R_s(\text{CO}_2/\text{H}_2\text{S})$, vs pressure, P , and mole fractions of the coexisting component (H₂S/CO₂) were used:

$$\log[R_s(\text{CO}_2)] = a_{00} + a_{01} \cdot C_{\text{H}_2\text{S}} + a_1 \cdot \log(P) + a_2 \cdot \log(P)^2,$$

$$\log[R_s(\text{H}_2\text{S})] = a_{00} + a_{01} \cdot C_{\text{CO}_2} + a_1 \cdot \log(P) + a_2 \cdot \log(P)^2,$$

to match measurement data as shown in Figure 5.13 and Figure 5.14, respectively for CO₂ and H₂S. The resultant coefficients are given in Table 5.6.

Table 5.5. Analysis of gas-in-brine solution measurements.

Pressure P [bars]	Injected gas solution R_s(gas) [gas m ³ /brine m ³]	CO ₂ solution R_s(CO₂) [CO ₂ m ³ /brine m ³]	H ₂ S solution R_s(H₂S) [H ₂ S m ³ /brine m ³]	CO ₂ concentration C_{CO2} [mole fraction]	H ₂ S concentration C_{H2S} [mole fraction]
1.0	0.00	0.000	0.000	0.0000	0.0000
20.0	3.20	2.472	0.693	0.0070	0.0010
39.7	5.80	4.480	1.256	0.0127	0.0019
97.2	7.09	5.476	1.536	0.0155	0.0023
155.0	7.31	5.646	1.583	0.0160	0.0024

Table 5.6. Coefficients of RS models.

Quantity	Model coefficients			
	a₀₀	a₀₁	a₁	a₂
R _s (CO ₂)	-0.5604	0.0	1.1871	-0.2685
R _s (H ₂ S)	-1.1126	0.0	1.1871	-0.2685

5.2 MODEL CALIBRATION

The simulation model of the Borzęcin structure of the construction described above were subsequently calibrated based on 3 groups of data: pressures at well bottom-holes, water-gas ratios of individual well productions, CO₂ concentrations of gas produced by selected wells. The results of the calibration process are given in:

- Bottomhole pressures: Figure 5.15, Figure 5.16, Figure 5.17, Figure 5.18, Figure 5.19, Figure 5.20, Figure 5.21, Figure 5.22, Figure 5.23, Figure 5.24, Figure 5.25, Figure 5.26, Figure 5.27, Figure 5.28, Figure 5.29, Figure 5.30, Figure 5.31, Water-gas ratios:
- Figure 5.32, Figure 5.33, Figure 5.34, Figure 5.35, Figure 5.36, Figure 5.37, Figure 5.38, Figure 5.39, Figure 5.40, Figure 5.41, Figure 5.42, Figure 5.43, Figure 5.44, Figure 5.45, Figure 5.46, Figure 5.47,
- CO₂ concentration of produced gas: Figure 5.48, Figure 5.49, Figure 5.50, Figure 5.51, Figure 5.52.

The calibration process concluded with very precise match of the model results to the measured data. In order to obtain this match, several modifications of model parameters were introduced. The main modification divided the model into 3 partially separated regions (western, central and eastern ones) as shown in Figure 5.4. This division was necessary due to 3 different measured pressure trends as can be seen in Figure 2.30. As no faults, macro-fractures or other structure barriers were recognized in the structural geological setting, lithological barriers were assumed to separate the regions. In order to precisely match the pressure trends in this regions, transmissibility properties of those barriers together with effective pore volumes of the regions were determined and/or modified appropriately. Other global parameters of the model, that were subject to change, include: aquifer characteristics and vertical vs horizontal permeability anisotropy. In addition, local



transport properties were modified in several drainage well zones in order to match their water-gas ratios and produced gas composition.

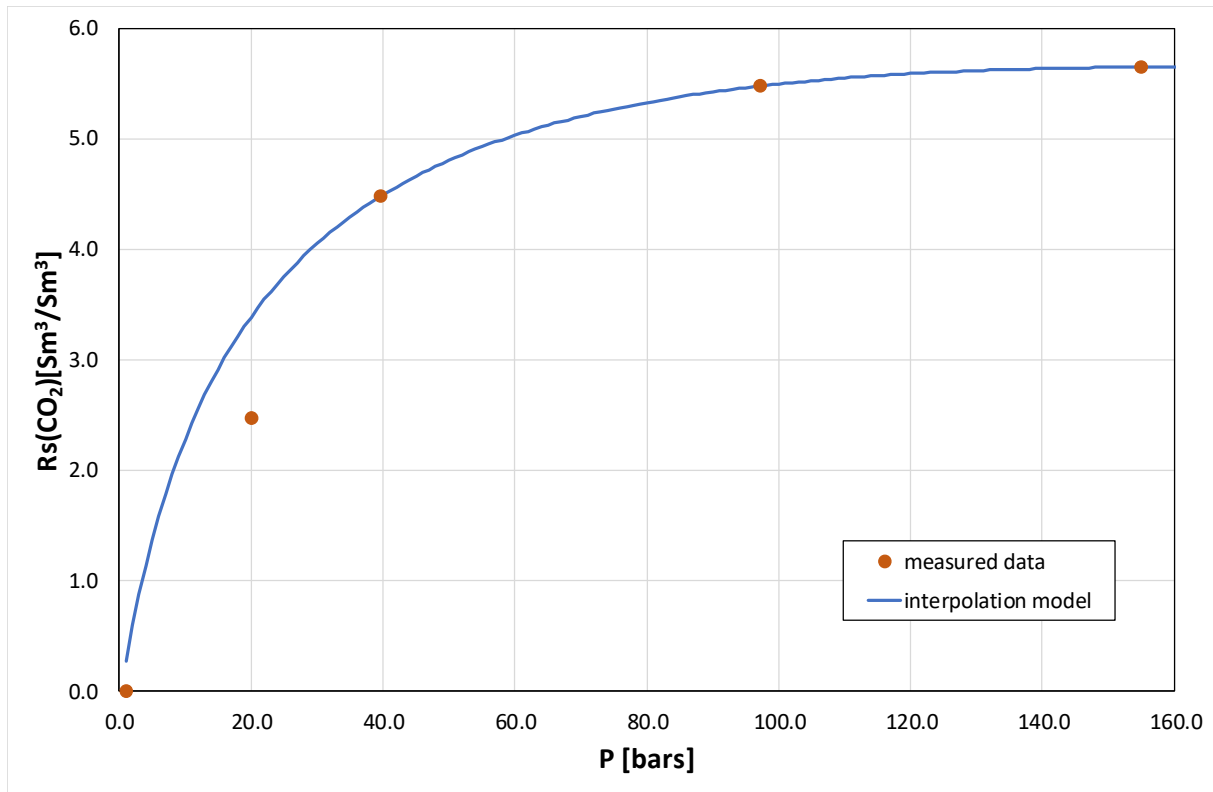


Figure 5.13. Solution of CO_2 in reservoir brine under reservoir conditions vs pressure.

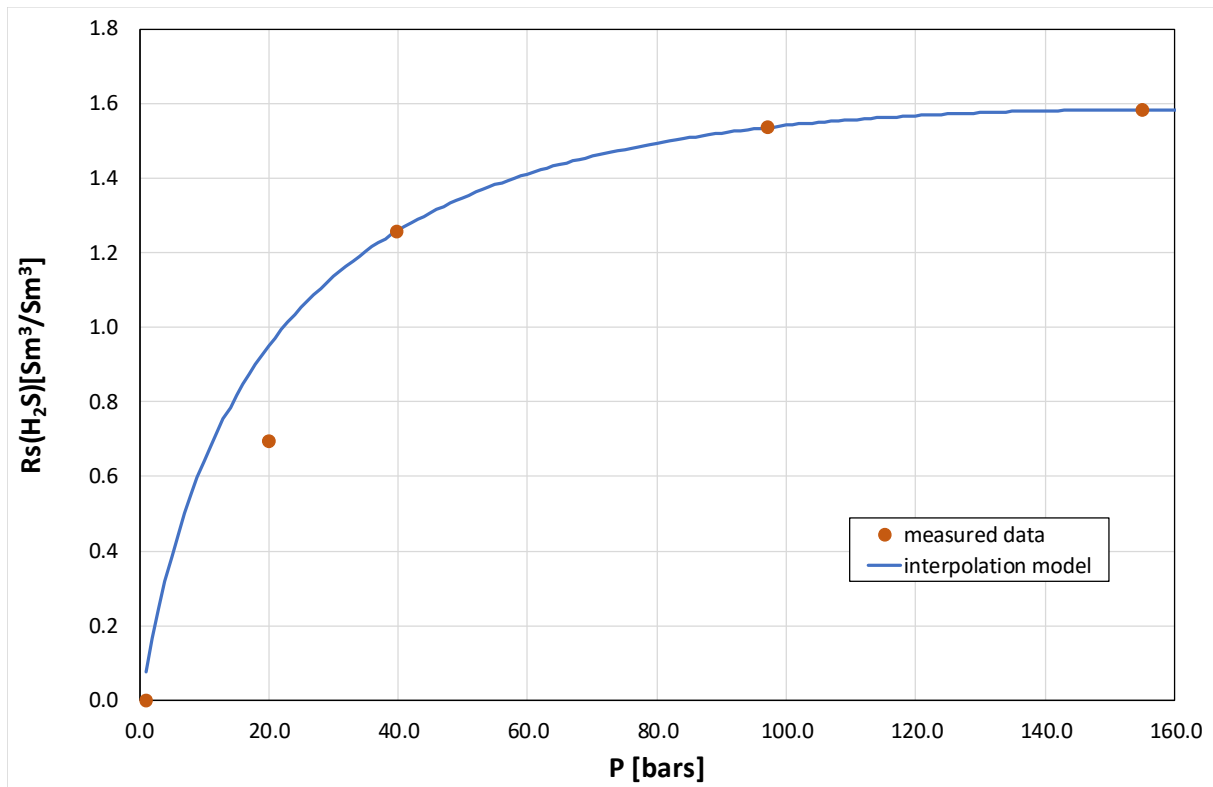


Figure 5.14. Solution of H_2S in reservoir brine under reservoir conditions vs pressure.

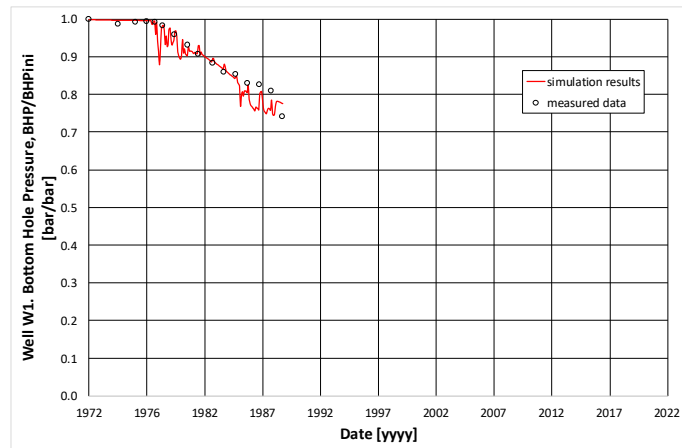


Figure 5.15. Model calibration. Comparison of measured bottom hole pressure and simulation results. Well W1.

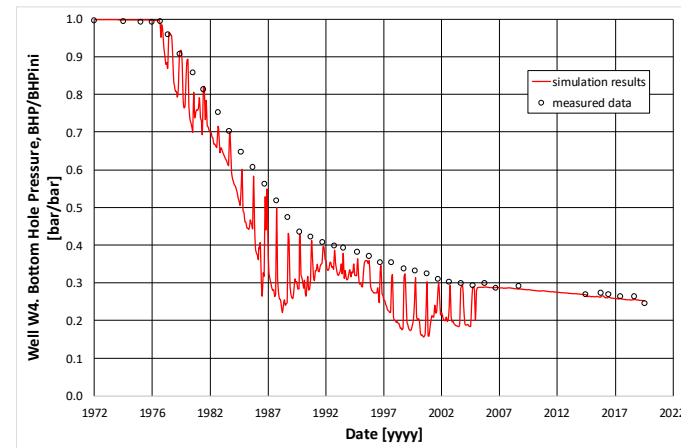


Figure 5.16. Model calibration. Comparison of measured bottom hole pressure and simulation results. Well W4.

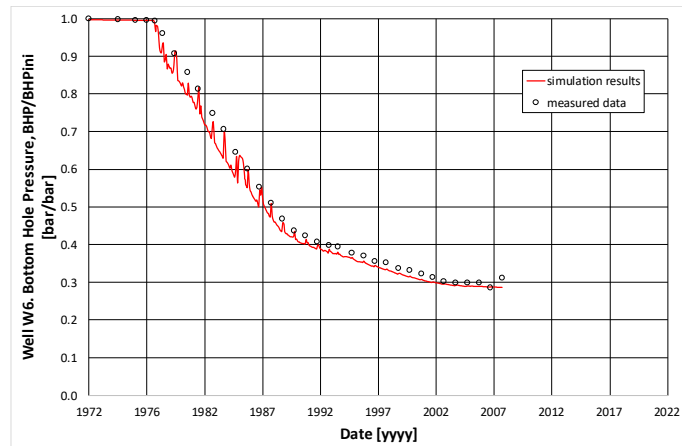


Figure 5.17. Model calibration. Comparison of measured bottom hole pressure and simulation results. Well W6.

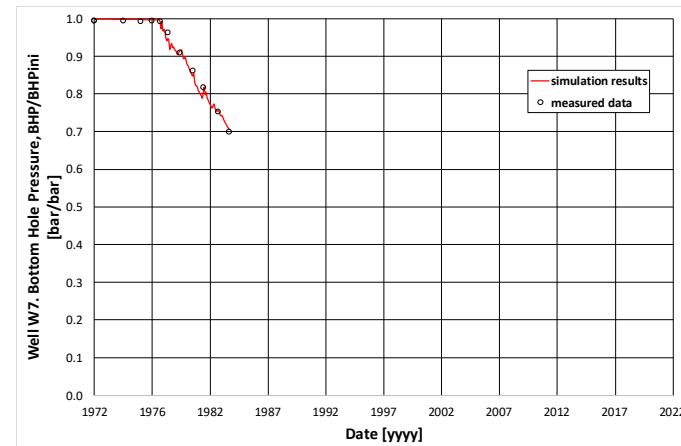


Figure 5.18. Model calibration. Comparison of measured bottom hole pressure and simulation results. Well W7.

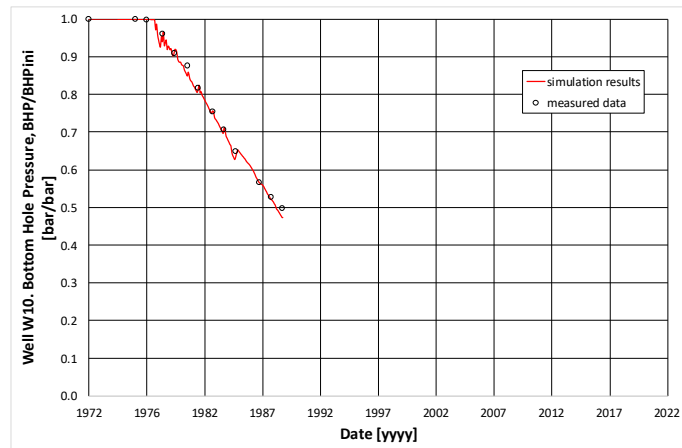


Figure 5.19. Model calibration. Comparison of measured bottom hole pressure and simulation results. Well W10.

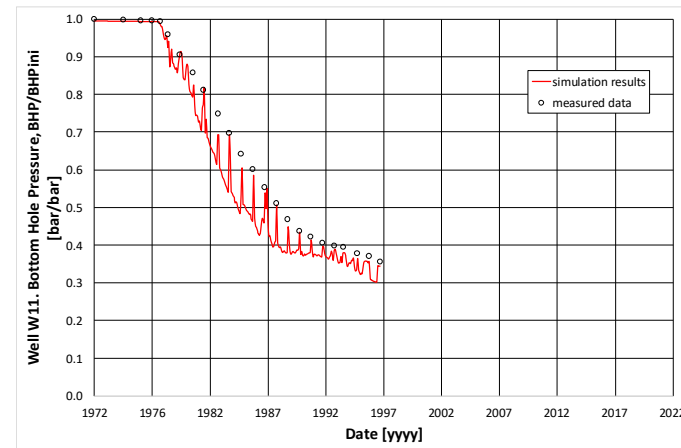


Figure 5.20. Model calibration. Comparison of measured bottom hole pressure and simulation results. Well W11.

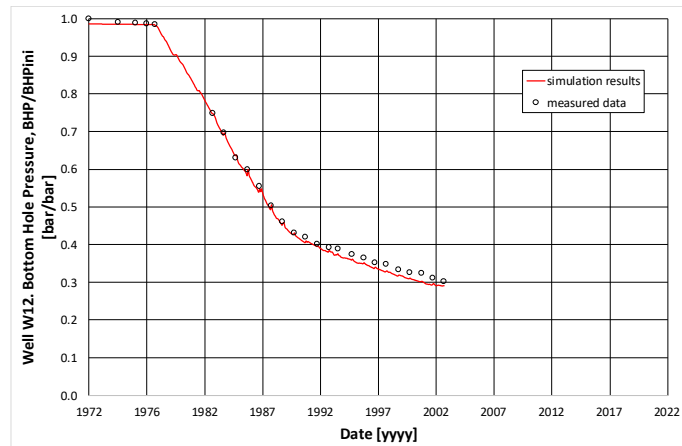


Figure 5.21. Model calibration. Comparison of measured bottom hole pressure and simulation results. Well W12

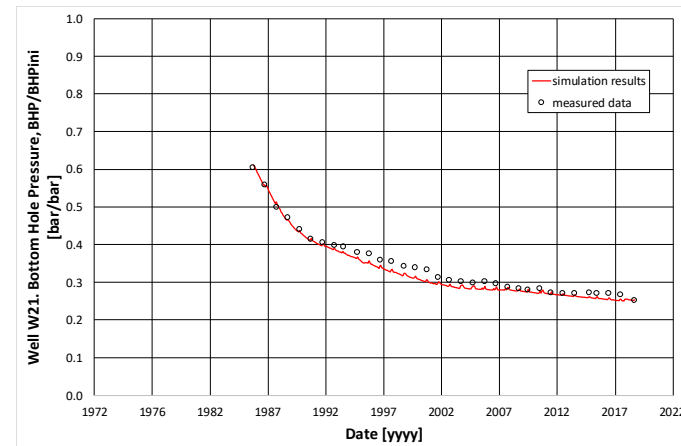


Figure 5.22. Model calibration. Comparison of measured bottom hole pressure and simulation results. Well W21.

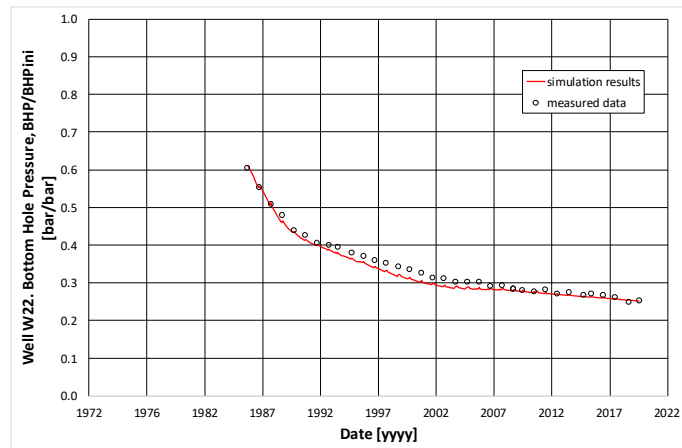


Figure 5.23. Model calibration. Comparison of measured bottom hole pressure and simulation results. Well W22.

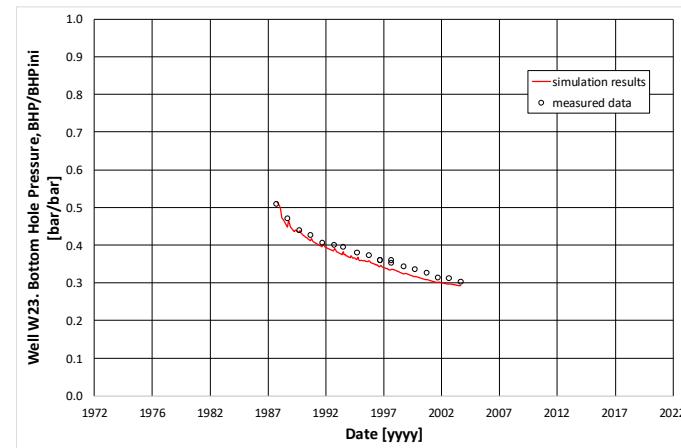


Figure 5.24. Model calibration. Comparison of measured bottom hole pressure and simulation results. Well W23.

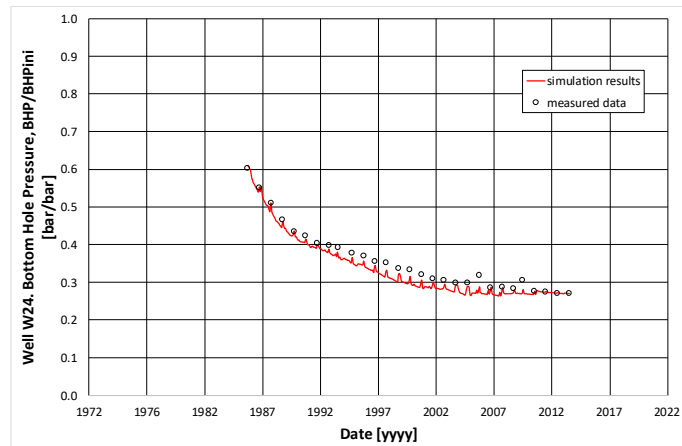


Figure 5.25. Model calibration. Comparison of measured bottom hole pressure and simulation results. Well W24.

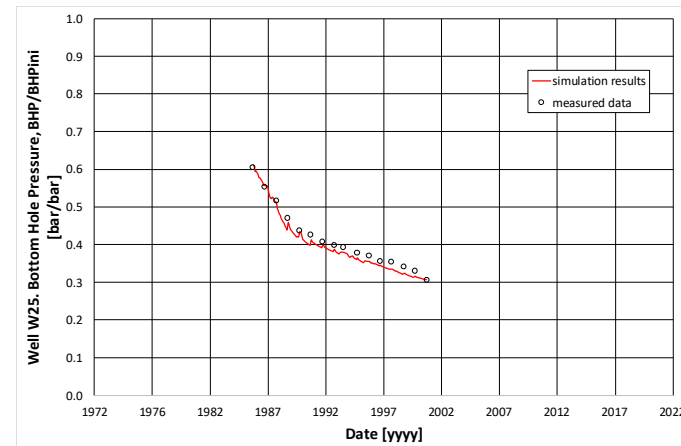


Figure 5.26. Model calibration. Comparison of measured bottom hole pressure and simulation results. Well W25.

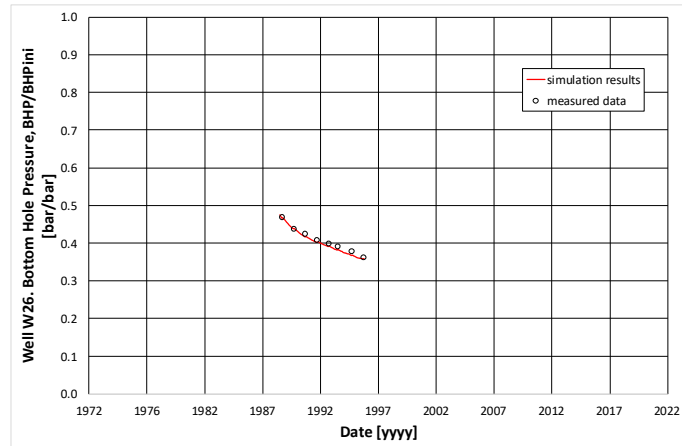


Figure 5.27. Model calibration. Comparison of measured bottom hole pressure and simulation results. Well W26.

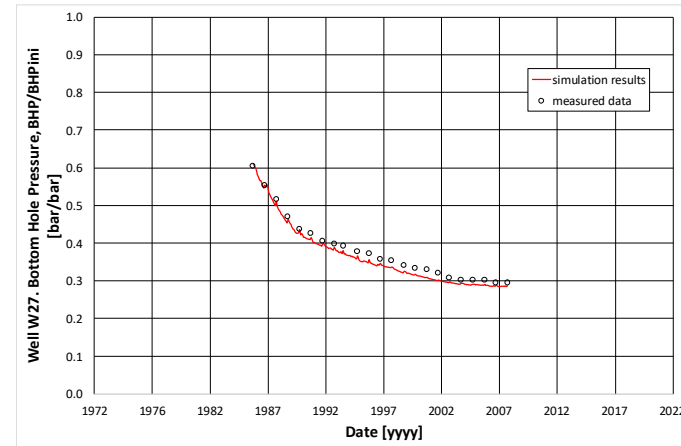


Figure 5.28. Model calibration. Comparison of measured bottom hole pressure and simulation results. Well W27.

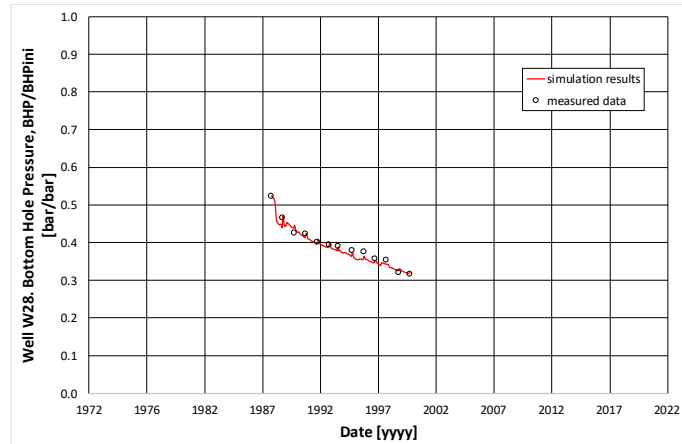


Figure 5.29. Model calibration. Comparison of measured bottom hole pressure and simulation results. Well W28.

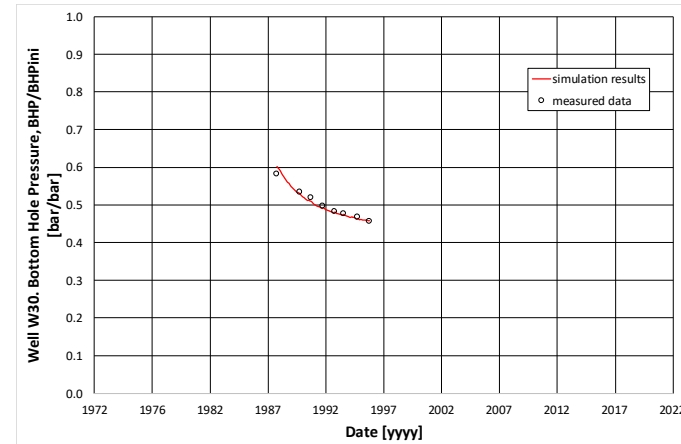


Figure 5.30. Model calibration. Comparison of measured bottom hole pressure and simulation results. Well W30.

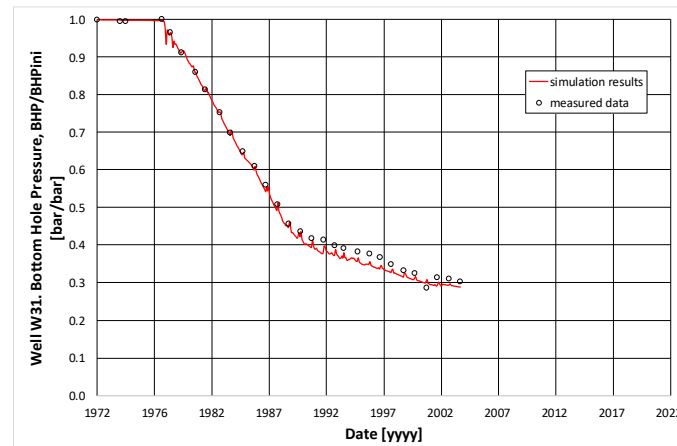


Figure 5.31. Model calibration. Comparison of measured bottom hole pressure and simulation results. Well W31.

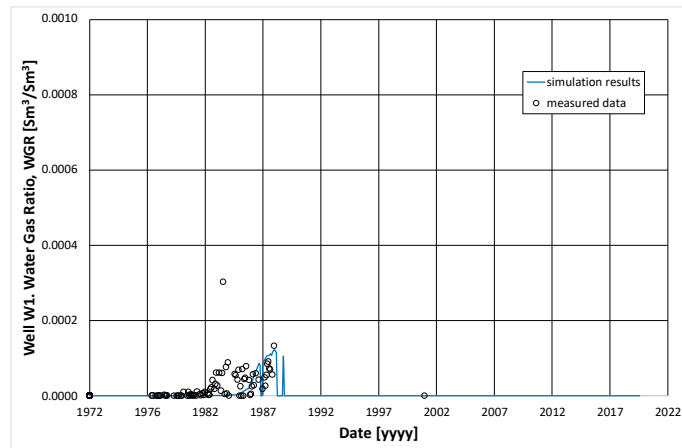


Figure 5.32. Model calibration. Comparison of measured water-gas ratio and simulation results. Well W1.

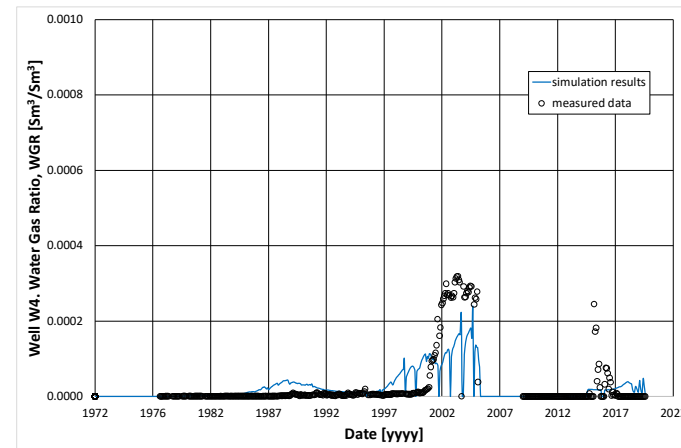


Figure 5.33. Model calibration. Comparison of measured water-gas ratio and simulation results. Well W4.

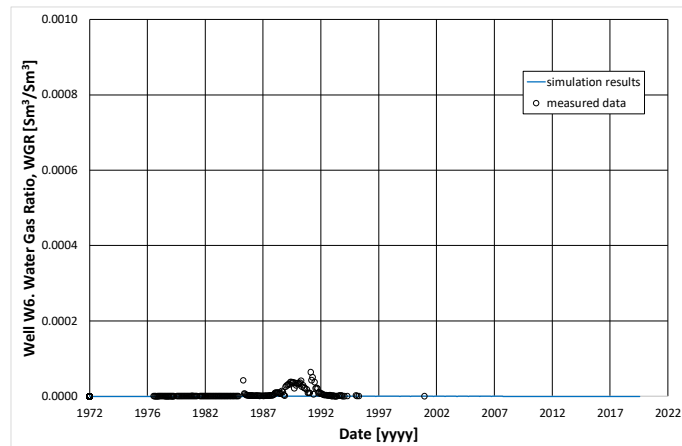


Figure 5.34. Model calibration. Comparison of measured water-gas ratio and simulation results. Well W6.

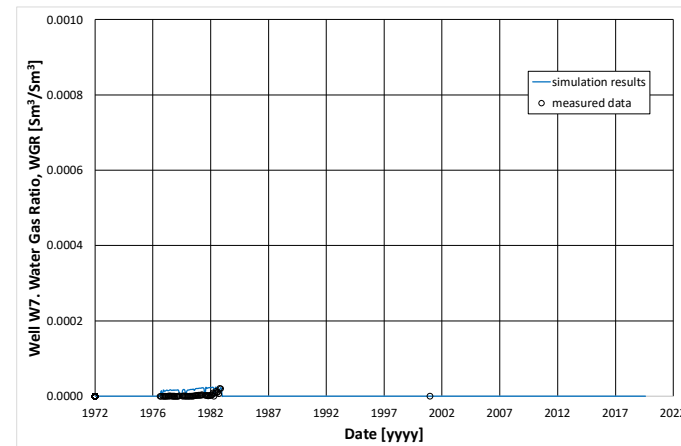


Figure 5.35. Model calibration. Comparison of measured water-gas ratio and simulation results. Well W7.

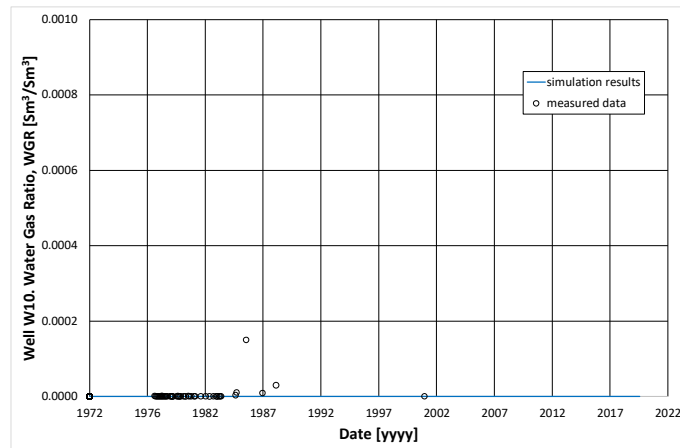


Figure 5.36. Model calibration. Comparison of measured water-gas ratio and simulation results. Well W10.

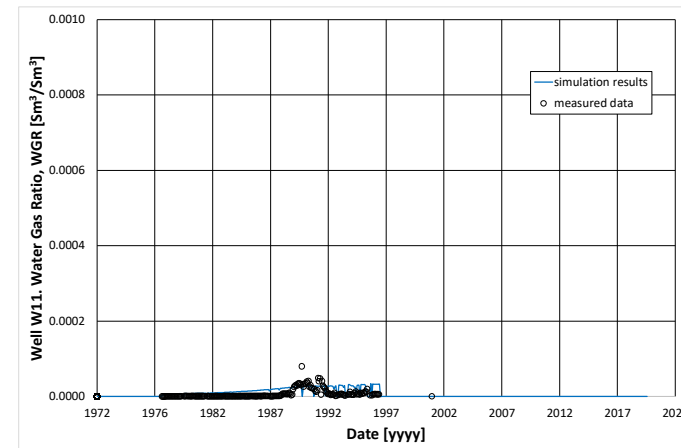


Figure 5.37. Model calibration. Comparison of measured water-gas ratio and simulation results. Well W11.

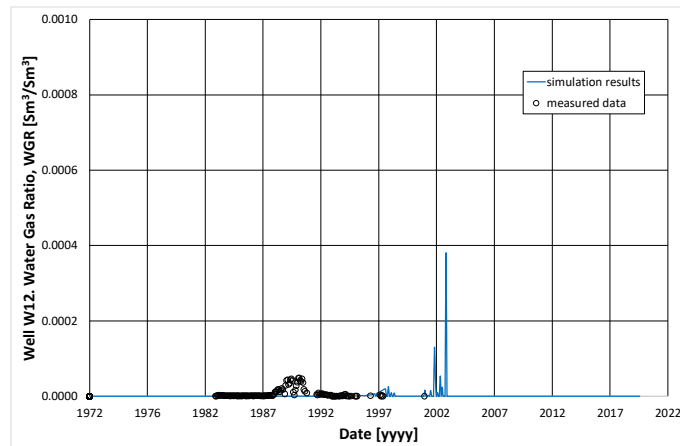


Figure 5.38. Model calibration. Comparison of measured water-gas ratio and simulation results. Well W12.

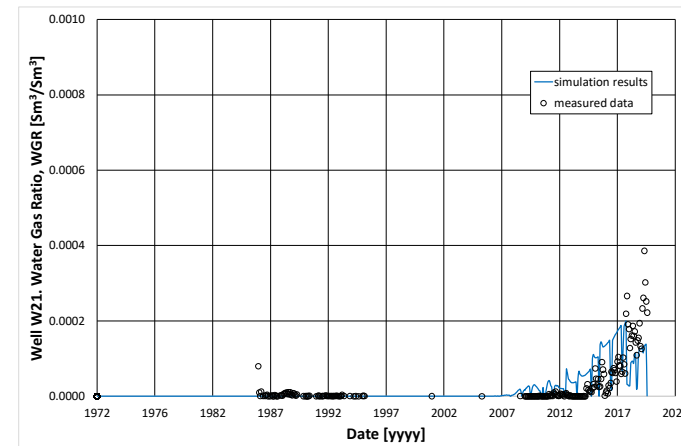


Figure 5.39. Model calibration. Comparison of measured water-gas ratio and simulation results. Well W21.

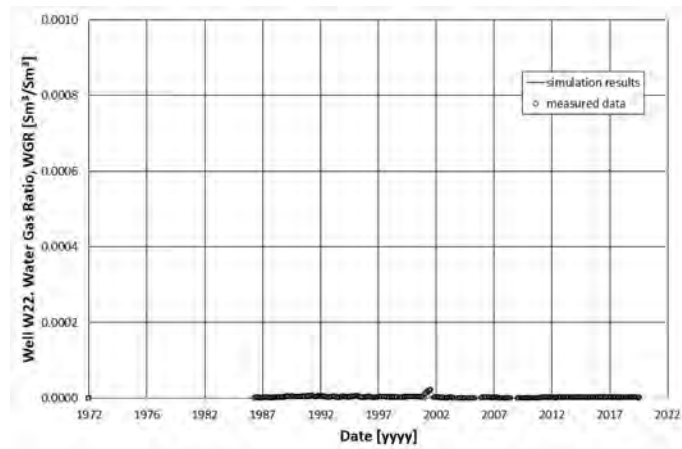


Figure 5.40. Model calibration. Comparison of measured water-gas ratio and simulation results. Well W22.

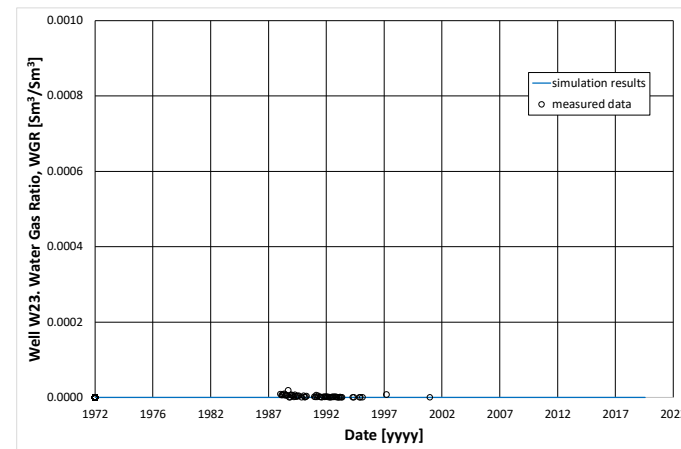


Figure 5.41. Model calibration. Comparison of measured water-gas ratio and simulation results. Well W23.

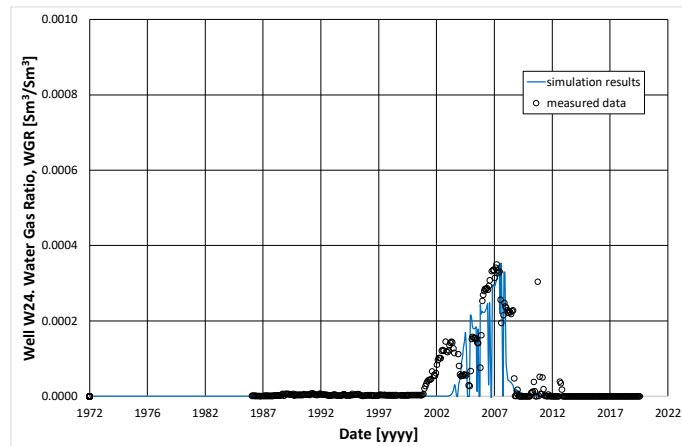


Figure 5.42. Model calibration. Comparison of measured water-gas ratio and simulation results. Well W24.

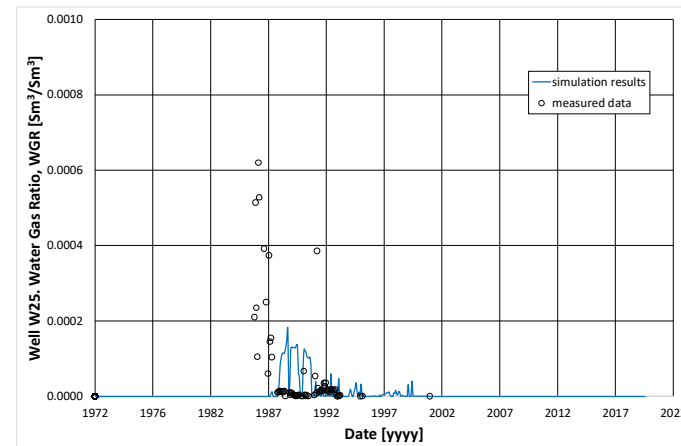


Figure 5.43. Model calibration. Comparison of measured water-gas ratio and simulation results. Well W25.

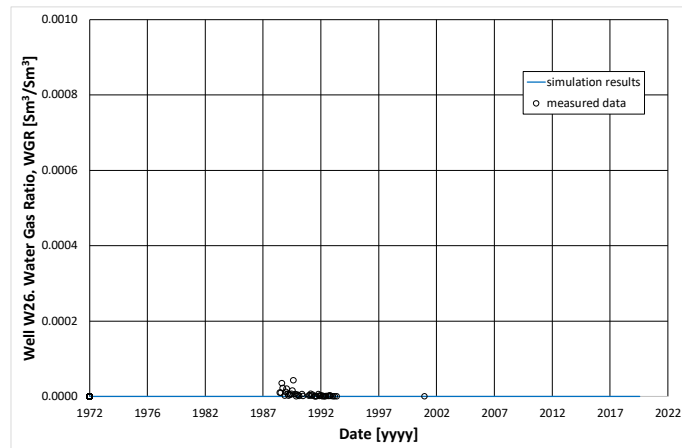


Figure 5.44. Model calibration. Comparison of measured water-gas ratio and simulation results. Well W26.

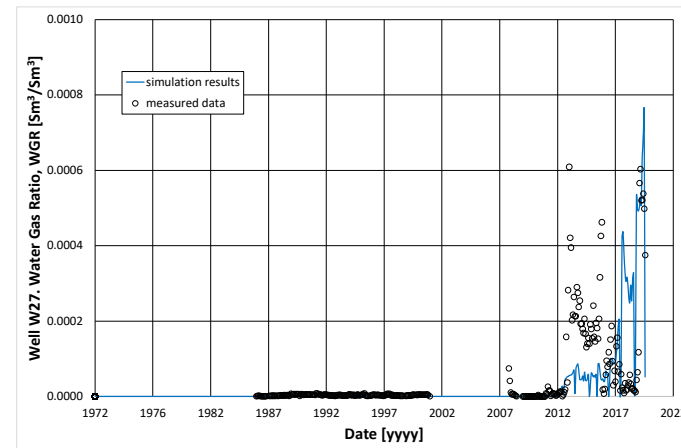


Figure 5.45. Model calibration. Comparison of measured water-gas ratio and simulation results. Well W27.

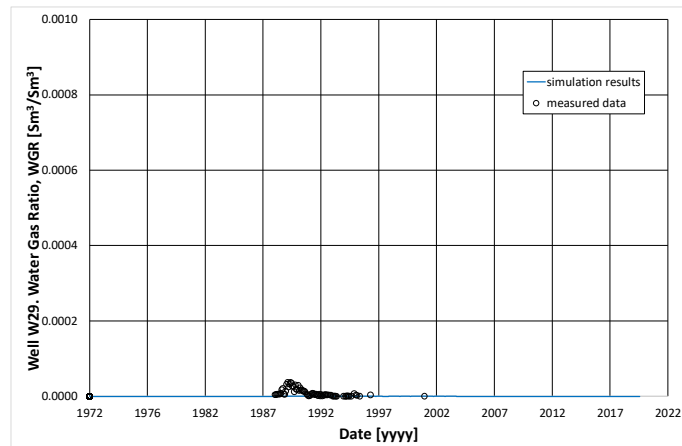


Figure 5.46. Model calibration. Comparison of measured water-gas ratio and simulation results. Well W29.

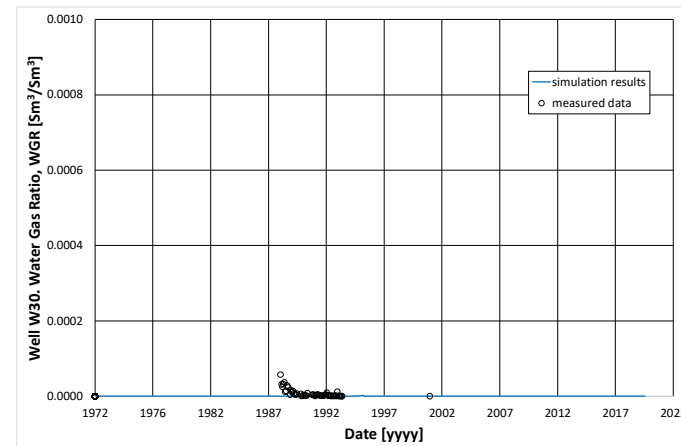


Figure 5.47. Model calibration. Comparison of measured water-gas ratio and simulation results. Well W30.

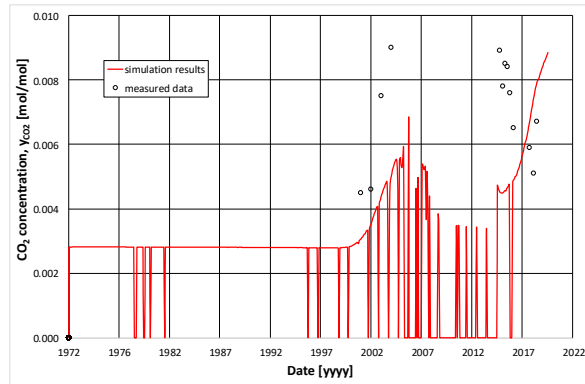


Figure 5.48. Model calibration. Comparison of measured CO₂ concentration and simulation results in gas produced by well W4.

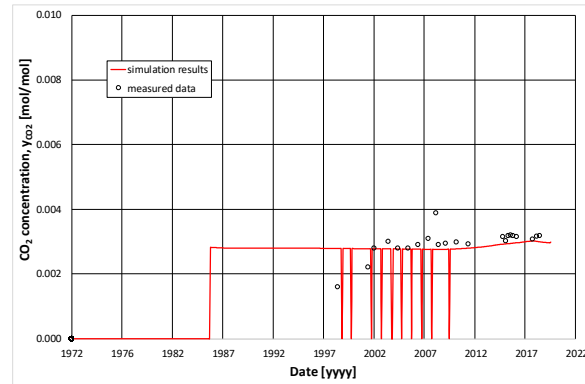


Figure 5.49. Model calibration. Comparison of measured CO₂ concentration and simulation results in gas produced by well W21.

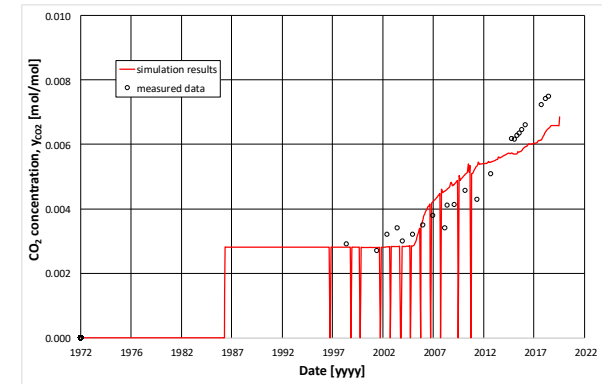


Figure 5.50. Model calibration. Comparison of measured CO₂ concentration and simulation results in gas produced by well W22.

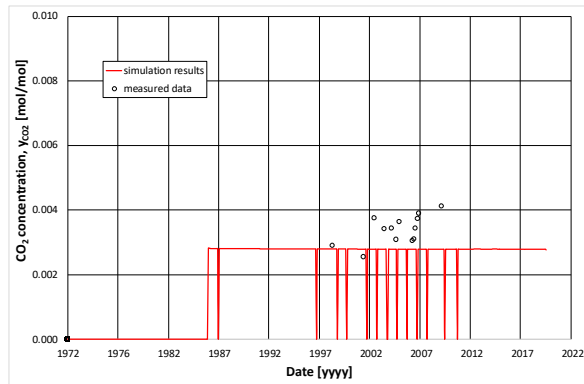


Figure 5.51. Model calibration. Comparison of measured CO₂ concentration and simulation results in gas produced by well W27.

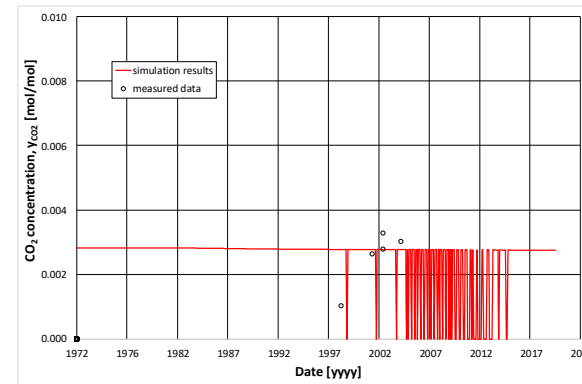


Figure 5.52. Model calibration. Comparison of measured CO₂ concentration and simulation results in gas produced by well W31.



5.3 SUMMARY AND CONCLUSIONS

This chapter includes continuation tasks concerning the modelling of the Borzęcin structure. Based on the geological model described in Chapter 4, a dynamic simulation model of the structure is constructed that implements the geological data supplemented with other required components such as: well technical data, reservoir fluid models (thermodynamic model of gas with varying composition, reservoir brine properties, reservoir fluid transport properties), initial reservoir conditions (pore pressures and fluid saturations), boundary reservoir conditions (models of surrounding and underlying aquifers). Upon the model construction it was calibrated against historical production data (gas production and injection rates, bottomhole pressures and water-gas ratios of the producing wells, CO₂ concentration of gas produced by individual wells).

In the next chapter, details of the project simulation results including reservoir pressure and fluid saturation distributions are used to analyse particular processes taking place in the structure during the project under consideration and to assess their consequences in terms of leakage risk.

6 Geomechanical model

6.1 GEOMECHANICAL DESCRIPTION

For the purposes to determine additional structure characteristics, such as formation breakdown pressure and variation of geomechanical state caused by reservoir pressure changes and presence of boreholes, a geomechanical model of the Borzęcin structure was used. That model was constructed within SECURE Work Package 4 by several authors of this deliverable (W.S., A.G., P.L., A.R.) and was subject to geomechanical simulations.

The geomechanical model was generated by the significant extension of the dynamic simulation model and included 3 additional parts:

- overburden – from the Borzęcin top up to the ground surface,
- sideburden – to encompass large lateral structures,
- underburden – to encompass Carboniferous horizons below the Rotliegend formation.

The 3D view of the geomechanical model is shown in Figure 6.1.

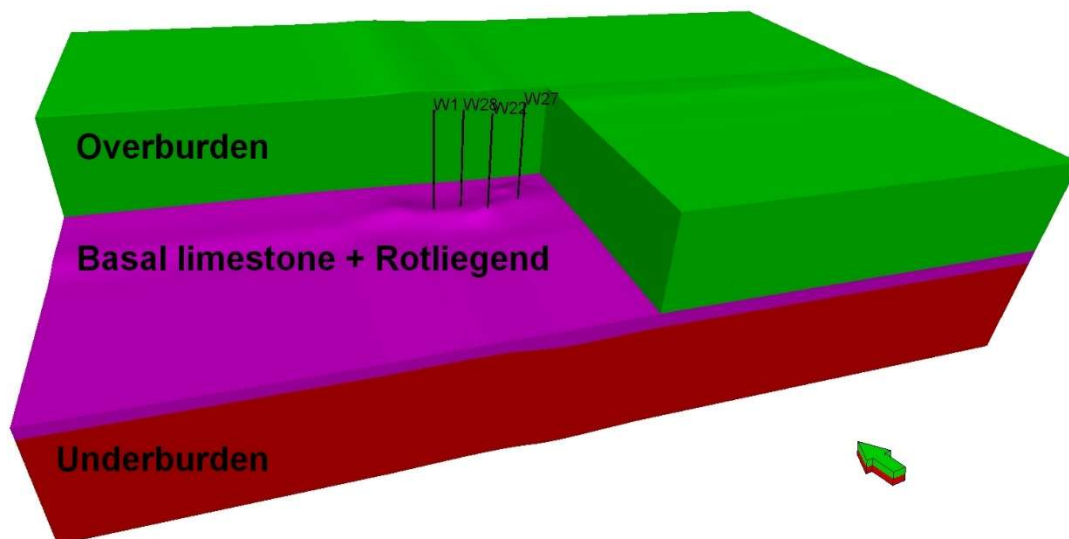


Figure 6.1. 3D view of the geomechanical model.

Geological and geomechanical parameters of that model were obtained from several sources including both the Borzęcin wells and wells penetrating neighbouring formations. The list of the geomechanical parameters include the following quantities shown in the associated figures:

- Young modulus – Figure 6.2,
- Poisson's ratio – Figure 6.3,
- unconfined compressive strength – Figure 6.4,
- friction angle – Figure 6.5,
- Biot constant – Figure 6.6,
- tensile strength – Figure 6.7.

6.2 GEOMECHANICAL SIMULATIONS

The basic geomechanical simulation results comprise stress and strain tensors. In the following, distributions of stress tensor main values (vertical, minimum horizontal, maximum horizontal ones) and volumetric strain are shown in the Figure 6.8, Figure 6.9, Figure 6.10, Figure 6.11, respectively, for 4 dates of operation: initial values (1972), the end of production phase (1996), the beginning of the injection phase with the presence of the well W28 (1996), and after 10 years of the injection (2006).

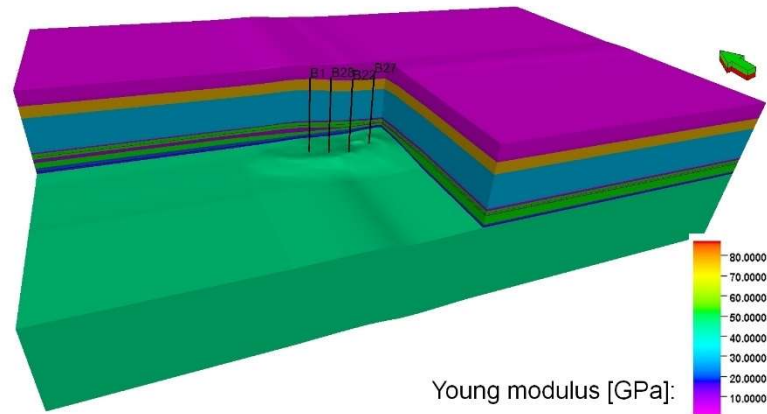


Figure 6.2. Geomechanical model input data. Young modulus.

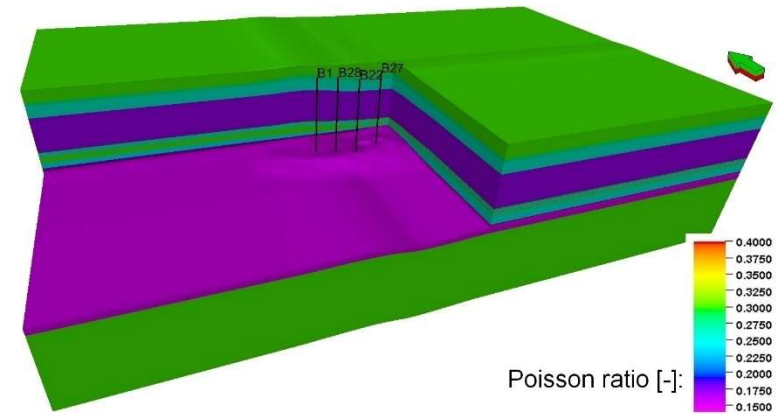


Figure 6.3. Geomechanical model input data. Poisson ratio.

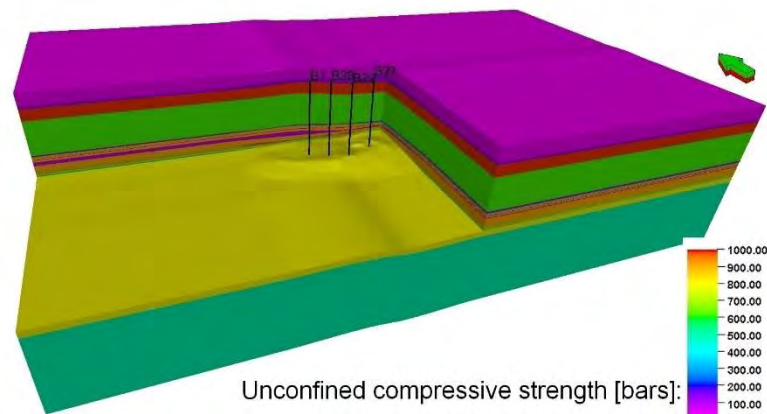


Figure 6.4. Geomechanical model input data. Unconfined compressive strength.

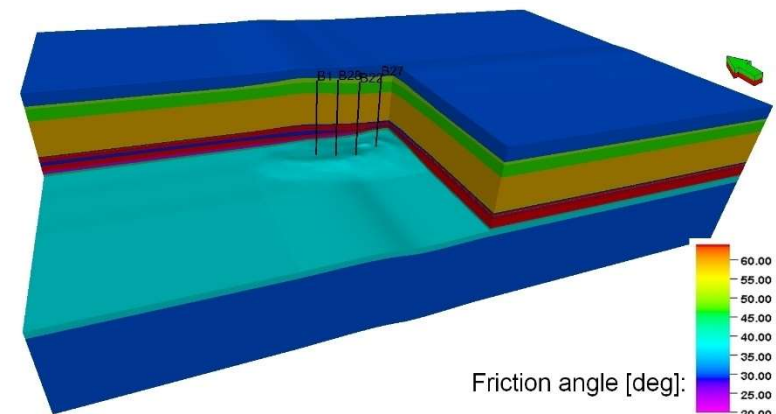


Figure 6.5. Geomechanical model input data. Friction angle.

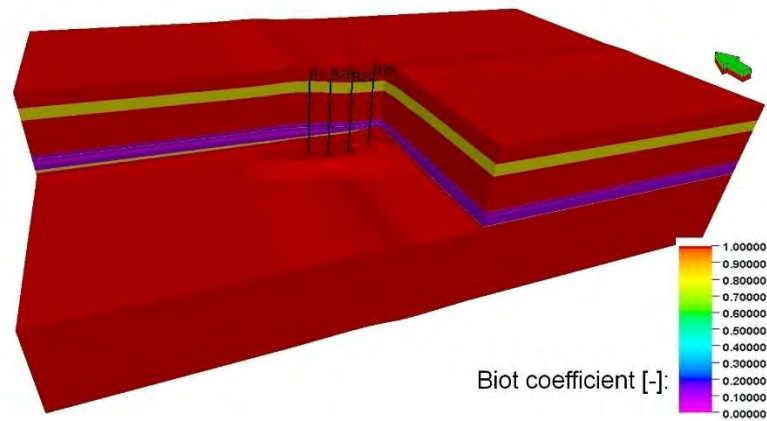


Figure 6.6. Geomechanical model input data. Biot coefficient.

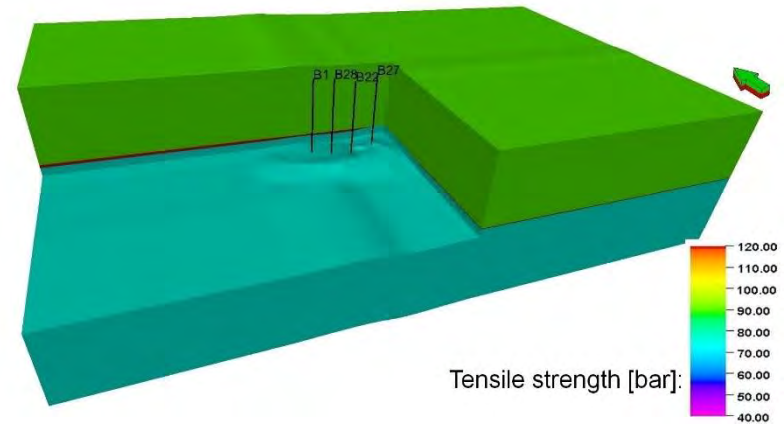
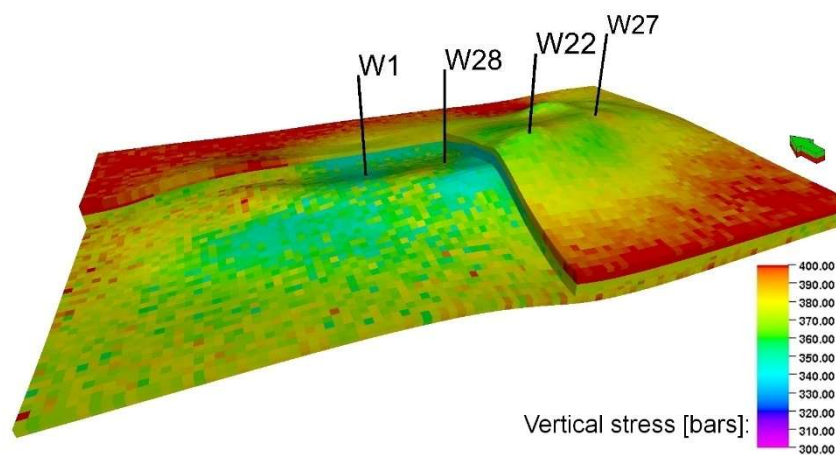
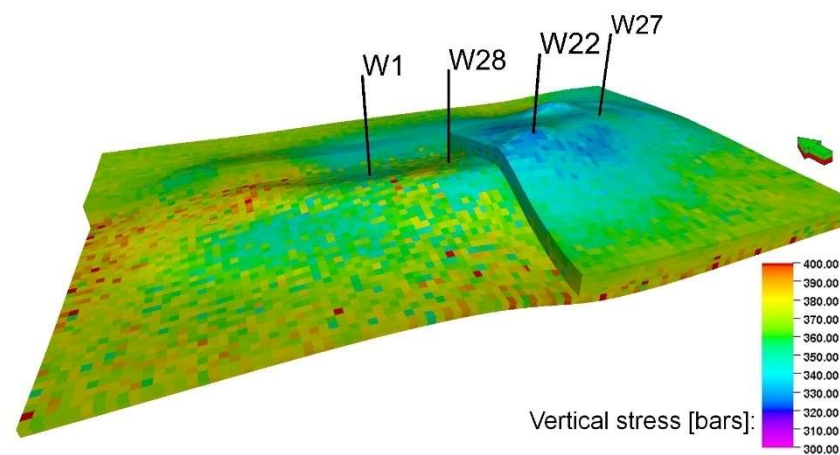


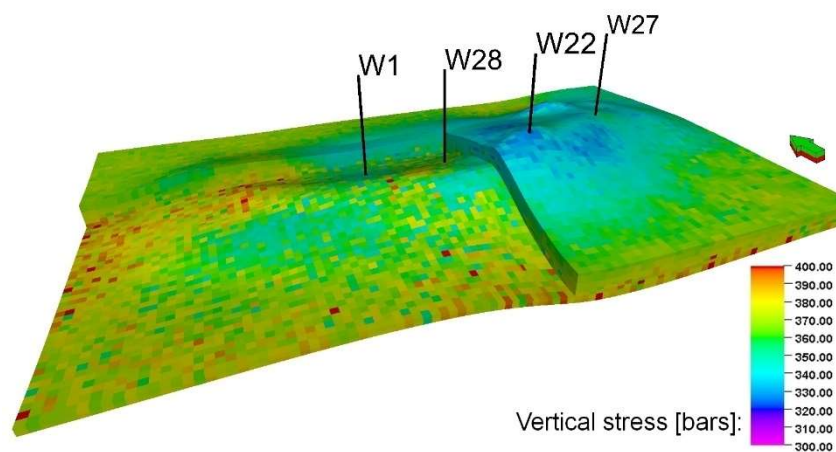
Figure 6.7. Geomechanical model input data. Tensile strength.



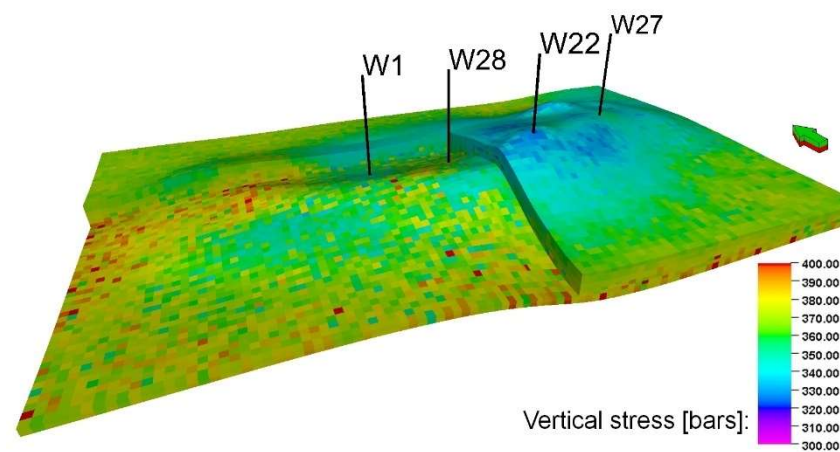
initial values (1972)



end of production phase (1996)

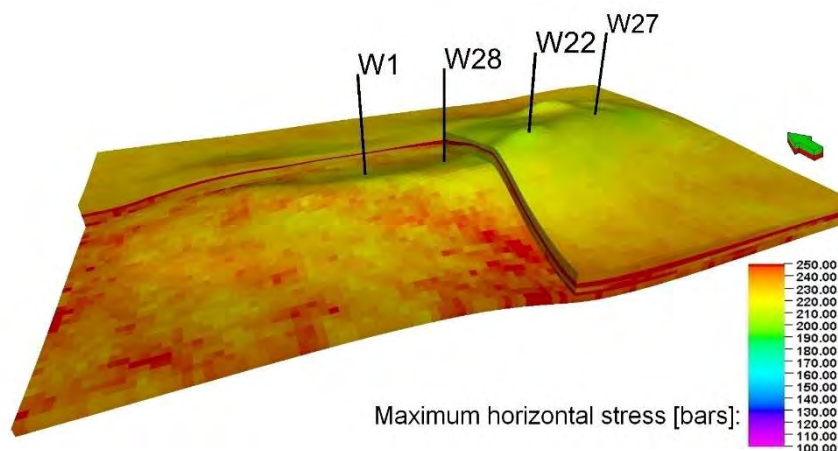


beginning of injection phase with well W28 (1996)

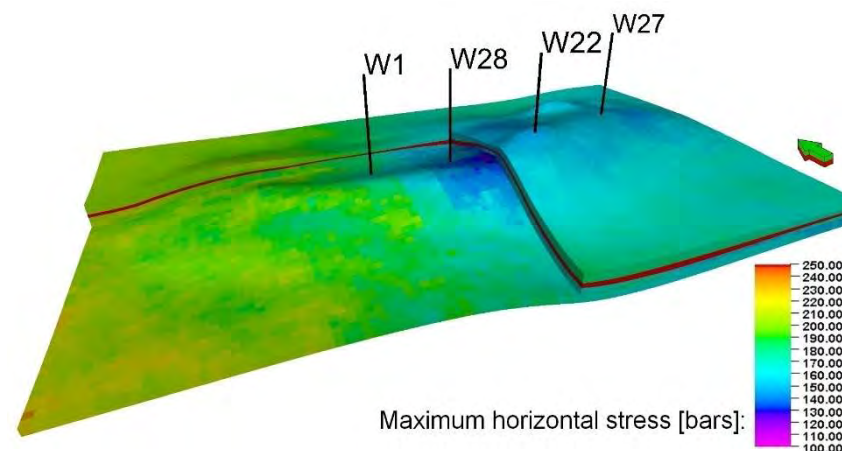


after 10 years of injection (2006)

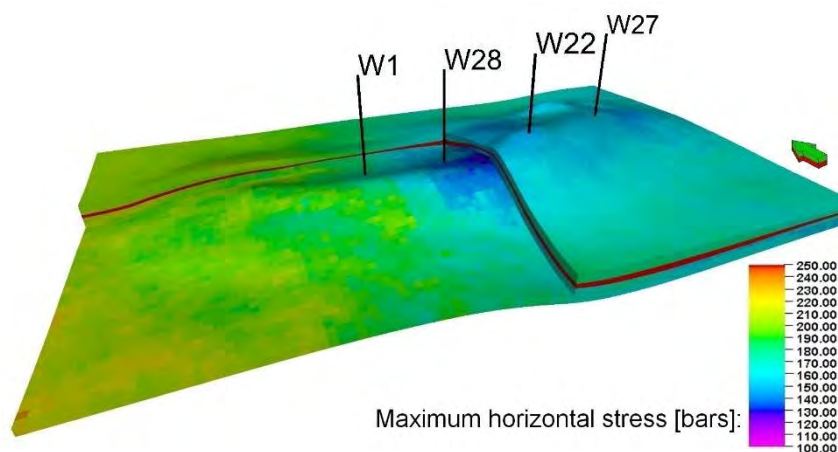
Figure 6.8. Distribution of vertical stress.



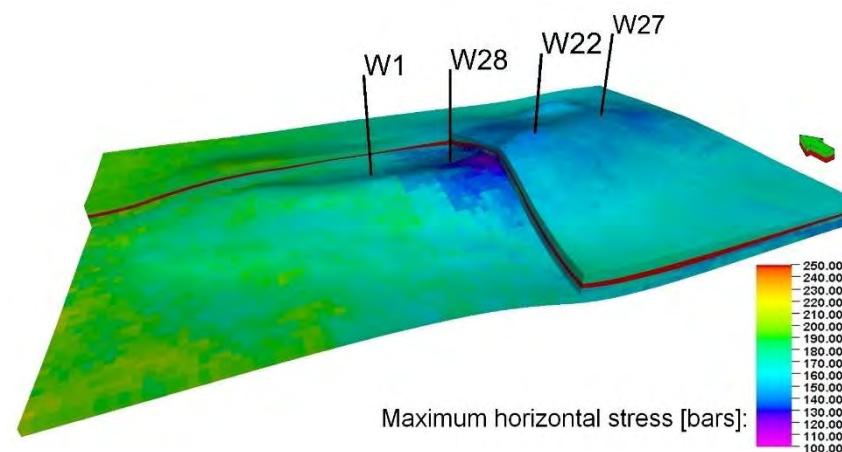
initial values (1972)



end of production phase (1996)

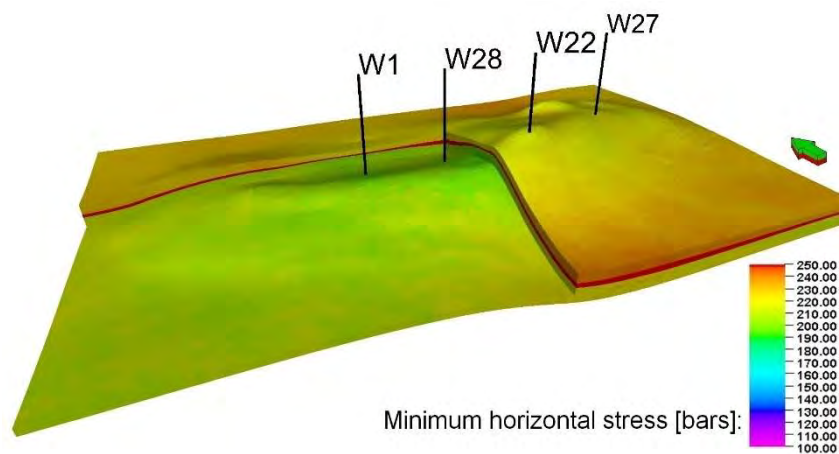


beginning of injection phase with well W28 (1996)

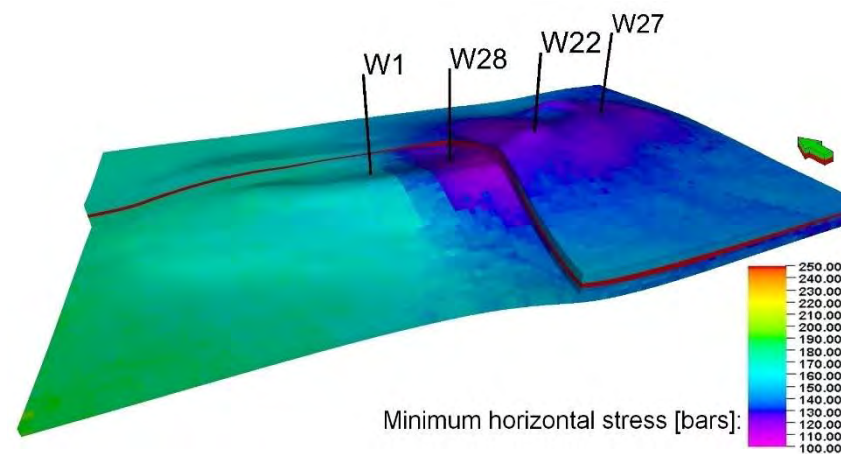


after 10 years of injection (2006)

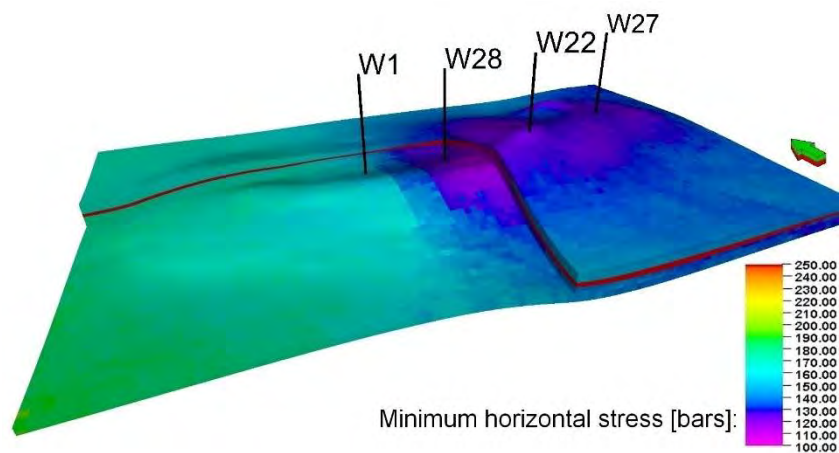
Figure 6.9. Distribution of maximum horizontal stress.



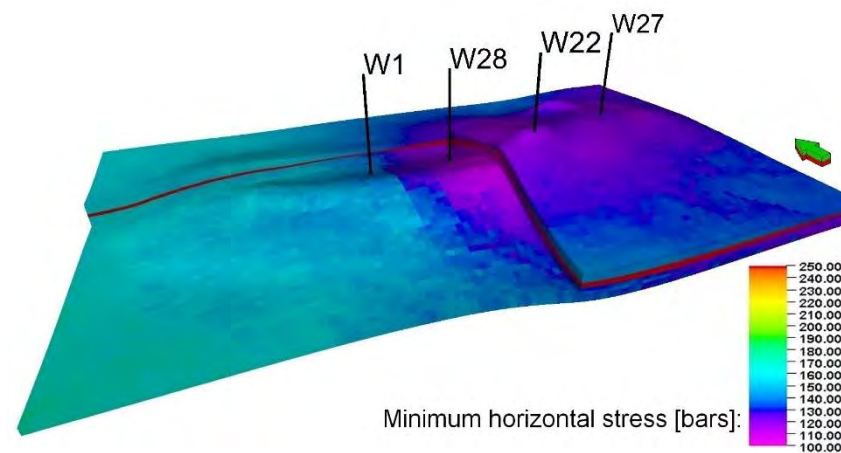
initial values (1972)



end of production phase (1996)

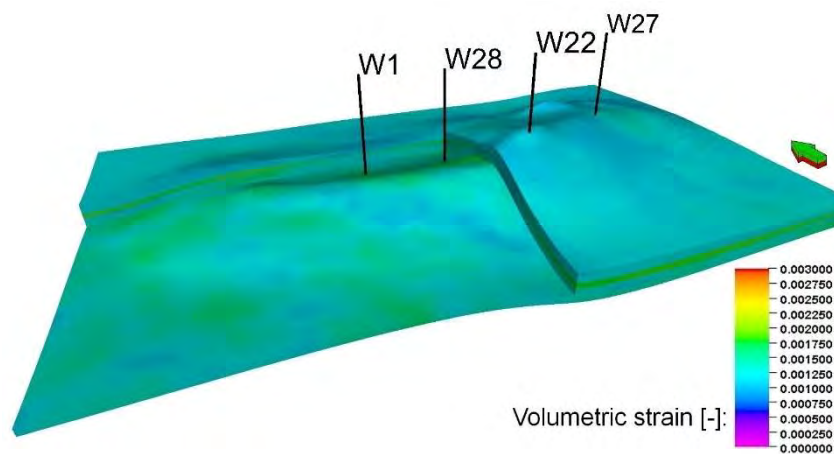


beginning of injection phase with well W28 (1996)

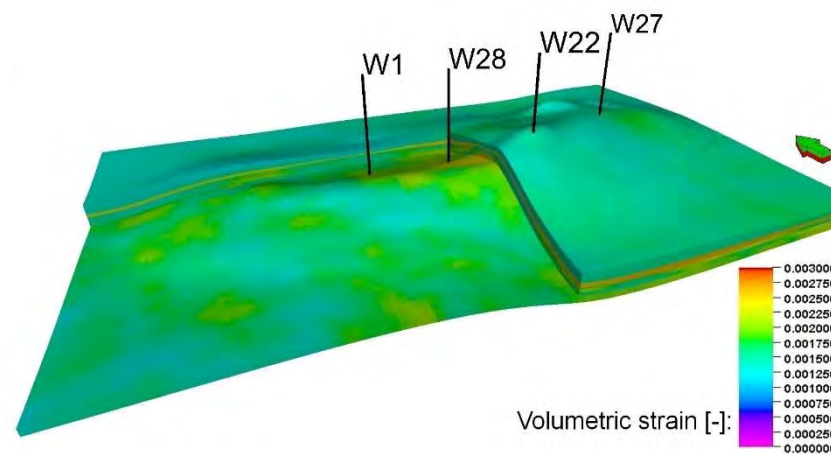


after 10 years of injection (2006)

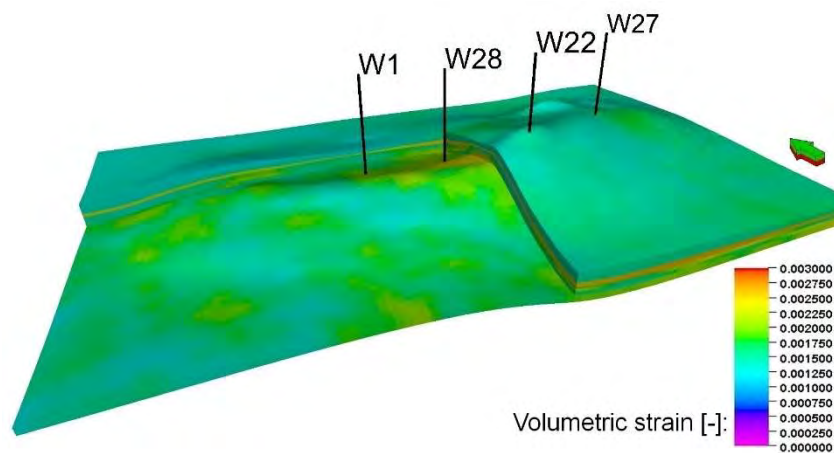
Figure 6.10. Distribution of minimum horizontal stress.



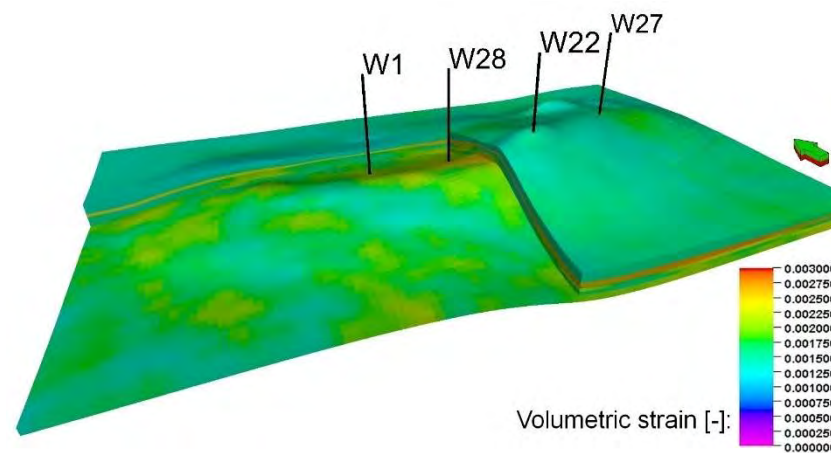
initial values (1972)



end of production phase (1996)



beginning of injection phase with well W28 (1996)



after 10 years of injection (2006)

Figure 6.11. Distribution of volumetric strain.



6.3 SUMMARY AND CONCLUSIONS

This chapter includes a concise description of the geomechanical model constructed within another work package (WP4) of the SECURE Project by the authors of this deliverable. Simulation results of the structure geomechanical state at 4 different moments of the project operation are presented in this chapter and will be used as important input data to assess particular leakage risk along the injecting well to be included as a part of deliverable D2.5.



7 Analysis of simulation results – detailed description of the ongoing sequestration process

7.1 PROCESS BASIC PARAMETERS

The calibrated model of the Borzęcin structure is used for the detailed analysis of processes taking place during the sequestration project. Some analysis refers to the pore pressure evolution within the Borzęcin structure. As indicated by the bottom-hole pressures reported in Chapter 2 and reconstructed in Chapter 5 as a result of the model calibrated process, three partially separated regions are identified within the Borzęcin structure. Average pressures of those regions significantly decline (as shown in Figure 7.1) and presently they assume a small fraction of the initial value.

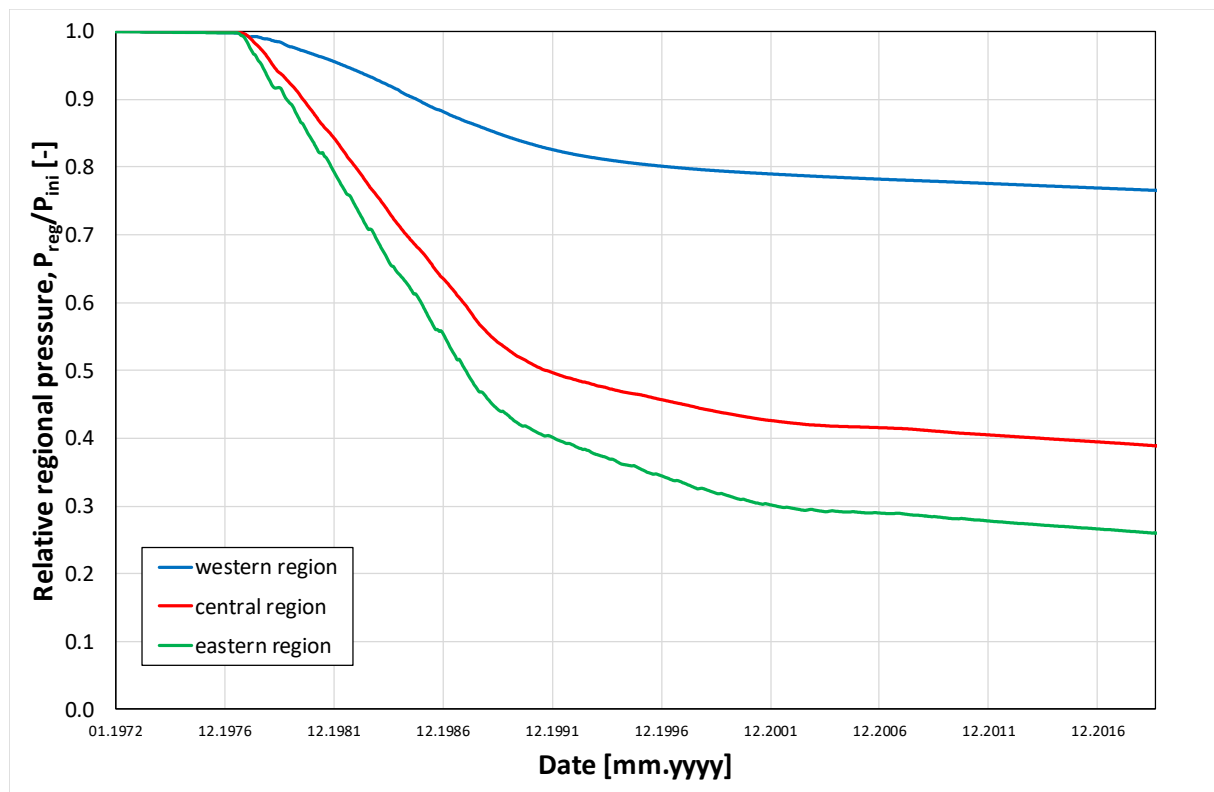


Figure 7.1. Evolution of relative average regional pressures.

These reductions take place despite the behaviour of the surrounding and underlying aquifers. The amount of total water encroachment is minor compared to the original water in place (see Figure 7.2 and Figure 7.3) yet it cannot be neglected as it is relevant when considering the pressure and water-to-gas ratio reconstructions of the producing wells.

Detailed pressure distributions within the structure volume are shown in Figure 7.4, Figure 7.5 and Figure 7.6 along the vertical cross section, at the structure top and bottom, respectively.

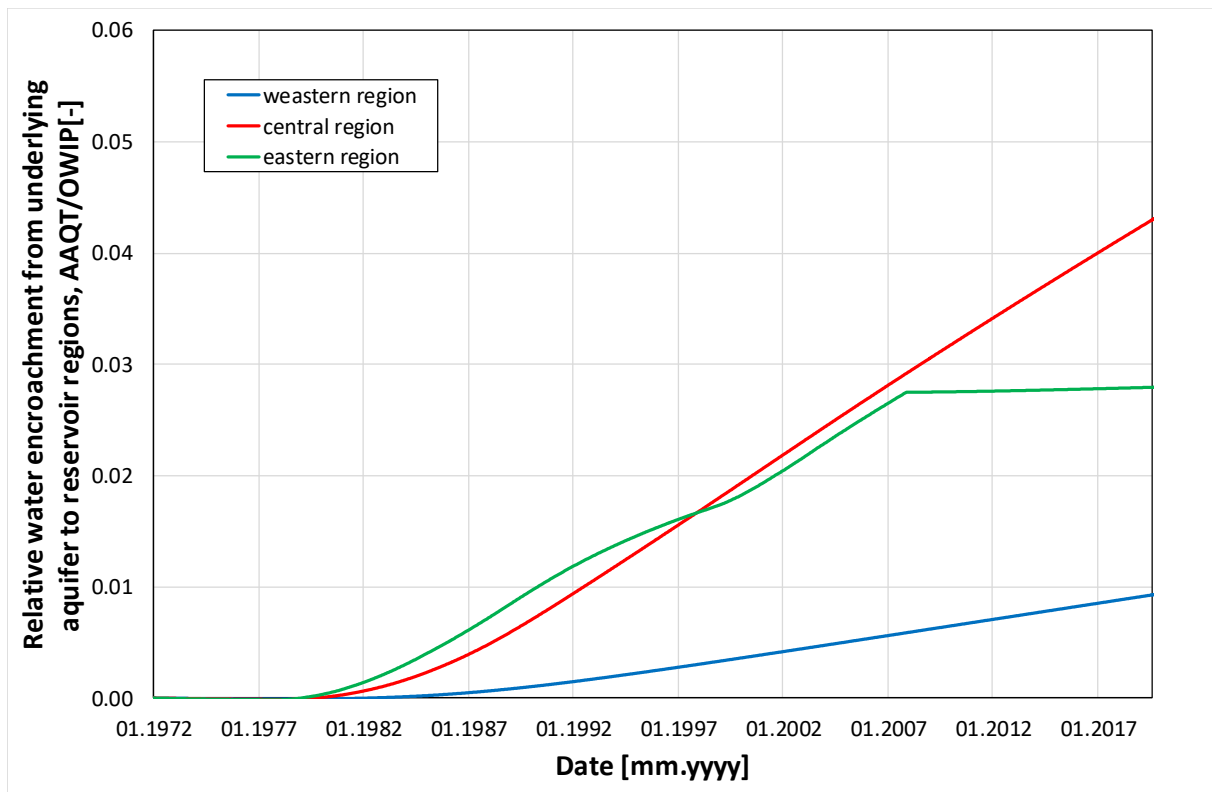


Figure 7.2. Relative water encroachment from underlying aquifer to reservoir regions.

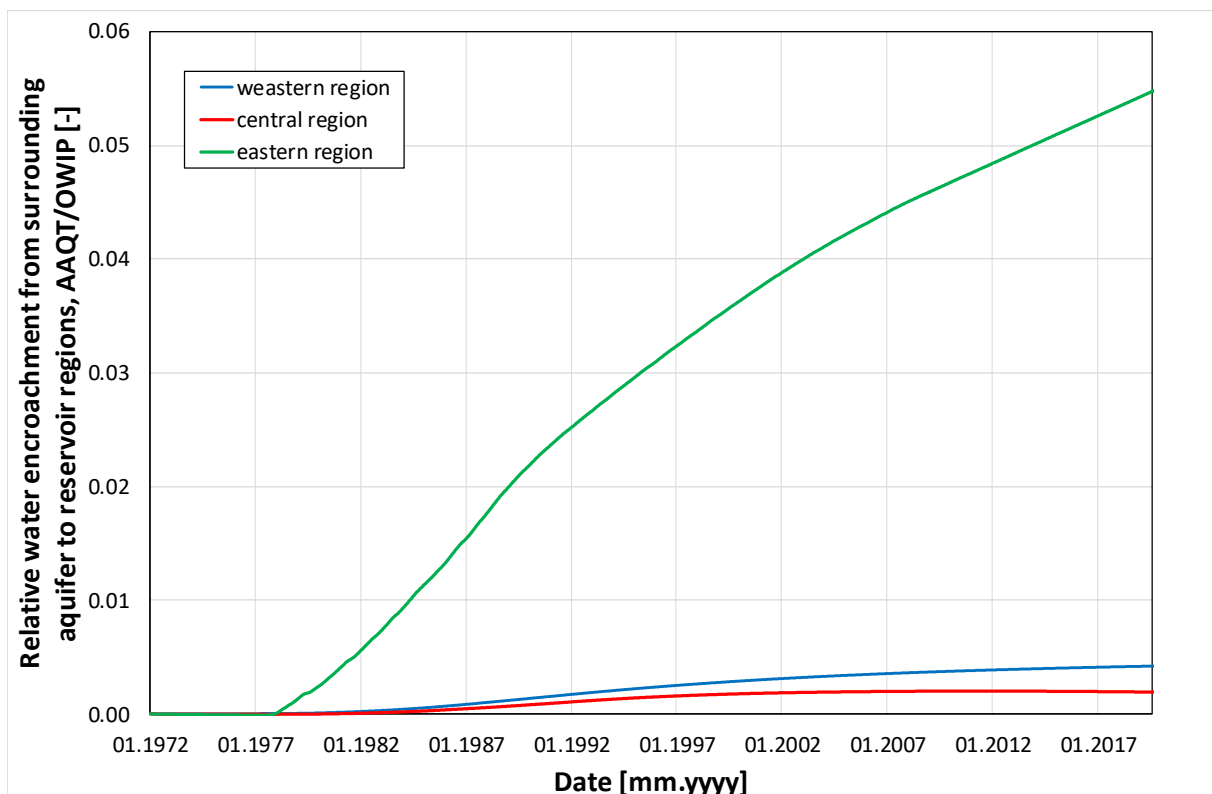


Figure 7.3. Relative water encroachment from surrounding aquifer to reservoir regions.

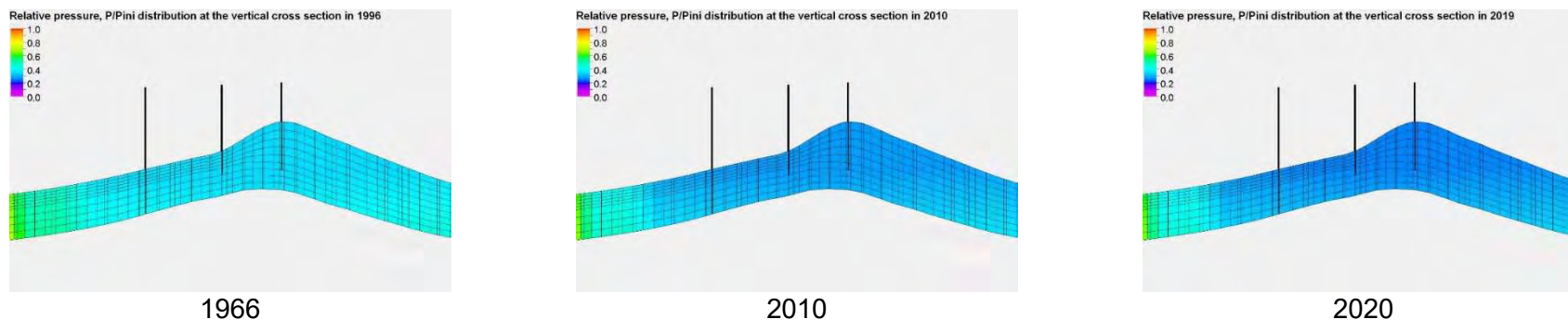


Figure 7.4. Relative pressure distribution along the vertical cross section connecting wells: W29, W22, W11.

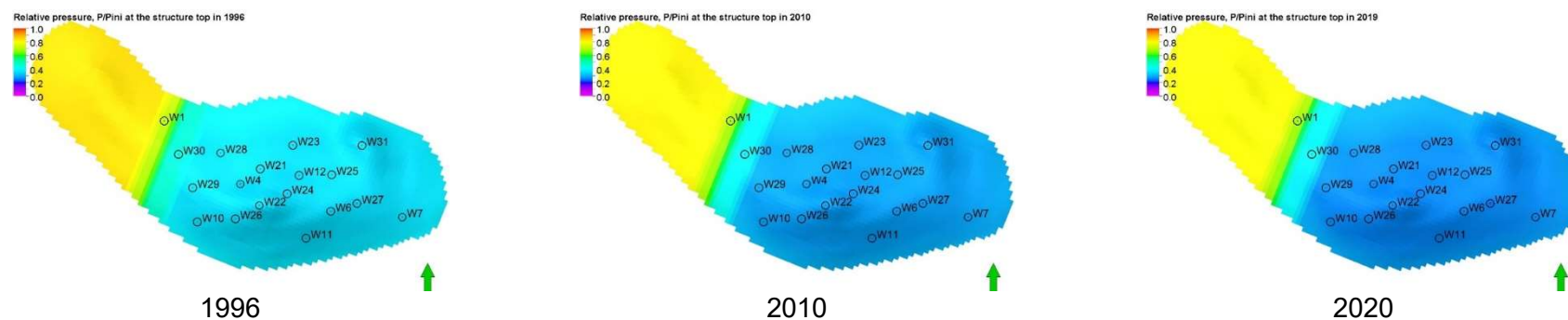


Figure 7.5. Relative pressure distribution at the structure top.

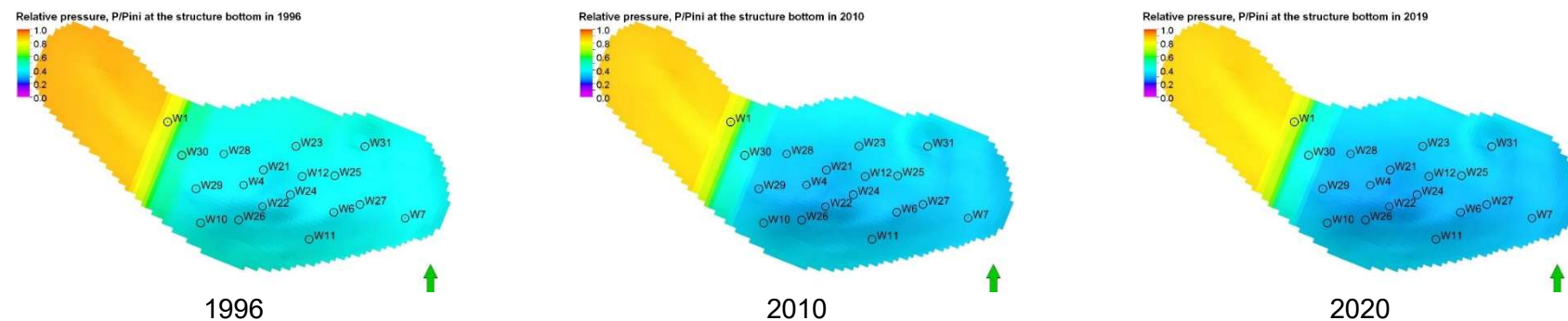


Figure 7.6. Relative pressure distribution at the structure bottom.



A local maximum pressure is observed along the completion interval of the injecting well W28. Its time evolution is shown in Figure 7.7 and does not exceed 40% of the reservoir initial pressure.

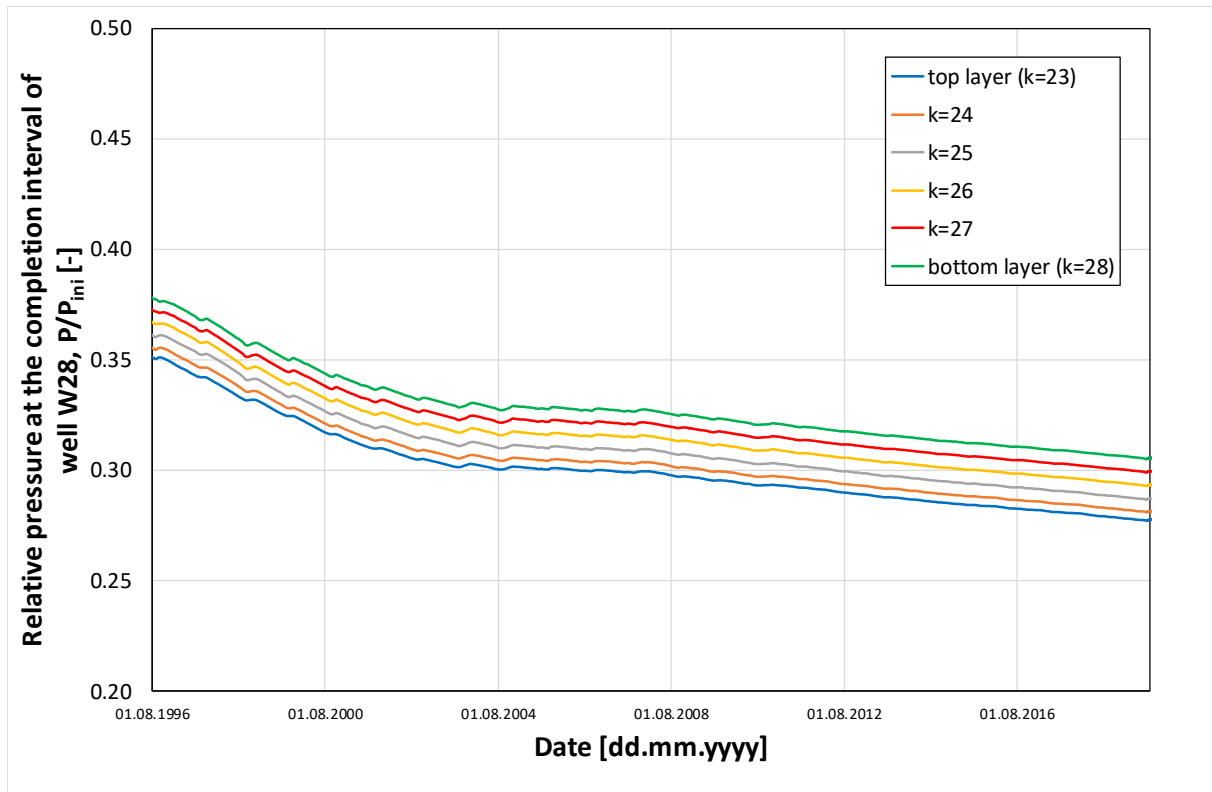


Figure 7.7. Relative pressure at the completion interval of well W28.

7.2 LEAKAGE RISK FACTOR ANALYSIS

This maximum pressure is compared with the formation breakdown (fracturing) pressure, P_{bd} , as calculated from the geomechanical model simulations according to the formula by Terzaghi [16]:

$$P_{bd} = 3\sigma_{h,min} - \sigma_{h,max} + T_0 - P_p$$

where:

- $\sigma_{h,min}$ – minimum horizontal stress,
- $\sigma_{h,max}$ – maximum horizontal stress,
- T_0 – tensile strength,
- P_p – pore pressure.

The calculated breakdown pressure distribution within the Borzęcin structure is shown in Figure 7.8. The maximum pore pressure during the injection phase of the acid gas sequestration project is much lower than the formation breakdown pressure. Consequently, there is no risk of any induced fractures to be generated and no leakage risk due to fracture pathways.

Another potential leakage pathway may occur through the caprock above the reservoir rock. Its sealing properties are, first of all, determined by threshold displacement pressure. This pressure for the Borzęcin structure can be estimated by analysing initial pressure profile across gas zone vs hydrostatic pressure profile in the caprock at the highest point of the caprock – reservoir rock boundary and by taking into account the complete sealing properties of the caprock under those conditions. This pressure profile is shown in Figure 7.9 and the threshold displacement pressure is found to be 9.2 bars.

As the maximum pressure at the structure caprock – reservoir rock boundary is much reduced compared to the initial pressure, the pressure step across the boundary never exceeds the estimated threshold displacement pressure. Consequently, there is no leakage risk due to pathways developed in the caprock.

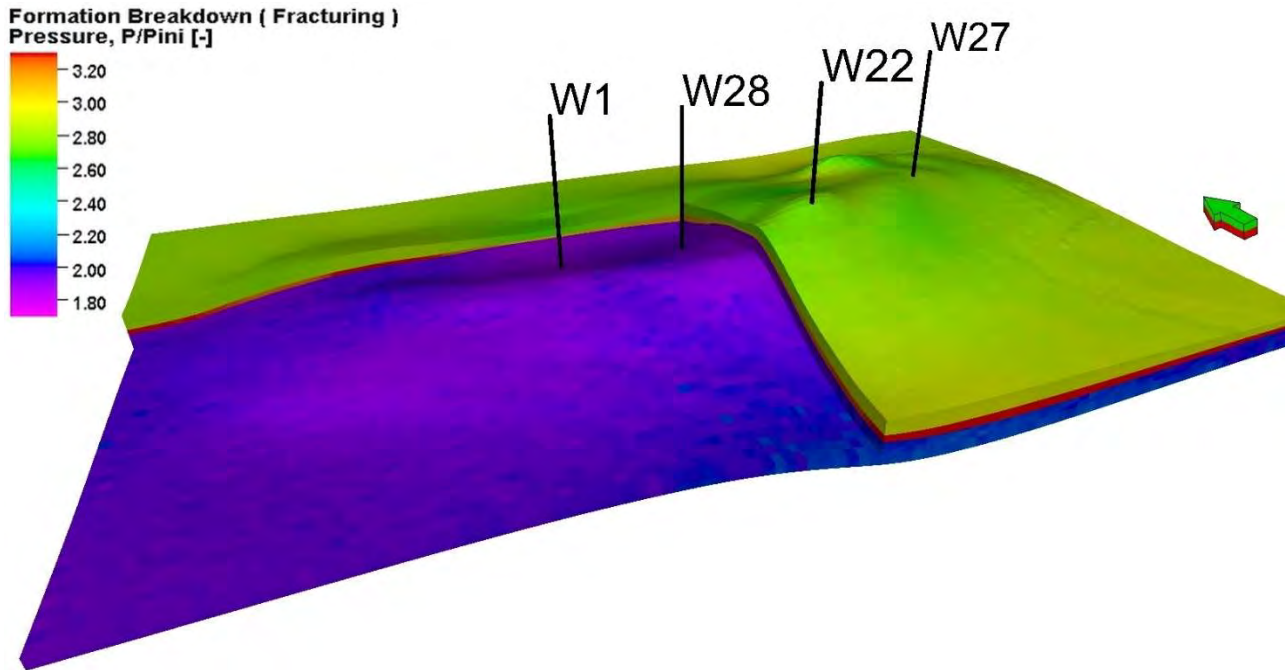


Figure 7.8. Distribution of the formation breakdown pressure within the Borzęcin structure.

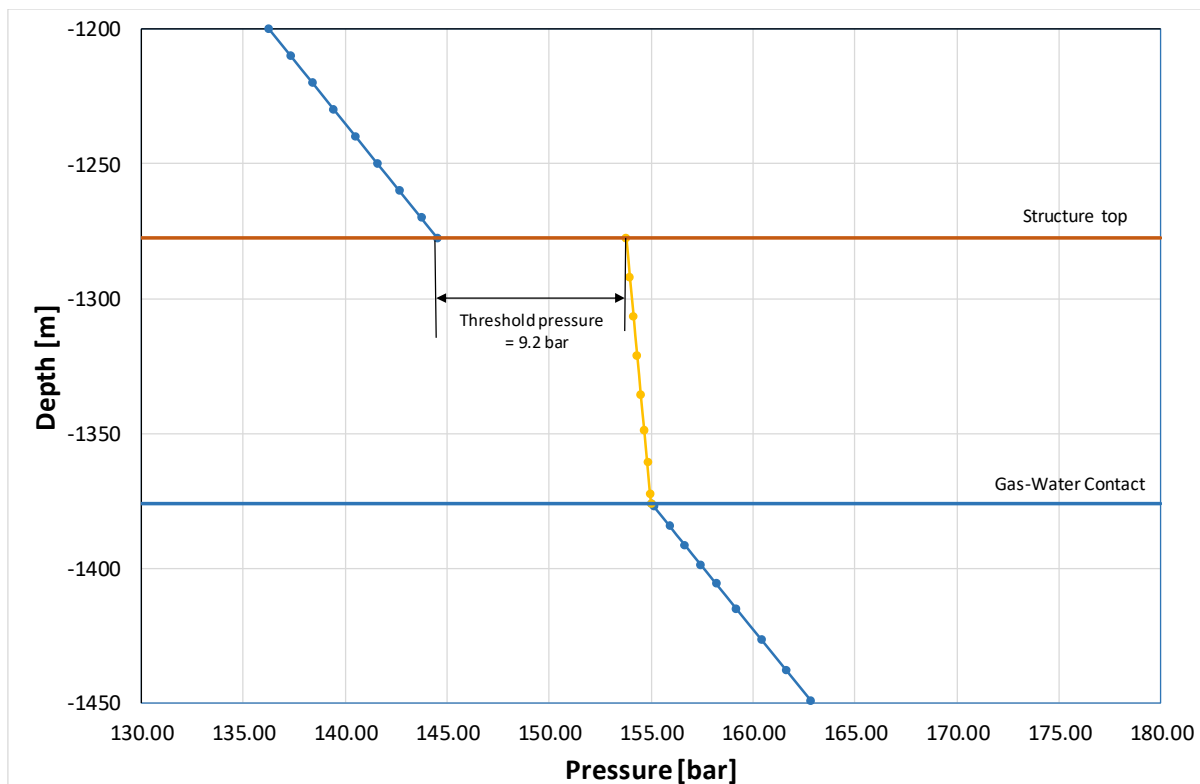


Figure 7.9. Diagram for the estimation of the threshold displacement pressure at the caprock – reservoir rock boundary under initial conditions.



Another significant characteristic of the acid gas sequestration project is the extension of the gas plume containing the injected acid gases. As the acid gases are injected into the water-bearing zone, their presence in the water phase also requires closer examination. The distribution of relevant quantities are shown in the following figures:

- gas saturation – Figure 7.10, Figure 7.11, Figure 7.12,
- CO₂ concentration in the gas phase – Figure 7.13, Figure 7.14, Figure 7.15,
- brine saturation – Figure 7.16, Figure 7.17, Figure 7.18,
- CO₂ solution in the brine phase – Figure 7.19, Figure 7.20, Figure 7.21.

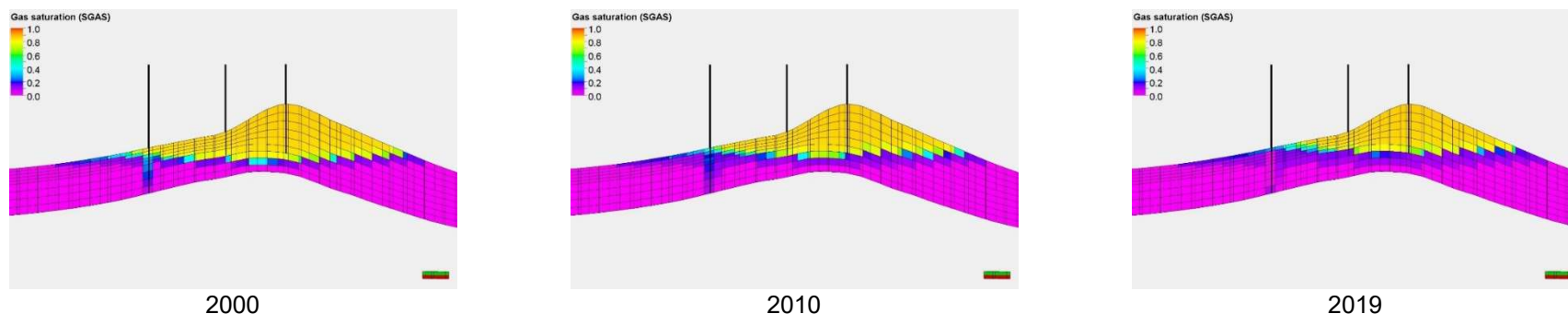


Figure 7.10. Distribution of gas saturation along the vertical cross section (A-A') connecting wells: W29, W22, W11.

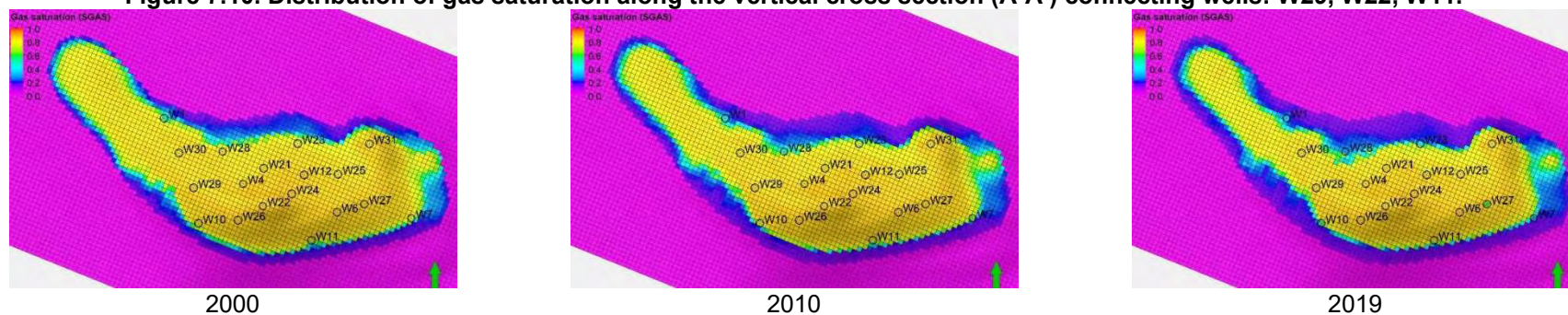


Figure 7.11. Distribution of gas saturation at the structure top.

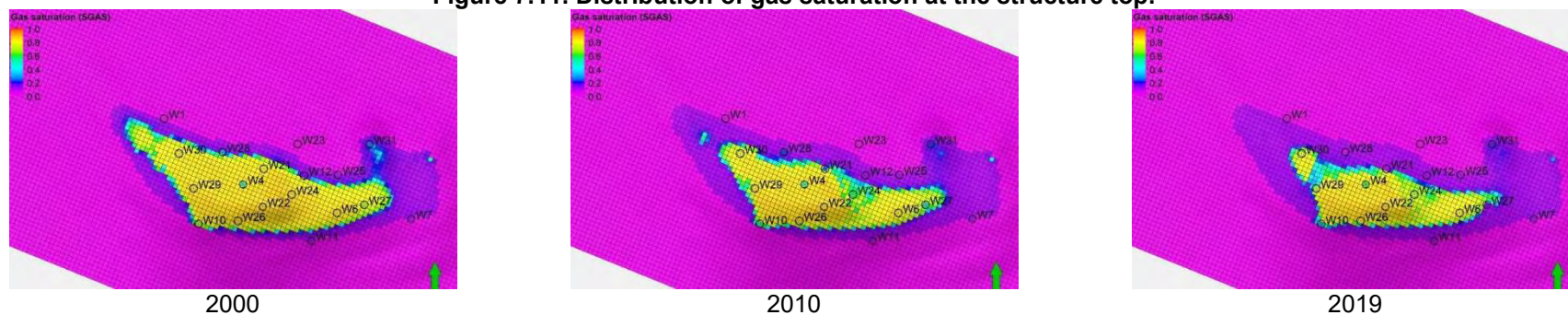


Figure 7.12. Distribution of gas saturation at the structure mid depth.

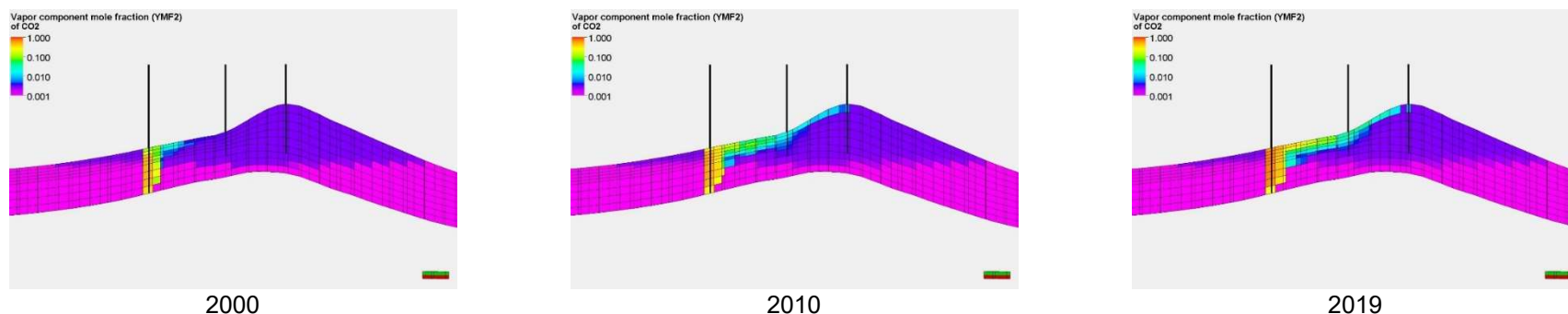


Figure 7.13. Distribution of CO₂ concentration in the gas phase along the vertical cross section (A-A') connecting wells: W29, W22, W11.

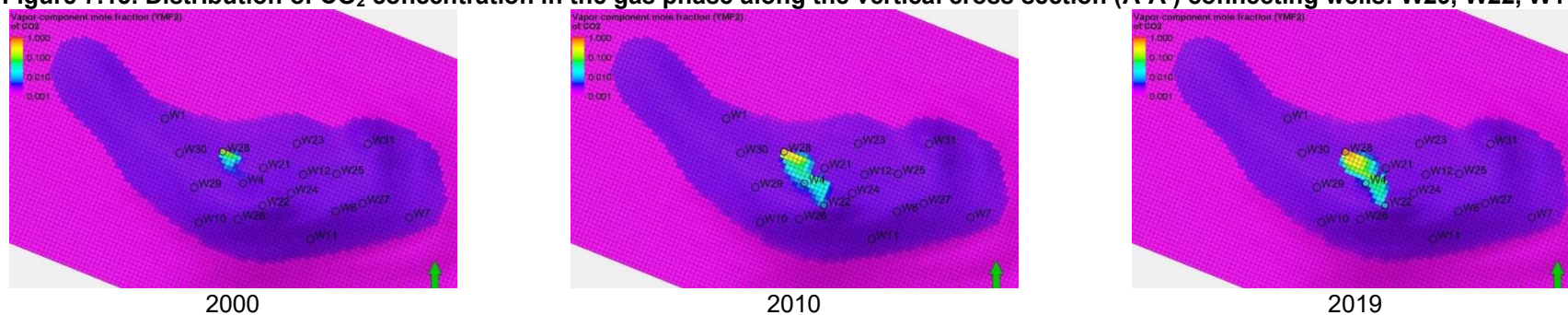


Figure 7.14. Distribution of CO₂ concentration in the gas phase at the structure top.

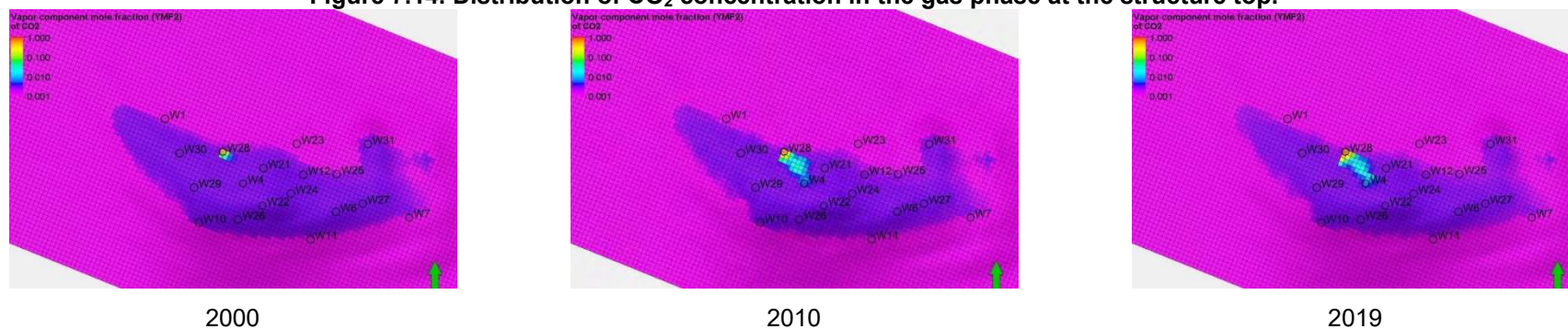


Figure 7.15. Distribution of CO₂ concentration in the gas phase at the structure mid depth.

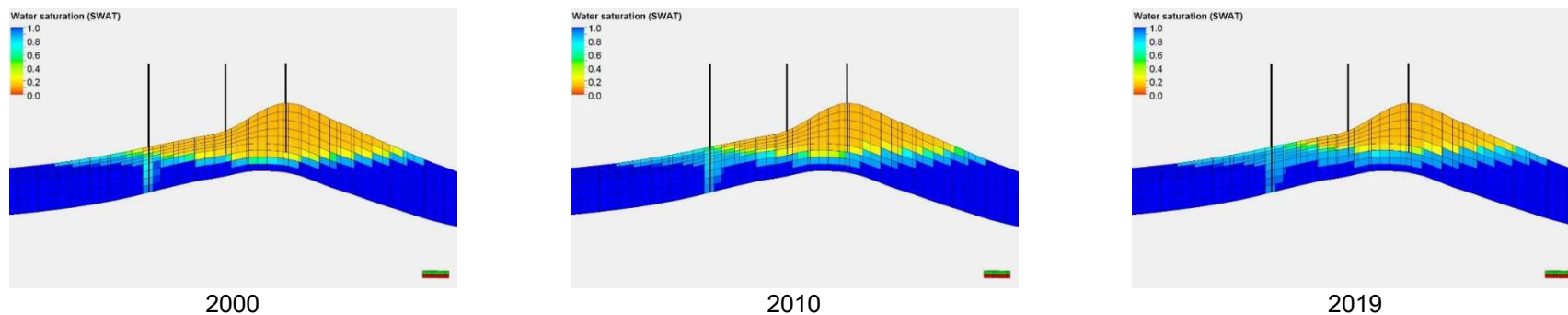


Figure 7.16. Distribution of brine saturation along the vertical cross section (A-A') connecting wells: W29, W22, W11.

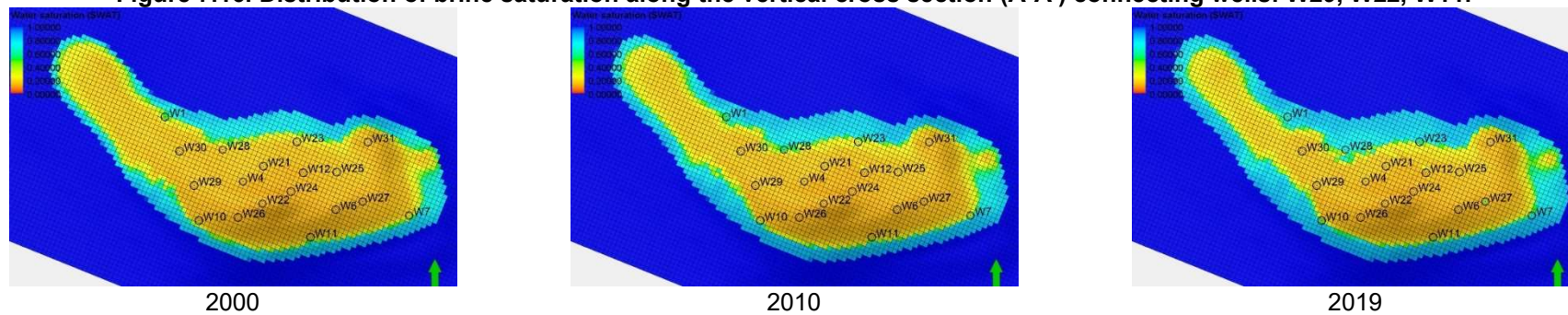


Figure 7.17. Distribution of brine saturation at the structure top.

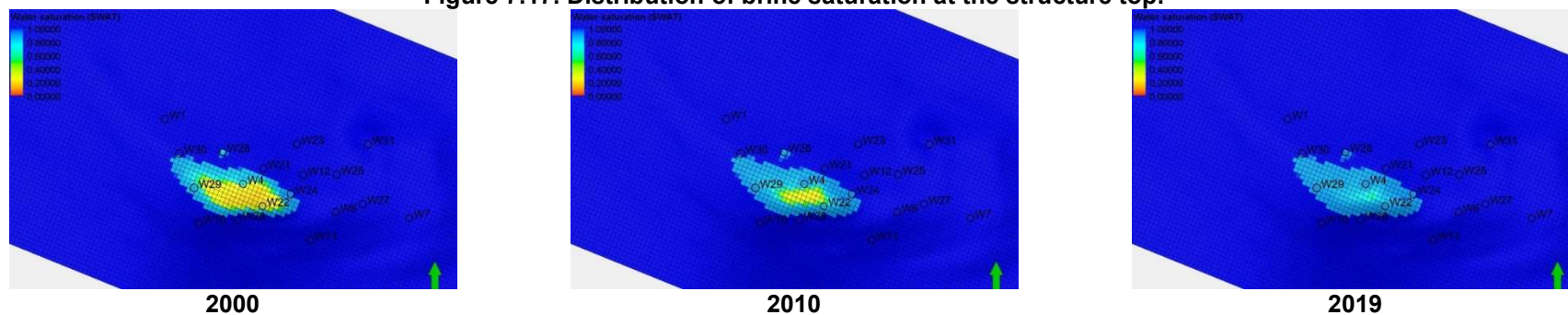


Figure 7.18. Distribution of brine saturation at the structure mid depth.

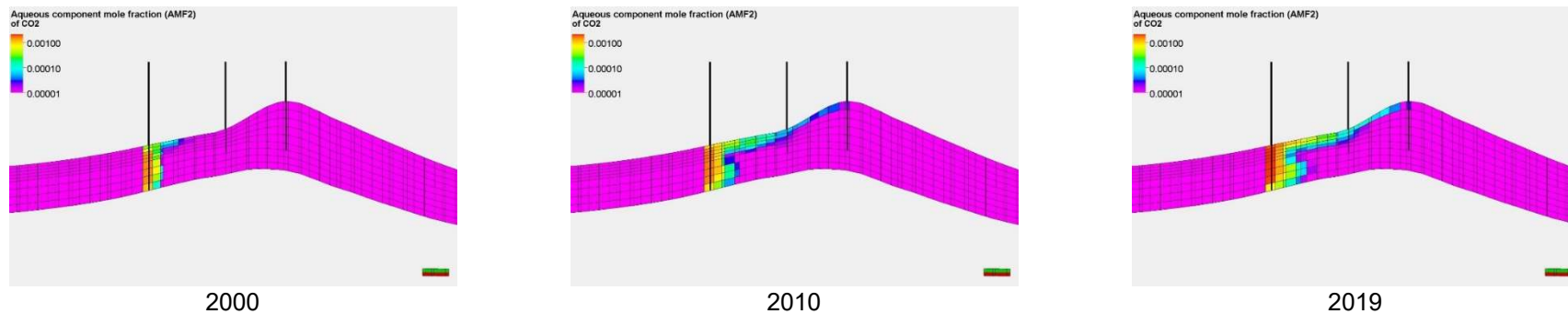


Figure 7.19. Distribution of CO2 solution in brine (immobile at $S_w < 0.1$, mobile otherwise) along the vertical cross section (A-A') connecting wells: W29, W22, W11.

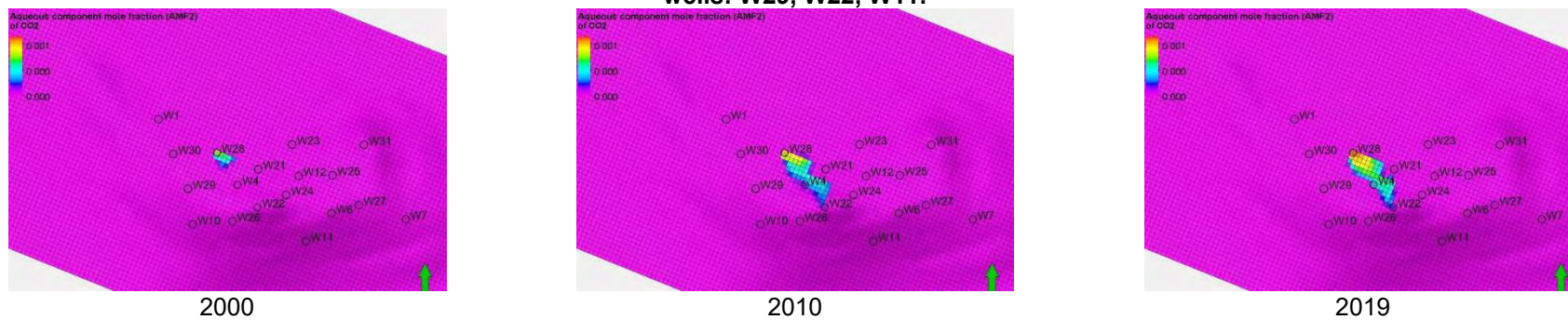


Figure 7.20. Distribution of CO2 solution in brine (immobile at $S_w < 0.1$, mobile otherwise) at the structure top.

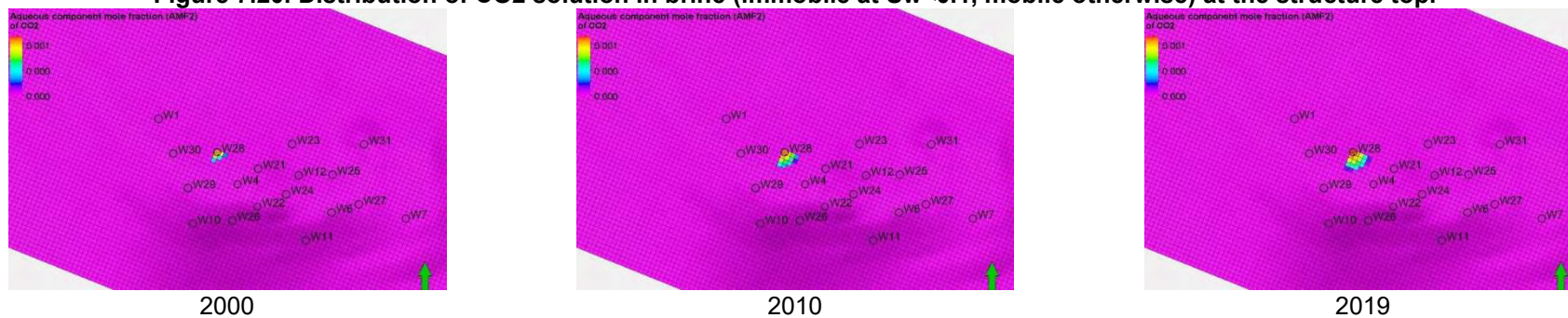


Figure 7.21. Distribution of CO2 solution in brine (immobile at $S_w < 0.1$, mobile otherwise) at the structure mid depth.

As seen in the above figures, the extension of the gas plume containing CO₂ as well as the CO₂ dissolved in the brine are confined within the initial gas cap extension (Figure 5.7) being the reservoir contour up to present day. Consequently, there is no leakage risk due to either gas containing CO₂ or brine with dissolved CO₂ to spill out beyond the structural trap of the Borzęcin structure.

Another potential leakage risk is related to the variation of geomechanical status along the existing wells and, in particular, along the injecting well. An example of maximum horizontal stress distribution in the injecting well zone is shown in Figure 7.22, for 3 different dates: initial (1972), before well W28 drilling (1996), after well W28 completion (1996), 10 years of well operation (2006).

These results together with other parameters (well design, its geophysical and cementing logs) will be used to estimate leakage risk within Task 2.2 of the SECURE project and reported in Deliverable D2.5.

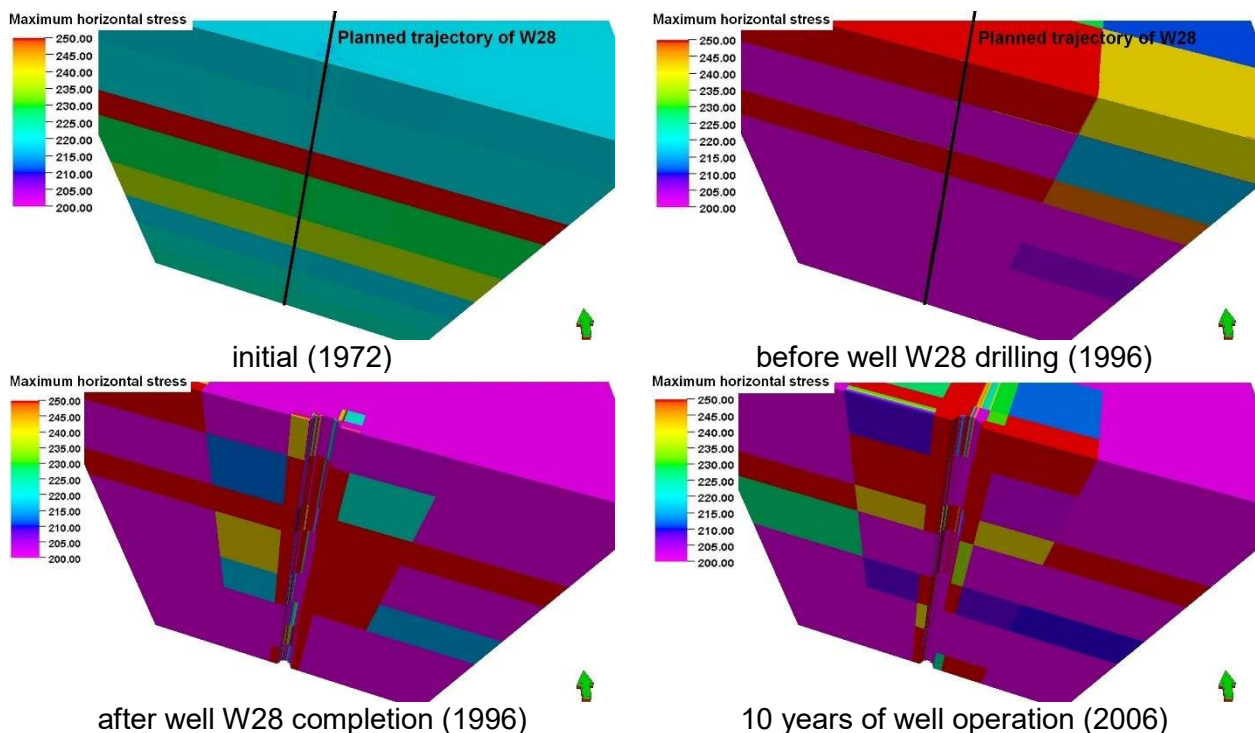


Figure 7.22. Distribution of maximum horizontal stress in the well W28 zone.

7.3 SUMMARY AND CONCLUSIONS

Simulation results of the acid gas injection process obtained from the calibrated model of the Borzęcin structure were used to analyse key factors of the process. In particular, the distribution of reservoir fluid saturations and pore pressures determined consequences of the process with respect to the injected gas leakage factor.

The former included gas and brine saturations together with the concentration of the injected gas (CO₂) in these fluids in order to characterize migration of their mobile components. This analysis provides direct data to assess the risk of the injected gas leakage beyond the structural trap.

The reservoir pressure distribution allows a determination of risks of other leakage events: through the reservoir caprock and via any induced fractures. In the first case the pressure step across the caprock – reservoir rock boundary is determined based on the simulation results and compared with the threshold displacement pressure of the caprock. This threshold pressure is available from the measurements of the caprock samples and/or can be estimated from the initial pressure vertical profile in the gas reservoir as shown in the analysed case of the Borzęcin structure.

For the assessment of the leakage possibility via the induced fractures, reservoir pressure distribution obtained from results of the simulation results has to be compared to the formation breakdown (fracturing) pressure. This pressure can be determined in the appropriate well tests and/or calculated using the geomechanical model of the structure as it is the case of the Borzęcin structure.



Also, the assessment of the leakage risk through wells requires a set of input data that are available from both the dynamical and geomechanical models of the analysed wells and their surroundings.

In the case of the Borzęcin project, results of its simulation modelling clearly show no leakage risk – a conclusion consistent with the measurement results presented in Chapter 3. However, in general, it should be emphasized that lack of measuring evidences during the project operation is not a sufficient condition for leakage-free sequestration process. This is caused by typically prolonged migration processes of the gas to leak upwards all the way from the sequestration site to the surface where it can be detected. Therefore, the long-term simulation modelling of sequestration projects proves to be a unique method for the quantitative leakage risk analysis.

Thus, the procedure based upon the sequestration project modelling and presented in this chapter should be recommended as a general leakage risk analysis approach.



8 Simulation forecasts and result analysis for the continuation scenario of the acid gas sequestration

8.1 SIMULATON FORECAST ASSUMPTIONS

The current Borzęcin project will probably continue until the producing wells are watered-out or are too contaminated with the acid gas components. Therefore, a prediction of its operation is simulated using the model described above. For these purposes, the production rate is extrapolated for the current production decline trend as shown in Figure 8.1. The contribution of 4 currently producing wells (W4, W21, W22, W27) is adopted from recently observed values (Figure 8.2). The simulation of the injection phase is performed for the next 20 years that is followed by a 100 years relaxation phase.

The whole amount of the produced CO₂ and H₂S is assumed to be reinjected back to the water-bearing zone of W28 as it has been done so far. Yearly amount of injected gases is shown in Figure 8.3. Composition of CO₂ and H₂S in the injected stream is presented in Figure 8.4.

8.2 SIMULATION FORECAST RESULTS AND ANALYSIS

As a result of the assumed future project schedule, average reservoir pressures continue to slowly decline till the end of the injection phase. Then the pressures are built up (Figure 8.5) due to aquifer activities (Figure 8.6, Figure 8.7).

The CO₂ concentrations in the gas produced by individual wells and total reservoir production are shown in Figure 8.8.

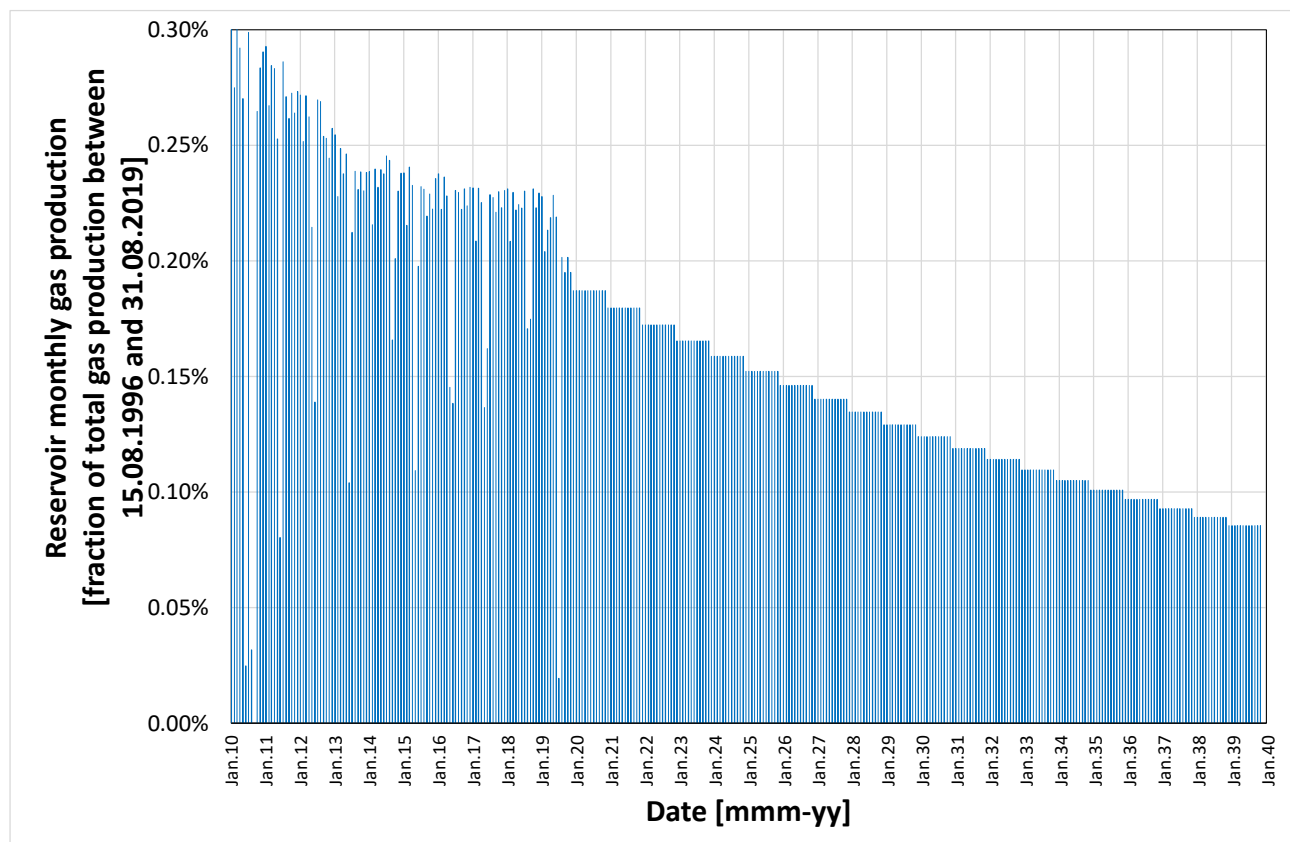


Figure 8.1. Reservoir monthly gas production. Extrapolation of the historical production decline trend.

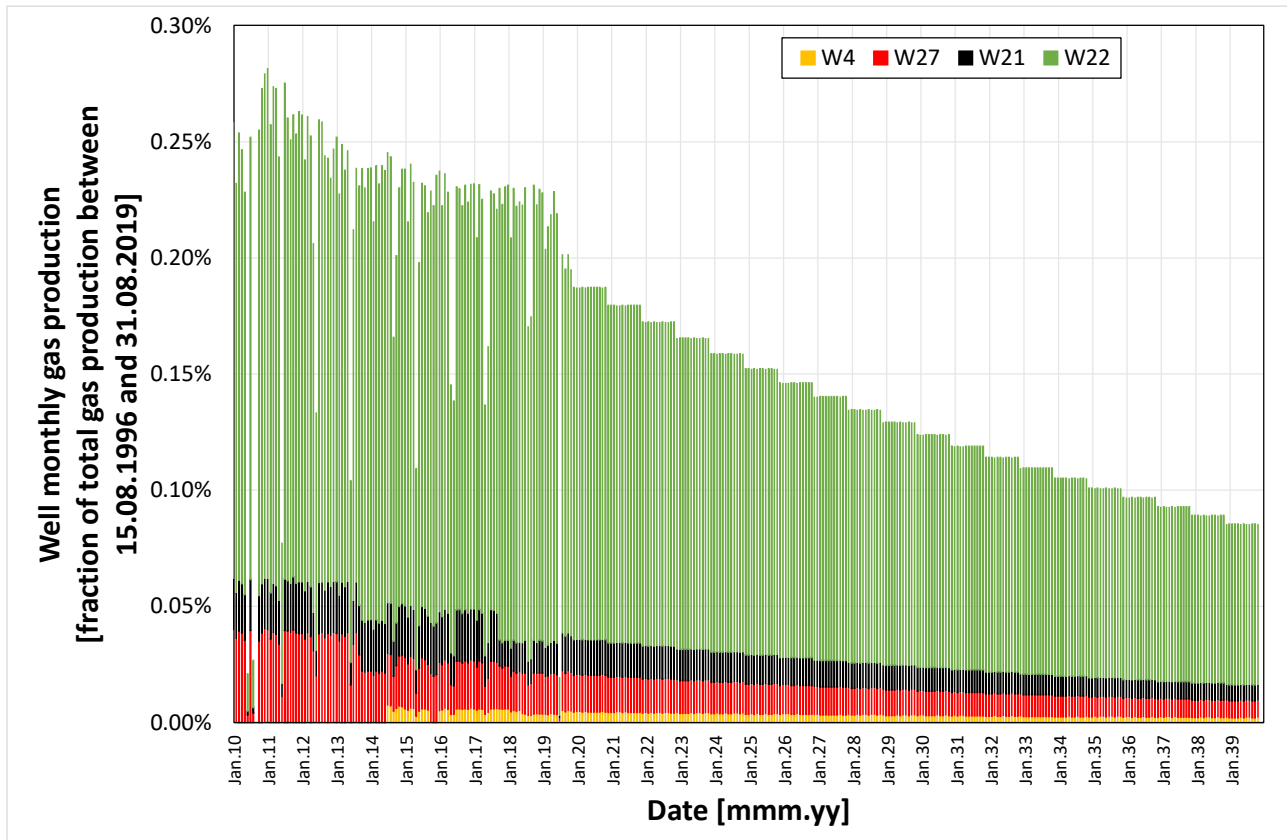


Figure 8.2. Well monthly gas production. Historical well contribution to the reservoir production rate.

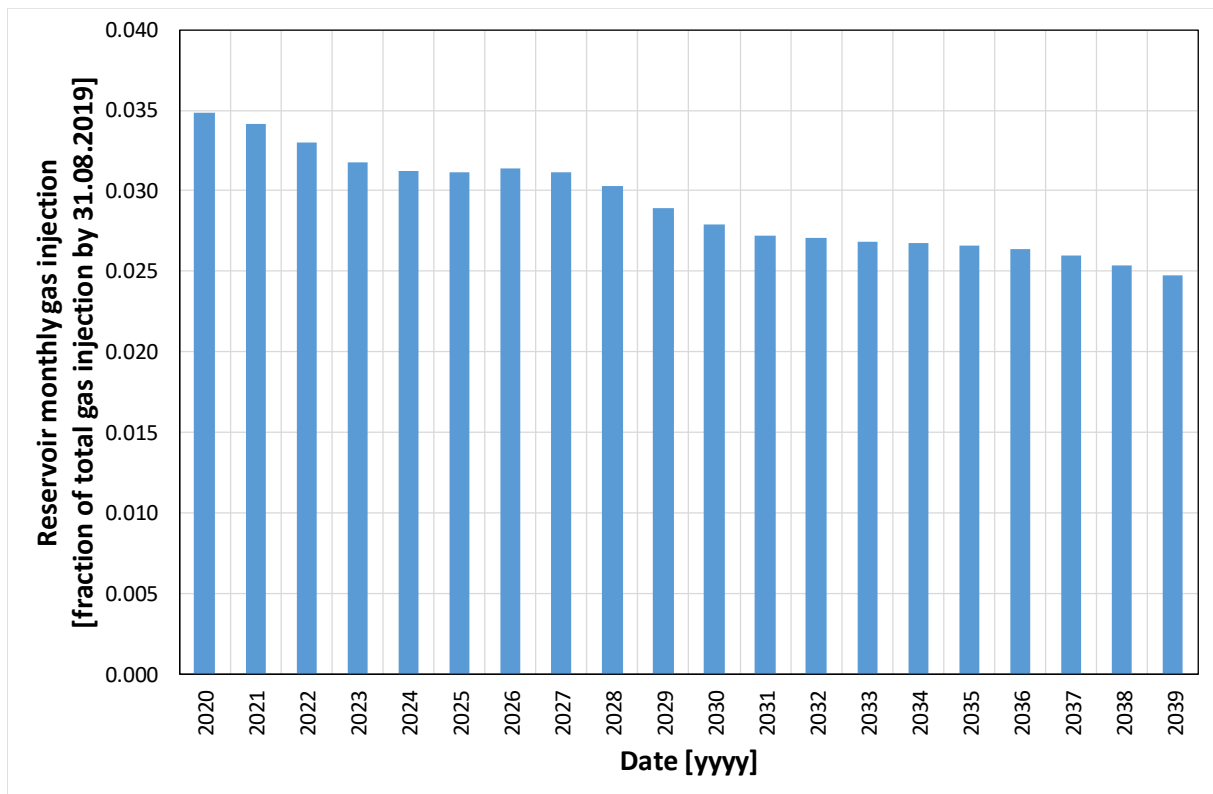


Figure 8.3. Reservoir monthly gas injection by well W28. Balanced CO₂ and H₂S production.

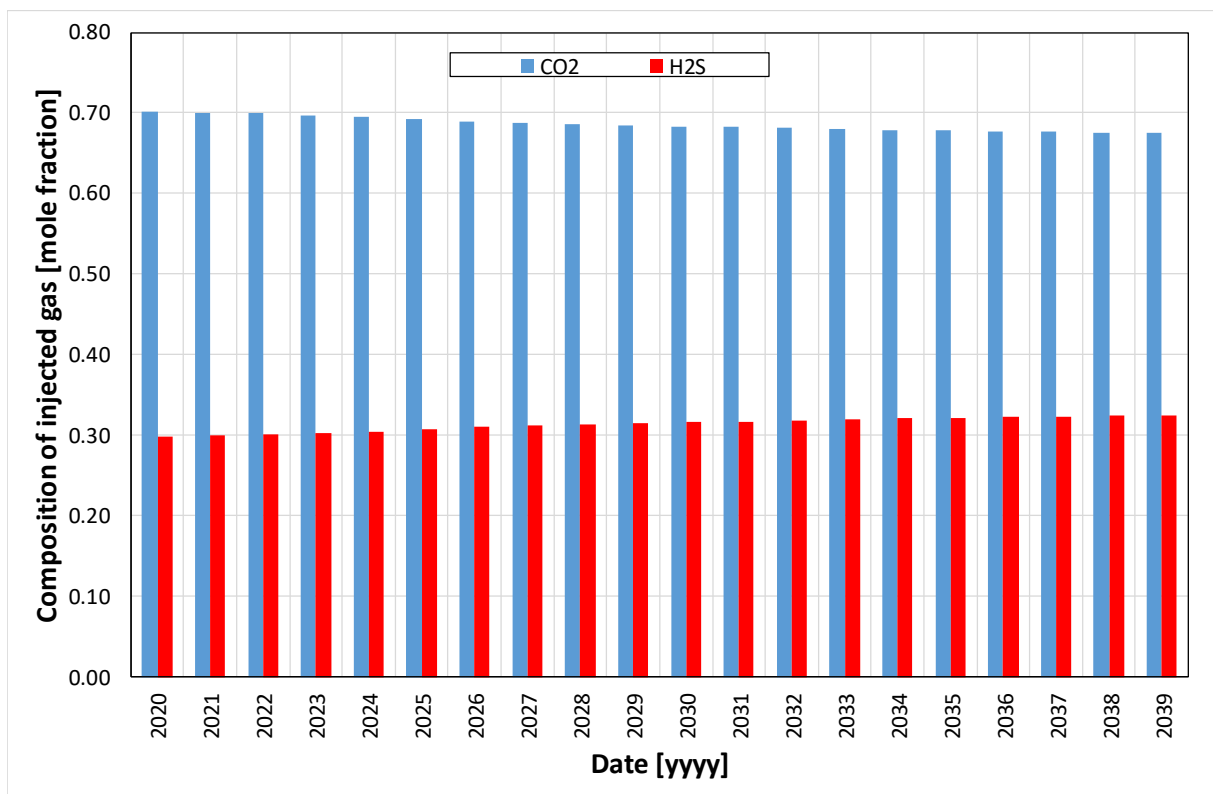


Figure 8.4. Composition of gas injected by W28.

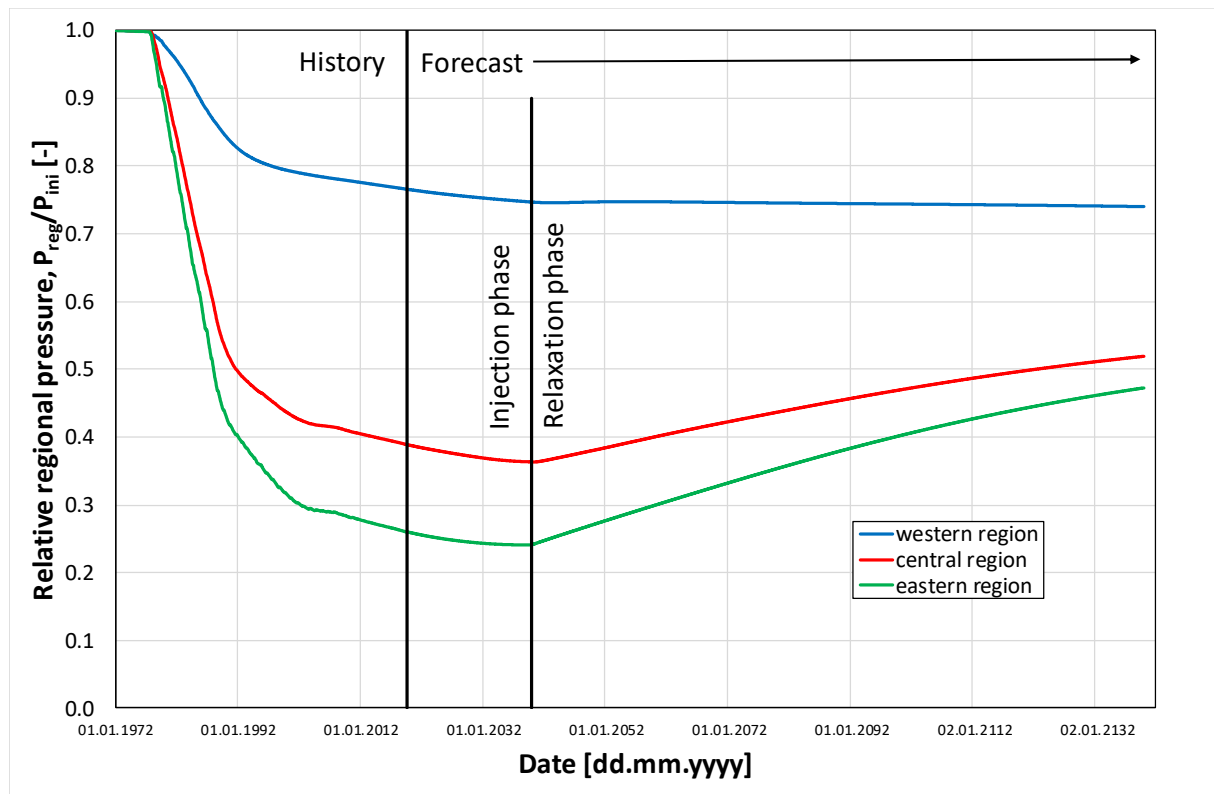


Figure 8.5. Evolution of average regional pressures.

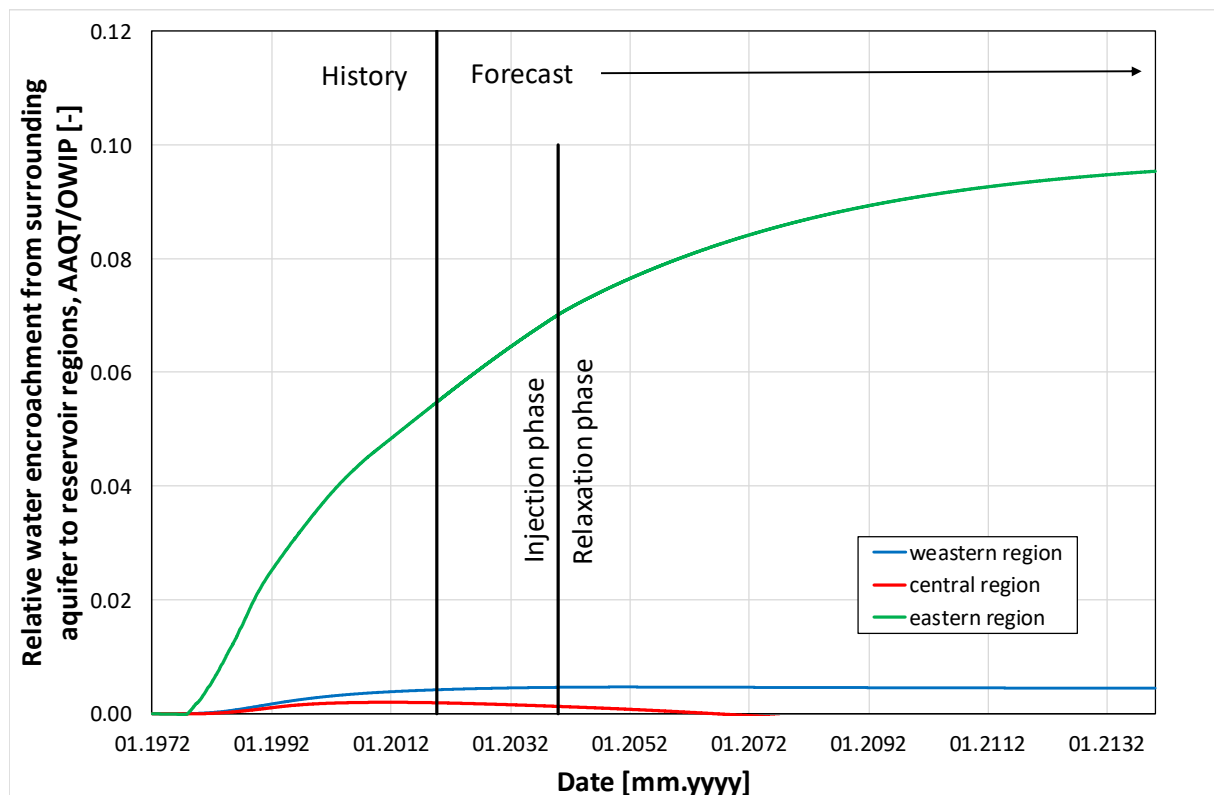


Figure 8.6. Relative water encroachment from surrounding aquifer to reservoir regions.

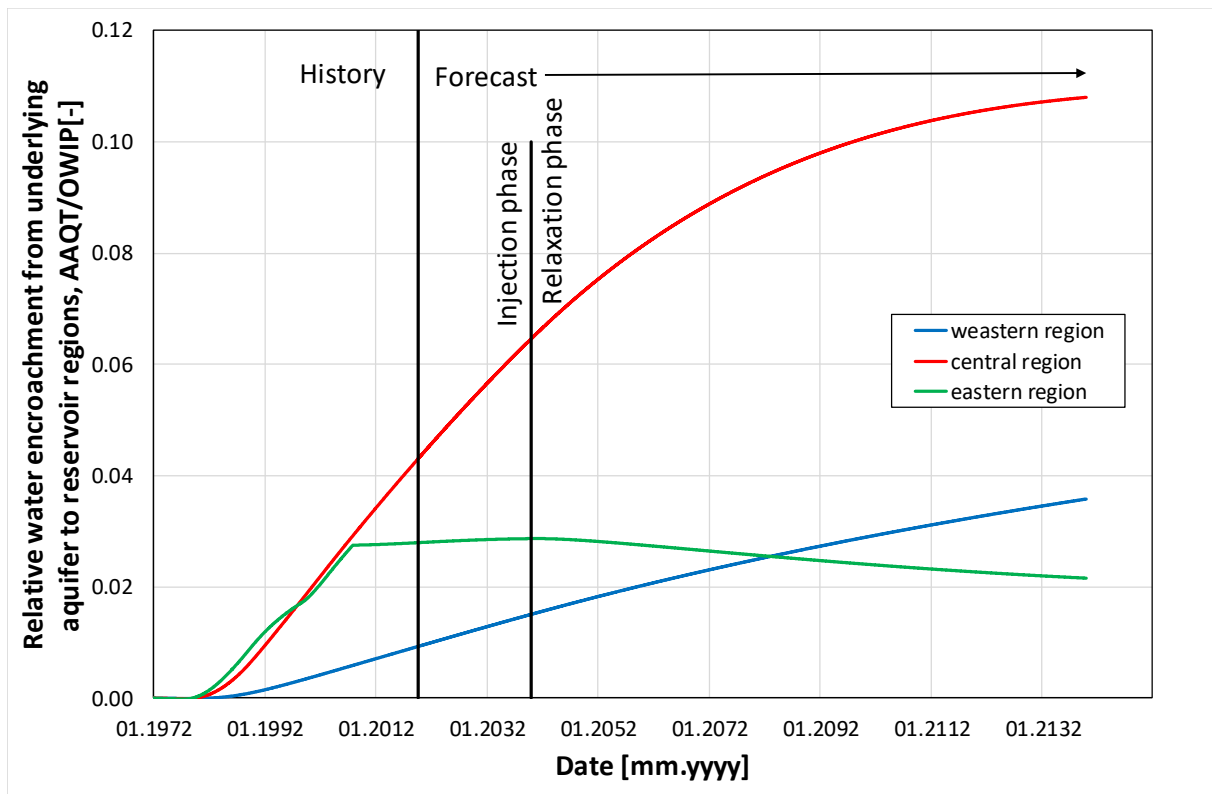


Figure 8.7. Relative water encroachment from underlying aquifer to reservoir regions.

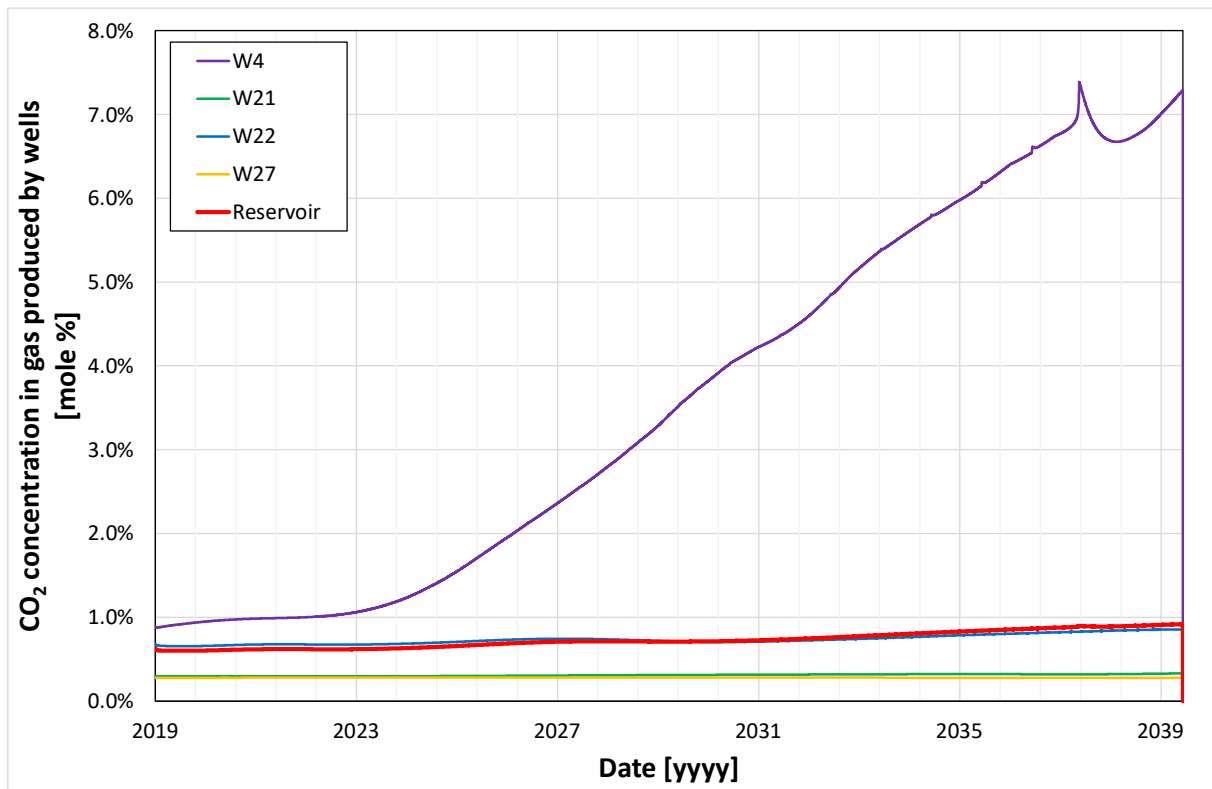


Figure 8.8. CO₂ concentration in gas produced by wells W4, W21, W22, W27 and of total reservoir production.



The assumed production and injection schedule causes the variation of the average composition of the gas in place (GIP). The composition of CO₂ and H₂S increases twice at that time yet stays at the very low level (Figure 8.9) and, as a consequence the other, dominant components (hydrocarbons and N₂) are practically constant (Figure 8.10).

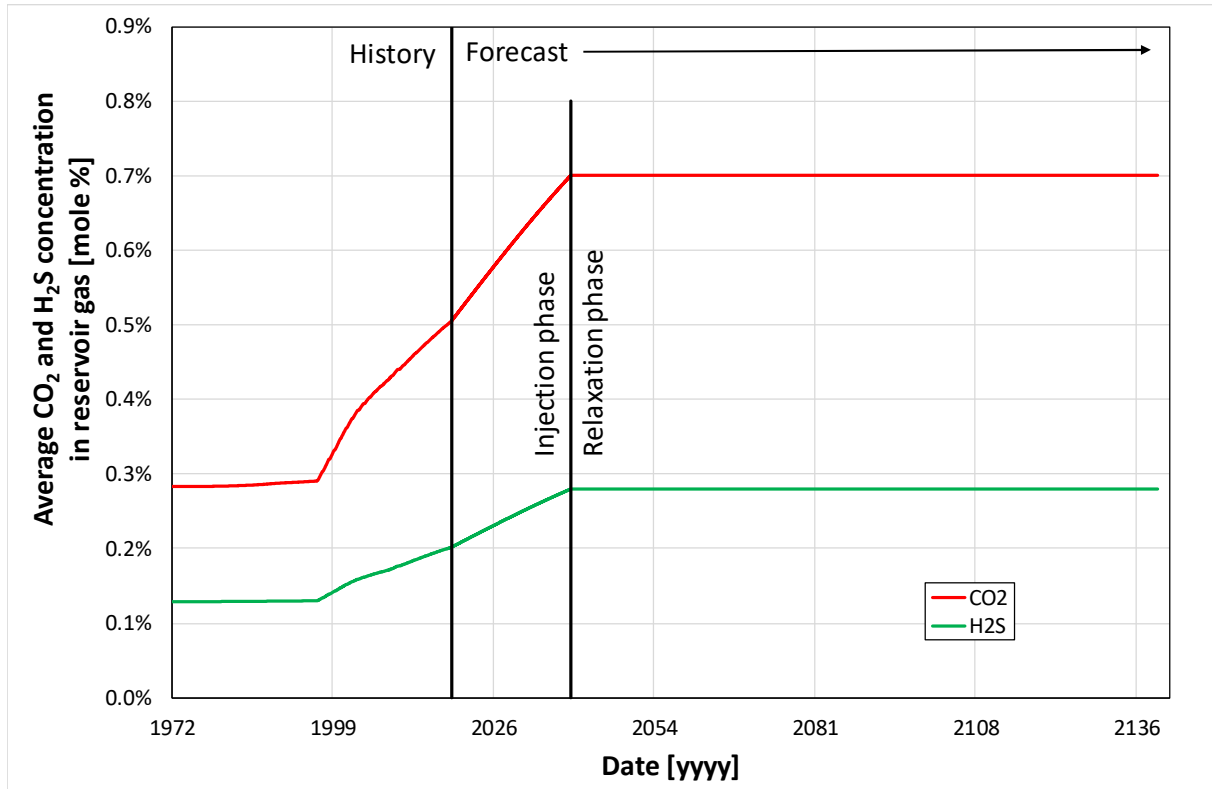


Figure 8.9. Average composition of reservoir gas - CO₂ and H₂S components.

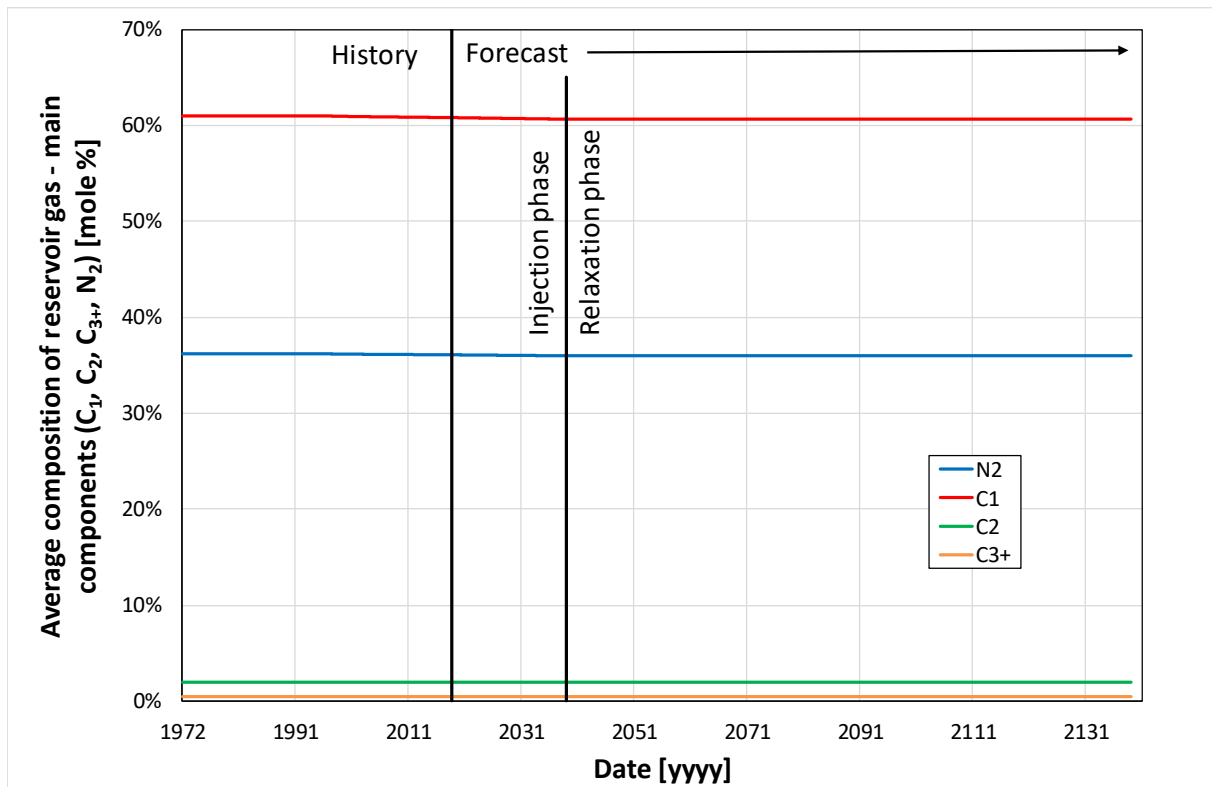


Figure 8.10. Average composition of reservoir gas - main components (C₁, C₂, C₃₊, N₂).



The reservoir production and injection activities during the injection phase (until 2039) followed by the relaxation phase (until 2139) together with aquifer activities result in varying contribution of different CO₂ phases to the total amount of CO₂ present in the structure, that can be seen in Figure 8.11.

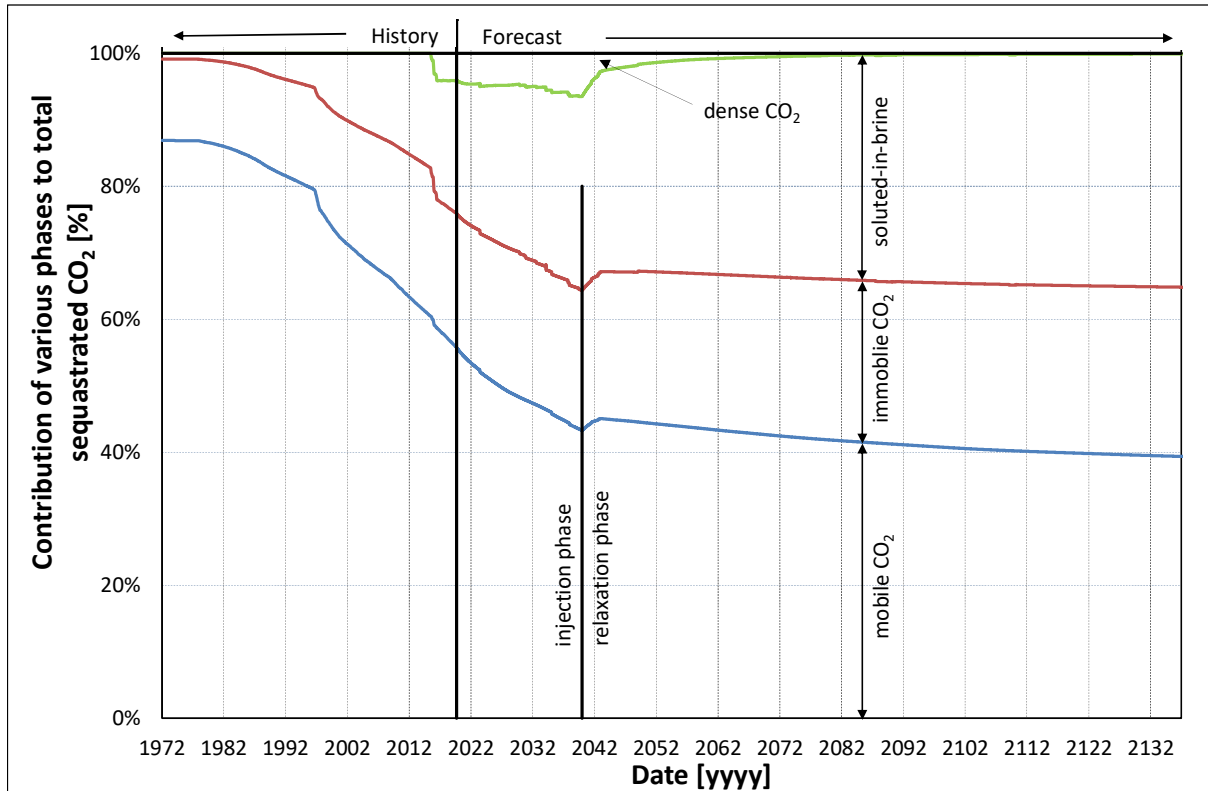


Figure 8.11. Contribution of various phases to total CO₂ in reservoir.

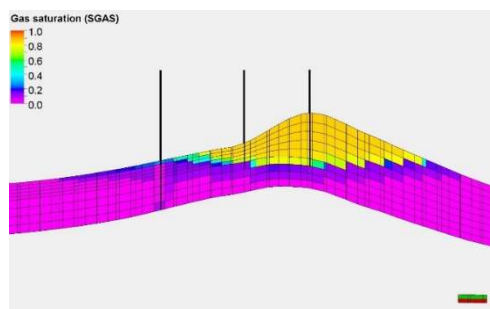
Detailed results of the CO₂ distribution in the Borzęcin structure follow from and are presented as:

- gas saturation: Figure 8.12, Figure 8.13, Figure 8.14,
- CO₂ concentration in the gas phase: Figure 8.15, Figure 8.16, Figure 8.17,
- brine saturation: Figure 8.18, Figure 8.19, Figure 8.20,
- CO₂ solution in brine: Figure 8.21, Figure 8.22, Figure 8.23,
- pressure distributions: Figure 8.24, Figure 8.25, Figure 8.26.

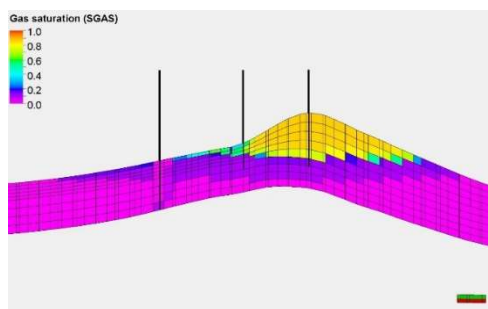
As the production rate (and, consequently, the injection rate) in the analysed forecast are relatively small, the modelled estimates of basic reservoir parameters (pressures and saturations) at the end of the injection phase (2039) do not differ significantly from those at the end of the historical activities (2019). The conclusions concerning the various risk factors are presented in Chapter 7.

Greater changes of the reservoir parameters can be observed at the end of the relaxation phase (2139). Due to the water encroachment from the aquifers to the reservoir zone, the final reservoir pressures (Figure 8.5) increase above the minimum values by up to about 20% of the initial pressure level. That increase can be seen in Figure 8.24, Figure 8.25, Figure 8.26. The maximum local pressure is observed at the deepest layer of the structure bottom and amounts to less than 60% of the initial reservoir pressure at the end of the relaxation phase. This result effectively eliminates the leakage risk across caprock or via induced fractures for the reasons described in Chapter 7.

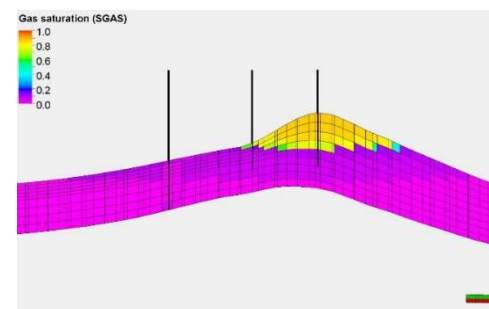
As a consequence of average reservoir pressure increase during the relaxation phase, a shrinkage of the gas cap containing the CO₂ component can be observed in the gas saturation distributions in Figure 8.12, Figure 8.13, Figure 8.14. The amount of CO₂ dissolved in the brine increases as shown in Figure 8.21, Figure 8.22, Figure 8.23 with no risk of brine migration beyond the structure limit. Consequently, there is no leakage risk due to either gas containing CO₂ or brine with dissolved CO₂ to spill out beyond the structural trap of the Borzęcin structure.



Injection start (2020)

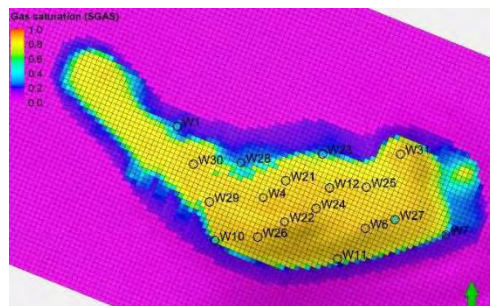


Injection end (2039)

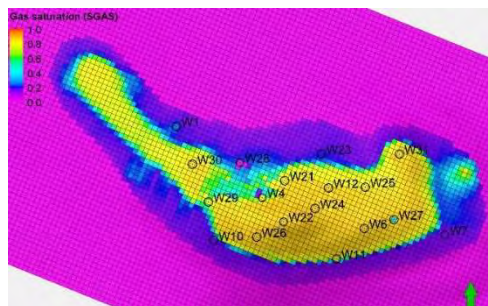


after 100 years of relaxation (2139)

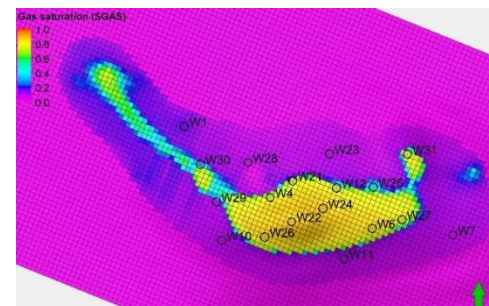
Figure 8.12. Distribution of gas saturation along the vertical cross section (A-A') connecting wells: W29, W22, W11.



Injection start (2020)

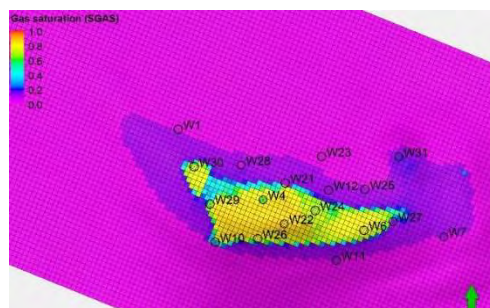


Injection end (2039)

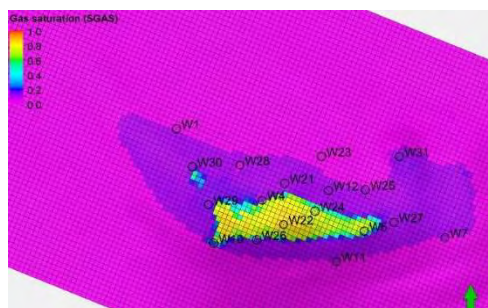


after 100 years of relaxation (2139)

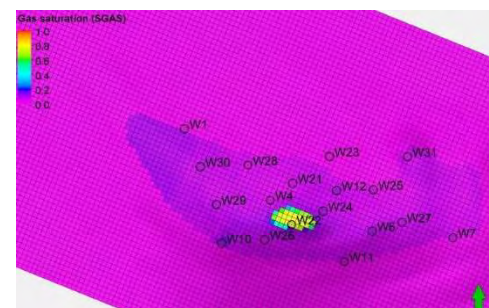
Figure 8.13. Distribution of gas saturation at the structure top in year.



Injection start (2020)

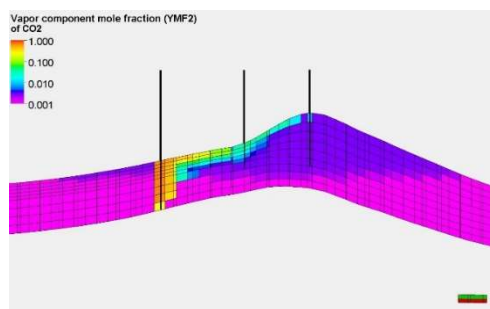


Injection end (2039)

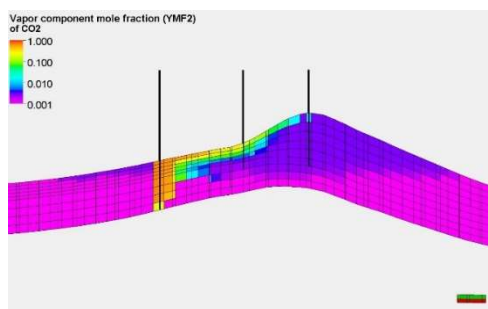


after 100 years of relaxation (2139)

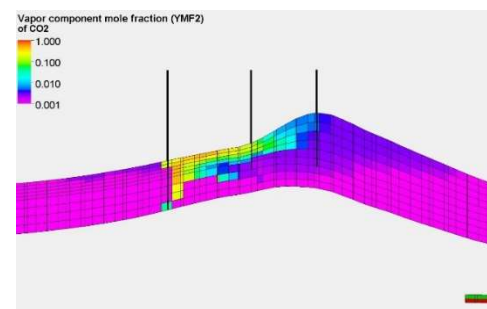
Figure 8.14. Distribution of gas saturation at the structure mid depth in year.



Injection start (2020)

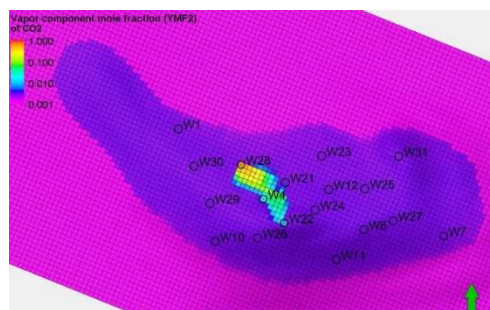


Injection end (2039)

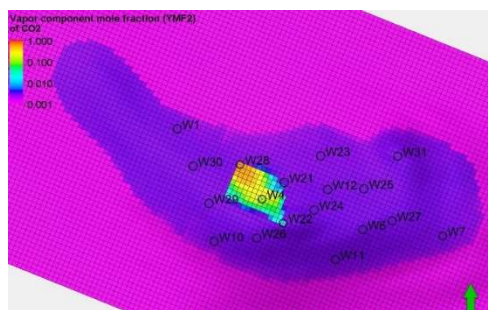


after 100 years of relaxation (2139)

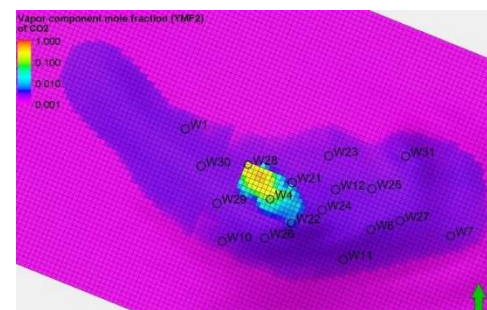
Figure 8.15. Distribution of CO₂ concentration in the gas phase along the vertical cross section (A-A') connecting wells: W29, W22, W11.



Injection start (2020)

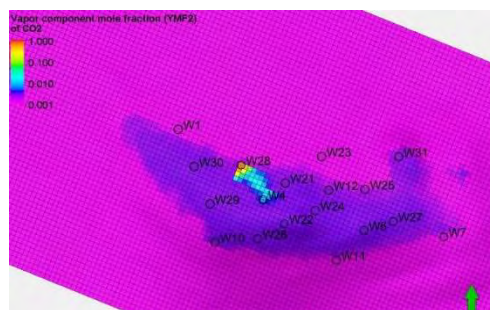


Injection end (2039)

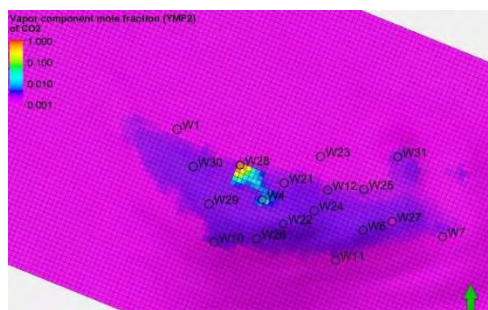


after 100 years of relaxation (2139)

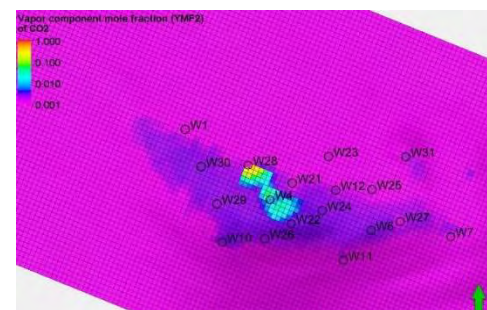
Figure 8.16. Distribution of CO₂ concentration in the gas phase at the structure top.



Injection start (2020)

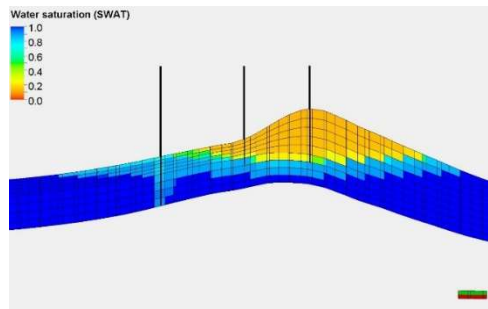


Injection end (2039)

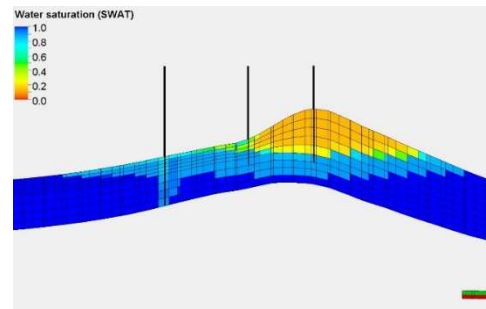


after 100 years of relaxation (2139)

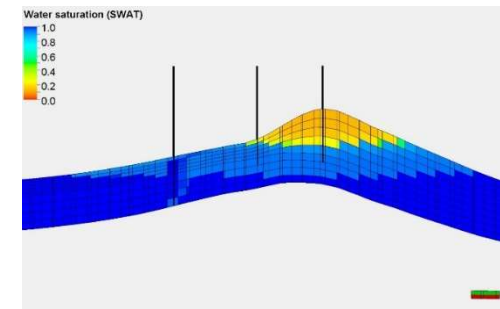
Figure 8.17. Distribution of CO₂ concentration in the gas phase at the structure mid depth.



Injection start (2020)

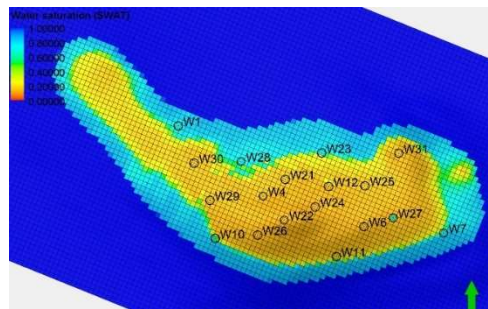


Injection end (2039)

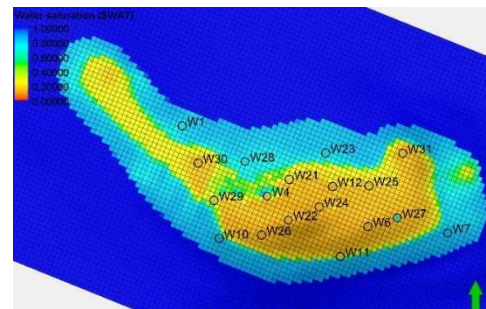


after 100 years of relaxation (2139)

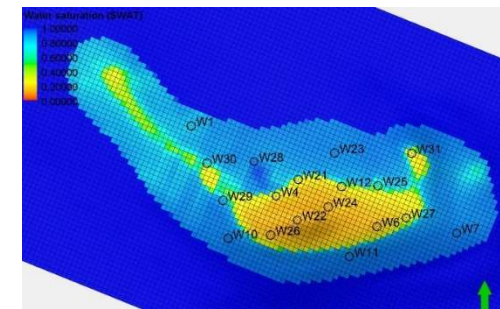
Figure 8.18. Distribution of brine saturation along the vertical cross section (A-A') connecting wells: W29, W22, W11.



Injection start (2020)

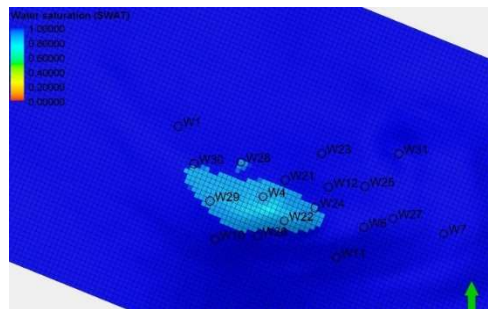


Injection end (2039)

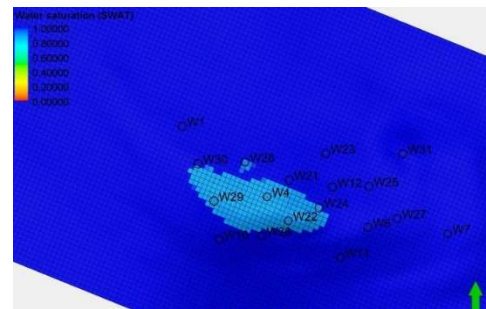


after 100 years of relaxation (2139)

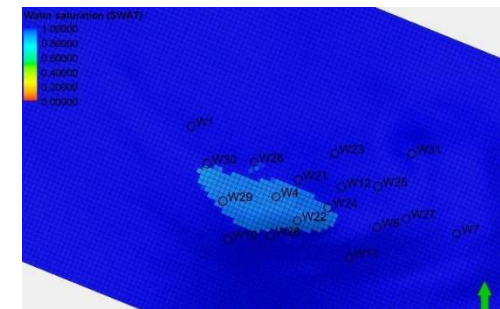
Figure 8.19. Distribution of brine saturation at the structure top.



Injection start (2020)

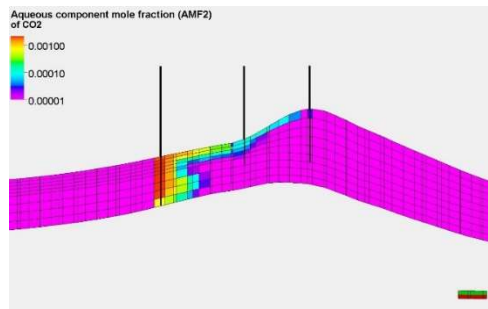


Injection end (2039)

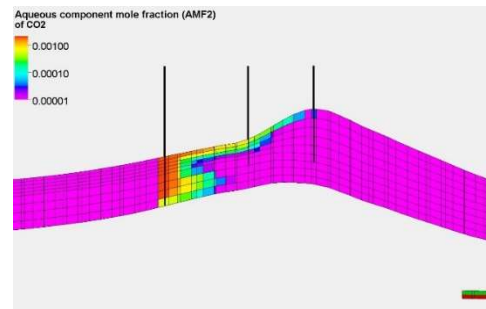


after 100 years of relaxation (2139)

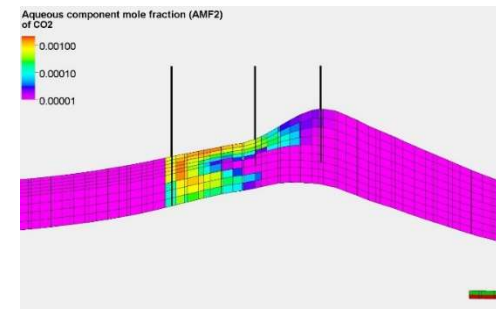
Figure 8.20. Distribution of brine saturation at the structure mid depth.



Injection start (2020)

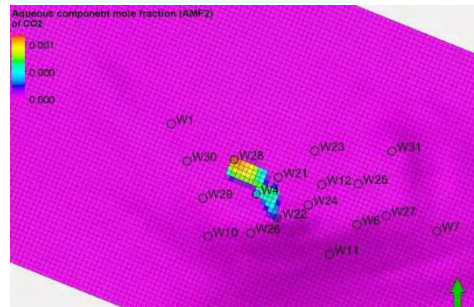


Injection end (2039)

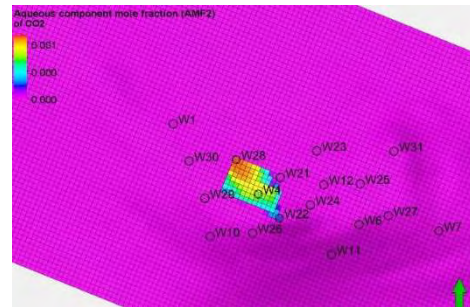


after 100 years of relaxation (2139)

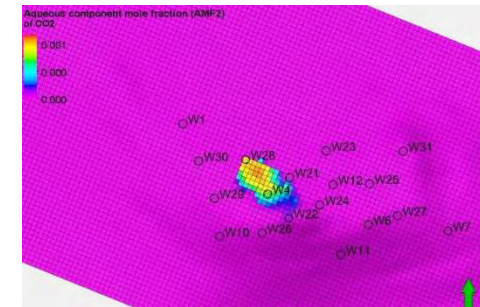
Figure 8.21. Distribution of CO2 solution in brine along the vertical cross section (A-A') connecting wells: W29, W22, W11.



Injection start (2020)

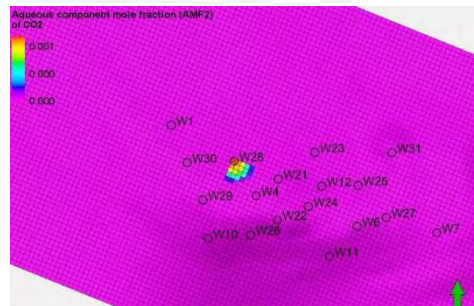


Injection end (2039)



after 100 years of relaxation (2139)

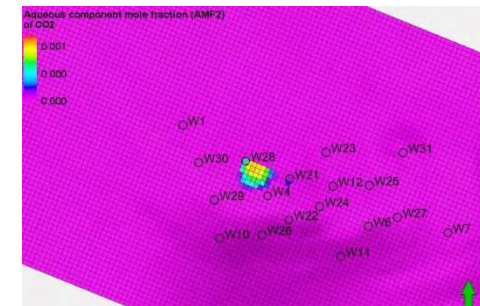
Figure 8.22. Distribution of CO2 solution in brine at the structure top.



Injection start (2020)

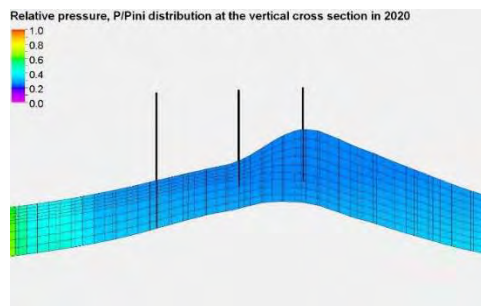


Injection end (2039)

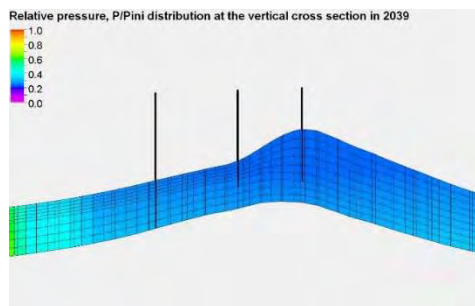


after 100 years of relaxation (2139)

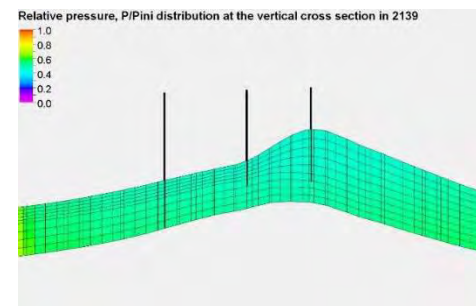
Figure 8.23. Distribution of CO2 solution in brine at the structure mid depth.



Injection start (2020)

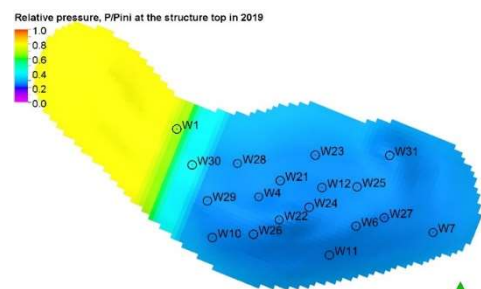


Injection end (2039)

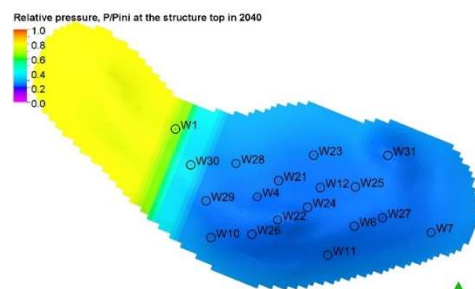


after 100 years of relaxation (2139)

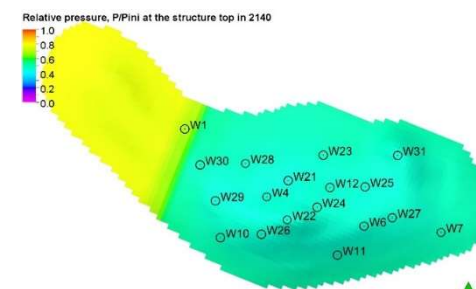
Figure 8.24. Figure 9. Relative pressure distribution along the vertical cross section (A-A') connecting wells: W29, W22, W11.



Injection start (2020)

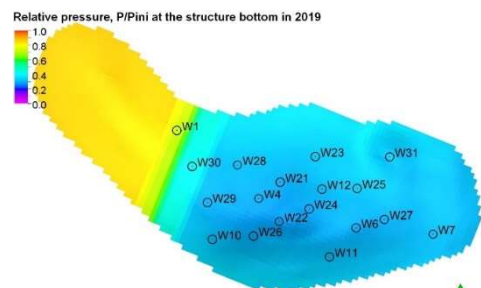


Injection end (2039)

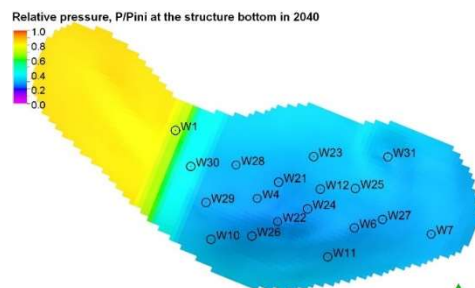


after 100 years of relaxation (2139)

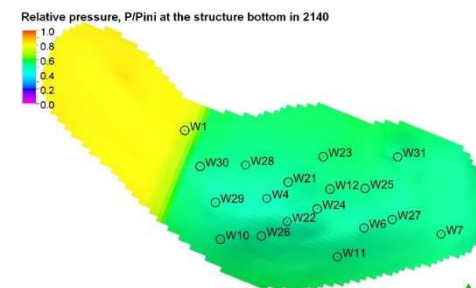
Figure 8.25. Relative pressure distribution at the structure top.



Injection start (2020)



Injection end (2039)



after 100 years of relaxation (2139)

Figure 8.26. Relative pressure distribution at the structure bottom.



8.3 SUMMARY AND CONCLUSIONS

This chapter includes a simulation forecast of the analysed project obtained with the use of the structure numerical model previously constructed and calibrated. Results of the forecast are analysed with respect to the leakage risk factors using the procedure described in Chapter 7. It should be emphasized that the forecast includes a long-time relaxation period extending beyond the injection schedule of the project. During the relaxation period, a significant redistribution of pressures and fluid saturations may occur that affects leakage risk factors. Therefore, performing project simulation forecasts comprising relaxation period of sufficient duration is a key requirement for the complete sequestration project analysis. Again, the application of the project numerical modelling proves to be a necessary tool of the project assessment.



9 Storage capacity analysis for a hypothetical full-scale CO₂ sequestration scenario at Borzęcin

9.1 SIMULATON FORECAST ASSUMPTIONS

At present, the reservoir properties of the Borzęcin structure are characterized by the following:

- the amount of gas in place is reduced to 85% of the original gas in place (Figure 2.29),
- the average reservoir pressure is also significantly reduced, in particular, it reaches less than 30% of the initial pressure in the dominant eastern region of the structure (Figure 7.1),
- most of the producing wells can be converted to injection wells at relatively low cost,
- also, other elements of the existing surface installation can be converted for the purposes of an alternative sequestration project.

All the above points suggest that the Borzęcin facility can be considered as a potential site of a large-scale CO₂ sequestration project. In the following, reservoir characteristics of such a project are presented as the results of simulation studies.

The existing system of wells does not cover the whole area of the Borzęcin reservoir. In particular, the western region of the reservoir does not include any operating well. Therefore, one additional well (W40) is assumed to complete the existing system of wells in the location shown in Figure 9.1.

As a result, 17 wells (W4, W6, W7, W10, W11, W12, W21, W23, W22, W24, W25, W26, W27, W28, W29, W30, W31) cover the eastern region, a single well (W30) covers the central regions, and 2 wells (W1, W40) cover the western region.

All the wells are assumed to be completed in the water-bearing layers below the gas cap. The nominal, maximum injection rate is set at 400 000 Sm³/d and the bottom-hole injection pressure is limited to 200 bars.

Multiple scenarios of the CO₂ injection project were performed with the calibrated model of the Borzęcin structure and tested against the following risk determining factors:

- no spill-out of the injected CO₂ beyond the structural trap,
- maximum pressure in the structure volume below the fracturing pressure,
- maximum pressure step across the caprock-reservoir rock boundary below the threshold displacement pressure.

It should be noted that all the above factors are directly dependent upon the degree of the structure filling with the sequestered gas and thus uniquely determine its capacity. Another leakages risk factor – deteriorated well integrity – is not studied here. Its influence upon the structure sequestration capacity is more complex and depends on various factors not necessarily related to the overall project characteristics and thus is much difficult to predict.

The optimum scenario that fulfils the above criteria and maximizes the injected CO₂ amount was calculated. The characteristics of the optimum scenario are presented below.

9.2 SIMULATION FORECAST RESULTS AND ANALYSIS

The injection time interval lasts from 01.2020 to 05.2029. The total injection rate is constant up to 12.2027 and is slightly reduced afterwards (Figure 9.2). Most of the injected CO₂ moves to the eastern region of the structure (Figure 9.3). The total volume of the injected CO₂ exceeds that of the original gas in place (OGIP) and amounts to 135% of OGIP (Figure 9.4). Most of the sequestered CO₂ (79%) becomes a mobile gas, approximate 20% is in the immobile gas saturation, the rest is dissolved in the reservoir brine (Figure 9.5).

The average reservoir pressures in the 3 structure regions significantly increase during the injection phase of the project and slightly decline during the relaxation phase (Figure 9.6). This pressure behaviour results not only from the injection schedule but also from the aquifer activities. During the sequestration project the reservoir water is pushed back to the aquifers (Figure 9.7, Figure 9.8) and this process effectively increases the reservoir volume available to the injected CO₂. The maximum pressure in the structure volume is observed at the end of the injection phase. Its values at that time are presented in Figure 9.9. The maximum local pressure is found along the injecting well trajectories and its absolute maximum amounts to 108% of the initial



reservoir pressure (Figure 9.10). This value is much below the formation breakdown pressure of the corresponding reservoir rock (Figure 7.8). Hence, there is no risk of the gas leakage via a fracture pathway.

Depth of the structure top [m b. s. l.][0]

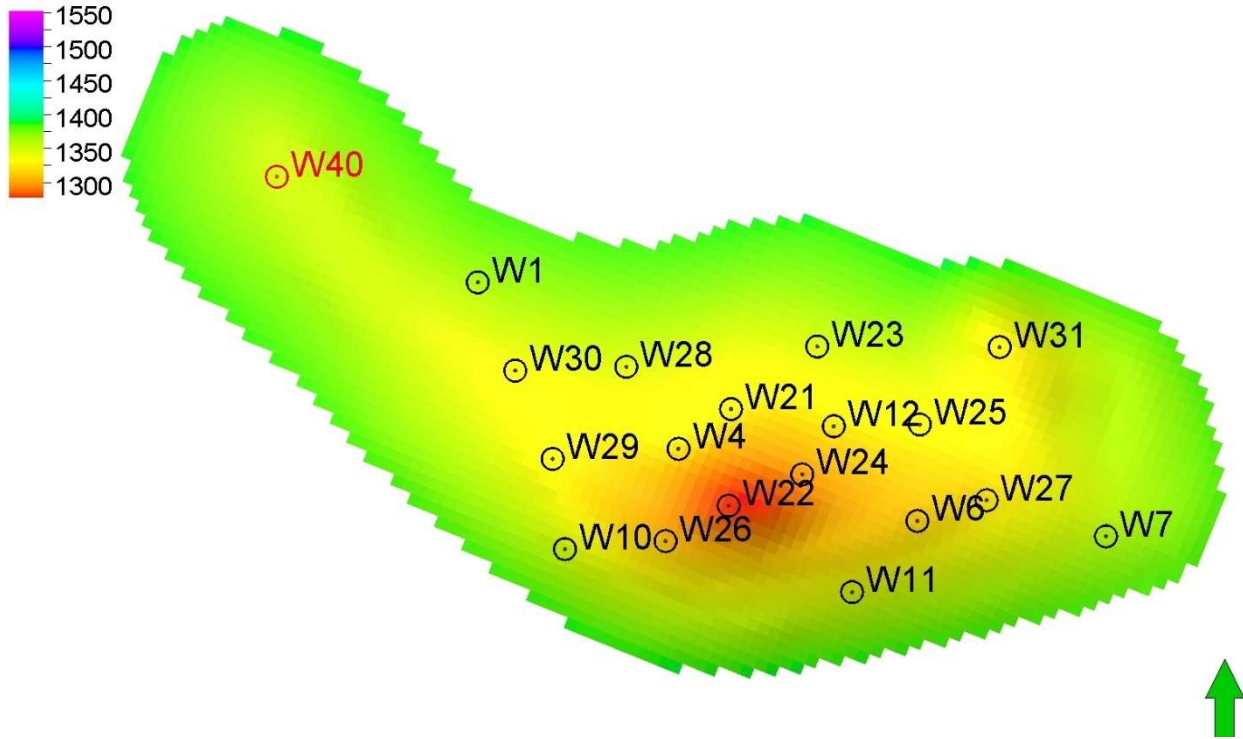


Figure 9.1. Localization of the injecting wells including W40.

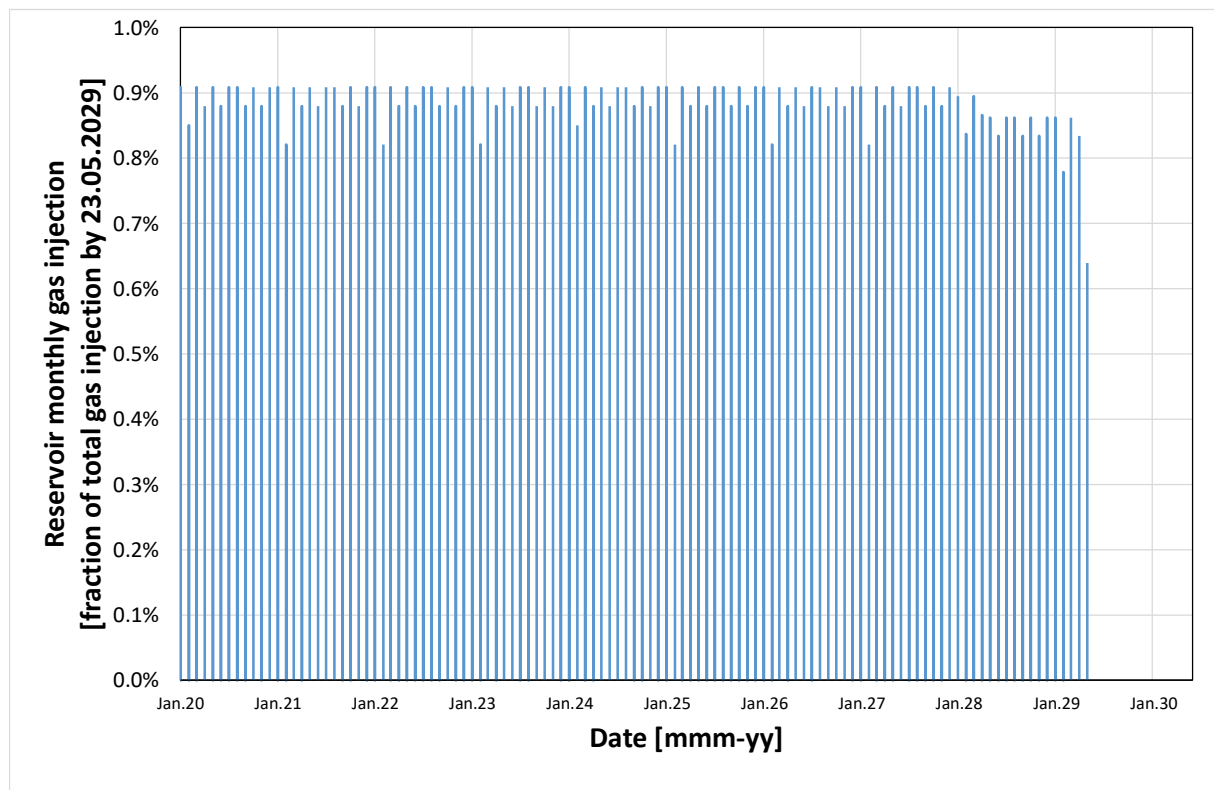


Figure 9.2. Reservoir monthly CO₂ injection.

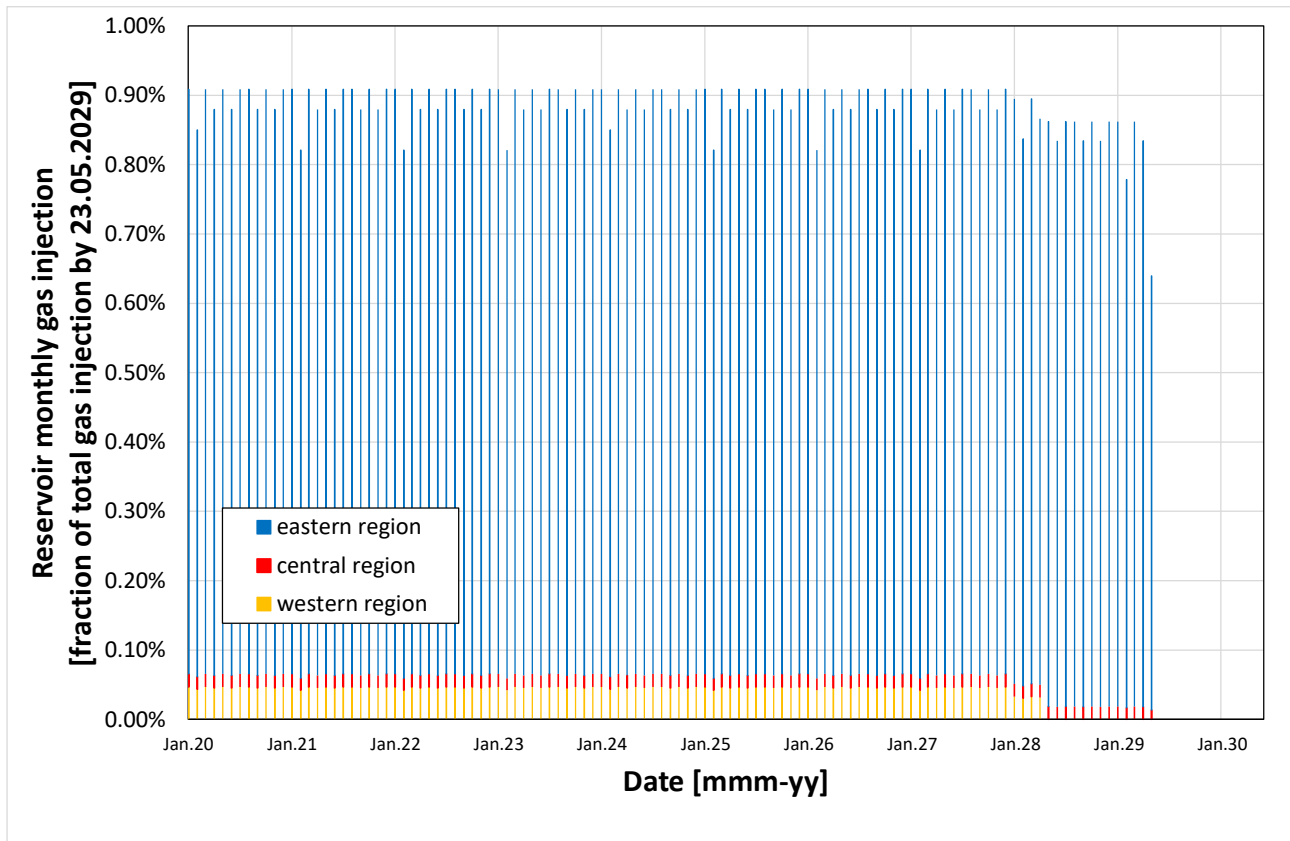


Figure 9.3. Regional monthly CO₂ injection.

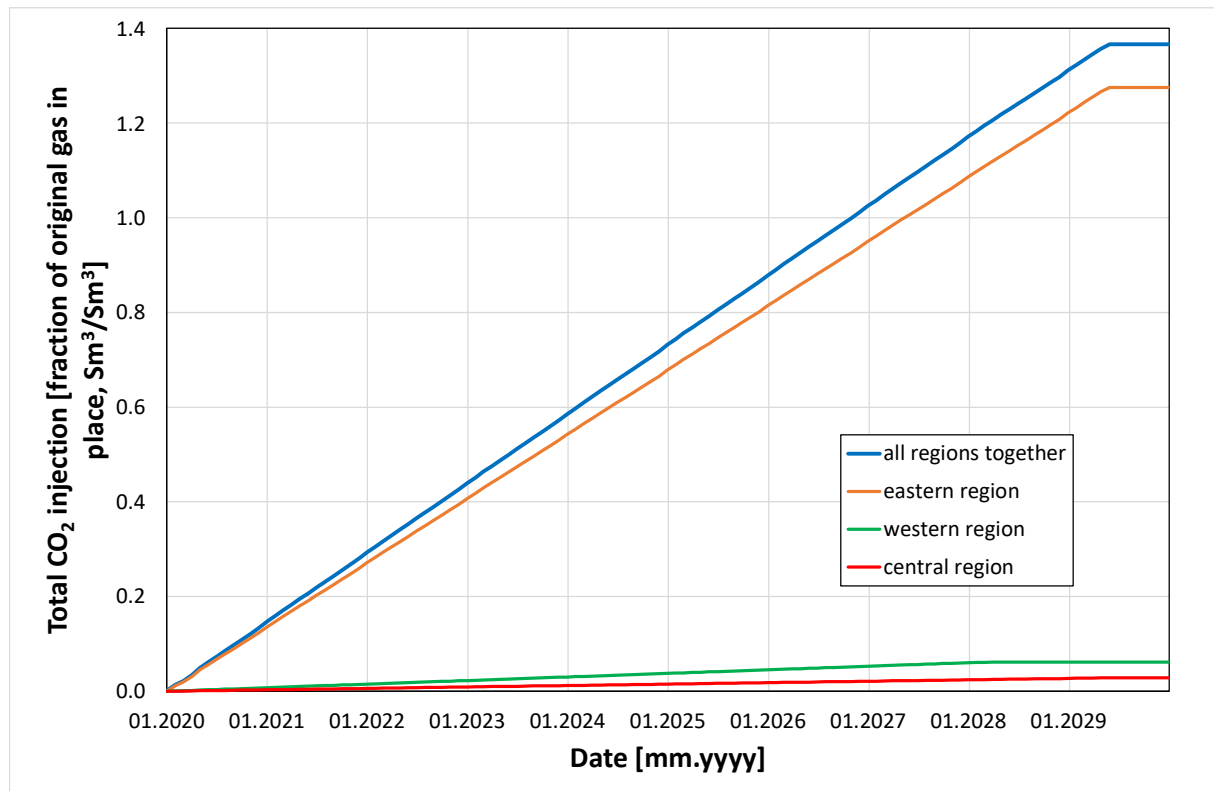


Figure 9.4. Evolution of total CO₂ injection.

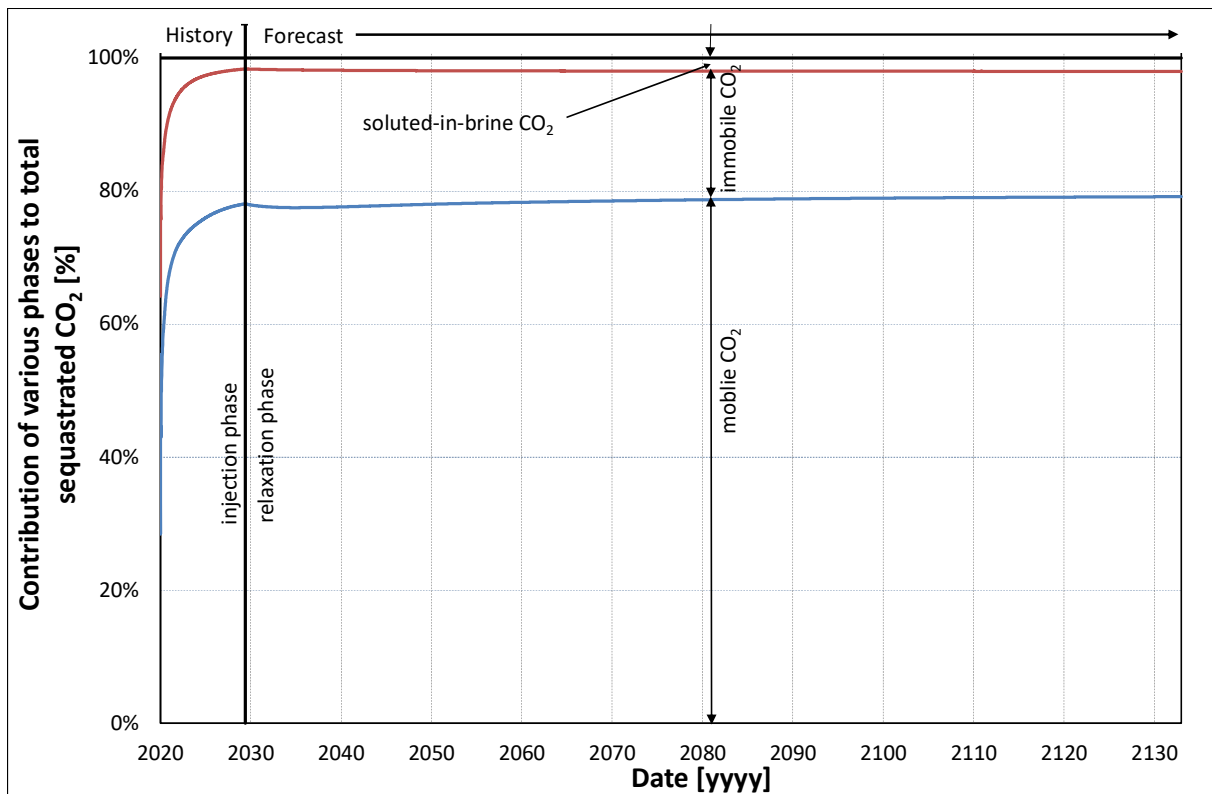


Figure 9.5. Contribution of trapping mechanisms to the total sequestration.

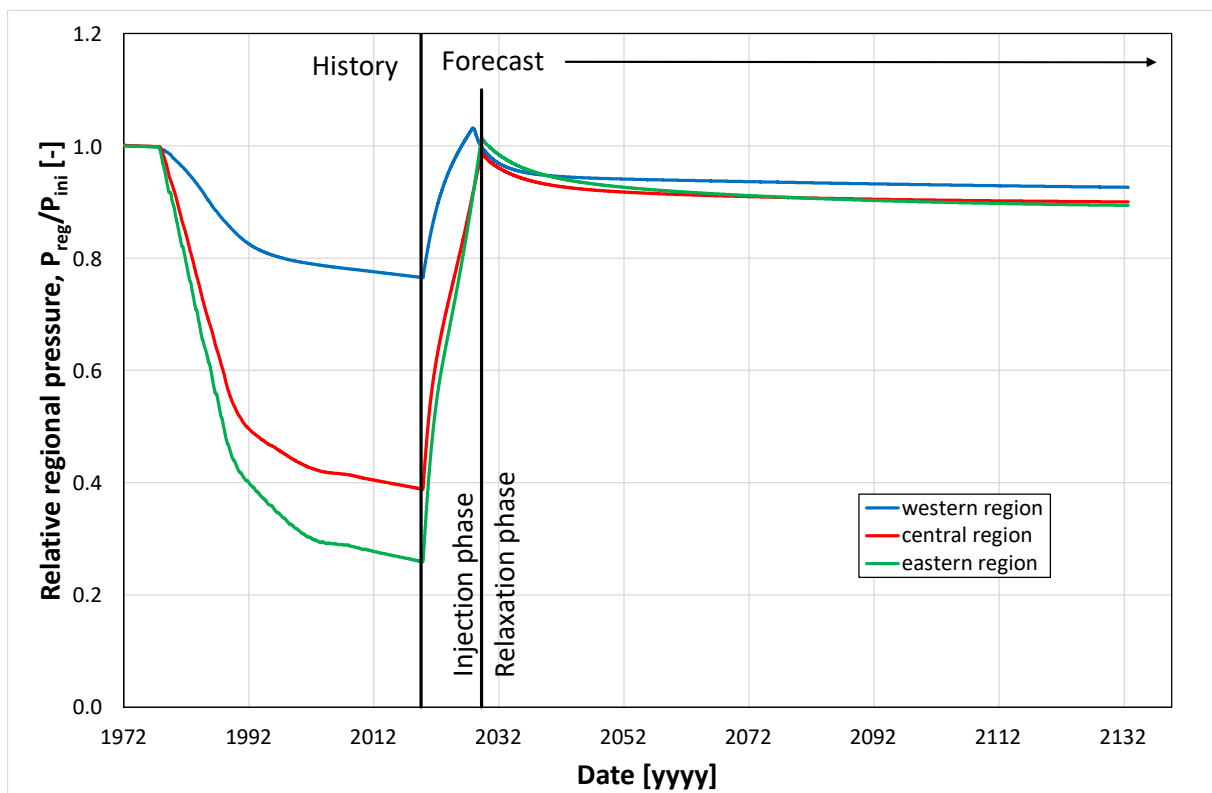


Figure 9.6. Average reservoir pressure.

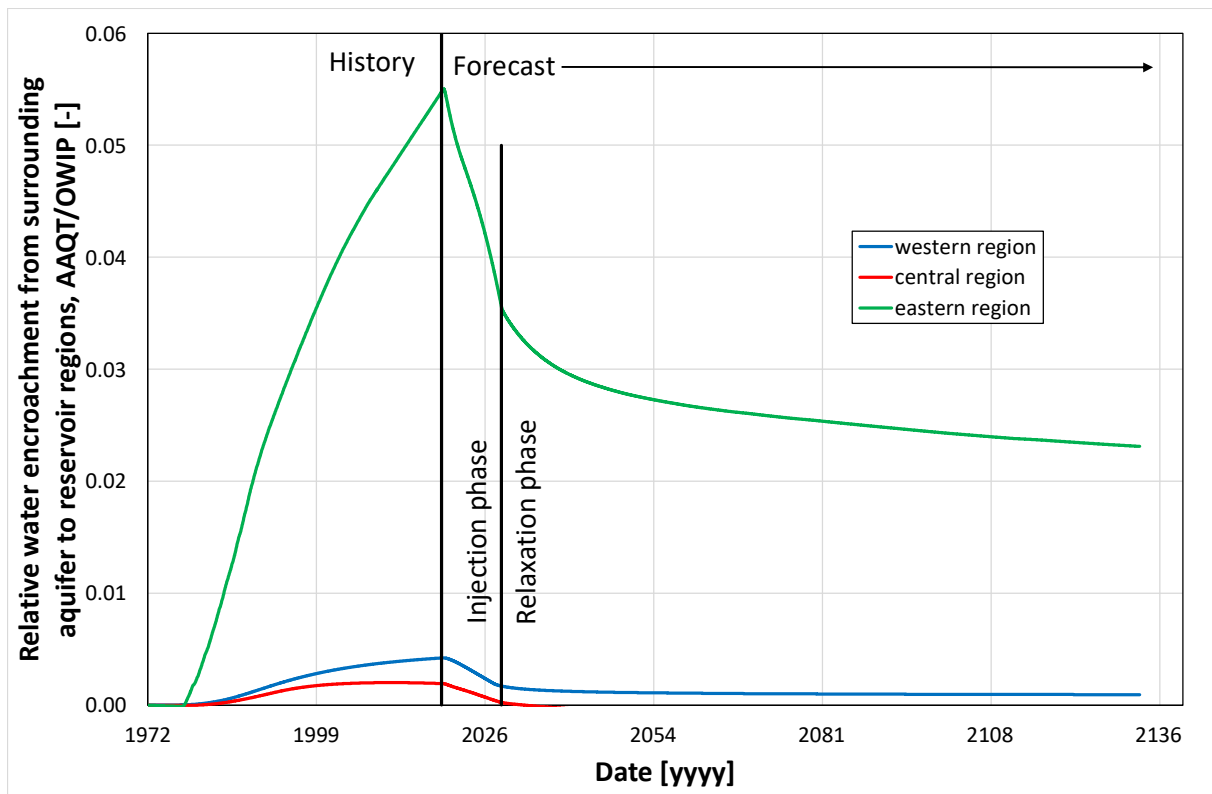


Figure 9.7. Relative water encroachment from surrounding aquifer to reservoir regions.

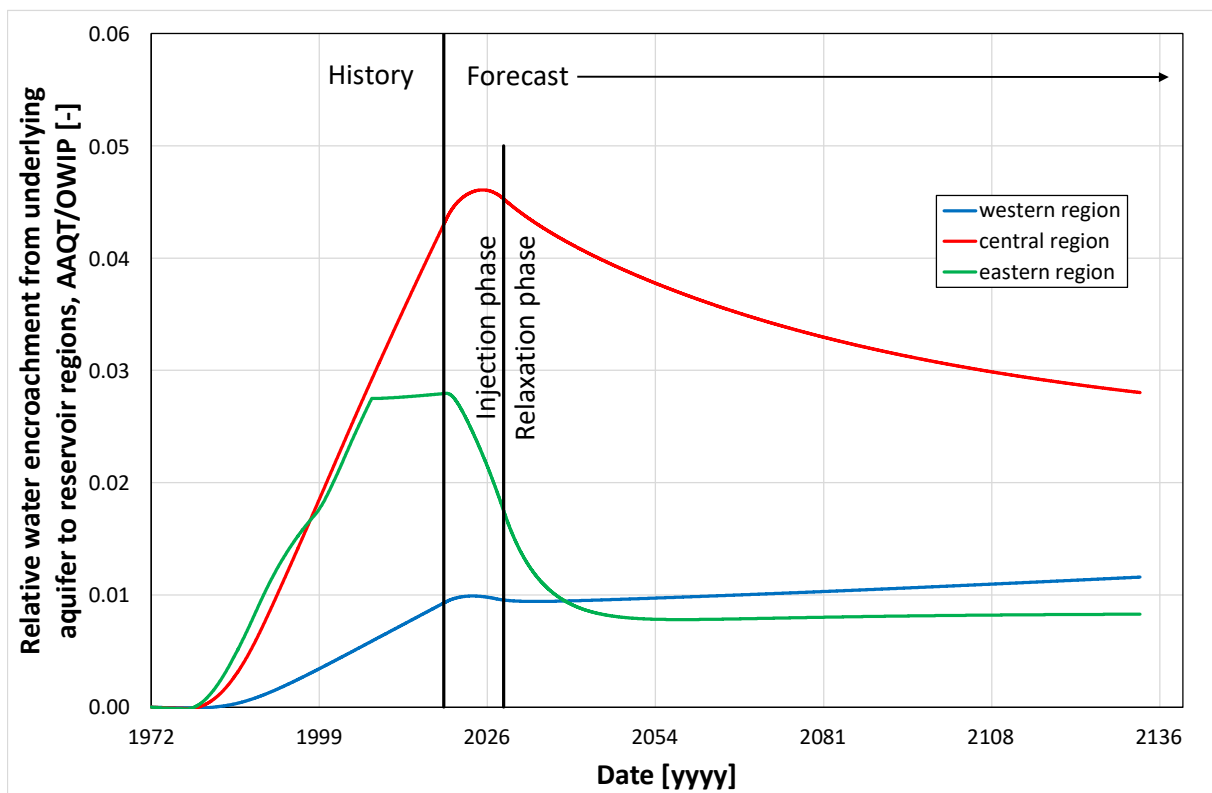


Figure 9.8. Relative water encroachment from underlying aquifer to reservoir regions.

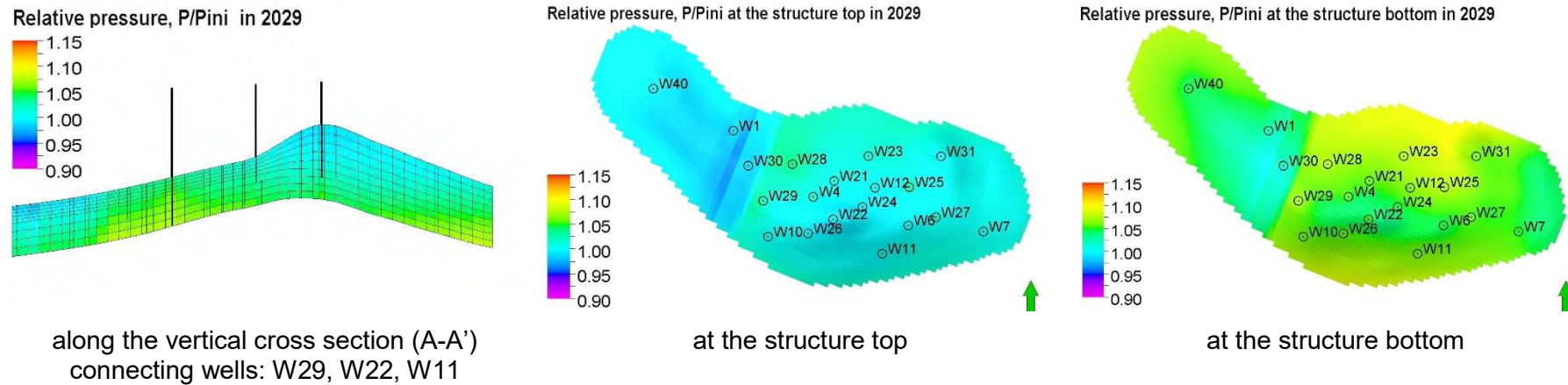


Figure 9.9. Reservoir pressure distribution at the end of the injection phase (2029).

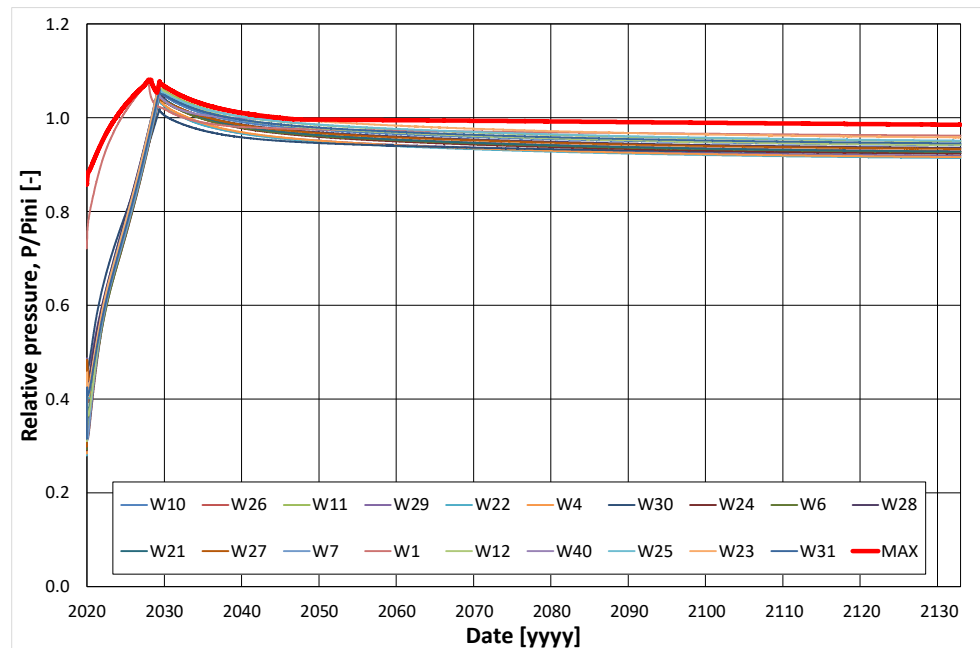


Figure 9.10. Maximum pressures along well trajectories. Maximum pressures among all well trajectories.



The next factor of the leakage risk refers to the pressure step across the caprock-reservoir rock boundary. That step, as a function of time, reaches its maximum value at the end of the injection phase (2029). The distribution of the step pressure at that time is shown in Figure 9.11. The maximum value of the step takes place in the neighbourhood of W22 which is the highest structure point and its evolution with time is shown in Figure 9.12.

Pressure step at the caprock-reservoir boundary (2029)

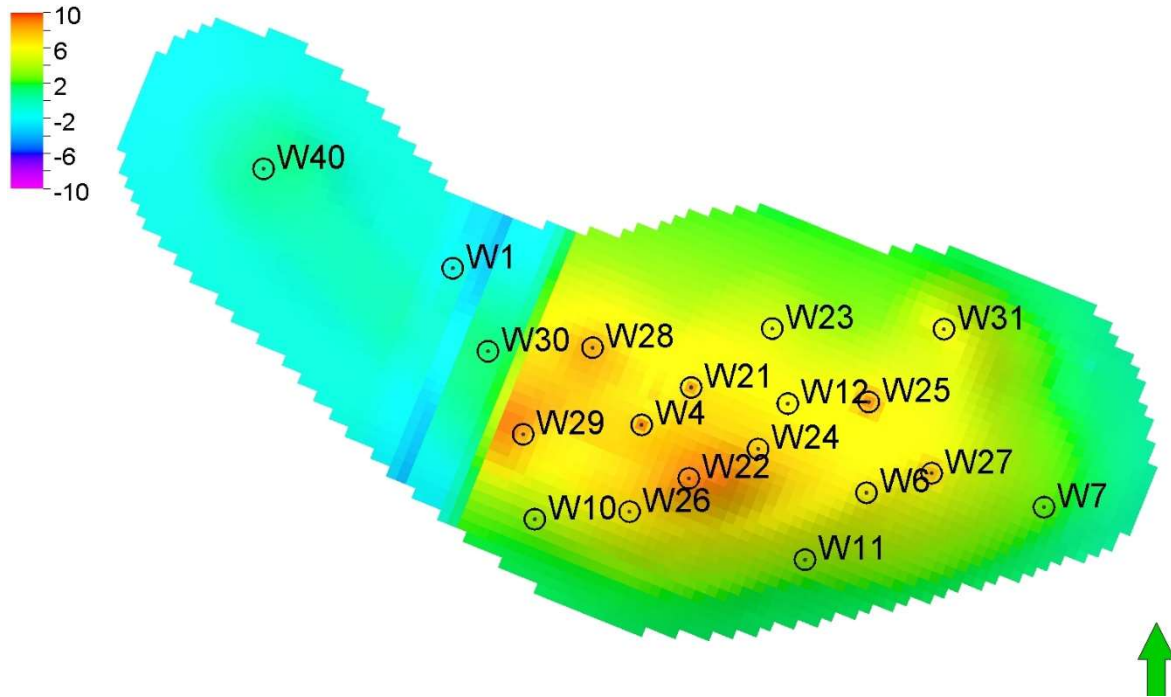


Figure 9.11. Distribution of pressure step across the caprock-reservoir rock boundary in 2029.

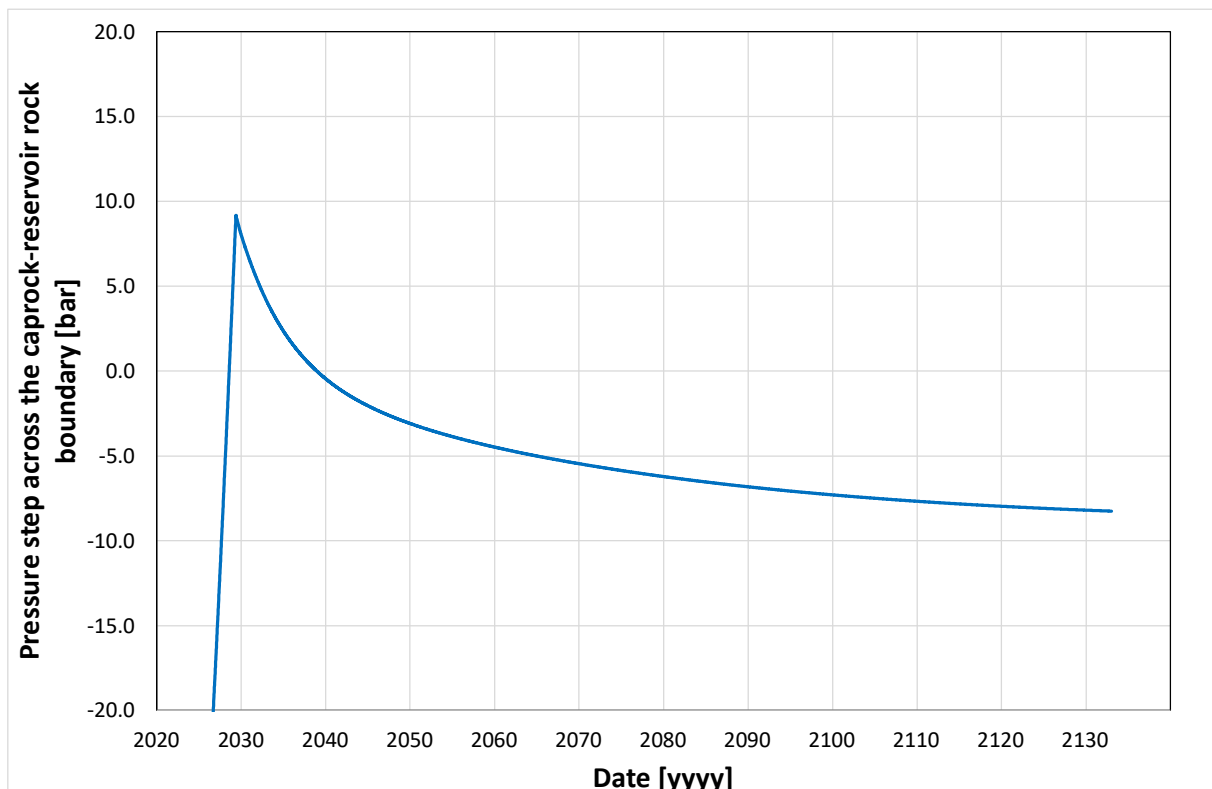


Figure 9.12. Pressure step across the caprock-reservoir rock boundary at the high structure point.

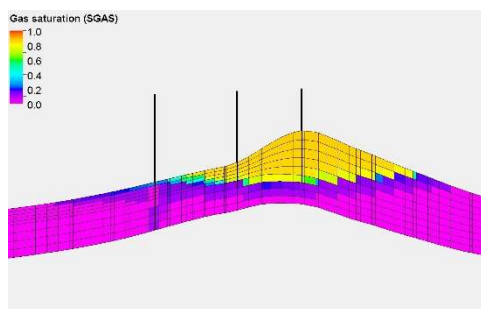


It is worth emphasising the criterion of the pressure step across the caprock-reservoir rock boundary not exceeding the threshold displacement pressure (9.2 bars in Figure 7.9). This is relevant as it is among the risk factors that effectively limits the amount of the injected CO₂, hence, determines the sequestration capacity of the structure.

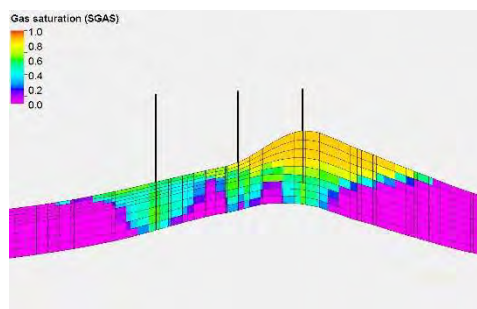
Another important factor to ensure the effectiveness of the sequestration process (in addition to avoiding the injected gas spill-out beyond the structural trap) is the homogeneity of the injected gas distribution across the structure volume. The corresponding results of the significant parameters are shown in the following figures:

- gas saturation – Figure 9.13, Figure 9.14, Figure 9.15,
- CO₂ concentration in the gas phase – Figure 9.16, Figure 9.17, Figure 9.18,
- brine saturation – Figure 9.19, Figure 9.20, Figure 9.21,
- CO₂ solution in the brine phase – Figure 9.22, Figure 9.23, Figure 9.24.

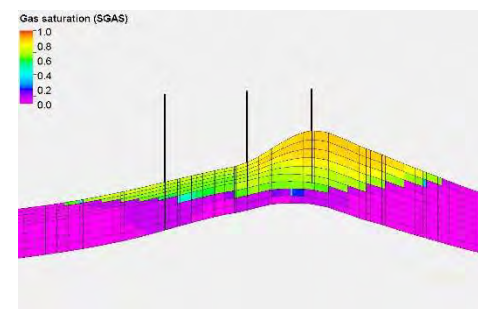
It should be noted that in order to determine the key parameters of the sequestration process it is required to extend the examination of the project beyond the end of the injection phase. This allows for the elongated relaxation phase that typically results in redistribution of fluid saturations and compositions as well as reservoir pressure variation to be included in modelling.



Injection start (2020)

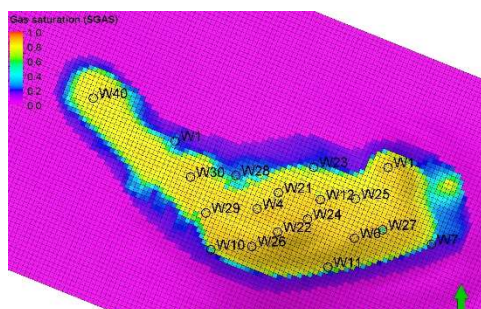


Injection end (2029)

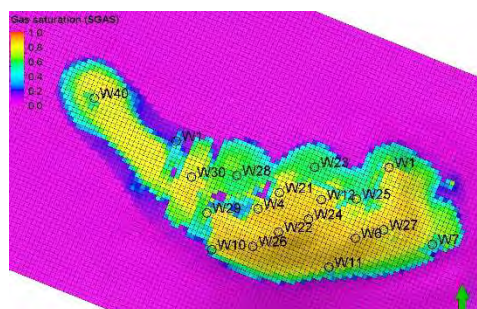


after 100 years of relaxation (2129)

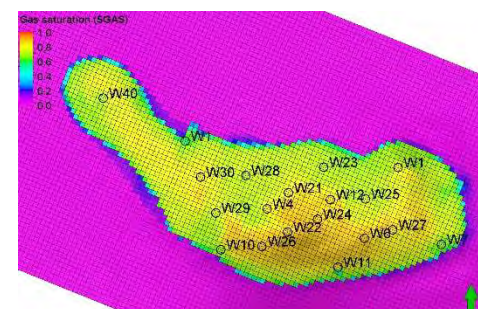
Figure 9.13. Distribution of gas saturation along the vertical cross section (A-A') connecting wells: W29, W22, W11.



Injection start (2020)

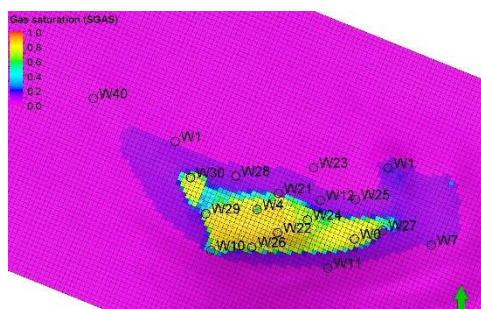


Injection end (2029)

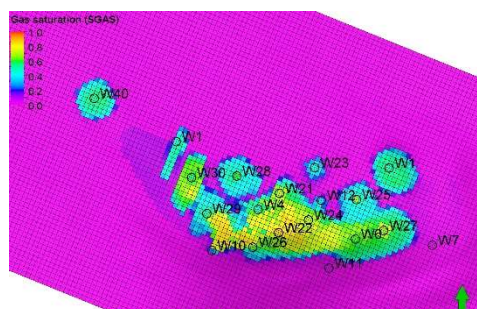


after 100 years of relaxation (2129)

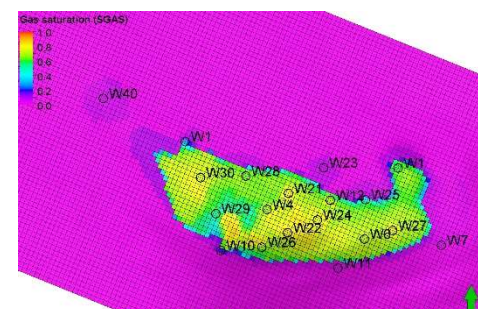
Figure 9.14. Distribution of gas saturation at the structure top.



Injection start (2020)



Injection end (2029)



after 100 years of relaxation (2129)

Figure 9.15. Distribution of gas saturation at the structure mid depth.

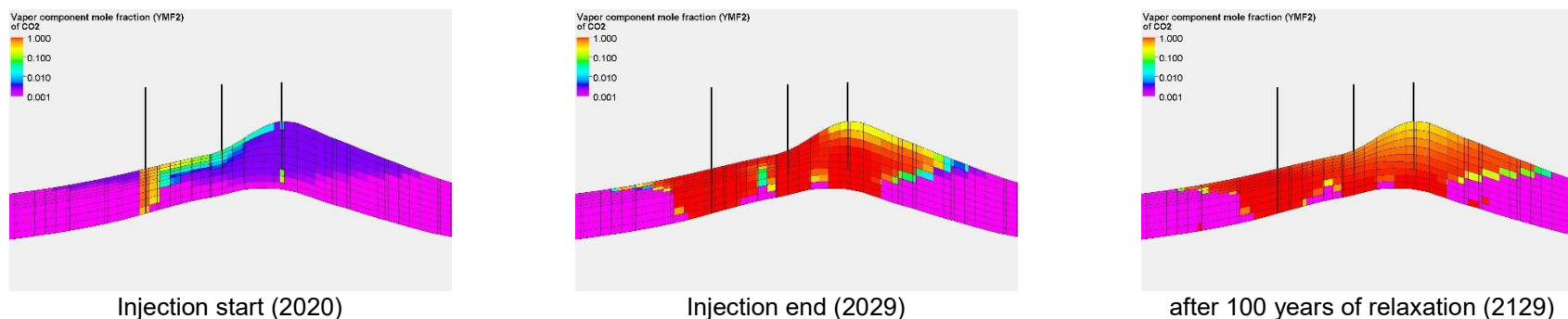


Figure 9.16. Distribution of CO2 concentration in the gas phase along the vertical cross section (A-A') connecting wells: W29, W22, W11.

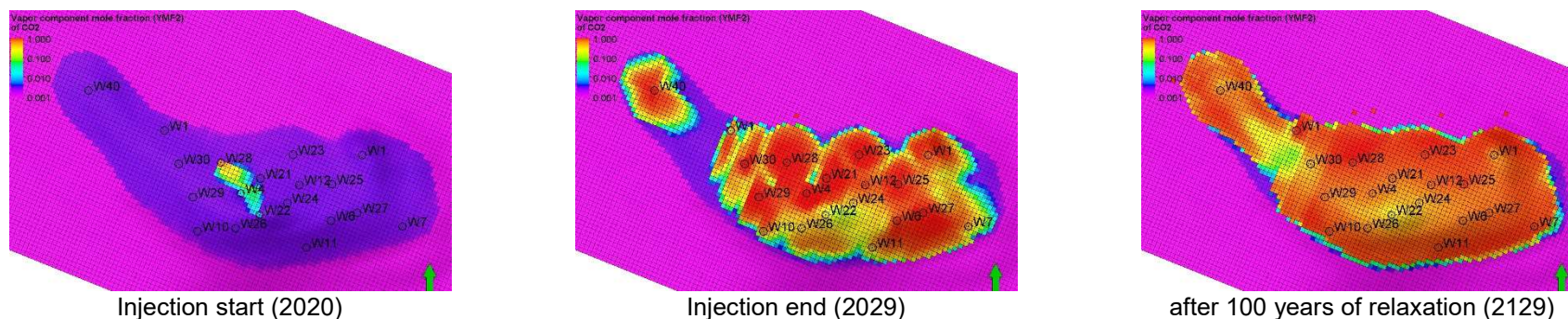


Figure 9.17. Distribution of CO2 concentration in the gas phase at the structure top.

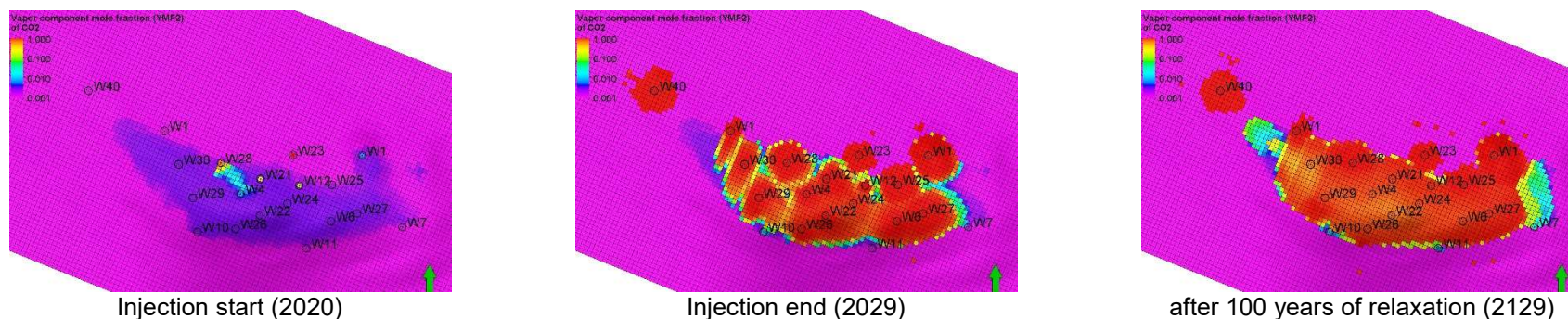
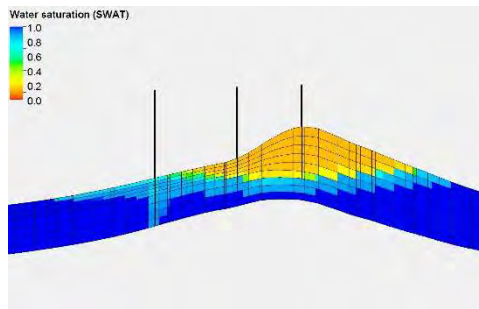
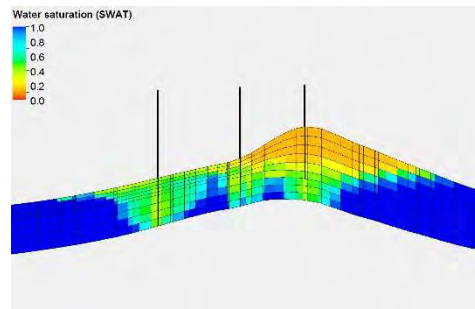


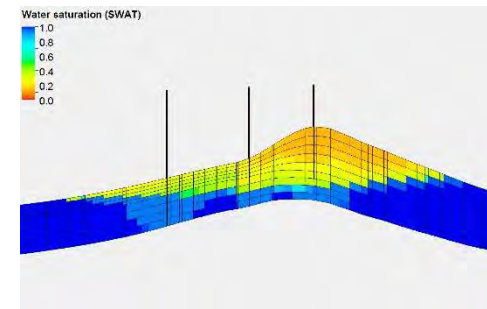
Figure 9.18. Distribution of CO2 concentration in the gas phase at the structure mid depth.



Injection start (2020)

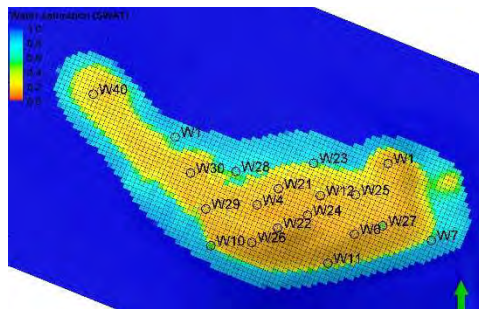


Injection end (2029)

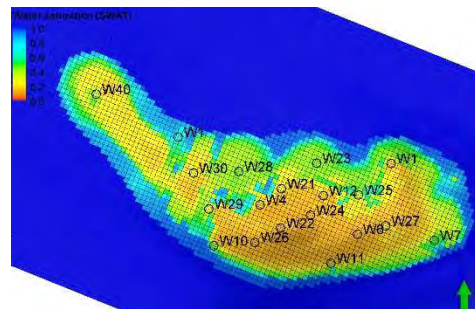


after 100 years of relaxation (2129)

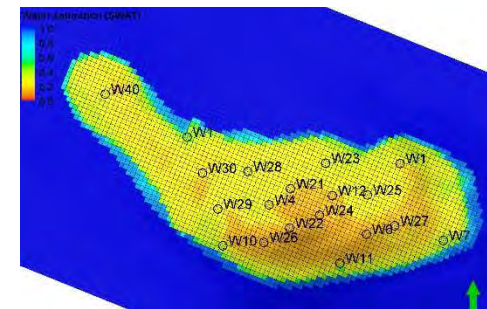
Figure 9.19. Distribution of brine saturation along the vertical cross section connecting wells: W29, W22, W11.



Injection start (2020)

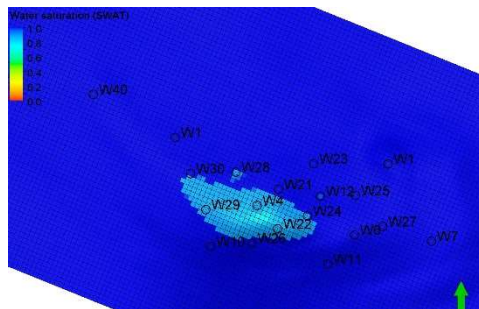


Injection end (2029)

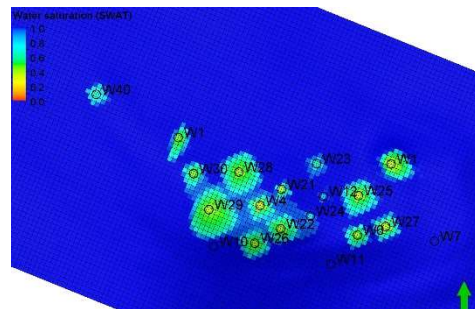


after 100 years of relaxation (2129)

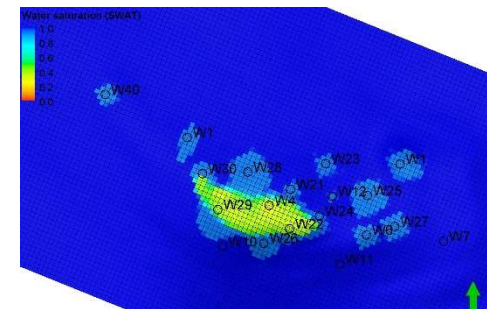
Figure 9.20. Distribution of brine saturation at the structure top.



Injection start (2020)

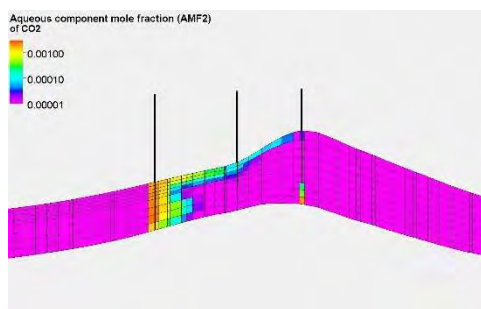


Injection end (2029)

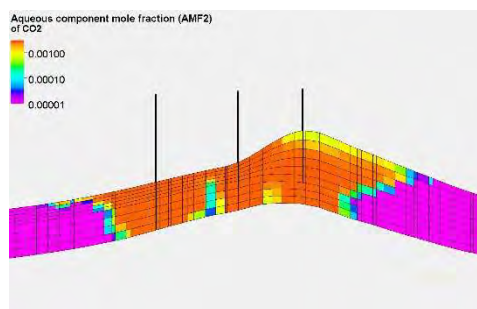


after 100 years of relaxation (2129)

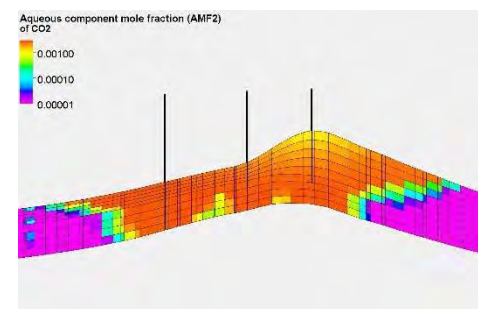
Figure 9.21. Distribution of brine saturation at the structure mid depth.



Injection start (2020)

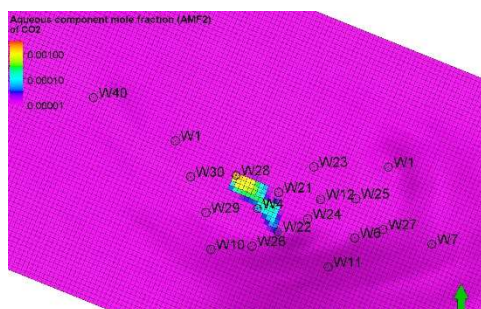


Injection end (2029)

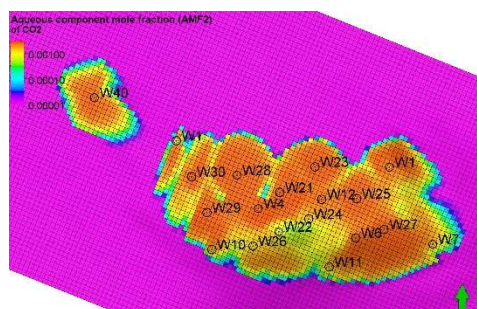


after 100 years of relaxation (2129)

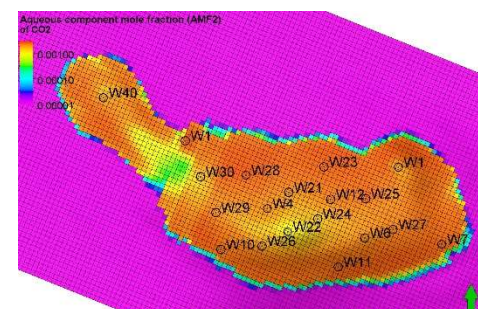
Figure 9.22. Distribution of CO2 solution in brine along the vertical cross section connecting wells: W29, W22, W11.



Injection start (2020)

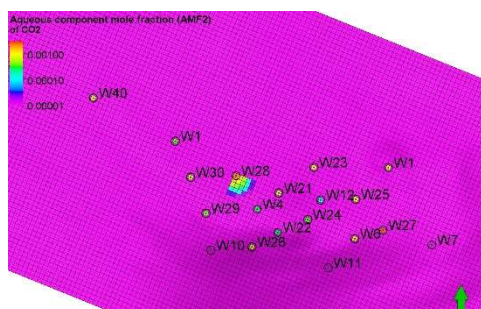


Injection end (2029)

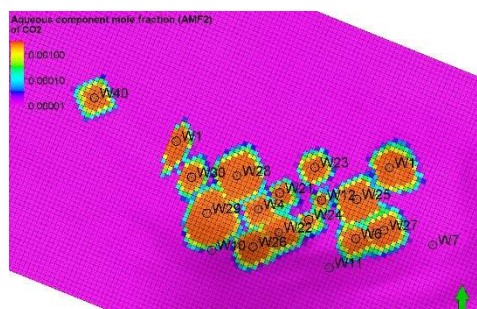


after 100 years of relaxation (2129)

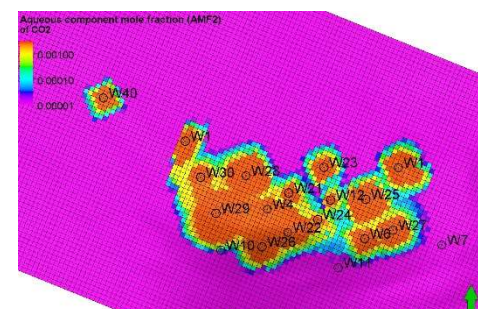
Figure 9.23. Distribution of CO2 solution in brine at the structure top.



Injection start (2020)



Injection end (2029)



after 100 years of relaxation (2129)

Figure 9.24. Distribution of CO2 solution in brine at the structure mid depth.



9.3 SUMMARY AND CONCLUSIONS

This chapter includes the simulation forecast of an alternative scenario for the CO₂ sequestration project in the Borzęcin structure. This scenario maximizes the sequestration capacity of the structure while maintaining a leakage free operation of the sequestration process. The scenario of maximum sequestration capacity is a result of the optimization procedure using multiple simulation forecasts. Capability of performing the optimization procedure proves to be another significant advantage of the numerical modelling tool applied to the sequestration project assessment.



10 Summary and Conclusions of the deliverable

This deliverable reports on the effects of long-term sequestration processes in the Borzęcin structure. It comprises an extended set of data and various modelling tasks necessary to describe significant processes and effects taking place in the Borzęcin structure during the acid gas sequestration project. The report includes detailed description of the operational history of the project. Its key components consist of gas production data of the Borzęcin gas field (since 1972) and concomitant (since 1996) acid gas injection data of the injection activities targeted at the water-bearing zone underlying the gas cap of the Borzęcin field. The rate and composition of the injected gas have followed that of the field production gas as the injected gas has originated from the sweetening process of the produced gas. As a consequence, the composition of the injected gas has stayed roughly constant and included about 78% of CO₂ and 20% of H₂S.

Although the acid gas has been injected into the water-bearing zone, yet the injected gas has migrated to the producing wells completed only in the gas-bearing zone of the Borzęcin structure that is evidenced by the composition of the produced gas that contains, in general, increasing amount of acid gas components. This fact indicates migration paths of the injected gas induced by buoyance mechanisms in the water-bearing zone and by pressure gradients in the gas cap of the structure. These migration paths have taken place due to the limited effects of acid gas solution in the reservoir brine and significantly dominated over the migration of the brine saturated with the dissolved gas. The detailed description of all the involved mechanisms leading to the effective migration of the gas injected to the structure can be given only by the application of the simulation model described below. The above migration effects of the injected gas also result in making a few leakage risks possible. They include leakage pathways across the caprock and as a spill-out beyond the structural trap in addition to the pathways via induced fractures and along well trajectories.

Bottomhole sampling of reservoir water saturated with gas was an essential source of knowledge concerning the phenomena occurring in the sequestration structure as a consequence of the acid gas injection. The results of solution gas analysis revealed that the acid gas injected into the aquifer through the B-28 injector well migrate southwards towards the B-4 well. The investigations proved that this is the main direction of the injected acid gas plume propagation. B-4 well is closest to the B-28 (injector well) and is located in the direction consistent with the expected migration of acid gas, as indicated above, migrates towards shallower parts of the structure, driven by gravity forces and by pressure depression caused by continuous gas production.

The chemical analysis of produced gas confirmed the inflow of the injected acid gas into the gas produced by the B-4 well. Furthermore, an increased concentration of CO₂ was also recorded in the gas produced by the B-22 well, which may indicate that the migration zone of the injected acid gas is going to affect the major production well.

The high dynamics of individual system phases occurring in the structure of the Borzęcin reservoir implies temporal and spatial variability in the isotope composition detected in the analysed gas. The system is subject to periodic disturbances related to the process of gas production, reinjection of acid gases and water coming from outside of the reservoir.

Based on the physiochemical parameters and hydrochemical indicators, it can be stated that the bottom water underlying the Borzęcin reservoir, to which acid gas is injected is a calcium chloride type brine. The values of hydrochemical coefficients indicate a high degree of metamorphosis of the brine analysed. It is a quality typical of highly metamorphosed fossil brines originating from formations with very high hydrogeological sealing.

The PVT studies of produced natural gas as well as reinjected acid gas allowed for the phase behaviour analysis of tested fluids. Both experimental studies and computer simulations showed that under current thermobaric conditions, there is no risk of condensation of the liquid phase at any of the stages of the natural gas production and acid gas reinjection processes. The determining factor here, apart from the gas composition, is low reservoir pressure and above all, the reservoir temperature exceeding the critical temperature concerning both tested gases.

The ability to dissolve the produced and reinjected gases in the reservoir water was also examined. The studies showed that acid gas has excellent solubility in Borzęcin reservoir water about 20 times higher than of the produced gas. This is a positive phenomenon when concerning acid gas sequestration within an active gas reservoir. The dissolution of CO₂ and H₂S in the reservoir water delays the breakthrough of these components into the natural gas zone.

The soil air analyses carried out so far did not reveal surface leaks of acid gases injected into the Borzęcin structure. Periodically elevated hydrocarbon concentrations at some of the wells are likely to occur due to



natural gas exhalation. To ascertain what their origin is, it is recommended to perform long-term monitoring tests on the identified wells.

The process of injecting CO₂ and/or other acid gases is typically associated with significant potential corrosivity of metal tubing and/or casing components of the injecting wells. In the analysed case of the Borzęcin project relevant corrosion tests were performed and showed relatively high corrosion rate reaching 0.18 mm/year. This effect confirms the necessity of corrosion monitoring and possible replacement of the corroded components during the sequestration project.

The injection of CO₂ and/or other acid gases may affect properties of the cement used in injecting well constructions. This clearly requires the use of appropriate cement types. The cement used in the Borzęcin project wells was subject to long-time laboratory tests of the influence of CO₂ upon the cement properties. As a result, no signs of carbonate corrosion were found and the presence of CO₂ environment increased the cement compressive strength over time as compared to the natural gas environment.

The remaining part of the report comprises modelling tasks of the Borzęcin structure and project aimed at the description of significant processes taking place in the structure and determining analysis of leakage risk factors. These tasks began with a detailed description of the geological setting of the Borzęcin structure that is subsequently quantified into the numerical model that includes both structural and parametric properties of the structure.

Based on the geological model, the dynamic simulation model of the structure was constructed that implemented the geological data supplemented with other required components such as: well technical data, reservoir fluid models (thermodynamic model of gas with varying composition, reservoir brine properties, reservoir fluid transport properties), initial reservoir conditions (pore pressures and fluid saturations), boundary reservoir conditions (models of surrounding and underlying aquifers). Upon the model construction it was calibrated against historical production data (gas production and injection rates, bottom hole pressures and water-gas ratios of the producing wells, CO₂ concentration of gas produced by individual wells). The positive results of the calibration process helped verify the model and was a useful step in analysing particular processes taking place in the structure during the project under consideration and to assess their consequences in terms of leakage risks.

In addition to the dynamic simulation model, a concise description of the geomechanical model constructed within another work package (WP4) of the SECURE project by the authors of this deliverable was presented and the simulation results of the structure geomechanical state at 4 different time intervals of the project operation were given and will be used as important input data to assess particular leakage risk along the injecting well to be included as a part of deliverable D2.5.

Simulation results of the acid gas injection process obtained from the calibrated model of the Borzęcin structure were used to analyse key factors of the process. In particular, the distribution of reservoir fluid saturations and pore pressures determined consequences of the process with respect to injected gas leakage factors. The former included gas and brine saturations together with the concentration of the injected gas (CO₂) in these fluids in order to characterize migration of their mobile components. That analysis provided direct data to assess the risk of the injected gas leakage beyond the structural trap.

The reservoir pressure distribution allowed a determination of risks of other leakage events: through the reservoir caprock and via the induced fractures. In the first case the pressure step across the caprock – reservoir rock boundary was determined based on the simulation results and compared with the threshold displacement pressure of the caprock. This threshold pressure is available from the measurements of the caprock samples and/or can be estimated from the initial pressure vertical profile in the gas reservoir as shown in the analysed case of the Borzęcin structure.

For the assessment of the leakage possibility via the induced fractures, reservoir pressure distribution obtained as the simulation results was compared to the formation breakdown (fracturing) pressure. That pressure can be determined in the appropriate well tests and/or calculated using the geomechanical model of the structure as it was the case of the Borzęcin structure. Also, the assessment of the leakage risk through wells requires a set of input data that are available from both the dynamical and geomechanical models of the analysed wells and their surroundings.

In the case of the Borzęcin project, results of the simulation modelling clearly showed **no leakage risk – a conclusion consistent with the measurement results** presented in the measuring part of the deliverable. However, in general, it should be emphasized that lack of measuring evidences during the project operation is not a sufficient condition for leakage-free sequestration process. This is caused by typically prolonged



migration processes of the gas to leak upwards all the way from the sequestration site to the surface where it can be detected. Therefore, the long-term simulation modelling of sequestration projects proves to be a unique method for the complete leakage risk analysis.

In order to assess the future consequences of the sequestration project and to make their analyses, its simulation forecast was performed with the use of the structure numerical model. Results of the forecast were analysed with respect to the leakage risk factors using the above procedure. It should be emphasized that the forecast included a long-time relaxation period extending beyond the injection schedule of the project. During the relaxation period, a significant redistribution of pressures and fluid saturations may occur and usually does occur that affects leakage risk factors. Therefore, performing project simulation forecasts comprising relaxation period of sufficient duration is a key requirement for a thorough analysis of the sequestration project. Again, the application of the project numerical modelling proved to be a necessary tool of the project assessment.

As the current project of the acid gas injection to the Borzęcin structure does not take all the advantages of the structure and its installation, the simulation forecast of an alternative scenario for the large scale CO₂ sequestration project in the Borzęcin structure was performed. This scenario maximized the sequestration capacity of the structure while maintaining a leakage risk-free operation of the sequestration process. The scenario of maximum sequestration capacity was found as a result of the optimization procedure using multiple simulation forecasts. Capability of performing the optimization procedure proved to be another significant advantage of the numerical modelling tool applied to the sequestration project assessment.

General conclusions concerning the significance of measuring and modelling tasks and their mutual relation in the analysis of a sequestration project and, in particular, in the assessment of leakage risk follow.

Obviously, the modelling tasks and their results heavily depend on various types of monitoring data. They mostly include typical production data (fluid injection/production, bhps, etc.). Only few of them are specific to the acid gas sequestration project. They include the content of the injected gas components in samples of reservoir fluids (gas and brine) obtained from the monitoring/producing wells. Those data are of a significant value for the model effective calibration/verification. Another issue, not discussed in the deliverable, is the question of the uniqueness of such a model as a typical inverse problem. However, this is not specific to the sequestration modelling. If accepted, the simulation model of any sequestration project becomes a valuable source of various detailed characteristics of the project not available with another tool or method. Moreover, the simulation model presents an addition value of performing project forecasts and studying future project behaviour. In particular, a very important relaxation phase of the project usually takes hundreds of years and it may affect the key results of the project.

Hence, measuring data (including monitoring ones) are required to generate a proper simulation model and the model is necessary to better understand and describe most of the project characteristics.

An important point refers to the question of leakage risk analysis. The monitoring data (such as soil gas detection) provides hard and direct information about leakage presence or absence. However, these data are limited by their space extent and, obviously, to the past and present time. Then simulation results may provide unique way to assess leakage risks that are not easily and quickly detectable. This confirms the merits of the modelling approach to the problem of leakage risk assessment.



11 References

- [1] Lubaś J, Szott W: *15-year experience of acid gas storage in the natural gas structure of Borzęcin – Poland*. Nafta-Gaz 2010; 66 (5): 333–338
- [2] Lubaś J, Szott W, Jakubowicz P: *Effects of Acid Gas Reinjection on CO₂ Concentration in Natural Gas Produced from Borzęcin Reservoir*. Nafta-Gaz 2012; R. 68, nr: 405–410
- [3] https://sequestration.mit.edu/tools/projects/in_salah.html
- [4] <https://www.co2-cato.org/cato/locations/regions/western-netherlands/gdf-k12-b-offshore-co2-injection-project>
- [5] Polish Oil and Gas Company: *Historical production data of the Borzęcin reservoir - reportet by Polish Oil and Gas Company (POGC) - various reports in free format 1972 -2019*. Unpublished 2019
- [6] Pleśniak Ł, Orion-Jędrysek M, Jakubiak M, Bucha M, Krajniak J, Matusiewicz M, et al.: *Ocena migracji składników gazu ziemnego w złożu Borzęcin na podstawie wyników analiz izotopów trwałych wodoru i węgla*. Nafta-Gaz 2017; 73 (1): 27–35. DOI: 10.18668/ng.2017.01.03
- [7] Hosgormez H, Etiope G, Yalçın MN: *New evidence for a mixed inorganic and organic origin of the Olympic Chimaera fire (Turkey): A large onshore seepage of abiogenic gas*. *Geofluids*, vol. 8, John Wiley & Sons, Ltd; 2008. DOI: 10.1111/j.1468-8123.2008.00226.x
- [8] Kotarba MJ, Nagao K: *Composition and origin of natural gases accumulated in the Polish and Ukrainian parts of the Carpathian region: Gaseous hydrocarbons, noble gases, carbon dioxide and nitrogen*. *Chemical Geology* 2008; 255 (3–4): 426–438. DOI: 10.1016/j.chemgeo.2008.07.011
- [9] Collins, A.G.: *Geochemistry of oilfield waters* 1974
- [10] Józwiak K: *Variability of concentrations of gases in the air of the vadose zone in the natural and agriculturally converted environments*. *Przegląd Geologiczny* 2017; Vol. 65 (nr 11/1)
- [11] Geofizyka Toruń Grupa PGNiG: *Multifinger Imaging Tool Reports 2002 – 2018*. Unpublished 2018
- [12] Filar B, Rzepka M: *Risk management of CO₂ geological storage*. *Prace Instytutu Nafty i Gazu* 2012
- [13] Tikhomirov V V.: *Hydrogeochemistry Fundamentals and Advances: Groundwater Composition and Chemistry, Volume 1*. vol. 1. Hoboken, NJ, USA: John Wiley & Sons, Inc.; 2016. DOI: 10.1002/9781119160434
- [14] Polish Oil and Gas Company: *Geological Documentation of the Borzęcin Natural Gas Reservoir*. Unpublished 1999
- [15] Szott W, Gołabek A, Milek K: *Simulation studies of acid gas sequestration in aquifers underlying gas reservoirs*. *Prace Instytutu Nafty i Gazu* 2009; 165: 1–89
- [16] Guo B, Lyons WC, Ghalambor A: *Petroleum Production Engineering, A Computer-Assisted Approach*. Elsevier Inc.; 2007. DOI: 10.1016/B978-0-7506-8270-1.X5000-2